# New Initiators for the Controlled Production of Copolymers (Alternative Format Thesis)

Kirk, Sarah

*Award date:*
2017

*Awarding institution:*
University of Bath

# New Initiators for the Controlled Production of Copolymers

Sarah Megan Kirk

A thesis submitted for the degree of Doctor of Philosophy

University of Bath

Department of Chemistry

January 2017


# Contents

# Acknowledgements

Firstly I would like to thank Dr Matthew Jones for all the support and supervision during my PhD, I have thoroughly enjoyed my time working here. I am grateful to the University of Bath for the facilities, the CSCT for providing me with the opportunity to carry out this project, and the EPSRC for the funding which made this possible. I would also like to thank my secondary supervisor Dr Marianne Ellis for her contributions. Many thanks go to Drs John Lowe and Tim Woodman for their training, advice and NMR spectroscopy services. Thanks also to Dr Anneke Lubben for training and use of mass spectrometry services.

My experience in the Jones group has been an excellent one and I owe a lot of that to its past and current members: Helena Quilter, Heather Parker, James Beament, Tom Clarke, Rhodri Owen, Tom Forder and Stuart Hancock. They have provided me with guidance and laughter during my time here. A special thank you to my lab and office buddy Paul McKeown, cheers for putting up with me over the years! Another thank you goes to members of the 5W 3.11 lab for making the experience particularly enjoyable. Thanks also to David Liptrot for his help and invaluable support during my PhD.

I reluctantly thank my housemates over the four years of my time in Bath - Stephen Bradley, Andy Paterson, Chris Davey, you guys are okay. I owe part of my sanity over the past few years to Bristol Roller Derby, not only for providing a hobby where I can smash people on skates but also a group of great friends. I don't know where I would be (literally!) without James McDonald and Rob Farrow, who have provided me with a place to live in these final months of thesis writing. Finally, I am grateful to my parents for supporting me over the many years of my pursuit of education in the sciences, my love and thanks to you both.

# Abstract

The topic of the production and characterisation of biopolymers, with a specific focus on polylactide is introduced in Chapter 1. Previously reported initiators for the production of polylactide and other biopolymers and copolymers are discussed, with a focus on zinc, group 2, aluminium and group 4 initiators. This chapter puts into context the research carried out for this thesis.

Chapter 2 investigates the effect of dinuclear *vs* mononuclear aluminium salen complexes featuring a naphthalene backbone. All the initiators synthesised in this chapter were found to yield atactic PLA during the ROP of *rac*-lactide, however the dinuclear complex was found to achieve high conversions of polylactide within 2 hours. A kinetic investigation was performed in order to understand this effect. It was found that at the same concentration of initiating metal centres, the $k_{app}$ values were comparable between mononuclear and dinuclear species, thus ruling out the possibility of cooperative effects between the metal centres in the dinuclear complex accelerating the polymerisation rate. Investigation into the copolymerisation of lactide and caprolactone using these initiators found that lactide was selectively consumed in the first instance, however the final copolymer product was found to be random in nature due to transesterification reactions. This work has been published in Dalton Transactions, 2016.

Chapter 3 reports the synthesis of a range of aluminium and zinc complexes using Schiff base ligands featuring an NHBoc moiety and {ONN} ligands with both an amine and imine group. For the aluminium NHBoc complexes, it was found that either 2:1 or 1:1 ligand to metal complexes would form, depending on the steric bulk of the substituent groups on the phenolate ring. These aluminium initiators were all found to produce atactic PLA. Zinc complexes were also formed using these NHBoc ligands, in 2:1 ligand to metal centre ratio. These initiators produced high molecular weight PLA in an uncontrolled manner when no coinitiator was employed. It is proposed that these zinc complexes undergo the activated monomer mechanism when benzyl alcohol is utilised as a coinitiator. For the tridentate zinc complexes Zn(**10**)Me and Zn(**12**)Me, two stereoisomers were observed in the solution-state NMR spectrum. These initiators were found to produce mildly heterotactic PLA, in high conversions after one hour at ambient temperature.

Chapter 4 discusses the relationship between salen and salalen ligands featuring a phenylene backbone and their complexes with aluminium, zirconium and hafnium. It was found that the

salen ligand formed dinuclear metal complexes, with the exception of zirconium *tert*-butoxide. The dinuclear salen complexes were found to have high activity but little selectivity, producing atactic PLA. The aluminium salalen complex was found to be slightly isoselective, and the zirconium isopropoxide salalen complex even more so. At a reduced temperature of 50 °C, the latter yielded PLA with a $P_r$ value of 0.15. This complex was taken forward for copolymerisation studies of lactide and caprolactone, it was found to produce a copolymer that is 'blocky' in character. This work has been published in Organometallics, 2016.

Chapter 5 details the synthetic procedures for all ligands, complexes and polymers reported in this thesis, along with details of general experimental methods and techniques utilised.

# Abbreviations

| | |
|---|---|
| Å | Angstrom |
| BDI | β-diketiminate |
| BnOH | benzyl alcohol |
| br. s | broad singlet |
| calc | calculated |
| CL | caprolactone |
| corr | corrected |
| d | doublet |
| D | Diffusion coefficient |
| DCM | dichloromethane |
| dd | doublet of doublets |
| ddd | doublet of doublet of doublets |
| dt | doublet of triplets |
| DOSY | diffusion-ordered spectroscopy |
| DSC | differential scanning calorimetry |
| ESI | electrospray ionisation |
| *fac* | facial |
| GPC | gel permeation chromatography |
| $k_{app}$ | apparent rate constant |
| $k_{init}$ | rate constant of initiation |
| $k_{prop}$ | rate constant of propagation |
| $L_x$ | average block length |
| LA | Lactide |
| m | Multiplet |
| MALDI | matrix-assisted laser desorption ionisation |
| *mer* | meridonal |
| $M_n$ | number average molecular weight |
| $M_w$ | weight average molecular weight |
| NMR | nuclear magnetic resonance |
| obs | observed |
| PBL | polybutyrolactone |

| | |
|---|---|
| PCL | polycaprolactone |
| PDI | polydispersity index |
| PEF | polyethylene furanoate |
| PET | polyethylene terephthalate |
| PLA | polylactide |
| $P_m$ | probability of meso enchainment |
| ppm | parts per million |
| $P_r$ | probability of racemic enchainment |
| R | randomness factor |
| RI | refractive index |
| ROP | ring-opening polymerisation |
| s | singlet |
| SPS | solvent purification system |
| t | triplet |
| td | triplet of doublets |
| $T_c$ | crystallisation temperature |
| td | triplet of doublets |
| $T_g$ | glass transition temperature |
| THF | tetrahydrofuran |
| $T_m$ | melting temperature |
| tol | toluene |

# Publications and Presentations



Dalton Transactions

PAPER

View Article Online
View Journal | View Issue

Cite this: *Dalton Trans.*, 2016, **45**, 13846

## Monomeric and dimeric Al(III) complexes for the production of polylactide†

Sarah M. Kirk,[a,b] Helena C. Quilter,[a,b] Antoine Buchard,[b] Lynne H. Thomas,[b] Gabriele Kociok-Kohn[b] and Matthew D. Jones*[b]

Received 19th July 2016,
Accepted 3rd August 2016

DOI: 10.1039/c6dt02861f

www.rsc.org/dalton

A series of monometallic and bimetallic Al(III) complexes with substituted naphthyl based Schiff base ligands have been prepared and characterised. When 1-aminonaphthalene based ligands were reacted with $AlMe_3$ monometallic complexes were isolated, however, with 1,5 and 1,8-diaminonaphthalene based ligands bimetallic complexes were formed. In all cases 4-coordinate tetrahedral Al(III) centres were observed in the solid state and in solution. There was little difference in rate of polymerisation of *rac*-lactide between the monometallic and bimetallic complexes based on 1,5-diaminonaphthalene. However, for the 1,8-diaminonaphthalene the complex was an order of magnitude faster than the monometallic and the analogous 1,5-system. Moreover, this complex was active at room temperature, which is rare for aluminium initiators, and PLA with a high degree ($P_m$ = 0.82) of isotacticity was observed.

## Introduction

Polylactide has been extensively researched in recent years. This is due to the fact that it is biodegradable, renewable and biocompatible.[1] It has found many uses from high value biomedical applications (sutures and drug delivery vesicles) to commodity packaging materials. Polylactide (PLA) is prepared *via* ring opening polymerisation of the cyclic ester lactide (LA), the monomer is available in various stereoforms – meso, racemic or chirally pure.[2] When *rac*-lactide (*rac*-LA) is polymerised either atactic, heterotactic or isotactic PLA can be prepared.[3] The physical properties (melting temperature, $T_g$, rate of degradation) are intrinsically linked to the polymers microstructure.[3] In the literature there are complexes based on group 4,[4] zinc,[5] indium,[6] aluminium,[7] rare earth metals[8] and groups 1–3[5a,9] that are capable of imparting selectivity during the polymerisation. It is fair to say that aluminium initiators are amongst some of the successful in the literature, since the early work of Spassky,[7e] Chisholm,[7a] Feijen,[7g,h] Coates and Gibson[7c,10] there have been a multitude of aluminium complexes with salan, salen and salalen ancillary ligands reported.[7] Moreover it is also fair to say that there is still a significant degree of serendipity in choice of ligand–metal in terms of rate of polymerisation and stereocontrol observed in the resultant PLA. Currently, there has been interest in the preparation of multimetallic catalysts, with the hope there will be beneficial cooperativity between the metal centres and enhancement in the catalytic properties. There are only a limited number of dinuclear complexes for the polymerisation of cyclic esters.[6c,11] For example, Carpentier has shown that for dinuclear aluminium systems based on biphenyl ligands the rate of polymerisation is almost an order of magnitude faster than the monometallic complex.[12] This is believed to be due to the fact that in these examples the aluminium centres can potentially be close enough to cooperate (within 3.0 Å) and this potentially may facilitate a dual activation mechanisms. Further evidence for the existence of cooperation between aluminium centres has be demonstrated by Yao and co-workers.[13] They prepared a series of Al–alkyl complexes of piperazidine ligands and observed a 2–8 times rate enhancement in polymerisation activity. Redshaw suggests that cooperative effects are present in aluminium complexes as long as they are not linked in an aluminoxane [Al–O–Al] and they suggest a favourable Al–Al distance of around 6 Å for ε-caprolactone polymerisation.[14] Chen has pioneered the use of bimetallic Al(III) complexes for the ROP of lactide and ε-caprolactone.[15] Importantly they have shown that it is possible to induce stereoselectivity with such complexes.[15a] Very recently Mazzeo has highlighted the importance of cooperativity in the polymerisation of *rac*-LA initiated with Al(III) salen complexes with Al···Al distance the key parameter. They propose that this is due to synergic interactions during the alcoholysis and polymer growth steps.[16] In this paper we have prepared a series of

[a]Doctoral Training Centre in Sustainable Chemical Technologies, University of Bath, Bath BA2 7AY, UK
[b]Department of Chemistry, University of Bath, Bath BA2 7AY, UK.
E-mail: mj205@bath.ac.uk

†Electronic supplementary information (ESI) available: Representative NMR spectra, GPCs and homonuclear decoupled NMR spectra. CCDC 1491894–1491898. For ESI and crystallographic data in CIF or other electronic format see DOI: 10.1039/c6dt02861f

ORGANOMETALLICS

Article

pubs.acs.org/Organometallics

# Zirconium vs Aluminum Salalen Initiators for the Production of Biopolymers

Sarah M. Kirk,[†,‡] Gabriele Kociok-Köhn,[‡] and Matthew D. Jones*[,‡]

[†]Doctoral Training Centre in Sustainable Chemical Technologies and [‡]Department of Chemistry, University of Bath, Bath BA2 7AY, U.K.

Supporting Information

**ABSTRACT:** Herein we report the synthesis and full characterization (NMR and solid-state structures) for a series of Zr(IV), Hf(IV), and Al(III) salalen complexes, together with salen bimetallic counterparts. With the salalen ligand, $1H_2$, monometallic complexes were observed in solution and solid state. Complex $Zr(1)(O^iPr)_2$ was able to produce isotactic polylactide (PLA) from *rac*-lactide ($P_m$ up to 0.85) in solution at 50 °C; in the melt (130 °C) this reduced to ca. 0.75. Al(**1**)Me was significantly less active and produced PLA with only a very modest isotactic enchainment ($P_m \approx 0.6$). $Zr(1)(O^iPr)_2$ was also able to produce copolymers with lactide and $\varepsilon$-caprolactone, producing copolymers of a "blocky" nature.

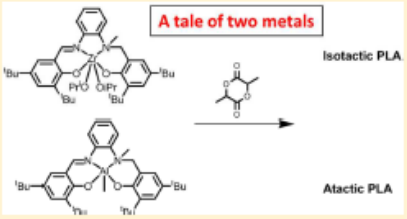


## INTRODUCTION

Research into polylactide (PLA) has exploded in recent years.[1] The reason is the favorable properties of the final polymer (biodegradability and biocompatibility) coupled with the fact that the starting material lactide (LA) can be sourced from annually renewable raw materials. PLA is prepared by the ring-opening polymerization (ROP) of the cyclic ester monomer, LA. The properties of the polymer (thermal transitions and degradation profiles) are correlated to the polymer's tacticity (either atactic, heterotactic, or isotactic). The tacticity can be controlled by the judicious choice of ligand and metal combination; however, clear structure−activity relationships are lacking in the area, and there is an element of serendipity in initiator design. There are a multitude of metal centers that can be applied for the controlled ROP of *rac*-LA, for example Al(III),[2] Zn(II),[3] In(III),[4] groups 1 and 2,[5] group 3,[6] group 4,[7] and the lanthanides.[6d,8] Further, the use of bimetallic complexes is promising to be an alternative research strategy.[2i,9] The majority of these examples utilize salan or salen ligands. In recent years the use of salalen ligands has been a promising avenue of research.[7r,8i,10] For example, we have prepared a series of salalen ligands with aliphatic linkers and have shown that the polymer microstructure can be changed from moderately isotactic to moderately heterotactic by subtle changes to the ligand backbone.[7r,10a,e] Using similar ligands to these, Yao was able to prepare a series of efficient initiators for the production of heterotactic PLA ($P_r$ up to 0.85), and the tacticity was related to the ionic radii of the complexes, with the ligand's steric bulk appearing not to have any effect on tacticity.[8i] Wu and co-workers[11] have prepared binuclear magnesium and zinc initiators based on heptadentate salalen systems. The complexes were found to be efficient initiators for the controlled polymerization of L-lactide; they observed that the mechanism of initiation varied with temperature. At 130 °C the classical coordination insertion mechanism was in operation, whereas at lower temperature an external initiator was required and polymerization proceeded via an "activated monomer" mechanism. When *rac*-LA was used, only very modest isotactic PLA was prepared (probability of isotactic linkages, $P_m$, up to 0.59). Al(III) salalen complexes have been used to excellent effect by Kol, Lamberti, and Mazzeo.[10b,12] They have prepared an Al(III) complex of a chiral salalen ligand based on an aminoethylpyrrolidine backbone and have isolated gradient isotactic multiblock PLA. The mechanism is a combination of enantiomorphic-site control and chain-end control.

## RESULTS AND DISCUSSION

As part of our continuing studies concerning the utilization of salalen ligands for the production of PLA, we have prepared a salalen ligand with a planar and rigid backbone, $1H_2$, Scheme 1.[7r,10a,d,e,13] This ligand has been previously prepared by Nozaki and utilized for $CO_2$/epoxide alternating copolymerizations. Surprisingly, given the relative ease and scale of synthesis, there are no characterized examples of solid-state structures with such a ligand system.[14] We have also prepared a salen, $2H_2$, Scheme 2, as a comparison. $1H_2$ can be prepared on a gram scale from commercially available (or readily synthesizable) materials in a day.

All complexes have been characterized by $^1H$ and $^{13}C\{^1H\}$ NMR spectroscopy, elemental analysis, and single-crystal X-ray diffraction. $Zr(1)(O^iPr)_2$ crystallizes in the monoclinic space group $P2_1/c$ with the isopropoxides *cis* to one another, and the

Received: September 10, 2016
Published: November 8, 2016





DOI: 10.1021/acs.organomet.6b00718
Organometallics 2016, 35, 3837−3843

References for publications:

S. M. Kirk, H. C. Quilter, A. Buchard, L. H. Thomas, G. Kociok-Kohn and M. D. Jones, *Dalton Transactions*, 2016, **45**, 13846-13852.

S. M. Kirk, G. Kociok-Kohn and M. D. Jones, *Organometallics*, 2016, **35**, 3837-3843.

Posters presented at external conferences:

*Novel Schiff Base Aluminium Complexes for the Production of Polylactide.*
13th International Symposium for Advancing the Chemical Sciences (ISACS13), Challenges in Inorganic and Materials Chemistry, Royal Society of Chemistry
Dublin, July 2014

*Novel Initiators for the Production of Polylactide and Copolymers*
Frontiers in Green Materials, Institution of Civil Engineers
London, December 2015

# 1. Introduction

Some of the most commonly used polymers today include polyethylene (PE), polypropylene (PP), polyethylene terephthalate (PET, shown in Figure 1.01) and polystyrene (PS), which are all derived from crude oil and are non-biodegradable. The longevity of these plastics was originally considered a highly beneficial property, but as a result of the huge increase in use of disposable plastic material it became evident that most of these plastics long outlive their purpose – in fact, it is difficult to determine exactly what the life span of plastic is in landfill as crude oil based plastic has only existed for less than a century.[1] Sustainable development was defined in the Brundtland report for the United Nations as "*development that meets the needs of the present without compromising the ability of future generations to meet their own needs*".[2] It is clear that continuing to use only oil-based, non-degradable plastics is unsustainable as crude oil is non-renewable and space in landfill is limited. As a result of this, a drive exists to produce polymers that will degrade without harming the environment, ideally made from materials derived from renewable sources.

In recent years an initiative has been taken by fizzy drinks producers such as Coca-Cola to reduce the impact of PET bottles, by partially producing the plastic from plant material. This project, called PlantBottle™, involves replacing the source of the ethylene glycol from one that is crude oil based to a bio-based source by converting plant matter into ethanol and subsequently ethylene glycol.

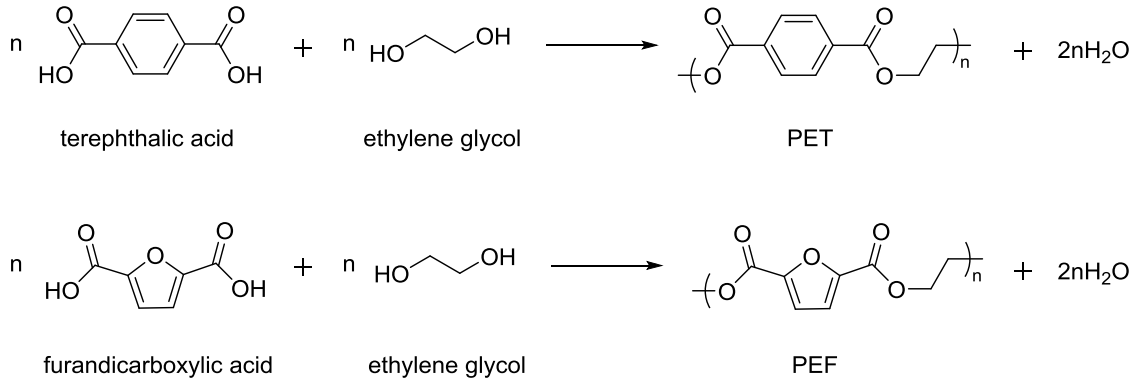


**Figure 1.01: Synthesis of PET and PEF**

Taking this further, a bio-derived polymer polyethylene furanoate (PEF, Figure 1.01) has been developed, which is an alternative to PET that is 100% renewable. In place of terephthalic acid, furandicarboxylic acid (FDCA) is used.[3] This is derived from fructose, which undergoes several dehydration steps to hydroxymethylfurfural which is then oxidised to FDCA.[4] As well as being a

more sustainable polymer, PEF has even been shown to have higher barrier properties than PET due to the decreased flexibility of the furan ring.[5]

## 1.1 Biopolymers

Biopolymers are divided into two categories: polymers that occur naturally, and polymers synthesised from naturally-occurring materials.[6] Examples of polymers in the former category include cellulose, chitosan and polyhydroxybutyrates (PHB).[7,8] This project is based on biopolymers that belong to the latter category. Figure 1.02 shows a few examples of synthetic biopolymers that are produced from cyclic esters including polylactide, which will be the focus of this report.

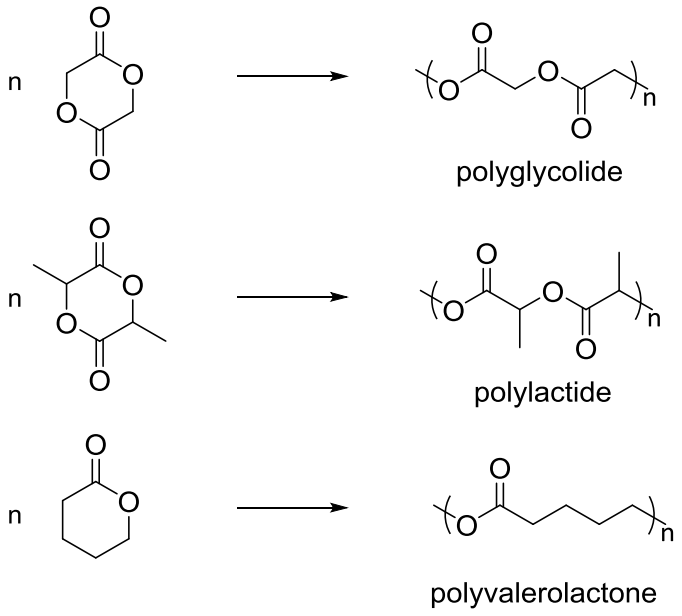


**Figure 1.02: Some synthetic biopolymers made from cyclic esters.**

## 1.2 Polylactide

Polylactide, or polylactic acid (PLA), is a biodegradable, biocompatible polymer produced by the ring-opening polymerisation of lactide, a cyclic dimer of lactic acid, usually initiated with a metal alkoxide (Figure 1.03). Polylactide is a linear aliphatic thermoplastic, whose uses include packaging,[9] biomedical tools such as implants, stents and sutures. It is also a useful material for tissue engineering applications and for drug delivery.[10]

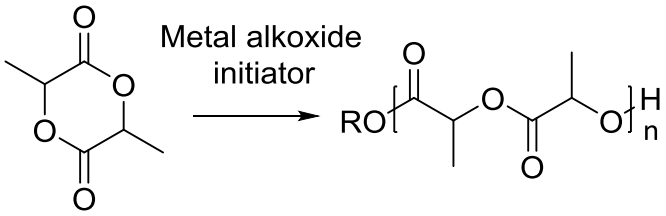


**Figure 1.03: Ring-opening polymerisation of lactide *via* a metal alkoxide initiator**

Figure 1.04 shows the life cycle of polylactide. Lactic acid is produced by the fermentation of plant material which is then converted into lactide (LA), either by dehydration or oligomerisation and subsequent depolymerisation into lactide, the latter of which is a more cost-effective way of producing lactide.[11] This is then polymerised to polylactide and once used for its purpose, can be composted and broken back down into lactic acid and finally, carbon dioxide and water.[12]

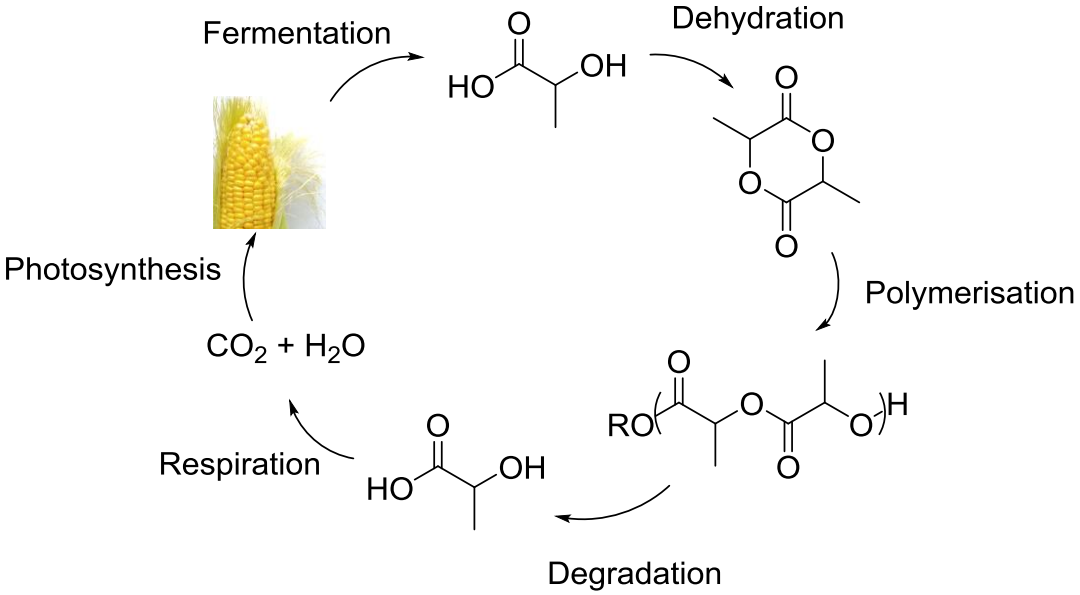


**Figure 1.04: Life cycle of PLA**

A life cycle analysis was carried out comparing a drink bottle made using polylactide, compared to a polyethylene terephthalate (PET) bottle. It was found that polylactide performed well in categories such as fossil fuel consumption and climate change, producing only 17.2 kg of $CO_2$ per 1000 bottles of PLA whereas PET produces 38.2 kg.[13] However, polylactide fails in the land use and eutrophication categories. For example, PLA produces 95.4 g of $PO_4^{3-}$ per 1000 bottles, compared to 38.8 g for 1000 PET bottles. Lactic acid is produced by fermentation of starchy plant material such as corn or potatoes, using bacteria or yeast. To avoid the land use issues, waste streams could be used instead to contribute to lactic acid feedstocks. For example, a study found that waste potato starch can be used for lactic acid production, yielding 52 $gL^{-1}$ from 100 $gL^{-1}$ of

starch.[14] Although this could not provide enough lactic acid to meet demand, it could contribute to feedstocks, reducing the need for crops.

## 1.3 Lactic acid and lactide

L-Lactic acid is a naturally occurring alpha-hydroxy acid. Poly(lactic acid) can be made by the polymerisation of lactic acid (Figure 1.05), however this occurs *via* an equilibrium.[15] Water is produced as a by-product of this reaction, which is undesirable due to extra energy needed to remove it to drive forward the reaction.[16]

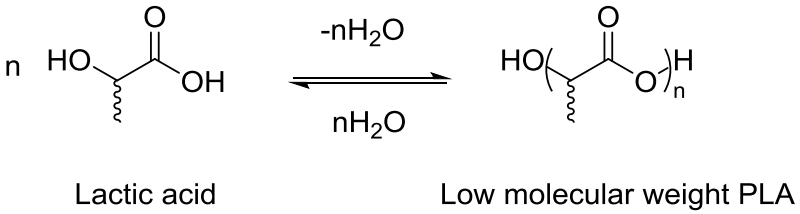


**Figure 1.05: Polycondensation of lactic acid**

To overcome these barriers, lactic acid is converted into lactide. Although this can be achieved by dehydration of lactic acid, industrially this is done by oligomerisation of lactide acid and subsequent depolymerisation into lactide. This can then undergo ring-opening polymerisation, which is thermodynamically favourable due to the release of ring-strain.[17]

Lactide occurs as three stereoisomers: *meso*-lactide, D-lactide and L-lactide (Figure 1.06). The use of these isomers can affect the tacticity of the resulting polymer.

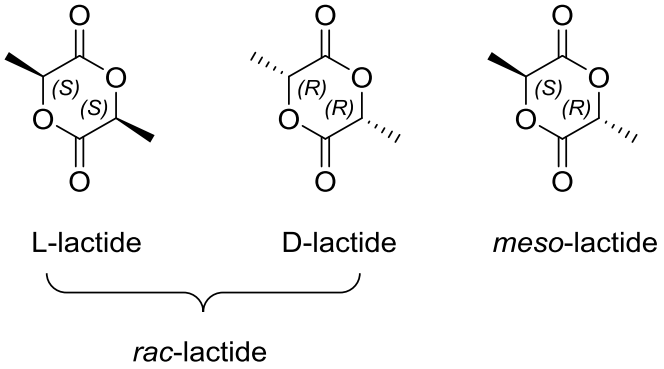


**Figure 1.06: *rac*- and *meso*- lactide**

Figure 1.07 shows all of the possible stereochemical outcomes (also known as 'tacticities') of lactide polymerisation (excluding transesterification), depending on the isomer feed. Isotactic PLA is produced when only one isomer is used, or can be produced using *rac*-lactide if the initiator employed is isoselective. Atactic polylactide is produced using a feed of *rac*-lactide when the initiator has no selectivity for L- or D-lactide, so a random polymer is produced. If

*meso*-lactide is used as the monomer feed, then syndiotactic PLA is produced. Finally, heterotactic PLA can be produced using a feed of *rac*-lactide and a heteroselective initiator. This stereochemistry occurs if the initiator preferentially inserts onto the alternate monomer to the previous insertion. As a result, an alternating chain of D- and L- lactide is produced, known as heterotactic PLA.

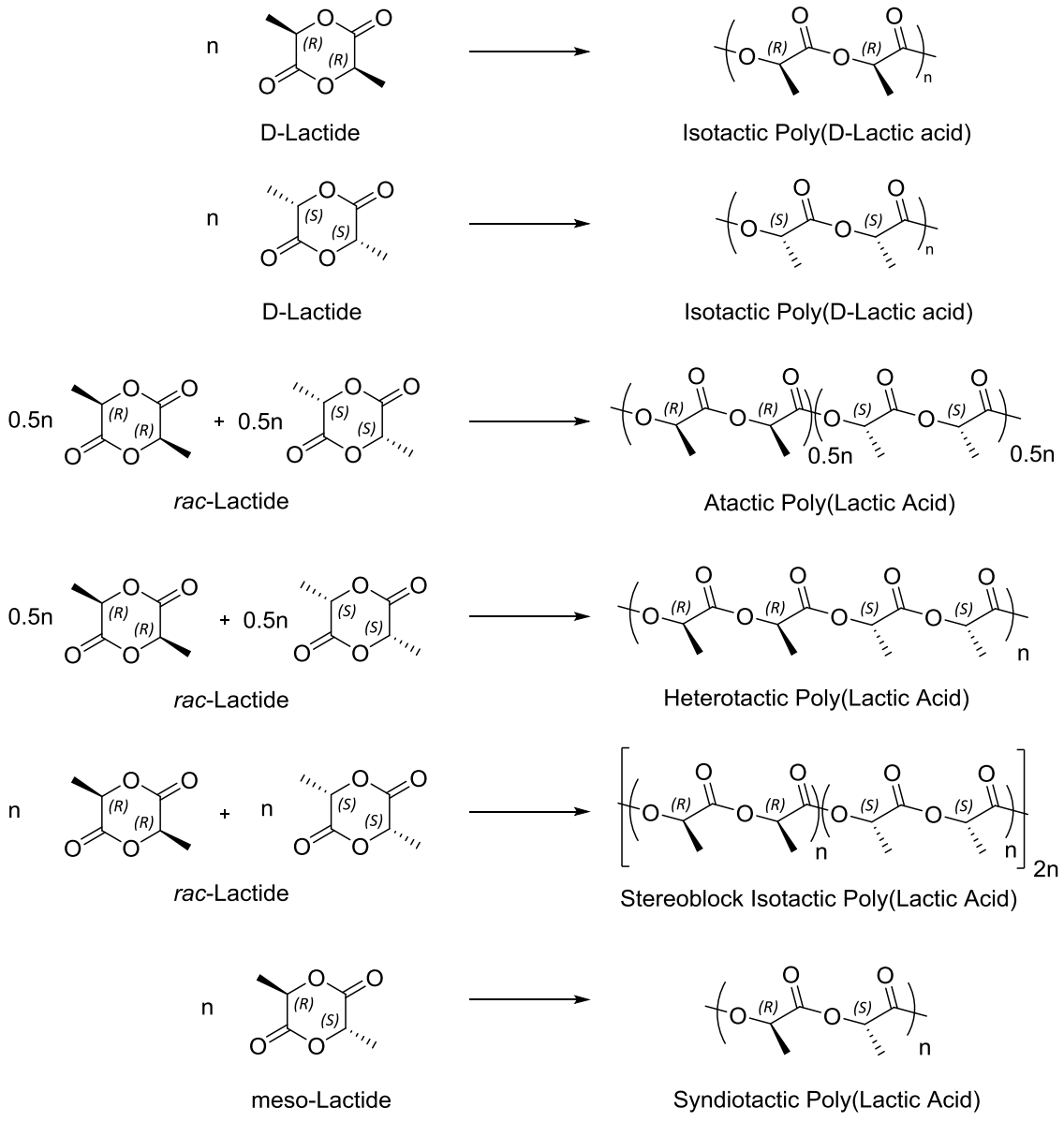


**Figure 1.07: Possible tacticities of PLA currently accessible**

## 1.4 Mechanisms

The ring-opening polymerisation of lactide typically occurs *via* a coordination-insertion mechanism when using a metal alkoxide initiator (Figure 1.08). For the initiation step, the metal centre coordinates with the oxygen of the carbonyl then the alkoxide attacks the carbonyl carbon. The ring-opening occurs by cleavage of the acyl-oxygen bond. The next monomer

coordinates with the metal centre and the polymer chain propagates. This is an example of a 'living' polymerisation, as there is no termination step in this mechanism. Termination can be induced by either cyclisation of the polymer chain (*vide infra*) or quenching of the reaction by addition of alcohol or an alcohol-containing end group. It is also possible to use an organocatalyst for this reaction,[18-20] however this will not be covered as the focus of this work is inorganic catalysis. The kinetics of the reaction are important for controlling chain growth: if $k_{initiation} >> k_{propagation}$ then the molecular weight distribution will be narrow.

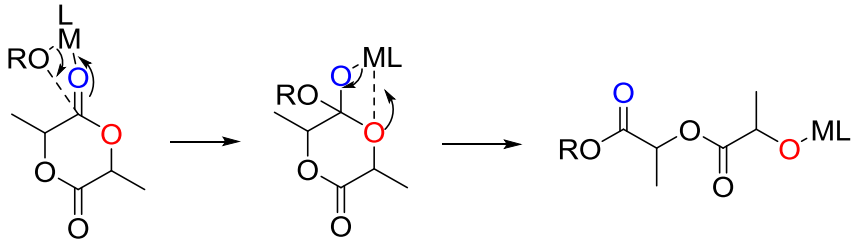


**Figure 1.08: Coordination insertion mechanism of the ring-opening polymerisation of lactide**

If charged initiators are employed, the reaction occurs *via* an ionic mechanism, either anionic (Figure 1.09) or cationic.[21, 22] Anionic ROP is initiated by nucleophilic attack on the carbonyl resulting in acyl bond cleavage.[23] The resulting alkoxide ion at the end of the chain then undergoes further nucleophilic attack.

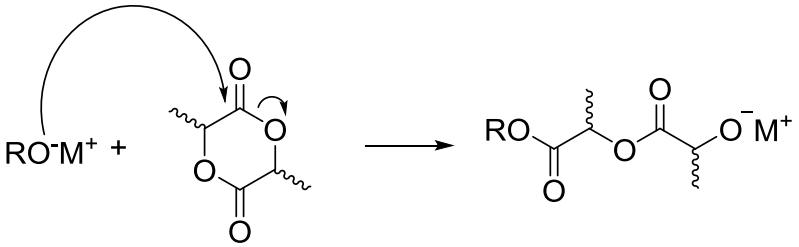


**Figure 1.09: Anionic mechanism for ROP of lactide**

Transesterification is a side-reaction that can occur between polylactide chains in a intermolecular chain transfer (Figure 1.10). This is undesirable as polymers that have undergone transesterification exhibit larger molecular weight distributions, which manifests itself in an increase in the polydispersity index.[24] This also results in a loss of stereocontrol in the polymer.

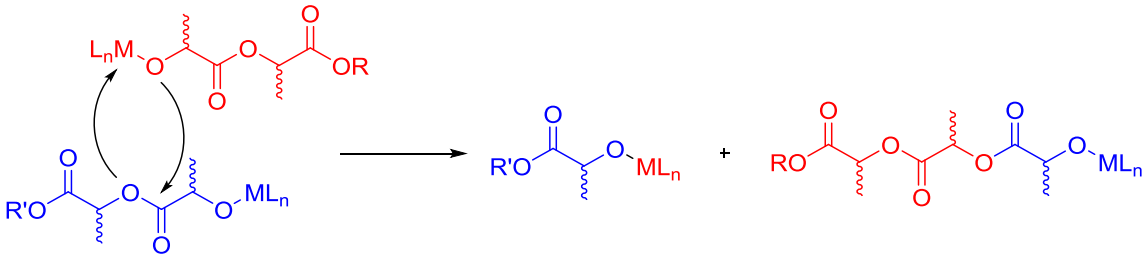

**Figure 1.10: Intermolecular transesterification reaction**

Intramolecular transesterification occurs when the metal 'backbites' into the same polymer chain that it is initiating, resulting in a macrocycle (Figure 1.11).

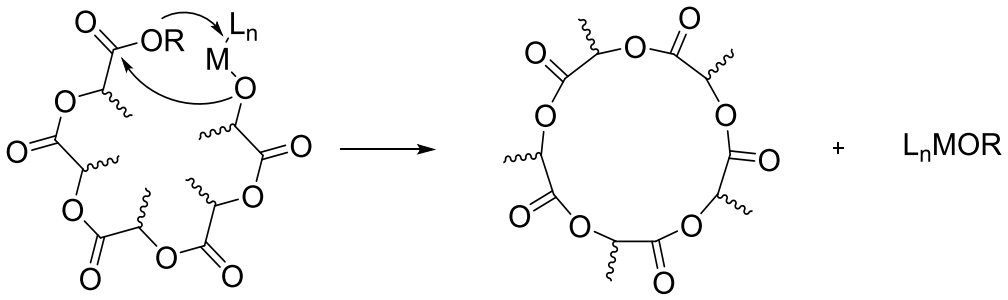

**Figure 1.11: Intramolecular transesterification reaction**

Where a living polymerisation can be quenched on addition of an alcohol, 'immortal' polymerisations cannot.[25] In this polymerisation type, addition of alcohol will simply cause the polymer chains to rearrange, with the number of chains proportional to the amount of alcohol added.[26] In the example shown in Figure 1.12, four equivalents of alcohol are added to the polymerisation, resulting in 4 polymer chains per initiator, and an active initiator that is still able to polymerise.

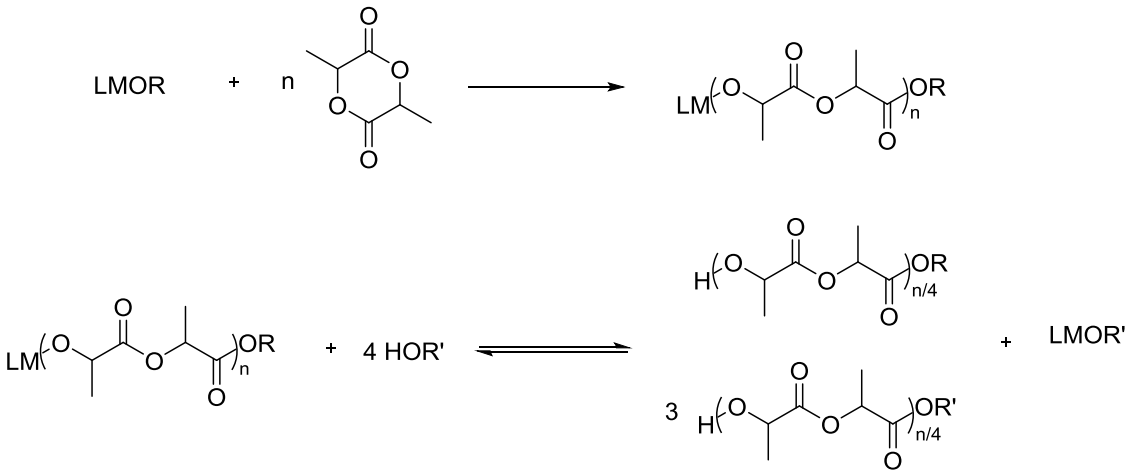

**Figure 1.12: Immortal polymerisation**

Polylactide degrades by hydrolysis of the ester linkages (Figure 1.13). This process is autocatalytic once it has begun, as the carboxylic acid end groups catalyse the ester hydrolysis.[27] For use in medical implants, this is a useful trait, as the device will degrade after its function has been performed, thus no surgery would be require to remove it after use. The eventual degradation product, lactic acid, is metabolised by the body.[28]

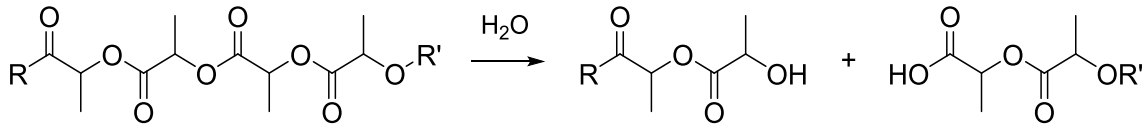


**Figure 1.13: Hydrolytic degradation of polylactide**

Polylactide can biodegrade under composting conditions.[29-31] A study of PLLA degradation in an anaerobic solid state digester, reaching a maximum temperature of 70 °C, found that 99 % mineralisation (by $CO_2$ measurement) was achieved after 40 days.[32] It has also been shown that polylactide degrades under gamma and electron beam radiation, by random chain scission.[33, 34] This change in molecular weight needs to be taken into account when using polylactide for biomedical applications if the polymer is to be sterilised by radiation methods.

## 1.5 Polymer characterisation

### 1.5.1. Gel Permeation Chromatography

Gel permeation chromatography (GPC) is a technique used to determine the molecular weights of polymers. This is a type of size exclusion chromatography where the polymer chains interact with pores in the column. The largest chains are forced to take the shortest path and thus elute first, followed by increasingly smaller polymer chains. For each peak on the chromatograph, the molecular weight and polydispersity is measured. Figure 1.14 shows a typical GPC trace.

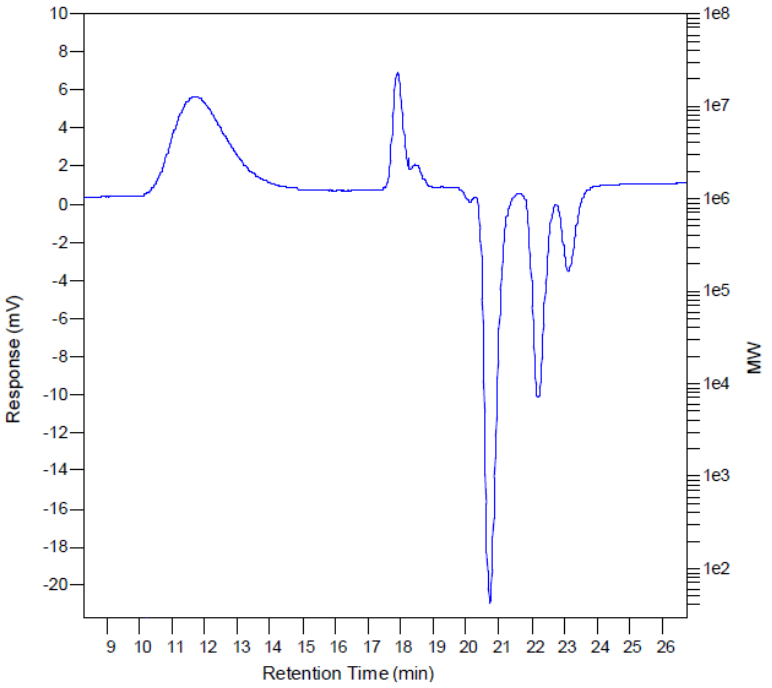


**Figure 1.14: A typical GPC trace for PLA**

Various detection methods are possible, the most commonly used being refractive index (RI). This method compares the measured RI of the sample to external polymer standards, for example, polystyrene. If the polymer has a different viscosity and hydrodynamic radius to the polymer standard, a correction factor will need to be applied to account for this difference. For polylactide against a polystyrene standard, the frequently used correction factor is 0.58.[35] Other detection methods available include viscometry and light scattering. For single detection viscometry measurements, the intrinsic viscosity and concentration of the polymer sample is measured and compared to a calibrant.[36, 37] For light scattering, light is bounced off of the sample at an angle (or multiple angles) in order to determine the molecule's size, which can be used to calculate the weight average molecular weight.[38] The three methods above can be combined in a triple detection instrument, to give better accuracy of the molecular weights.

The polydispersity index (PDI) is determined as a ratio of molecular weights (equation 1.01). A perfectly monodisperse sample would have a PDI of 1. A narrow molecular weight range indicates a 'living and controlled' polymerisation, which does not undergo high levels of transesterification and yields high molecular weight polymers.[39]

$$PDI = \frac{M_w}{M_n}$$

**Equation 1.01**

### 1.5.2 MALDI-Tof Mass Spectrometry

Matrix-assisted laser desorption ionisation time-of-flight (MALDI-ToF) is a mass spectrometry technique. It uses a soft ionisation technique and can be used for large molecules such as polymers and proteins.[40, 41] The analyte is mixed with a matrix compound in solution, such as 4-hydroxycinnamic acid or 2,5-dihydroxybenzoic acid.[42] The matrix is usually acidic, to act as a proton source to allow the analyte to ionise, and also UV active in order to absorb laser irradiation efficiently.[43] The use of non-acidic matrices such as sodium acetate can also facilitate ionisation. This technique is useful for determining the end-group of the polymer chain and the molecular weight.[44] In the case of polylactide and other polyesters, it can also determine if the polymer has transesterified. This is determined by the spacing between the peaks – for PLA it should be 144 $gmol^{-1}$, for each repeating lactide unit. However, if transesterification has occurred, the spacing would be 72 $gmol^{-1}$, for half a lactide unit (or one lactic acid unit). Figure 1.15 shows a typical MALDI-ToF spectrum for a transesterified polylactide sample.

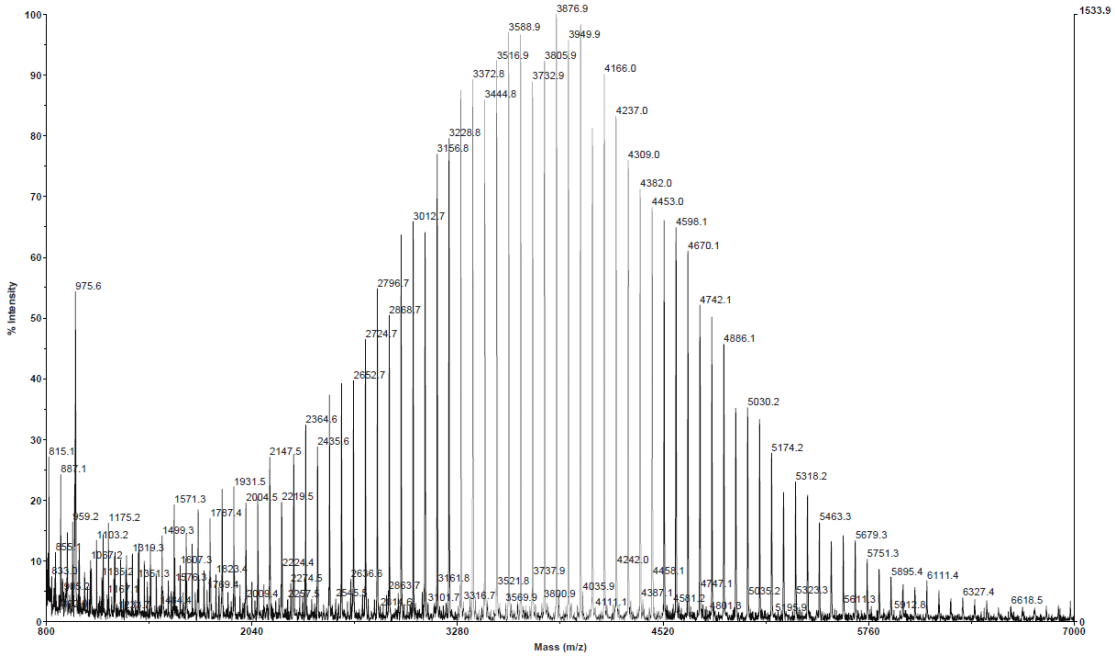


**Figure 1.15: Example spectrum of polylactide analysed *via* MALDI-ToF mass spectrometry.[45] This polymer has transesterified, as shown by the spacing of 72 $gmol^{-1}$**

Figure 1.16 shows a theoretical MALDI-ToF spectrum for a polymer containing a benzyl alcohol end group. This shows how this technique can be used for end-group analysis.

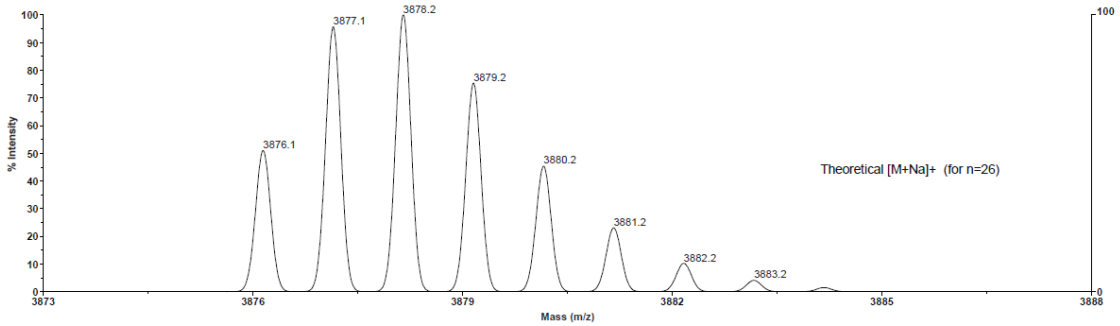


**Figure 1.16: Theoretical MALDI-ToF mass spectrum for the benzyl end group of polylactide**

### 1.5.3 DSC

Differential scanning calorimetry (DSC) is a technique where the thermal properties of a material are analysed. This is carried out by heating a sample in a pan and comparing that sample to a blank reference which is heated at the same rate. During the analysis several events may occur at different temperatures, including glass transition ($T_g$), melting ($T_m$) and crystallisation ($T_c$). These can be measured as the heat capacity of the material will change at these temperatures, causing a spike or trough to appear on the trace.

### 1.5.4 NMR spectroscopy

Nuclear magnetic resonance (NMR) spectroscopy is an invaluable tool in polymer characterisation. The simplest method of calculating the conversion of monomer into polymer taking an NMR sample of the crude polymerisation mixture. Figure 1.17 shows the proton NMR of a crude polymerisation, zoomed in on the methine proton region between 4.9 and 5.3 ppm. The monomer and polymer resonances are clearly distinguishable, conversion of lactide into PLA can be calculated by relative integration of these two resonances.

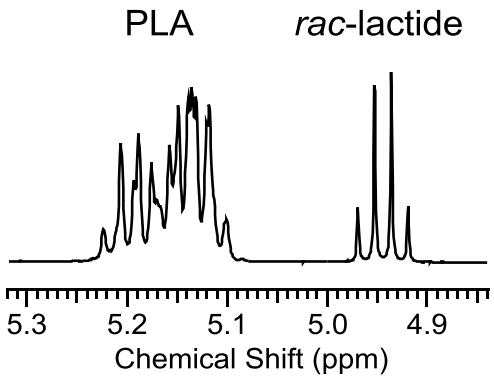


**Figure 1.17: $^1$H NMR spectrum of crude polymerisation mixture, zoomed into methine proton region**

The stereochemistry of the polymer can be determined by proton homonuclear decoupled NMR spectroscopy.[46] The methyl region of the spectrum is irradiated (~1.6 ppm), resulting in five

resonances in the methine region. Groups of four repeating units, known as tetrads, have the arrangements sis, iss, ssi, iii and isi, where s denotes a syndiotactic link and i denotes an isotactic link. Relative integrations of these resonances can be used to calculate a probability relating to the tacticity of the polymer.[47]

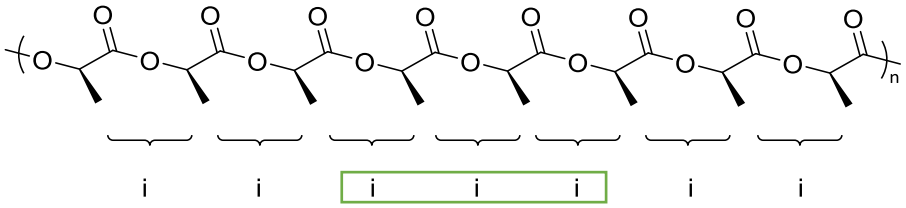


**Figure 1.18: Isotactic PLA**

Purely isotactic PLA (Figure 1.18) has only isotactic linkages, resulting in one resonance in the methine region of the homonuclear decoupled NMR (Figure 1.19).[48]

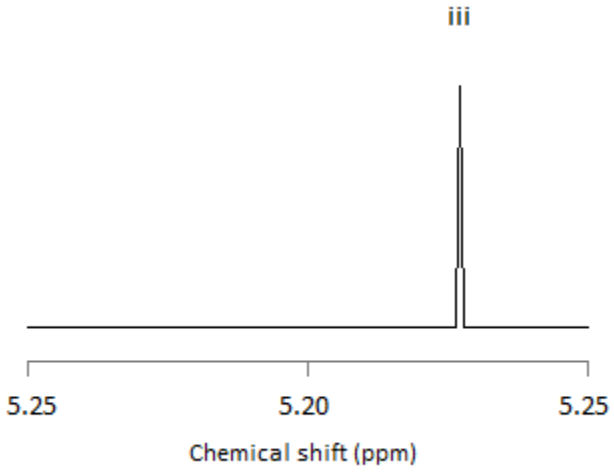


**Figure 1.19: Diagram of homonuclear decoupled $^{1}$H NMR spectrum of isotactic PLA methine region**

Heterotactic PLA (Figure 1.20) has two possible tetrad arrangements, isi and sis. This results in two resonances in the methine region of the NMR spectrum, at a 1:1 ratio (Figure 1.21).

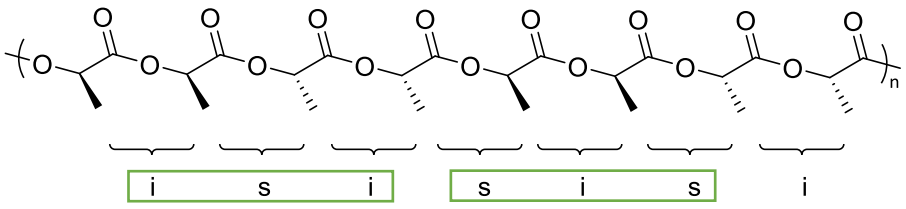


**Figure 1.20: Heterotactic PLA**

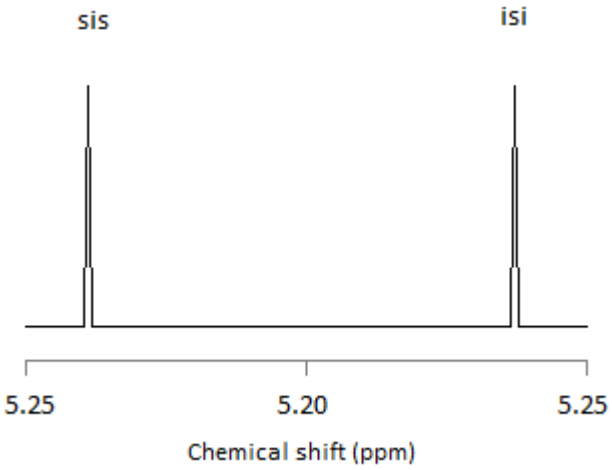


**Figure 1.21: Diagram of NMR spectrum of heterotactic PLA methine region**

Atactic PLA consists of random linkages (Figure 1.22). According to Bernoullian statistics, the five tetrads appear in a 1:1:1:3:2 ratio (Figure 1.23).

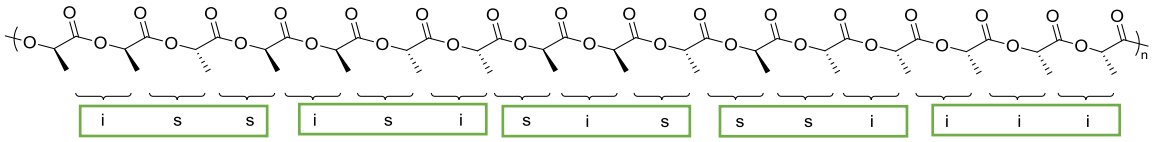


**Figure 1.22: Atactic PLA**

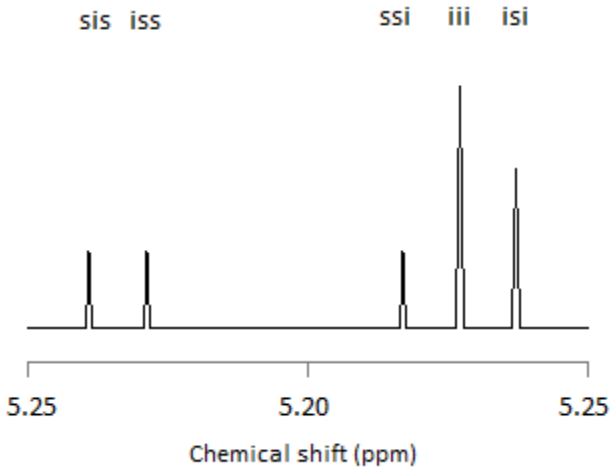


**Figure 1.23: Diagram of NMR spectrum of atactic PLA methine region**

The tacticity of the polymer is defined by the value $P_r$ which denotes the probability of racemic enchainment, i.e. the probability of the an alternate enantiomer of lactide to coordinate with the initiator in a racemic mix. This is calculated using equation 1.02, where [sis] is the relative integration of the sis resonance in the methine region of polylactide.[49] These values are determined by Bernoullian statistics (Table 1.01, page ).[47]

Equation 1.02 is derived from the data in Table 1.01. For entirely isotactic polylactide the $P_r = 0$, for atactic polylactide $P_r = 0.5$ as it is equally likely that L- or D- lactide could coordinate. For entirely heterotactic polylactide, $P_r = 1$. Alternatively, $P_m$ (probability of *meso* enchainment) is used in some publications. In this case, $P_m = 0$ is heterotactic PLA and $P_m = 1$ is isotactic.

$$P_r = \sqrt{2[sis]}$$

**Equation 1.02**

**Table 1.01: Probabilities of different tetrads occurring using Bernoullian statistics**[47]

| | **Probabilities based on Bernoullian statistics** | |
|---|---|---|
| **Tetrad** | *Rac*-lactide | *Meso*-lactide |
| **[iii]** | $P_m^2 + P_rP_m/2$ | 0 |
| **[iis]** | $P_rP_m/2$ | 0 |
| **[sii]** | $P_rP_m/2$ | 0 |
| **[sis]** | $P_r^2/2$ | $(P_m^2 + P_rP_m)/2$ |
| **[sss]** | 0 | $(P_r^2 + P_rP_m)/2$ |
| **[ssi]** | 0 | $P_rP_m/2$ |
| **[iss]** | 0 | $P_rP_m/2$ |
| **[isi]** | $(P_r^2 + P_rP_m)/2$ | $P_m^2/2$ |

The tacticity of the polymer is highly dependent on the initiator used. Typically, the stereochemistry is determined by one of two mechanisms: chain end control or enantiomorphic site control. In a chain end control mechanism, the growing chain dictates the stereochemistry of the subsequent coordinated monomer. For example, with a heteroselective initiator, if L-lactide was the most recently added monomer to the chain, the next monomer to be added would be D-lactide. For enantiomorphic site control the structure of the initiator, in particular any chirality, decides the stereochemical outcome of the polymer.

## 1.6 Other Biopolymers

### 1.6.1 Polycaprolactone

Polycaprolactone (PCL, Figure 1.24) is a semi-crystalline, hydrophobic polymer with a low melting point (up to 64 °C), a glass transition temperature of -60 °C and it is amenable to blending.[50, 51] Unlike PLA, whose eventual degradation product is lactic acid which is utilised by

the body, the degradation products of PCL cannot be processed or metabolised by the human body.[52] However, PCL is biocompatible (i.e. non-toxic) and can undergo hydrolytic degradation *in vivo*.

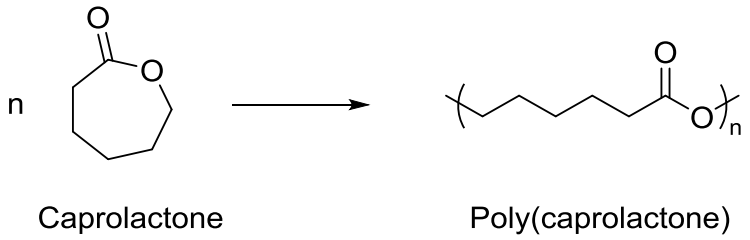


**Figure 1.24: Polymerisation of ε-caprolactone**

### 1.6.2 Polybutyrolactone

Polybutyrolactone (PBL), also known as polyhydroxybutyrate, is a naturally occurring polymer that is found in a variety of bacteria.[53] As well as being naturally produced in these organisms, it can be produced by the ring-opening polymerisation of β-butyrolactone (Figure 1.25). Different tacticities have been observed for this polymer which affect the properties of the polymer, for example syndiotactic polybutyrolactone has a melting point of 140-150 °C, lower than isotactic PBL (approx. 180 °C).[54] As with other polylactones, it is biodegradable and can be used in medical applications.[55]

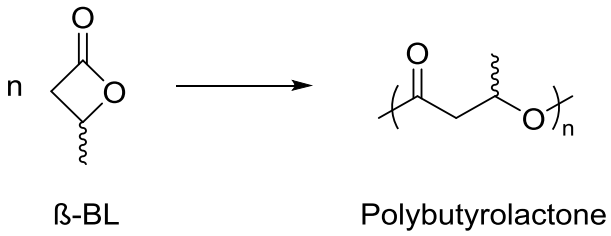


**Figure 1.25: Polymerisation of β-butyrolactone**

### 1.6.3 Polyglycolide

Polyglycolide (PGA) is a polymer produced *via* the ring-opening polymerisation of glycolide, a monomer very similar to lactide, but without the methyl groups on the ring (Figure 1.26). As a result of this no tacticity can be imparted onto the polymer. Polyglycolide is less hydrophobic than polylactide and as such, degrades at a faster rate.[56] PGA is hydrolysed to glycolic acid which then autocatalyses the hydrolysis of the polymer.[57]

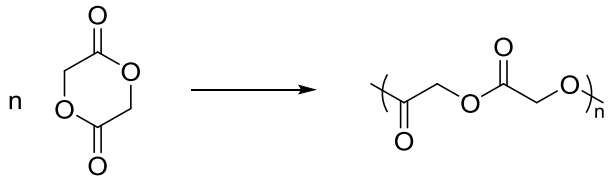

**Figure 1.26: Polymerisation of glycolide**

## 1.7 Copolymerisation

Lactide can be polymerised in the presence of other monomers to form copolymers. The most extensively researched lactide copolymers so far include poly(lactide-co-glycolide) and poly(lactide-co-caprolactone), the latter of which is depicted in Figure 1.27.[58, 59] With all cyclic esters, the more strained the ring, the more facile the ring-opening polymerisation.[60]

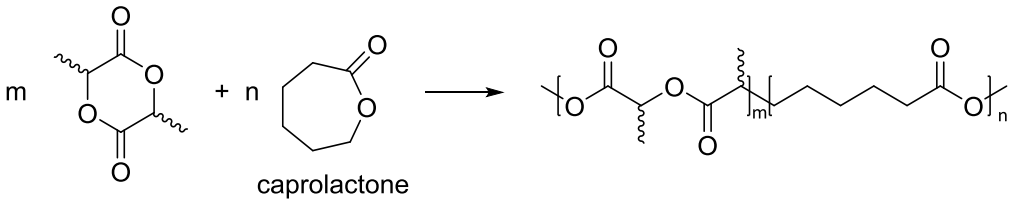


**Figure 1.27: Copolymerisation reaction of *rac*-lactide and ε-caprolactone**

As with homopolymers, there are different possible structural outcomes for copolymerisation, as demonstrated in Figure 1.28. In a one-pot synthesis, a block copolymer occurs if the catalyst is selective or more active for the polymerisation of one monomer over the other (site control), or when the subsequent addition of the same monomer is favoured (chain end control). A block copolymer can also be formed by sequential addition of monomers. For an alternating copolymer the other monomer is preferentially inserted - this is the natural outcome when homopolymerisation is not possible, e.g. for the polymerisation of ethylene glycol and terephthalic acid (see Figure 1.01). Random copolymerisation occurs when neither monomer is favoured and is equally likely to be incorporated into the copolymer.

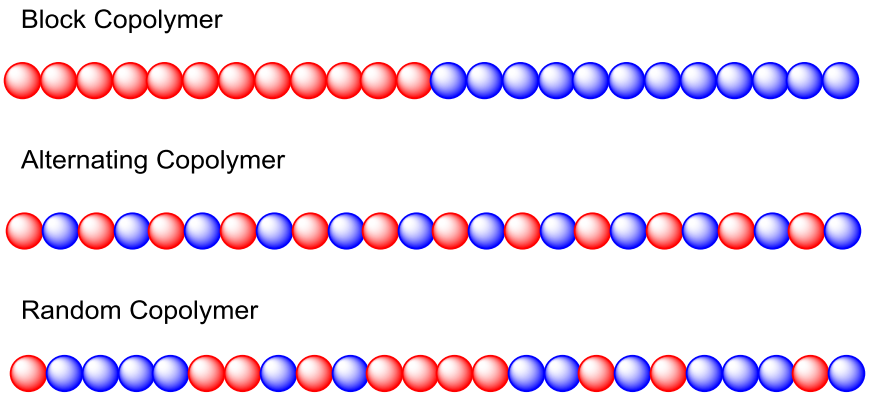


**Figure 1.28: Different possible copolymerisation outcomes, with the coloured spheres representing two different monomers**

If we call one monomer 'A' and the other 'B', the rate of addition of one monomer to another can be described using the rate constants ($k_{XX}$) in Equation 1.3.

$$A + A \xrightarrow{k_{AA}} AA$$

$$A + B \xrightarrow{k_{AB}} AB$$

$$B + A \xrightarrow{k_{BA}} BA$$

$$B + B \xrightarrow{k_{BB}} BB$$

**Equation 1.3**

Using the steady state approximation, an equation can be derived from the propagation rate laws, known as the Mayo-Lewis Equation (Equation 1.4).[61]

$$\frac{d[A]}{d[B]} = \frac{[A](r_1[A] + [B])}{[B]([A] + r_2[B])}$$

**Equation 1.4**

In this equation, the reactivity ratios, $r_1$ and $r_2$ are defined as:

$$r_1 = \frac{k_{AA}}{k_{AB}}$$

$$r_2 = \frac{k_{BB}}{k_{BA}}$$

These reactivity ratios refer to the likelihood of one monomer to insert onto the propagating polymer chain, with the other monomer at the growing chain end. For a block copolymer, $r_1 = r_2 > 1$, as both monomers show a preference for inserting onto a growing chain of the same monomer. For an entirely alternating copolymer $r_1 = r_2 = 0$, i.e. insertion into the same monomer

is impossible. As the reactivity ratio values for a copolymerisation approach zero, the copolymer is considered alternating. For a completely random copolymer $r_1 = r_2 = 1$, i.e. there is equal likelihood of either monomer inserting onto the growing polymer chain.[62]

## 1.8 Biopolymers for tissue engineering

Tissue engineering is a rapidly expanding, interdisciplinary field that has been defined as "*the development of biological substitutes that restore, maintain, or improve tissue function or a whole organ*".[63] The underlying principle of this is to remove cells from a subject (ideally the patient), culture those cells and attach them to a support, known as a scaffold.[64] Many different materials have been assessed for different tissue engineering applications, and each application requires materials with specialised properties. For example, it has been shown that the stiffness of a material can direct the differentiation of mesenchymal stem cells. Soft matrices encourage formation of nerve cells, whereas very stiff materials encourage osteocyte (bone cell) formation.[65]

Biopolymers are highly useful as tissue engineering materials, due to their processability – they can be easily moulded into the variety of shapes that may be needed for a specialised task. Whilst polylactide is an attractive material due to its biodegradability and biocompatibility, some of its other properties mean that it is not an ideal candidate. Once placed in the body, polylactide will degrade hydrolytically, however this occurs slowly due to the hydrophobicity of the polymer.[66]

To overcome some of the issues mentioned above, copolymers of polylactide are used for tissue engineering, in particular, poly(lactide-co-glycolide). It has been shown that varying the proportions of lactide and glycolide can alter the degradability, with higher ratios of glycolide leading to faster degradation. It was reported that 85:15 LA:GA degrades in 5-6 months, whereas 50:50 LA:GA degrades in 1-2 months.[67] This is important as the rate of degradation can be controlled, making it possible to tune the polymer to a unique specification.

The advantage of synthetic biopolymers is that the polymer chains can be modified to incorporate different compounds, including antibiotics, growth factors, anti-cancer treatments, etc. In one example, the anti-cancer drug Paclitaxel has been built into a modified PLA chain, which has a release rate of 50% after 22 hours.[68]

## 1.9 Initiators

Research into initiators for the ring-opening polymerisation is extensive and ranges from use of metal complexes to enzymes and metal-free organic initiators.[69] In the case of metal complexes,

a huge range of metal centres have been used for ROP of lactide, including tin, lithium potassium, calcium, zinc, magnesium, yttrium, aluminium, titanium, zirconium, hafnium, iron, indium and lanthanides.[70] The ring-opening polymerisation of lactide can be easily initiated, the difficulty lies in achieving molecular weight and stereocontrol.

Tin(II) 2-ethylhexanoate, or tin octanoate, $Sn(Oct)_2$, is the most commonly used initiator for the production of polylactide in industry (Figure 1.29) as it is inexpensive, highly active and can produce high molecular weight PLA in solvent free conditions.

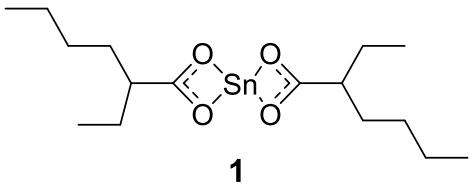


**1**

**Figure 1.29: Tin octanoate**

Despite these favourable characteristics $Sn(Oct)_2$ has some drawbacks, most notably a lack of stereoselectivity. Tin compounds are often toxic, which is of particular concern when using polymers for biomedical applications.[71] Although tin octanoate is FDA approved for use in food packaging, it is undesirable for use in tissue engineering where cells are cultured on the surface of the material.[72] For such applications, tin octanoate should be removed from the polymer before use. The mechanism of tin octanoate is suspected to proceed by the formation of a tin alkoxide species, generated by addition of alcohol, which can then undergo coordination-insertion.

Due to the large and varied literature available on the ROP of lactide, the focus henceforth will be on aluminium, zinc and group 4 initiators, as these are the metal centres employed in this project.

### 1.9.1 Zinc and Group 2 initiators

Zinc and Group 2 metals are appealing for use in polylactide initiators as they are non-toxic and cheaply available, thus making it suitable for biomedical applications. A variety of such initiators have been assessed for the ROP of lactide, a number of which will be discussed below. A summary of the data can be found in Table 1.02. One of the more well-known ligand types used with zinc and magnesium are β-diketiminates (BDI). Coates *et al* has used Zn(II) and Mg(II) BDI alkoxide initiators (Figure 1.30) to produce high selectivities from the ROP of *rac*-lactide in dichloromethane (DCM) at 20 °C.[73] Structure **3** shows the highest heterotactic bias, with high molecular weights and narrow polydispersities, indicating good molecular weight control. After

20 minutes at 20 °C, **3** produced PLA with a $P_r$ of 0.90, and after 120 minutes at 0 °C the $P_r$ was 0.94. Interestingly, this selectivity was not seen in a magnesium analogue **2**, which produced atactic PLA in two minutes.[73]

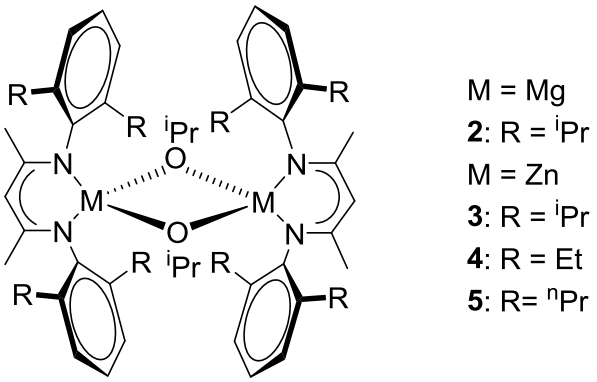


**Figure 1.30: Single site β-diketiminate zinc complexes[73]**

A tridentate phenolate ligand complexed with zinc was developed by Tolman *et al*.[74] It was found that this formed a dimer on addition of ethanol (Figure 1.31). Structure **7** was found to exist predominantly as a monomer in solution at room temperature. It is highly active, producing high molecular weight polymer at room temperature in just five minutes.[74] However the molecular weights obtained were lower than expected, possibly due to impurities causing chain-transfer, which also accounts for the high PDI values (1.34-1.42).

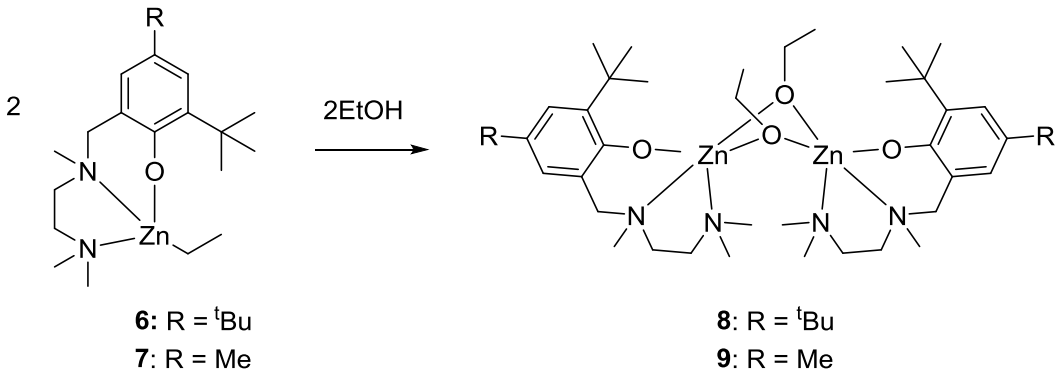


**Figure 1.31: Monomeric and dimeric zinc complexes[74]**

Considerable work has been carried out by Herres-Pawlis *et al.* on the use of bis(guanidine) ligands complexed with zinc for the ROP of lactide (Figure 1.32).[75] These initiators are air stable at ambient temperature, although structure **11** is hygroscopic. Melt polymerisation data was gathered for these complexes and structure **10** produced a high yield (82 %) and high molecular weight (58,800 $gmol^{-1}$) after 24 hours. Structure **11** was not as effective, with 63 % yield after 24 hours and lower molecular weight, which have been attributed to transesterification.

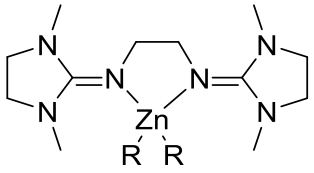


**10:** R = Cl
**11**: R = $OOCH_3$

**Figure 1.32: Zinc guanidine complex[75]**

More recently, high isotactic stereoselectivity has been achieved by employing chiral zinc initiators (Figure 1.33). Each of the structures **12**-**15** obtained high conversion (93-98 %) of lactide after 30 minutes at 50 °C, thus showing high activity.[76] Structure **15** achieved the highest isotacticity, $P_m$ = 0.86 (i.e. $P_r$ = 0.14). By lowering the temperature to 23 °C for 44 hours, a $P_m$ of 0.91 was achieved, the highest observed for any zinc system to date. This is proposed to be caused by enantiomorphic site control, due to the chirality of the ligand.

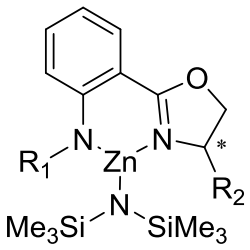


$R_1$ = 

$R_2$ = (S)$^i$Pr: **12**
$R_2$ = (R)Ph: **13**
$R_2$ = (S)$^s$Bu: **14**

$R_1$ = 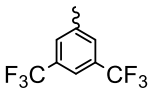


$R_2$ = (R)Ph: **15**

**Figure 1.33: Chiral zinc initiators[76]**

Some recent work by Cui *et al.* has shown that zwitterionic achiral zinc complexes (Figure 1.34) can also afford isoselectivity. Compound **16** gives high conversions after 8 hours at 30 °C in toluene, with $P_m$ values of up to 0.85 ($P_r$ = 0.15) and high molecular weights.[77] In THF, isotacticity drops slightly ($P_m$ = 0.74). Compounds **17**-**19** also show isotactic bias in THF, with $P_m$ values ranging from 0.69 to 0.73. Kinetic studies of these compounds showed that the complexes exhibit a chain-end control mechanism, where the isoselectivity is induced by the previously inserted lactyl unit.

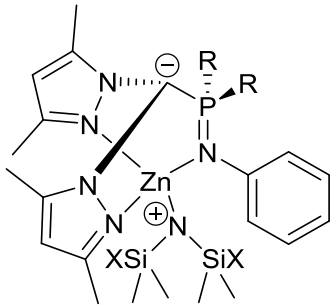


**16**: R = Ph, X = H
**17**: R = Ph, X = Me
**18**: R = Cy, X = H
**19**: R = Cy, X = Me

**Figure 1.34: Achiral zwitterionic zinc complex[77]**

Peng and coworkers developed zinc initiators (Figure 1.35) which formed dinuclear complexes on addition of benzyl alcohol. It was found that upon heating (>30 °C), the complex dissociated

into a monomeric species.[78] These complexes were employed for the ROP of L- and *rac*- lactide, ε-caprolactone and for the block copolymerisation of ε-caprolactone and either β-butyrolactone or valerolactone by sequential addition. For L- and *rac*- lactide, high conversions were achieved using **20** and **21** within 30 minutes at 30 °C in DCM. No selectivity was observed for the ROP of *rac*-lactide.

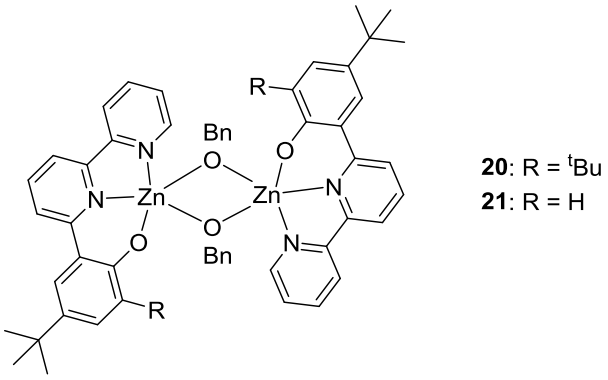


**Figure 1.35: Dinuclear zinc complexes prepared by Peng *et al.*[78]**

Chisholm *et al.* synthesised two BDI ligands and complexed them with butyl magnesium in THF (shown in Figure 1.36). In each case, a THF adduct formed.[79] These were utilised for the ROP of lactide at 25 °C in DCM or THF and were found to be highly active, both producing PLA from *rac*-lactide within 90 seconds. In DCM at 100:1 loading, the $P_r$ value of the polymer produced by **22** was 0.79 and PLA produced by **23** had a $P_r$ of 0.56. When carrying out the polymerisations in THF, the selectivity was greatly enhanced, with $P_r$ = 0.96 for **22** and $P_r$ = 0.94 for **23**, indicating that using THF as a coordinating solvent switches the selectivity towards highly heterotactic PLA. The complex **23** was also used for the ROP of ε-caprolactone, and found to be faster than for the ROP of *rac*-lactide, with $k_{app}$ = 0.42 $s^{-1}$ for *rac*-lactide and $k_{app}$ = 4.08 $s^{-1}$ for ε-caprolactone in DCM.

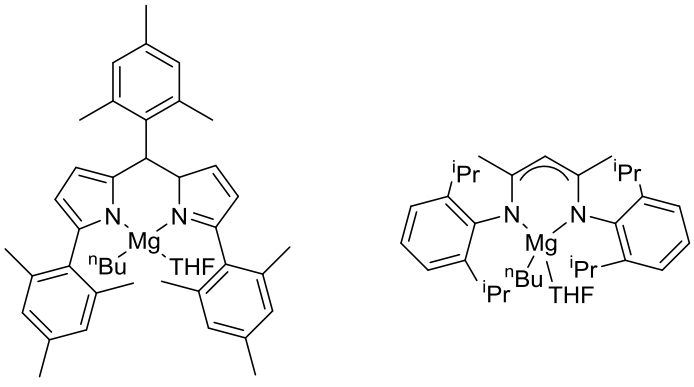


**22** **23**

**Figure 1.36: Magnesium complexes as reported by Chisholm *et al.*[79]**

Gibson and coworkers developed a potentially tridentate BDI ligand featuring a methoxy group, and complexed this with magnesium and zinc.[80] It was found that the ligand formed a tridentate

complex with magnesium (**24**) but the methoxy group did not bind to the zinc metal centre (**25**). When utilised for the ROP of *rac*-lactide, **24** achieved 81 % conversion within 8 minutes at 100:1 loading, however with a broad PDI of 1.78. The zinc complex **25** exhibited better molecular weight control at 100:1 loading, reaching 90 % conversion in 30 minutes with PDI = 1.15. No significant stereoselectivity was observed for either complexes.

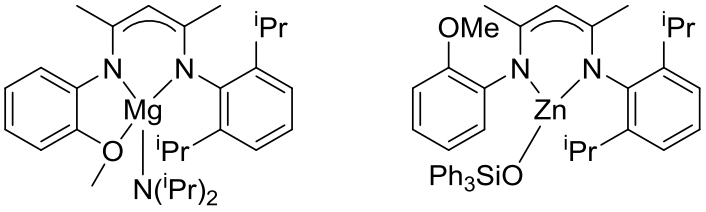


**24** **25**

**Figure 1.37: Magnesium and zinc BDI catalyst reported by Gibson *et al*.[80]**

Calcium and zinc complexes were synthesised by Darensbourg *et al*. using tridentate Schiff base ligands (Figure 1.38) and employed them for the ROP of L-lactide.[81] Complex **26** was found to have the highest turn-over frequency (TOF) of the three complexes, reaching 80 % conversion in 15 minutes in the melt at 110 °C, whereas **27** achieved 59 % conversion in the same time. It was found that **26** had good molecular weight control in the melt even at high initiator loadings, with PDI = 1.04 at 700:1 monomer to initiator loading. The zinc initiator **28** was considerably slower, yielding only 16 % conversion under the same conditions. Initiator **26** was also utilised for the ROP of *rac*-lactide, and was found to yield moderately heterotactic PLA ($P_r$ = 0.73). The complex was also found to successfully copolymerise L-lactide and trimethylene carbonate, producing a block copolymer with a $T_m$ of 150 °C.

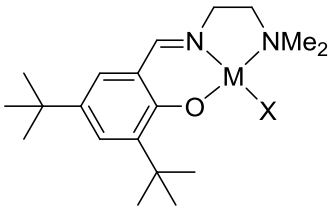


**26** M = Ca, X = $N(SiMe_3)_2$
**27** M = Ca, X = OMe
**28** M = Zn, X = $N(SiMe_3)_2$

**Figure 1.38: Calcium and zinc Schiff base complexes synthesised by Darensbourg *et al*.[81]**

Table 1.02 on page 24 shows polymerisation data for the ROP of *rac*-lactide using the zinc and group 2 initiators discussed above.

**Table 1.02: Summary comparing the zinc initiators listed above for the ROP of *rac*-lactide**

| Initiator | Conditions | Time (h) | LA:I | Conversion (%) | $M_n$ (Calc) ($gmol^{-1}$) | $M_n$ (Obs) ($gmol^{-1}$) | PDI | $P_r$ | Ref |
|---|---|---|---|---|---|---|---|---|---|
| **2** | DCM, 20 °C | 0.03 | 200:1 | 97 | | 29,700 | 1.29 | n.d. | 74 |
| **3** | DCM, 20 °C | 0.33 | 200:1 | 97 | | 37,900 | 1.10 | 0.90 | 74 |
| **4** | DCM, 20 °C | 8 | 200:1 | 97 | | 42,500 | 1.09 | 0.79 | 74 |
| **5** | DCM, 20 °C | 19 | 200:1 | 97 | | 35,800 | 1.18 | 0.76 | 74 |
| **8** | DCM, 25 °C | 0.08 | 650:1 | 96 | | 67,000 | 1.42 | n.d. | 75 |
| **9** | Melt, 135 °C | 24 | 500:1 | 82 | | 58,800 | 1.74 | n.d. | 75 |
| **10** | Melt, 135 °C | 24 | 500:1 | 63 | | 34,700 | 1.63 | n.d. | 76 |
| **11** | Tol, 50 °C | 0.5 | 100:1 | 98 | 14,100 | 30,000 | 1.30 | 0.23 | 76 |
| **12** | Tol, 50 °C | 0.5 | 100:1 | 96 | 13,800 | 18,000 | 1.07 | 0.24 | 77 |
| **13** | Tol, 50 °C | 0.5 | 100:1 | 96 | 13,800 | 30,200 | 1.10 | 0.20 | 77 |
| **14** | Tol, 50 °C | 0.5 | 100:1 | 93 | 13,400 | 37,400 | 1.23 | 0.14 | 77 |
| **15** | Tol, 23 °C | 44 | 100:1 | 96 | 13,800 | 52,200 | 1.32 | 0.09 | 77 |
| **16** | Tol, 30 °C | 8 | 200:1 | 96 | 2,760 | 5,100 | 1.37 | 0.15 | 78 |
| **16** | THF, 30 °C | 10 | 200:1 | 91 | 2,620 | 2,560 | 1.98 | 0.26 | 78 |
| **17** | THF, 30 °C | 36 | 200:1 | 73 | 2,100 | 1,810 | 1.67 | 0.27 | 78 |
| **18** | THF, 30 °C | 10 | 200:1 | 85 | 2,450 | 2,170 | 2.01 | 0.32 | 78 |
| **19** | THF, 30 °C | 36 | 200:1 | 74 | 2,130 | 1,980 | 1.79 | 0.31 | 78 |
| **20** | DCM, 30 °C | 0.5 | 200:1 | 99 | 14,377 | 15,246 | 1.11 | 0.52 | 79 |
| **21** | DCM, 30 °C | 1.5 | 200:1 | 99 | 14,377 | 7,576 | 1.08 | 0.50 | 79 |
| **22** | THF, 25 °C | 0.025 | 100:1 | 60 | | 20,200 | 1.94 | 0.96 | 80 |
| **23** | THF, 25 °C | 0.025 | 100:1 | 41 | | 21,600 | 1.28 | 0.94 | 80 |
| **24** | $C_6H_6$, 25 °C | 0.13 | 100:1 | 81 | | 23,000 | 1.78 | n.d. | 81 |
| **25** | $CDCl_3$, 25 °C | 0.5 | 100:1 | 90 | | 60,200 | 1.15 | n.d. | 81 |

In summary, it is possible to achieve both highly isotactic and heterotactic PLA from the ROP of *rac*-lactide using zinc and group 2 initiators, depending on the ligand employed. Zinc also exhibits high activity in many cases, producing high conversions in less than an hour.

### 1.9.2 Aluminium initiators

Aluminium has been a metal centre of great interest for the ROP of lactide, as many initiators reported exhibit high selectivity. A list of polymerisation data for the examples given below can be found in Table 1.03 on page 31. One of the simplest aluminium initiators for ROP of lactide is $Al(O^iPr)_3$. In a study by Degee *et al.*, it was found that it took between 40 and 83 hours to reach 100 % conversion of lactide at 125 °C in the melt.[82] This is a relatively slow rate of polymerisation for these conditions. Indeed, aluminium initiators are known to have lower activity for the ROP of lactide than with other metal centres.[70] It was found that addition of a Lewis base increased the rate of polymerisation for both $Al(O^iPr)_3$ and $Sn(Oct)_2$, with the former producing PLA of molecular weight 34,000 $gmol^{-1}$ in just one hour at 520:1 lactide to initiator ratio. No $P_r$ value is reported for the polymers produced in this work, it could be presumed that the polymers produced would be atactic due to the lack of ligand denticity, bulky groups or chirality.

One of the earliest well-defined aluminium initiators was reported by Spassky *et al.*, shown in Figure 1.39. This Schiff-group ligand class are known as salens. The ROP of lactide using this chiral initiator, described as (R)-SALBinaphtAlOCH$_3$, occurs *via* the coordination insertion mechanism, where the methoxide group on the aluminium inserts into the polymer chain.[83] This bulky structure affords PLA with narrow molecular weight distributions and little transesterification occurs, which suggests that the polymerisation is of living nature. This initiator exhibits selectivity for D-lactide over L-lactide (determined by optical activity) and produces stereocomplex PLA (determined by $T_m$ and $T_g$). This preference for D-lactide is attributed to the chirality of the initiator, with the R enantiomer of the ligand imparting selectivity for the (R,R) monomer.

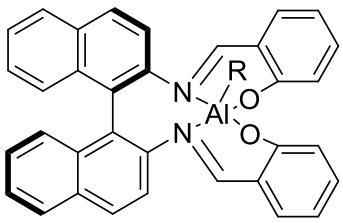


**29**: R = OMe

**Figure 1.39: Chiral salen initiator[83]**

Feijen *et al* reported highly isotactic PLA ($P_m$ up to 0.93) with an aluminium complex synthesised using a salen ligand previously reported by Jacobsen *et al.*, with a chiral (R,R)-*trans*-

diaminocyclohexyl backbone (Figure 1.40).[84] No evidence of polymer transesterification was observed despite long polymerisation times (up to 24 days). This exemplifies the living and controlled nature of the polymerisation using this initiator. In contrast to the binaphthyl system reported by Spassky, this initiator exhibited preference for L-lactide over D-lactide. This indicates that the chirality of the ligand plays an important role, and suggests an enantiomorphic site control mechanism. It was found that using the racemic equivalent of this complex also produced highly isotactic PLA.[85] In fact, for this complex, isotacticity was retained at high conversion, whereas with **30** the $P_m$ was found to be lower at higher conversions. It is suggested that this is due to tapering of the polymer as the L-lactide feed is exhausted and the initiator begins to consume D-lactide, whereas for the racemic version of **30**, the (S,S) enantiomer is consuming D-lactide at the same rate as the (R,R) is consuming L-lactide, which would cause less tapering in the polymer.

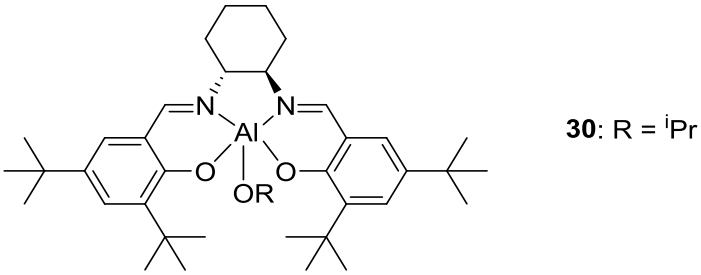


**Figure 1.40: Salen aluminium complex reported by Feijen *et al.*[84]**

Lin *et al.* synthesised a range of aluminium salen complexes with varying backbones (Figure 1.41). These were employed for ROP of lactide using benzyl alcohol as a co-initiator. Each structure produces PLA with a narrow molecular weight range (1.06-1.11), indicating a controlled, living polymerisation.[86] They all have high isoselectivity, with $P_m$ values between 0.94-0.97. Between the three structures, there is not a huge difference in activity or selectivity, which indicates that the backbone does not play a vital role in the polymerisation outcome in this instance, due to the similarity in flexibility of these backbones.

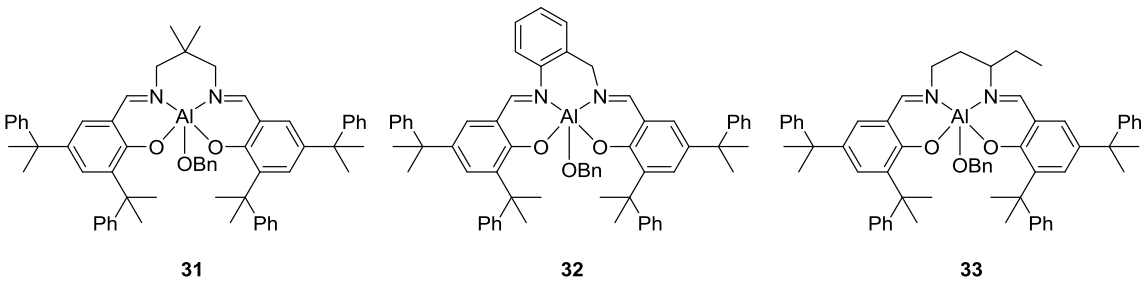


**Figure 1.41: Salen aluminium complexes with varying backbones on the ligand[86]**

Salans are another ligand class that have been complexed with aluminium and used to initiate ROP of lactide, using benzyl alcohol as a coinitiator. Gibson *et al.* synthesised a range of salan aluminium complexes (Figure 1.42).[87] These complexes are particularly interesting as the stereoselectivity can be tuned by changing the R groups. When $R_2$ = H (complexes **34** and **36**), the complex has isotactic bias and when $R_2$ = Me (complexes **35** and **37**), the complex has heterotactic bias. All the complexes produce PLA with narrow polydispersities, thus the polymerisations are well controlled and living.

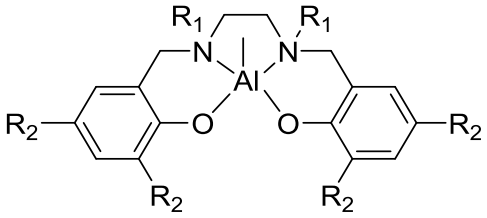


**34:** $R_1$ = Me, $R_2$ = H
**35:** $R_1$ = Me, $R_2$ = Me
**36:** $R_1$ = Bz, $R_2$ = H
**37:** $R_1$ = Bz, $R_2$ = Me

**Figure 1.42: Salan aluminium complexes[87]**

More recent work has been carried out with salalen ligands. These are ligands that contain a salen and a salan moiety and can exhibit both selectivity and high activity.[88] Figure 1.43 shows some salalen aluminium complexes developed by Jones *et al*. Structure **38** shows the best selectivity, with reasonable heterotactic bias ($P_r$ = 0.75). Structure **39** shows the highest activity, with near full conversion in 24 hours, however it does not exhibit selectivity ($P_r$ = 0.45). Structure **40** shows slight isoselectivity ($P_r$ = 0.39), but has the lowest activity with only 73 % conversion after 3 days. In the case of these structures, it appears that activity is compromised by increased selectivity.

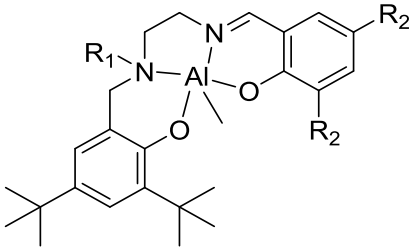


**38**: $R_1$ = Me, $R_2$ = H
**39**: $R_1$ = Ph, $R_2$ = H
**40**: $R_1$ = Me, $R_2$ = $^t$Bu
**41**: $R_1$ = Ph, $R_2$ = $^t$Bu

**Figure 1.43: Salalen aluminium complexes with ethylene backbone and varying amine and ring substituent groups[89]**

Kol and coworkers expanded on this ligand set, keeping the N-methyl group but varying substituents on both amine and imine phenolate groups.[90] Figure 1.44 shows these complexes. It was found that complexes **43** and **44** showed isoselectivity for the ROP of *rac*-lactide ($P_m$ = 0.72 and 0.69 respectively), whereas **42** was mildly heteroselective.

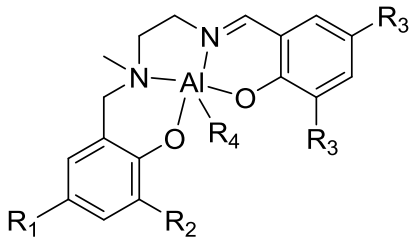

**42**: $R_1 = R_2 = Cl$, $R_3 = {}^tBu$, $R_4 = Me$
**43**: $R_1 = R_2 = {}^tBu$, $R_3 = Cl$, $R_4 = O^iPr$
**44**: $R_1 = Me$, $R_2 = Ad$, $R_3 = Cl$, $R_4 = O^iPr$

**Figure 1.44: Salalen aluminium complexes, reported by Kol *et al*.[90]**

In 2013 Jones *et al.* developed salalen ligands with a cyclohexane backbone and different substituents on each aromatic ring (Figure 1.45). Activity was lower for complexes with *tert*-butyl substituent groups, the slowest being structure **45** which had a conversion of 42 % after 4 days, which suggests the *tert*-butyl groups are hindering the polymerisations, presumably due to steric effects.[91] The most stereoselective complex was **48**, which had a $P_r$ of 0.73.

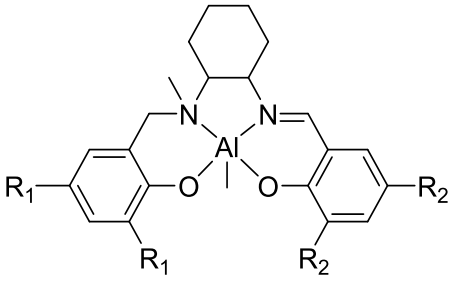

**45**: $R_1 = {}^tBu$, $R_2 = {}^tBu$
**46**: $R_1 = {}^tBu$, $R_2 = H$
**47**: $R_1 = {}^tBu$, $R_2 = Cl$
**48**: $R_1 = Cl$, $R_2 = Cl$

**Figure 1.45: Salalen aluminium complexes with a cyclohexane backbone.[91]**

A series of chiral salalen aluminium complexes with different phenyl substituents were synthesised by Kol and coworkers,[92] shown in Figure 1.46. Both the chirality and the substituents were found to have an effect on the selectivity of the initiator, for example, (S)-**49** produced heterotactic PLA whereas (S)-**50** and (S)-**51** yielded isotactic PLA. This suggests that bulky groups on the imine side favour isotactic PLA production and steric bulk on the amine side favours heterotacticity. In terms of chiral selectivity, *rac*-**51** was found to be less isoselective ($P_m = 0.70$) than its enantiopure equivalent (S)-**51**, which produced PLA with a $P_m$ of 0.82.

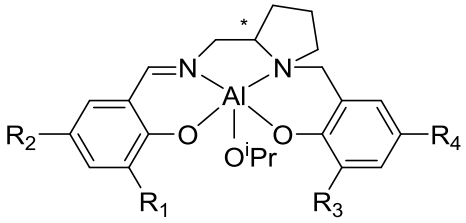

**49**: $R_1 = R_2 = Cl$, $R_3 = Ad$, $R_4 = Me$
**50**: $R_1 = Me$, $R_2 = Ad$, $R_3 = R_4 = Cl$
**51**: $R_1 = R_2 = {}^tBu$, $R_3 = R_4 = Cl$
**52**: $R_1 = R_2 = {}^tBu$, $R_3 = R_4 = I$

**Figure 1.46: Chiral salalen complexes prepared by Kol *et al*.[92]**

Dinuclear complexes have been of recent interest in the literature, as the higher number of metal centres in the initiator allow for faster polymerisation rates. In many examples, dinuclear

aluminium complexes have shown elevated activity compared to their mononuclear equivalents.

Yu and Wang synthesised a range of dinuclear aluminium salen and salan complexes (Figure 1.47).[93] Their structures were elucidated by X-ray crystallography and it was found that the aluminium centres orientated themselves on opposite sides of the complexes, made possible by rotation about the alkyl bridge. When compared to equivalent monomeric structures, it was found that the turnover frequencies of the dinuclear complexes were significantly elevated, e.g. from 0.91 $h^{-1}$ for the monomeric counterpart to 3.10 $h^{-1}$ for the dimeric complex **54**. This is attributed to a cooperative effect between the metal centres, which suggests that the solid state orientation is not retained during polymerisation, however it was stated that substituent effects cannot be ruled out.

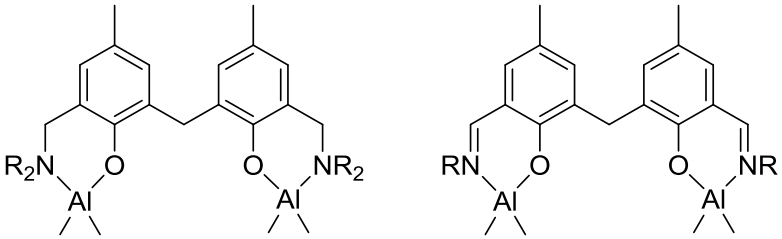


**53**: R = Me

**54**: R = 2,6-$^{i}Pr_2C_6H_3$

**55**: R = $^{t}Bu$

**Figure 1.47: Dinuclear aluminium complexes as reported by Yu and Wang[93]**

Research by Normand and coworkers showed that dinuclear aluminium complexes had significantly elevated activities compared to their mononuclear equivalent (Figure 1.48). The $k_{app}$ value reported for structure **57** (with two equivalents benzyl alcohol) was 12.2 x $10^{-3}$ $s^{-1}$, a 5 fold increase compared to **56** with one equivalent benzyl alcohol, which had a $k_{app}$ of 2.5 x $10^{-3}$ $s^{-1}$. This increased activity was attributed to interactions between the aluminium centres, facilitated by rotation about the phenyl-phenyl bond. The selectivities of these initiators were not reported, therefore polymers produced are assumed to be atactic.

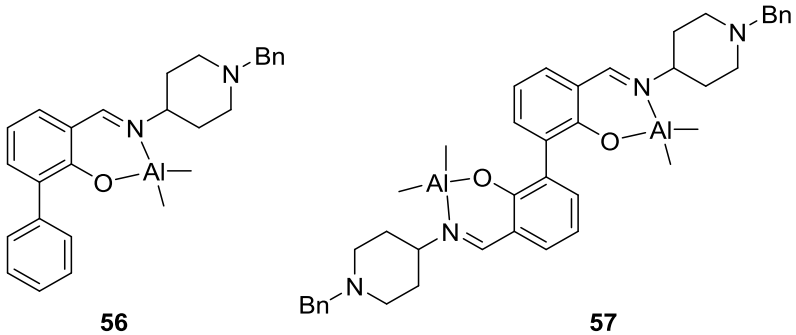


**56** **57**

**Figure 1.48: Mono- and dinuclear complexes as reported by Normand *et al.*[94]**

Chen *et al.* developed mononuclear and dinuclear aluminium complexes featuring a piperazidine backbone, which were utilised for the ROP of ε-caprolactone. Initial polymerisation results found that the dinuclear complex **59** was much faster at producing high conversions of polycaprolactone than the mononuclear complex **58**.[95] When ethanol was employed as a coinitiator, the result was more effective control of molecular weight with narrower PDIs. At 80 °C in toluene, it was found that the $k_{app}$ of the ROP of caprolactone using **58** was 4.68 x $10^{-5}$ $s^{-1}$, for **59** the $k_{app}$ = 1.51 x $10^{-4}$ $s^{-1}$. This increase in activity observed for the dinuclear complex **59** was attributed to cooperative effects between the metal centres in the complex.

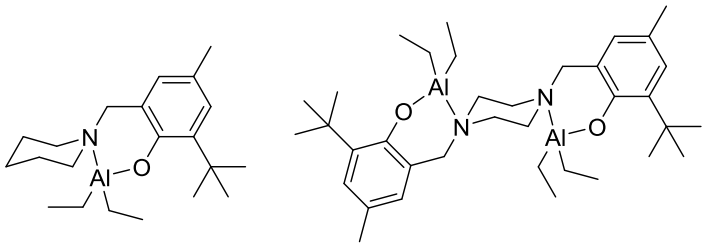


**58** **59**

**Figure 1.49: Mononuclear and dinuclear aluminium complexes synthesised by Chen *et al.*[95]**

A series of dinuclear aluminium complexes with different phenyl substituents was developed by Pang and coworkers.[96] These were investigated for the ROP of *rac*-lactide and ε-caprolactone. No mononuclear complexes of this type were produced for comparison. For the ROP of *rac*-lactide at 70 °C in toluene, it was found that complex **60** could achieve high conversion within a few hours with good molecular weight control, PDI values 1.12-1.18. The polymer was slightly isotactic, $P_m$ = 0.70 at 200:1 monomer to initiator loading. Complex **61** showed similar isoselectivity, with $P_m$ = 0.71 under the same conditions. Initiator **62** exhibited the highest selectivity of the three, producing isotactic PLA ($P_m$ = 0.92) within 10 hours at 70 °C. This suggests that the use of bulkier groups such as *tert*-butyl drives greater isoselectivity in this initiator type. For the ROP of ε-caprolactone, it was found that **60-62** produced polycaprolactone with good molecular weight control, in particular **62** (PDIs 1.06-1.18) in toluene at 40 °C.

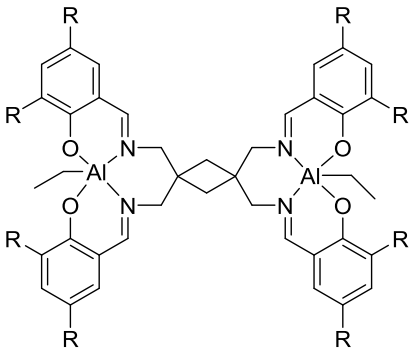


**Figure 1.50: Dinuclear aluminium complexes as synthesised by Pang *et al.*[96]**

Table 1.03 shows the polymerisation data for the aluminium initiators discussed above, including molecular weights and $P_r$ values, where reported.

**Table 1.03: Comparison of aluminium initiators listed above used for the ROP of *rac*-lactide**

| Initiator | Conditions | Time (h) | LA:I | Conversion (%) | $M_n$ Calc ($gmol^{-1}$) | $M_n$ (Obs) ($gmol^{-1}$) | PDI | $P_r$ | Ref |
|---|---|---|---|---|---|---|---|---|---|
| **$Al(O^iPr)_3$** | Melt, 125 °C | 40 | 520:1 | 100 | | 35,000 | 1.50 | n.d. | 83 |
| **29** | Tol, 70 °C | 113 | 75:1 | 90 | | 9,900 | 1.15 | n.d. | 84 |
| **30** | Tol, 70 °C | 288 | 62:1 | 85 | 7,600 | 7,700 | 1.06 | 0.07 | 85 |
| **31** | Tol, 70 °C | 12 | 100:1 | 96 | 14,000 | 13,900 | 1.10 | 0.03 | 87 |
| **32** | Tol, 70 °C | 12 | 125:1 | 97 | 14,600 | 14,000 | 1.09 | 0.06 | 87 |
| **33** | Tol, 70 °C | 12 | 100:1 | 72 | 10,900 | 10,500 | 1.06 | 0.03 | 87 |
| **34** | Tol, 70 °C | 23 | 100:1 | 97 | | 18,920 | 1.04 | 0.32 | 88 |
| **35** | Tol, 70 °C | 24 | 100:1 | 87 | | 12,725 | 1.09 | 0.80 | 88 |
| **36** | Tol, 70 °C | 21 | 100:1 | 98 | | 21,180 | 1.08 | 0.21 | 88 |
| **37** | Tol, 70 °C | 24 | 100:1 | 75 | | 13,350 | 1.06 | 0.83 | 88 |
| **38** | Tol, 80 °C | 72 | 100:1 | 86 | 12,500 | 6,620 | 1.07 | 0.75 | 90 |
| **39** | Tol, 80 °C | 24 | 100:1 | 98 | 14,200 | 9,050 | 1.39 | 0.45 | 90 |
| **40** | Tol, 80 °C | 72 | 100:1 | 73 | 10,600 | 11,900 | 1.05 | 0.39 | 90 |
| **41** | Tol, 80 °C | 24 | 100:1 | 96 | 13,950 | 11,925 | 1.11 | 0.43 | 90 |
| **42** | Tol, 80 °C | 24 | 100:1 | 63 | 9,100 | 6,300 | 1.07 | 0.55 | 91 |
| **43** | Tol, 80 °C | 120 | 100:1 | 52 | 7,500 | 8,700 | 1.06 | 0.28 | 91 |
| **44** | Tol, 80 °C | 168 | 100:1 | 54 | 7,800 | 9,400 | 1.07 | 0.31 | 91 |
| **45** | Tol, 80 °C | 96 | 100:1 | 42 | | 8,950 | 1.06 | 0.49 | 92 |
| **46** | Tol, 80 °C | 96 | 100:1 | 71 | | 12,200 | 1.07 | 0.54 | 92 |
| **47** | Tol, 80 °C | 96 | 100:1 | 97 | | 17,150 | 1.35 | 0.60 | 92 |
| **48** | Tol, 80 °C | 96 | 100:1 | 99 | | 19,350 | 1.15 | 0.73 | 92 |

| | | | | | | | | | |
|---|---|---|---|---|---|---|---|---|---|
| (S)-**49** | Tol, 80 °C | 24 | 100:1 | 75 | 10,800 | 8,500 | 1.07 | 0.76 | 93 |
| (S)-**50** | Tol, 80 °C | 24 | 100:1 | 42 | 6,100 | 6,800 | 1.05 | 0.18 | 93 |
| (S)-**51** | Tol, 80 °C | 24 | 100:1 | 78 | 11,200 | 9,000 | 1.07 | 0.18 | 93 |
| *rac*-**51** | Tol, 80 °C | 24 | 100:1 | 85 | 12,300 | 9,200 | 1.05 | 0.30 | 93 |
| (R)-**52** | Tol, 80 °C | 24 | 100:1 | 91 | 13,100 | 9,700 | 1.07 | 0.41 | 93 |
| **53** | Tol, 70 °C | 21 | 100:1 | 93 | 6,800 | 6,400 | 1.20 | n.d. | 94 |
| **54** | Tol, 70 °C | 16 | 100:1 | 93 | 6,800 | 7,000 | 1.16 | n.d. | 94 |
| **55** | Tol, 70 °C | 24 | 100:1 | 91 | 6,700 | 5,600 | 1.11 | n.d. | 94 |
| **56** | Tol, 110 °C | 8 | 500:1 | 74 | 10,700 | 12,100 | 1.06 | n.d. | 95 |
| **57** | Tol, 110 °C | 2 | 500:1 | 92 | 13,200 | 13,900 | 1.29 | n.d. | 95 |
| **60** | Tol, 70 °C | 3 | 200:1 | 82 | 11,900 | 11,600 | 1.16 | 0.30 | 97 |
| **61** | Tol, 70 °C | 3.6 | 200:1 | 87 | 12,600 | 11,300 | 1.16 | 0.29 | 97 |
| **62** | Tol, 70 °C | 6.6 | 200:1 | 85 | 12,200 | 10,500 | 1.10 | 0.09 | 97 |

In summary, aluminium initiators tend to have lower activities than other metal centres (compared to many of the zinc initiators listed in Table 1.02, for example). However, in many of the examples listed above, high selectivity has been observed, both isotactic and heterotactic, depending on the ligand structure of the initiator used.

### 1.9.3 Group 4 initiators

Group 4 initiators are a popular research area, as they often contain the alkoxide necessary for coordination-insertion mechanism, removing the requirement to add alcohol to the polymerisation reaction mixture as a coinitiator. For a summary of the polymerisation results for the initiators listed, see Table 1.04 on page 37.

In 2008, Davidson *et al.* used a tripodal trisphenolate ligand complexed with titanium, zirconium or hafnium (Figure 1.51). This showed unprecedented heterotactic selectivity, with a $P_r$ of 0.98 with complex **64** at room temperature in toluene after 48 hours.[97] This stereoselectivity is not fully understood but has been attributed to inversion of axial chirality during chain propagation which leads to alternating stereochemistry.

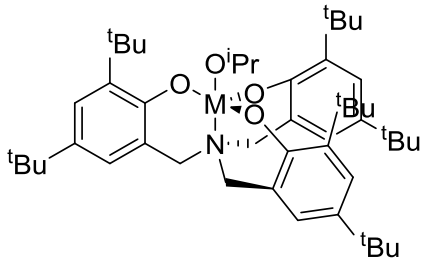


**63**: M = Ti
**64**: M = Zr
**65**: M = Hf

**Figure 1.51: Trisphenolate ligand system complexed with Ti, Zr, Hf[97]**

Huang *et al.* complexed a tripodal ligand with group 4 metals to form dinuclear complexes with high activity towards lactide polymerisation (Figure 1.52).[98] It was found that in solution at 100 °C, complexes **67** and **68** polymerised *rac*-lactide within an hour to high conversions with narrow PDIs. The titanium complex **66** was considerably slower under these conditions, producing high molecular weight polylactide within 12 hours, with a higher polydispersity of 1.39. No selectivity data was reported for these initiators.

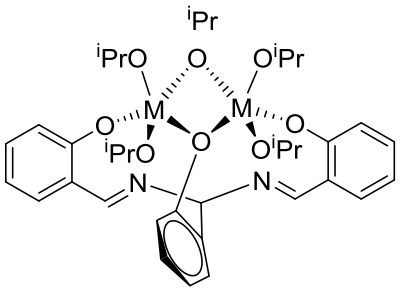


**66**: M = Ti
**67**: M = Zr
**68**: M = Hf

**Figure 1.52: Dinuclear group 4 complexes[98]**

Capacchione and coworkers developed group 4 metal complexes featuring thioetherphenolate ligands (Figure 1.53) and deployed them in the polymerisation of L-lactide.[99] High conversions were reached within hours in solution. Complexes **69** and **70** were also taken forward for the copolymerisation of L-lactide and ε-caprolactone in toluene at 100 °C. It was found that the copolymer produced by these initiators was random in nature.

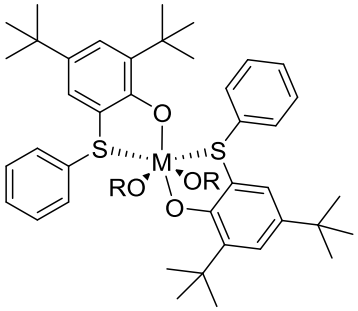


**69**: M = Ti, R = iPr
**70**: M = Zr, R = tBu
**71**: M = Hf, R = tBu

**Figure 1.53: Group 4 initiators synthesised by Capachhione *et al*.[99]**

A variety of {ONSO} tetradentate zirconium complexes were synthesised by Kol *et al.* (shown in Figure 1.54) and used for the melt polymerisations (140 °C) of L- and *rac*-lactide.[100] In the case of L-lactide, complexes **72-74** achieved high conversions in 15 minutes or less in the melt. For *rac*-lactide, polymerisations reached high conversions in less than 8 minutes, however little stereoselectivity was observed under melt conditions. It was found that by taking the temperature down to 70 °C and performing the polymerisation in toluene, higher heterotacticity ($P_r$ = 0.72) can be obtained within 20 hours for complex **72**. Under these conditions, complex **75** produced PLA with a $P_r$ value of 0.33, a switch in selectivity compared to the other initiators. It was proposed that complexes **72-74** were more fluxional type catalysts, which leads towards heterotactic-inclined PLA. For the more rigid catalyst **75**, more isotactically-inclined PLA was produced.

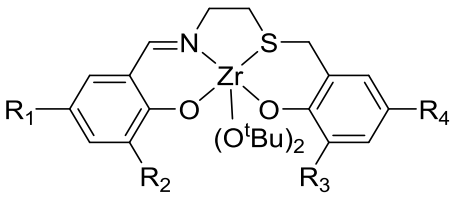


**72**: $R_1 = R_2 = {}^tBu$, $R_3 = R_4 = Cl$
**73**: $R_1 = R_2 = Cl$, $R_3 = R_4 = {}^tBu$
**74**: $R_1 = R_2 = R_3 = R_4 = {}^tBu$
**75:** $R_1 = Me$, $R_2 = Ad$, $R_3 = Ad$, $R_4 = Me$

**Figure 1.54: Zirconium complex with {ONSO} ligand[100]**

Kol *et al*. continued this investigation by developing an {ONSO} ligand featuring a phenyl backbone, illustrated in Figure 1.55.[101] Polymerisations of *rac*-lactide were carried out at 70 °C in toluene at 300:1 monomer to initiator loading. It was found that both **76** and **77** produced heterotactic PLA within 4 hours under these conditions, with $P_r$ = 0.75 and 0.78 respectively. The observed $M_n$ values were in agreement with the calculated $M_n$ values, indicating that the polymerisations were well controlled. Initiator **78** did not exhibit such stereoselectivity and produced PLA with a $P_r$ value of 0.52 under the same conditions. On reducing the temperature of the solution polymerisation to 50 °C, greater heteroselectivity could be achieved with initiator **76**, with $P_r$ = 0.81 for polymer produced at this temperature. At 50 °C, **78** was not able to polymerise lactide (0 % conversion after 24 hours).

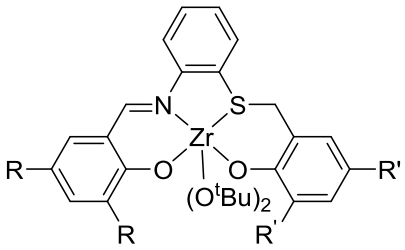


**76**: R = R' = Cl
**77**: R = R' = Br
**78**: R = Cl, R' = $^tBu$

**Figure 1.55: Phenyl-bridged {ONSO} zirconium complex[101]**

Chand *et al.* synthesised a two-ligand two-metal centre complex with bridging isopropoxide groups (Figure 1.56).[102] The most selective of these initiators featured hafnium metal centres with a *tert*-butyl group at $R_1$ and a methyl at $R_2$, complex **81**. With this, polylactide with a $P_r$ of 0.80 was produced at high conversions in just 5 minutes under solvent-free conditions, more heteroselective than the zirconium or titanium analogues. These complexes were also used for the ring-opening polymerisation of caprolactone, reaching high conversions in just minutes with narrow polydispersities. No copolymerisation data is reported for these initiators.

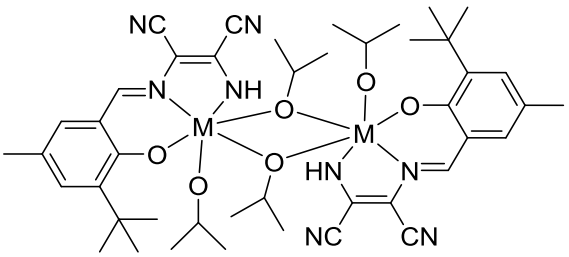


**79**: M = Ti
**80**: M = Zr
**81**: M = Hf

**Figure 1.56: Initiators synthesised by Chand *et al.* [102]**

A series of group 4 salalen complexes (Figure 1.57) were synthesised by Jones *et al*. and utilised for the melt and solution ROP of *rac*-lactide.[88] Under melt conditions at 130 °C using 300:1 monomer to initiator loading, the titanium initiators **82** and **83** produced atactic PLA in 15 minutes. Under the same conditions, zirconium complexes **84** and **85** yielded slightly heterotactic PLA, $P_r$ = 0.57 and 0.56 respectively. The best melt selectivity was observed for **86**, which produced isotactic PLA ($P_r$ = 0.30), however this took 48 hours to reach 75 % conversion. The other hafnium complex **87** showed no selectivity and required 24 hours to reach high conversion in the melt. The initiators **82-87** were also used for the solution ROP of *rac*-lactide at 80 °C using 100:1 monomer to initiator loading, but it was found that after 24 hours no enhancement of selectivity was observed compared to the results in the melt. In summary, the change of N-alkyl group only imparted a change in stereoselectivity with hafnium as the central metal.[88]

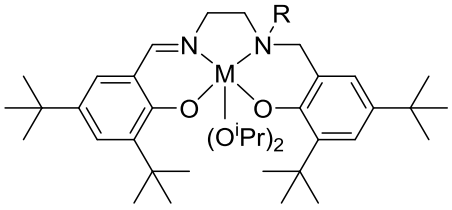


**82:** M = Ti, R = Me
**83:** M = Ti, R = Ph
**84:** M = Zr, R = Me
**85:** M = Zr, R = Ph
**86:** M = Hf, R = Me
**87:** M = Hf, R = Ph

**Figure 1.57: Group 4 salalen complexes reported by Jones *et al*.[88]**

Further investigation was carried out using this ligand type, this time with changes made to the substituents on the salen phenyl ring, illustrated in Figure 1.58.[103] It was found that for the ROP

of *rac*-lactide in toluene at 80 °C at 100:1 monomer loading, initiator **88** produced isotactic PLA ($P_r$ = 0.25) after just 2 hours. Complexes **89-91** also showed isoselectivity ($P_r$ = 0.30-0.35), however PDIs were broad, indicating poor molecular weight control (PDI = 1.54-1.77). Interestingly, if excess methanol was used for the work up of this polymer, it was observed that the sample would depolymerise into oligomers and methyl lactate. When employed in the melt at 130 °C at 300:1 monomer loading some isoselectivity is lost, e.g. $P_r$ = 0.40 for initiator **88**, at 77 % conversion after 15 minutes.

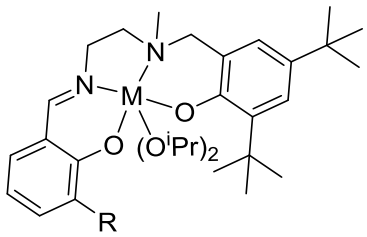


**88**: M = Zr, R = Me
**89**: M = Zr, R = H
**90**: M = Hf, R = Me
**91**: M = Hf, R = H

**Figure 1.58: More group 4 salalen complexes by Jones *et al*.[103]**

Chakraborty and coworkers utilised the (R,R)-*trans*-diaminocyclohexyl salen ligand to synthesise a zirconium and a hafnium salen complex.[104] It was found that for both metals, a dinuclear compound was formed (Figure 1.59). When utilised for the ROP of *rac*-lactide in the melt at 140 °C, both initiators exhibited excellent molecular weight control, with the observed $M_n$ values corresponding well with the expected values, and both producing polymer with a narrow PDI of 1.02. No $P_r$ values were reported, presumably because no selectivity was observed for these initiators. The initiators **92** and **93** were also employed for the ROP of other cyclic monomers; valerolactone, caprolactone and butyrolactone. The molecular weight control for the resulting polymers was as similarly well-controlled as was observed for the ROP of *rac*-lactide.

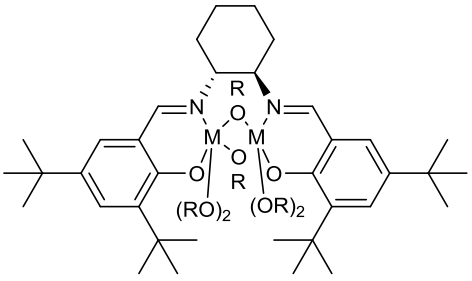


**92**: M = Zr, R = $^{i}$Pr
**93:** M = Hf. R = $^{t}$Bu

**Figure 1.59: Dinuclear group 4 salen complexes as reported by Chakraborty and coworkers[104]**

Table 1.04 shows the polymerisation data for the group 4 initiators discussed above, including molecular weights and $P_r$ values, where reported.

**Table 1.04: Comparison of Group 4 initiators listed above used for the ROP of *rac*-lactide (a) L-lactide used**

| Initiator | Conditions | Time (h) | LA:I | Conversion (%) | $M_n$ Calc ($gmol^{-1}$) | $M_n$ (Obs) ($gmol^{-1}$) | PDI | $P_r$ | Ref |
|---|---|---|---|---|---|---|---|---|---|
| **63** | Melt, 130 °C | 0.5 | 300:1 | 50 | | 37,100 | 1.38 | 0.50 | 98 |
| **64** | Melt, 130 °C | 0.1 | 300:1 | 78 | | 32,300 | 1.22 | 0.96 | 98 |
| **64** | Toluene, RT | 48 | 100:1 | 50 | | 11,700 | 1.09 | 0.98 | 98 |
| **65** | Melt, 130 °C | 0.5 | 300:1 | 95 | | 71,150 | 1.19 | 0.88 | 98 |
| **66** | Toluene, 100 °C | 12 | 500:1 | 78 | 56,200 | 23,600 | 1.39 | n.d. | 99 |
| **66** | Melt, 130 °C | 0.66 | 500:1 | 94 | 67,700 | 24,200 | 1.18 | n.d. | 99 |
| **67** | Toluene, 100 °C | 1 | 500:1 | 92 | 66,300 | 13,500 | 1.09 | n.d. | 99 |
| **68** | Toluene, 100 °C | 1 | 500:1 | 84 | 60,500 | 14,000 | 1.06 | n.d. | 99 |
| **69**[a] | Toluene, 100 °C | 8 | 100:1 | 84 | 6,100 | 6,000 | 1.18 | - | 100 |
| **70**[a] | Toluene, 100 °C | 1.25 | 100:1 | 90 | 13,000 | 8,900 | 1.10 | - | 100 |
| **71**[a] | Toluene, 100 °C | 1.5 | 100:1 | 82 | 11,700 | 8,100 | 1.24 | - | 100 |
| **72** | Melt, 140 °C | 0.1 | 300:1 | 92 | 39,500 | 16,300 | 1.55 | 0.63 | 101 |
| **72** | Toluene, 70 °C | 20 | 300:1 | 98 | 42,000 | 8,500 | 1.45 | 0.72 | 101 |
| **73** | Melt, 140 °C | 0.08 | 300:1 | 75 | 32,500 | 17,700 | 1.38 | 0.58 | 101 |
| **73** | Toluene, 70 °C | 20 | 300:1 | 87 | 37,500 | 14,700 | 1.50 | 0.65 | 101 |
| **74** | Melt, 140 °C | 0.11 | 300:1 | 97 | 42,000 | 20,300 | 1.57 | 0.50 | 101 |
| **74** | Toluene, 70 °C | 20 | 300:1 | 81 | 35,000 | 21,300 | 1.70 | 0.50 | 101 |
| **75** | Melt, 140 °C | 0.3 | 300:1 | 61 | 26,500 | 20,300 | 1.34 | 0.55 | 101 |
| **75** | Toluene, 70 °C | 20 | 300:1 | 18 | 8,000 | 18,000 | 1.17 | 0.33 | 101 |
| **76** | Toluene, 70 °C | 4 | 300:1 | 93 | 40,100 | 41,300 | 1.23 | 0.75 | 102 |
| **77** | Toluene, 70 °C | 4 | 300:1 | 97 | 41,900 | 48,600 | 1.26 | 0.78 | 102 |
| **78** | Toluene, 70 °C | 8 | 300:1 | 78 | 33,700 | 32,600 | 1.16 | 0.52 | 102 |
| **79** | Melt, 140 °C | 0.13 | 200:1 | 98 | 28,900 | 28,150 | 1.14 | 0.68 | 103 |

| | | | | | | | | | |
|---|---|---|---|---|---|---|---|---|---|
| **80** | Melt, 140 °C | 0.1 | 200:1 | 98 | 28,900 | 25,030 | 1.16 | 0.77 | 103 |
| **81** | Melt, 140 °C | 0.08 | 200:1 | 97 | 28,900 | 23,430 | 1.17 | 0.80 | 103 |
| **82** | Melt, 130 °C | 0.25 | 300:1 | 89 | | 38,000 | 1.44 | 0.50 | 89 |
| **83** | Melt, 130 °C | 0.25 | 300:1 | 98 | | 42,400 | 1.19 | 0.57 | 89 |
| **84** | Melt, 130 °C | 48 | 300:1 | 75 | | 24,400 | 1.32 | 0.30 | 89 |
| **87** | Melt, 130 °C | 24 | 300:1 | 96 | | 46,600 | 1.49 | 0.50 | 89 |
| **88** | Melt, 130 °C | 0.25 | 300:1 | 77 | | 97,300 | 2.40 | 0.40 | 104 |
| **88** | Toluene, 80 °C | 2 | 100:1 | 98 | | 30,500 | 1.54 | 0.25 | 104 |
| **89** | Toluene, 80 °C | 2 | 100:1 | 98 | | 21,600 | 1.65 | 0.35 | 104 |
| **90** | Toluene, 80 °C | 2 | 100:1 | 98 | | 18,400 | 1.54 | 0.35 | 104 |
| **91** | Toluene, 80 °C | 2 | 100:1 | 99 | | 20,200 | 1.77 | 0.30 | 104 |
| **92** | Melt, 140 °C | 0.8 | 200:1 | 100 | 28,900 | 29,500 | 1.02 | n.d. | 105 |
| **93** | Melt, 140 °C | 1.1 | 200:1 | 100 | 28,900 | 29,700 | 1.02 | | 105 |

To summarise the polymerisation results for lactide using Group 4 complexes, it appears that zirconium initiators are often faster than their titanium analogues. Heterotactic enchainment is frequently observed, the most notable example being with the zirconium trisphenolate (structure **64**).

## 1.10 Project aims

The aims of this project are:

- Develop new ligands based on salen and salalen structures shown above in order to investigate structure-activity relationships, with the aim to prepare isotactic PLA. A further aim is to compare mono and bimetallic Al(III) complexes to assess any potential cooperativity effects.
- Use these to create new initiators by complexation with inexpensive, earth-abundant metal centres, such as aluminium, zinc and zirconium.
- Employ these initiators for the ring-opening polymerisation of lactide and investigate their selectivities and molecular weight control.
- Further investigate the activity of initiators on the copolymerisation of lactide and caprolactone and assess the nature of the copolymer (e.g. random, block), with the aim of understanding the selectivity of the process.

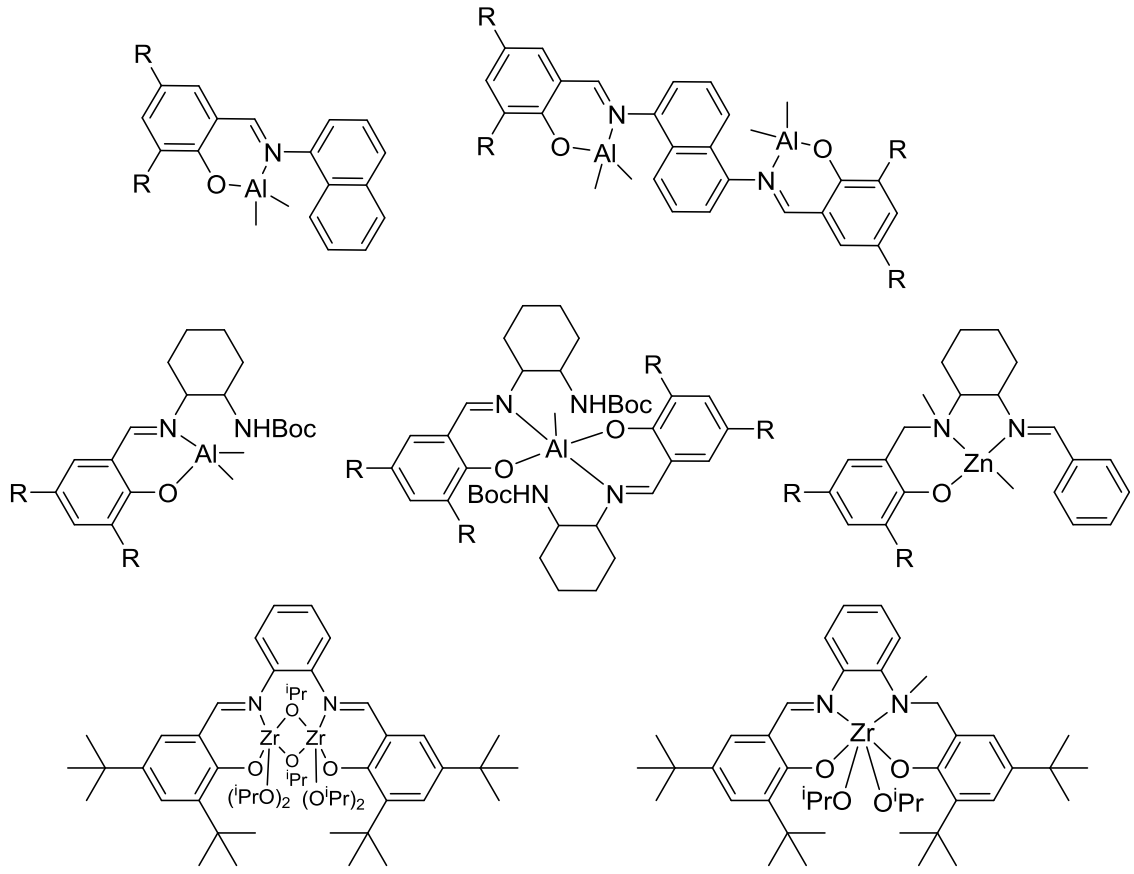


**Figure 1.60: Key initiators from this thesis. Top row, Chapter 2: mono- and dinuclear aluminium complexes featuring a naphthalene backbone. Middle row, Chapter 3: mono- and bis-ligated aluminium Schiff base complexes, {ONN} tridentate zinc complex. Bottom row, Chapter 4: dinuclear zirconium salen complex and mononuclear salalen complex.**

## 1.11 References


1. E. S. Stevens, *Green Plastics: An Introduction to the New Science of Biodegradable Plastics*, Princeton University Press, 2002.
2. *Our Common Future*, United Nations World Commission on Environment and Development, 1987.
3. A. Gandini, D. Coelho, M. Gomes, B. Reis and A. Silvestre, *J. Mater. Chem.*, 2009, **19**, 8656-8664.
4. J. J. Bozell and G. R. Petersen, *Green Chem.*, 2010, **12**, 539-554.
5. S. K. Burgess, J. E. Leisen, B. E. Kraftschik, C. R. Mubarak, R. M. Kriegel and W. J. Koros, *Macromolecules*, 2014, **47**, 1383-1391.
6. F. Siegmund and T. Gries, *Chem. Fibers Int.*, 2008, **58**, 28-29.
7. G. Mathur, A. Dua, A. R. Das, H. Kaur, S. Kukal, P. Sharma, N. Goswami, A. Sahai and A. Mathur, *Macromol. Symp.*, 2015, **347**, 27-31.
8. E. E. Abdel-Hady, H. F. M. Mohamed and S. S. Fareed, *Phys. Status Solidi C*, 2007, **4**, 3907-3911.
9. V. Siracusa, I. Blanco, S. Romani, U. Tylewicz, P. Rocculi and R. M. Dalla, *J. Appl. Polym. Sci.*, 2012, **125**, E390-E401.
10. M. S. Lopes, A. L. Jardini and R. M. Filho, *Procedia Eng.*, 2012, **42**, 1530-1542.
11. J. Lunt, *Polym. Degrad. Stab.*, 1998, **59**, 145-152.
12. T. M. Quynh, H. Mitomo, N. Nagasawa, Y. Wada, F. Yoshii and M. Tamada, *Eur. Polym. J.*, 2007, **43**, 1779-1785.
13. F. Gironi and V. Piemonte, *Environ. Prog. Sustainable Energy*, 2011, **30**, 459-468.
14. R. Palaniraj and P. Nagarajan, *Int. J. ChemTech Res.*, 2012, **4**, 1601-1614.
15. Y. S. Li, B. I. Zhang, X. M. Zhang and H. P. Li, *Xinyang Shifan Xueyuan Xuebao, Ziran Kexueban*, 2009, **22**, 209-211, 221.
16. S. Inkinen, M. Hakkarainen, A.-C. Albertsson and A. Södergård, *Biomacromolecules*, 2011, **12**, 523-532.
17. A. Duda and S. Penczek, *Macromolecules*, 1990, **23**, 1636-1639.
18. G. Nogueira, A. Favrelle, M. Bria, J. P. P. Ramalho, P. J. Mendes, A. Valente and P. Zinck, *React. Chem. Eng.*, 2016, **1**, 508-520.
19. O. Coulembier, T. Josse, B. Guillerm, P. Gerbaux and P. Dubois, *Chem. Commun.*, 2012, **48**, 11695-11697.
20. N. E. Kamber, W. Jeong, R. M. Waymouth, R. C. Pratt, B. G. G. Lohmeijer and J. L. Hedrick, *Chem. Rev.*, 2007, **107**, 5813-5840.
21. F. Hild, P. Haquette, L. Brelot and S. Dagorne, *Dalton Trans.*, 2010, **39**, 533-540.
22. M. Basko, *Pure Appl. Chem.*, 2012, **84**, 2081-2088.
23. M. J. Stanford and A. P. Dove, *Chem. Soc. Rev.*, 2010, **39**, 486-494.
24. V. T. Lipik, L. K. Widjaja, S. S. Liow, M. J. M. Abadie and S. S. Venkatraman, *Polym. Degrad. Stab.*, 2010, **95**, 2596-2602.
25. S. Asano, T. Aida and S. Inoue, *J. Chem. Soc., Chem. Commun.*, 1985, 1148-1149.
26. A. Routaray, N. Nath, T. Maharana and A. k. Sutar, *J. Macromol. Sci., Part A: Pure Appl. Chem.*, 2015, **52**, 444-453.
27. D. E. Henton, P. Gruber, J. Lunt and J. Randall, in *Natural fibers, biopolymers, and biocomposites*, ed. M. M. A.K. Mohanty, L.T. Drzal, Taylor & Francis, Boca Raton, FL, 2005, pp. 527-577.
28. H. R. Kricheldorf, *Chemosphere*, 2001, **43**, 49-54.
29. P. Sangwan and D. Y. Wu, *Macromolecular Bioscience*, 2008, **8**, 304-315.
30. D. D. Lu, X. W. Zhang, T. H. Zhou, Z. L. Ren, S. F. Wang and Z. Q. Lei, *Prog. Chem.*, 2008, **20**, 339-350.
31. G. Kale, R. Auras, S. P. Singh and R. Narayan, *Polymer Testing*, 2007, **26**, 1049-1061.
32. M. Itavaara, S. Karjomaa and J. F. Selin, *Chemosphere*, 2002, **46**, 879-885.

33. P. Benyathiar, S. Selke and R. Auras, *J. Polym. Environ.*, 2016, **24**, 230-240.
34. J. S. C. Loo, C. P. Ooi and F. Y. C. Boey, *Biomaterials*, 2004, **26**, 1359-1367.
35. T. Biela, A. Duda and S. Penczek, *Macromol. Symp.*, 2002, **183**, 1-10.
36. D. Cleverdon and P. G. Smith, *Chem. Ind.*, 1951, 937.
37. P. Castignolles and M. Gaborieau, *J Sep Sci*, 2010, **33**, 3564-3570.
38. A. C. Ouano and W. Kaye, *J. Polym. Sci., Polym. Chem. Ed.*, 1974, **12**, 1151-1162.
39. M. Moller, F. Nederberg, L. S. Lim, R. Kange, C. J. Hawker, J. L. Hedrick, Y. Gu, R. Shah and N. L. Abbott, *J. Polym. Sci., Part A: Polym. Chem.*, 2001, **39**, 3529-3538.
40. M. J. Weissenborn, J. W. Wehner, C. J. Gray, R. Sardzik, C. E. Eyers, T. K. Lindhorst and S. L. Flitsch, *Beilstein J. Org. Chem.*, 2012, **8**, 753-762, No. 786.
41. V. Mainini, G. Bovo, C. Chinello, E. Gianazza, M. Grasso, G. Cattoretti and F. Magni, *Mol. BioSyst.*, 2013, **9**, 1101-1107.
42. W. A. Korfmacher, *Using Mass Spectrometry for Drug Metabolism Studies*, Second Edition, CRC Press, 2009.
43. H. Pasch and W. Schrepp, *MALDI-TOF Mass Spectrometry of Synthetic Polymers*, Springer Berlin Heidelberg, 2003.
44. M. Florczak, A. Michalski, A. Kacprzak, M. Brzezinski, T. Biedron, A. Pajak, P. Kubisa and T. Biela, *React. Funct. Polym.*, 2016, **104**, 71-77.
45. S. M. Kirk, H. C. Quilter, A. Buchard, L. H. Thomas, G. Kociok-Kohn and M. D. Jones, *Dalton Trans.*, 2016, **45**, 13846-13852.
46. T. M. Ovitt and G. W. Coates, *J. Am. Chem. Soc.*, 2002, **124**, 1316-1326.
47. M. Cheng, D. R. Moore, J. J. Reczek, B. M. Chamberlain, E. B. Lobkovsky and G. W. Coates, *J. Am. Chem. Soc.*, 2001, **123**, 8738-8749.
48. T. M. Ovitt and G. W. Coates, *J. Polym. Sci., Part A: Polym. Chem.*, 2000, **38**, 4686-4692.
49. M. H. Chisholm, S. S. Iyer, M. E. Matison, D. G. McCollum and M. Pagel, *Chem. Commun.*, 1997, 1999-2000.
50. M. A. Woodruff and D. W. Hutmacher, *Prog. Polym. Sci.*, 2010, **35**, 1217-1256.
51. I. Engelberg and J. Kohn, *Biomaterials*, 1991, **12**, 292-304.
52. M. Vert, *J. Mater. Sci.: Mater. Med.*, 2009, **20**, 437-446.
53. A. Le Borgne and N. Spassky, *Polymer*, 1989, **30**, 2312-2319.
54. H. R. Kricheldorf and S.-R. Lee, *Macromolecules*, 1995, **28**, 6718-6725.
55. H. R. Kricheldorf and S. Eggerstedt, *Macromolecules*, 1997, **30**, 5693-5697.
56. R. A. Miller, J. M. Brady and D. E. Cutright, *J. Biomed. Mater. Res.*, 1977, **11**, 711-719.
57. S. Hurrell, G. E. Milroy and R. E. Cameron, *Polymer*, 2003, **44**, 1421-1424.
58. A. Meduri, T. Fuoco, M. Lamberti, C. Pellecchia and D. Pappalardo, *Macromolecules*, 2014, **47**, 534-543.
59. K. V. Zaitsev, Y. A. Piskun, Y. F. Oprunenko, S. S. Karlov, G. S. Zaitseva, I. V. Vasilenko, A. V. Churakov and S. V. Kostjuk, *J. Polym. Sci. Part A: Polym. Chem.*, 2014, **52**, 1237-1250.
60. W. Saiyasombat, R. Molloy, T. M. Nicholson, A. F. Johnson, I. M. Ward and S. Poshyachinda, *Polymer*, 1998, **39**, 5581-5585.
61. F. R. Mayo and F. M. Lewis, *J. Am. Chem. Soc.*, 1944, **66**, 1594-1601.
62. B. S. Beckingham, G. E. Sanoja and N. A. Lynd, *Macromolecules*, 2015, **48**, 6922-6930.
63. R. Langer and J. P. Vacanti, *Science*, 1993, **260**, 920-926.
64. B. O. Palsson, *Tissue Engineering*, Pearson Prentice Hall, 2004.
65. A. J. Engler, S. Sen, H. L. Sweeney and D. E. Discher, *Cell*, 2006, **126**, 677-689.
66. J. Huang, J. Xiong, J. Liu, W. Zhu and D. Wang, *J. Nanomater.*, 2013, 515741, 515711 pp.
67. B. D. Ulery, L. S. Nair and C. T. Laurencin, *J. Polym. Sci., Part B: Polym. Phys.*, 2011, **49**, 832-864.
68. Y. Yu, C.-K. Chen, W.-C. Law, J. Mok, J. Zou, P. N. Prasad and C. Cheng, *Mol. Pharmaceutics*, 2013, **10**, 867-874.
69. C. Jerome and P. Lecomte, *Adv. Drug Delivery Rev.*, 2008, **60**, 1056-1076.

70. R. H. Platel, L. M. Hodgson and C. K. Williams, *Polym. Rev.*, 2008, **48**, 11-63.
71. S. Daanmark, A. Finne-Wistrand, M. Wendel, K. Arvidson, A.-C. Albertsson and K. Mustafa, *J. Bioact. Compat. Polym.*, 2010, **25**, 207-223.
72. J. Hao, P. C. Granowski and M. C. Stefan, *Macromol. Rapid Commun.*, 2012, **33**, 1294-1299.
73. B. M. Chamberlain, M. Cheng, D. R. Moore, T. M. Ovitt, E. B. Lobkovsky and G. W. Coates, *J. Am. Chem. Soc.*, 2001, **123**, 3229-3238.
74. C. K. Williams, L. E. Breyfogle, S. K. Choi, W. Nam, V. G. Young, Jr., M. A. Hillmyer and W. B. Tolman, *J. Am. Chem. Soc.*, 2003, **125**, 11350-11359.
75. J. Boerner, S. Herres-Pawlis, U. Floerke and K. Huber, *Eur. J. Inorg. Chem.*, 2007, 5645-5651.
76. S. Abbina and G. Du, *ACS Macro Lett.*, 2014, **3**, 689-692.
77. Z. Mou, B. Liu, M. Wang, H. Xie, P. Li, L. Li, S. Li and D. Cui, *Chem. Commun.*, 2014, **50**, 11411-11414.
78. Y.-L. Hsieh, Y.-C. Lin, G.-H. Lee and C.-H. Peng, *Polymer*, 2015, **56**, 237-244.
79. M. H. Chisholm, K. Choojun, J. C. Gallucci and P. M. Wambua, *Chem. Sci.*, 2012, **3**, 3445-3457.
80. A. P. Dove, V. C. Gibson, E. L. Marshall, A. J. P. White and D. J. Williams, *Dalton Trans.*, 2004, 570-578.
81. D. J. Darensbourg, W. Choi and C. P. Richers, *Macromolecules*, 2007, **40**, 3521-3523.
82. P. Degee, P. Dubois, R. Jerome, S. Jacobsen and H.-G. Fritz, *Macromol. Symp.*, 1999, **144**, 289-302.
83. N. Spassky, M. Wisniewski, C. Pluta and B. A. Le, *Macromol. Chem. Phys.*, 1996, **197**, 2627-2637.
84. Z. Zhong, P. J. Dijkstra and J. Feijen, *Angew. Chem. Int. Ed.*, 2002, **41**, 4510-4513.
85. Z. Zhong, P. J. Dijkstra and J. Feijen, *J. Am. Chem. Soc.*, 2003, **125**, 11291-11298.
86. H.-L. Chen, S. Dutta, P.-Y. Huang and C.-C. Lin, *Organometallics*, 2012, **31**, 2016-2025.
87. P. Hormnirun, E. L. Marshall, V. C. Gibson, A. J. P. White and D. J. Williams, *J. Am. Chem. Soc.*, 2004, **126**, 2688-2689.
88. E. L. Whitelaw, M. D. Jones and M. F. Mahon, *Inorg. Chem.*, 2010, **49**, 7176-7181.
89. E. L. Whitelaw, G. Loraine, M. F. Mahon and M. D. Jones, *Dalton Trans.*, 2011, **40**, 11469-11473.
90. A. Pilone, N. De Maio, K. Press, V. Venditto, D. Pappalardo, M. Mazzeo, C. Pellecchia, M. Kol and M. Lamberti, *Dalton Trans.*, 2015, **44**, 2157-2165.
91. S. L. Hancock, M. F. Mahon and M. D. Jones, *Dalton Trans.*, 2013, **42**, 9279-9285.
92. A. Pilone, K. Press, I. Goldberg, M. Kol, M. Mazzeo and M. Lamberti, *J. Am. Chem. Soc.*, 2014, **136**, 2940-2943.
93. X.-F. Yu and Z.-X. Wang, *Dalton Trans.*, 2013, **42**, 3860-3868.
94. M. Normand, T. Roisnel, J. F. Carpentier and E. Kirillov, *Chem. Commun.*, 2013, **49**, 11692-11694.
95. L. Chen, W. Li, D. Yuan, Y. Zhang, Q. Shen and Y. Yao, *Inorg. Chem.*, 2015, **54**, 4699-4708.
96. X. Pang, R. Duan, X. Li and X. Chen, *Polym. Chem.*, 2014, **5**, 3894-3900.
97. A. J. Chmura, M. G. Davidson, C. J. Frankis, M. D. Jones and M. D. Lunn, *Chem. Commun.*, 2008, 1293-1295.
98. J.-X. He, Y.-L. Duan, X. Kou, Y.-Z. Zhang, W. Wang, Y. Yang and Y. Huang, *Inorg. Chem. Commun.*, 2015, **61**, 144-148.
99. F. Della Monica, E. Luciano, G. Roviello, A. Grassi, S. Milione and C. Capacchione, *Macromolecules*, 2014, **47**, 2830-2841.
100. A. Stopper, J. Okuda and M. Kol, *Macromolecules*, 2012, **45**, 698-704.
101. A. Stopper, K. Press, J. Okuda, I. Goldberg and M. Kol, *Inorg. Chem.*, 2014, **53**, 9140-9150.

102. D. Mandal, D. Chakraborty, V. Ramkumar and D. K. Chand, *RSC Adv.*, 2016, **6**, 21706-21718.
103. E. L. Whitelaw, M. G. Davidson and M. D. Jones, *Chem. Commun.*, 2011, **47**, 10004-10006.
104. T. K. Saha, V. Ramkumar and D. Chakraborty, *Inorg. Chem.*, 2011, **50**, 2720-2722.

# 2. Dinuclear *vs* mononuclear aluminium salen complexes

## 2.1 Preamble

As explained previously, salen ligands have been extensively researched. It has been shown that rigid salen ligands complexed with aluminium can be isoselective (Spassky *et al.*).[1] Other work on salens has shown that bimetallic aluminium salen complexes can show higher activity than monometallic complexes.[2,3] For example, Normand *et al.* found that the bimetallic complex (Figure 2.01) showed a 5-fold increase in activity for the polymerisation of lactide compared to the monometallic equivalent, with the $k_{app}$ = 0.0025 $s^{-1}$ for the mononuclear complex and $k_{app}$ = 0.0122 $s^{-1}$ for the dinuclear. This increase in activity was attributed to cooperative effects between the aluminium centres, facilitated by rotation about the phenyl-phenyl bond. The Al-Al distance in the dinuclear complex was found to be 8.0 Å, however it was calculated that this distance could become as low at 2.8 Å with rotation, allowing a synergic effect between the metals. Interestingly this increase in activity was not seen for the equivalent diindium complex vs. the mononuclear, which was attributed to a different ROP mechanism for indium (activated monomer instead of coordination-insertion).

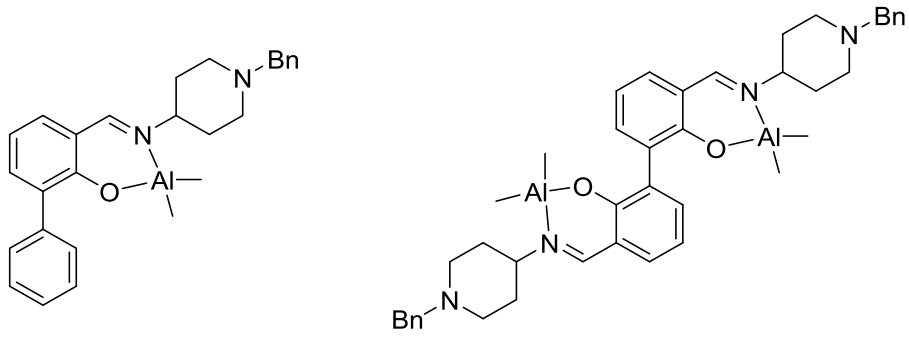


**Figure 2.01: Mononuclear and dinuclear aluminium complexes as prepared by Normand *et al.*[3]**

In this chapter, dinuclear and mononuclear aluminium Schiff-base complexes with a naphthalene backbone are synthesised and their activity and selectivity for the ring-opening polymerisation of lactide and caprolactone explored and compared. The purpose of this is to investigate to effect of a more rigid ligand on the activity different between mono- and dialuminium complexes, to determine if an Al-Al cooperative effect is possible with this system.

## 2.2 Synthesis of ligands and complexes

Previous work carried out by Jones *et al.* used salen ligands complexed with two equivalents of aluminium to form dinuclear complexes (Figure 2.02), which were then trialled for the ring-opening polymerisation of lactide.[4] It was found in this study that these initiators had no stereoselectivity for the ring-opening polymerisation of lactide, but did exhibit high activity with near full conversion reached in 2 hours. In this chapter, the effect of the two metal centres on activity is explored further and compared to analogous monometallic complexes.

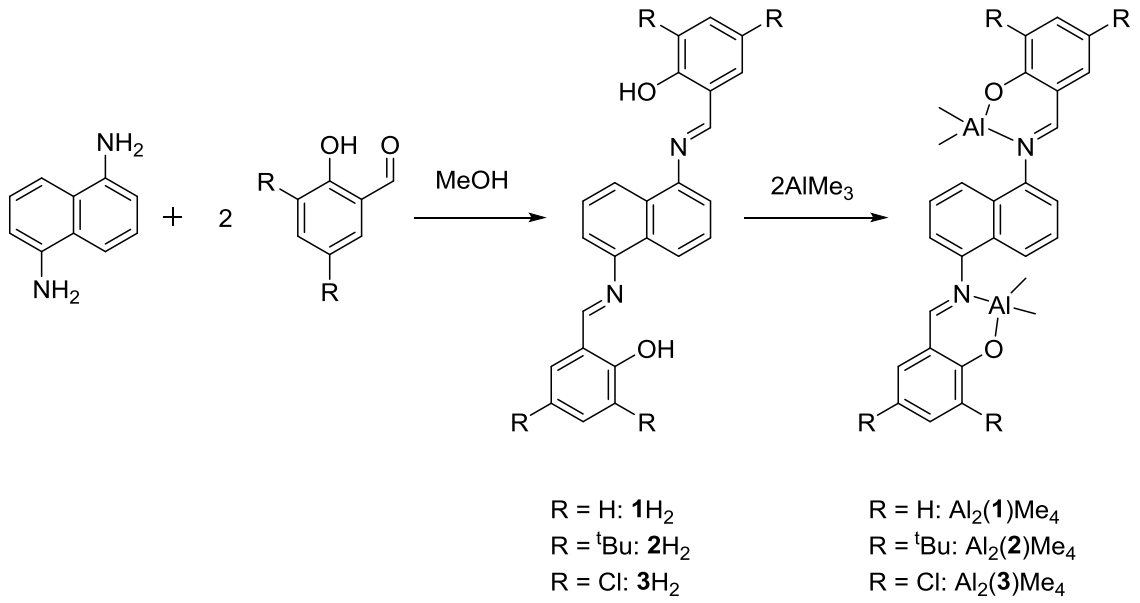


**Figure 2.02: Synthesis and structures of $Al_2$(1-3)$Me_4$**

Complexes $Al_2$(**1-3**)$Me_4$ were synthesised and crystallographic data for structures $Al_2$(**1**)$Me_4$ and $Al_2$(**2**)$Me_4$ were obtained, shown in Figures 2.03 and 2.04 respectively. Selected bond lengths and angles can be found in Table 2.01. Tau values ($\tau_4$ for four-coordinate structures) were calculated using Equation 2.1, as derived by Yang *et al.*, where α and β are the two largest angles.[5] When $\tau_4 = 0$, it has perfect square planar geometry, when $\tau_4 = 1$, there is perfect tetrahedrality.

$$\tau_4 = \frac{360 - (\alpha + \beta)}{141}$$

**Equation 2.1: Degree of tetrahedrality[5]**

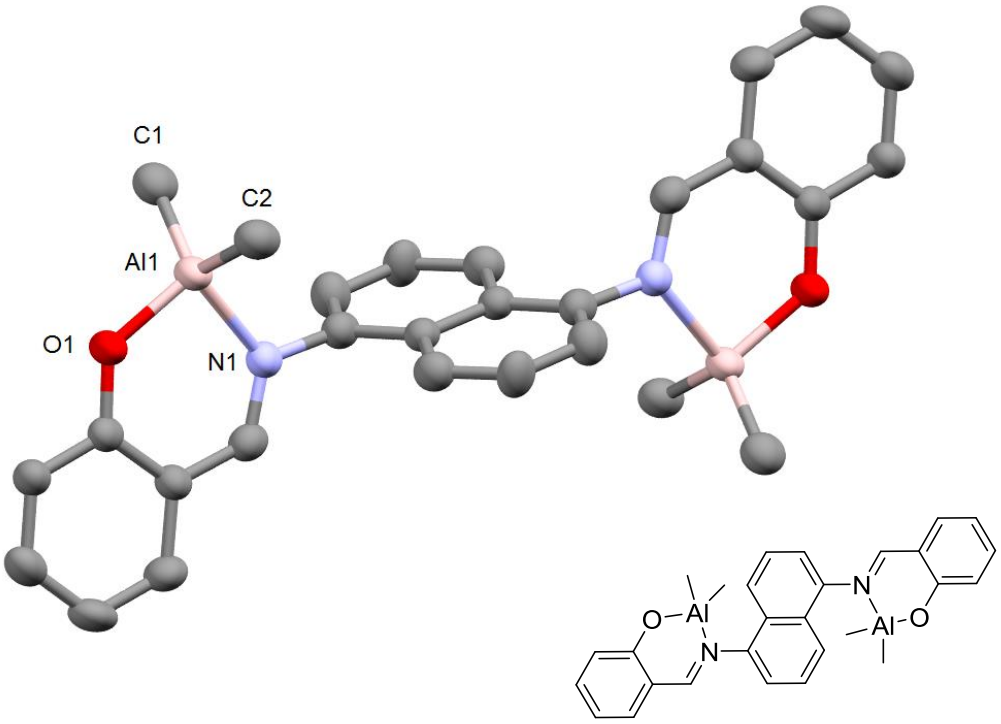


**Figure 2.03: Solid-state crystal structure of $Al_2$(1)$Me_4$. Hydrogen atoms have been omitted for clarity. Ellipsoids are shown at the 30 % probability level. One half occupied molecule of toluene was present in the asymmetric unit cell.**

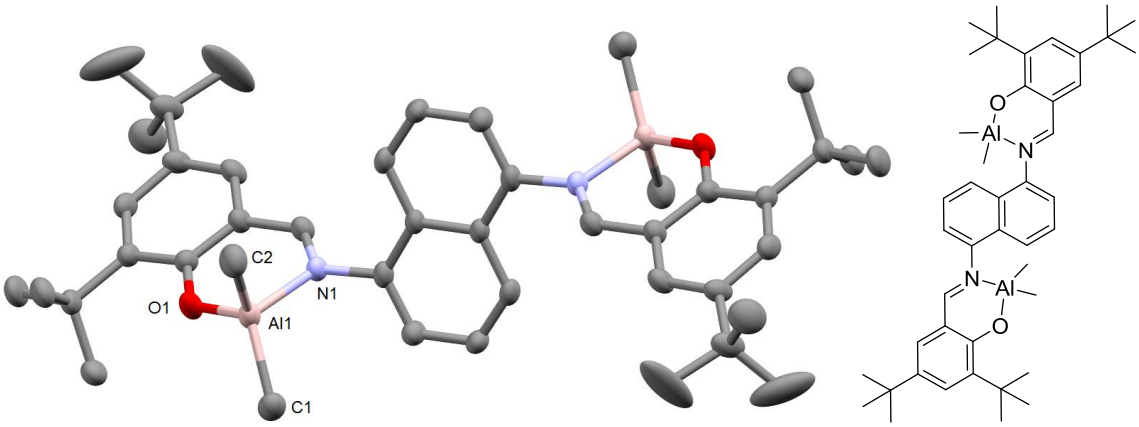


**Figure 2.04: Solid-state crystal structure for $Al_2$(2)$Me_4$. Hydrogen atoms have been omitted for clarity. Ellipsoids are shown at the 30 % probability level.**

Figure 2.05 shows complex **I**, a dinuclear complex synthesised by Cui *et al.* which has a similar structure to the complexes above and has been included in Table 2.01 for comparison.[6] In both complexes the aluminium metal centre has slightly distorted tetrahedral geometry ($\tau_4$ = 0.91 for $Al_2$(**1**)$Me_4$, $\tau_4$ = 0.90 for $Al_2$(**2**)$Me_4$), as exemplified by bond angles for N-Al-C1, which is 109.44(14)° for $Al_2$(**1**)$Me_4$ and 111.08(11)° for $Al_2$(**2**)$Me_4$ and for O-Al-C1, 111.16(14)° and 110.63(11)°. However, significant distortion in the N-Al-O angles, which are 94.07(10)° and 93.66(8)° respectively, appears to be a result of the steric environment imposed by the rigidity

of the ligand. Bond lengths Al-O are 1.777(2) Å and 1.772(2) Å respectively, and Al-N are 1.965(3) Å and 1.960(3) Å. These are comparable to previously reported values for **I**, with Al-O as 1.774(2) Å and Al-N as 1.969(3) Å.

**Table 2.01: Selected bond angles (°) and lengths (Å) for $Al_2(1)Me_4$ and $Al_2(2)Me_4$**

| | $Al_2(1)Me_4$ | $Al_2(2)Me_4$ | **I** |
|---|---|---|---|
| **Al-O1** | 1.777(2) | 1.772(2) | 1.774(2) |
| **Al-N1** | 1.965(3) | 1.960(3) | 1.969(3) |
| **Al-C1** | 1.950(4) | 1..952(3) | 1.939(4) |
| **Al-C2** | 1.966(4) | 1.955(3) | 1.950(4) |
| **N1-Al-O1** | 94.07(10) | 93.66(8) | 93.8(1) |
| **N1-Al-C1** | 109.44(14) | 111.08(11) | 107.7(2) |
| **O1-Al-C1** | 111.16(14) | 110.63(11) | 111.4(2) |
| **O1-Al-C2** | 112.01(14) | 113.37(11) | 112.2(1) |

In **I**, the two aluminium centres are adjacent, facing the same direction, unlike $Al_2$(**1**)$Me_4$ and $Al_2$(**2**)$Me_4$ where the two metal centres are facing away from one another. The calculated Al-Al distance for **I** is 7.914 Å, whereas it is 8.772 Å and 8.968 Å for $Al_2$(**1**)$Me_4$ and $Al_2$(**2**)$Me_4$ respectively, a difference caused by the larger backbone, creating more distance between the two metal centres.

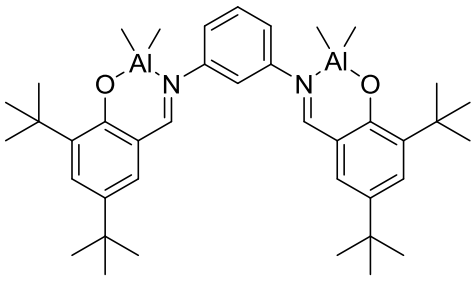


**I**

**Figure 2.05: Bimetallic aluminium complex reported by Cui *et al.*[6]**

**Figure 2.06** shows the $^1$H NMR spectrum of $Al_2$(**1**)$Me_4$, which confirms solid-state structure retention in solution. This is evidenced by the aluminium methyl resonances, which show as broad singlets (overlapping slightly) at -0.39 and -0.30 ppm. The imine resonance can also be seen at 7.31 ppm, which has an integral of 2H.

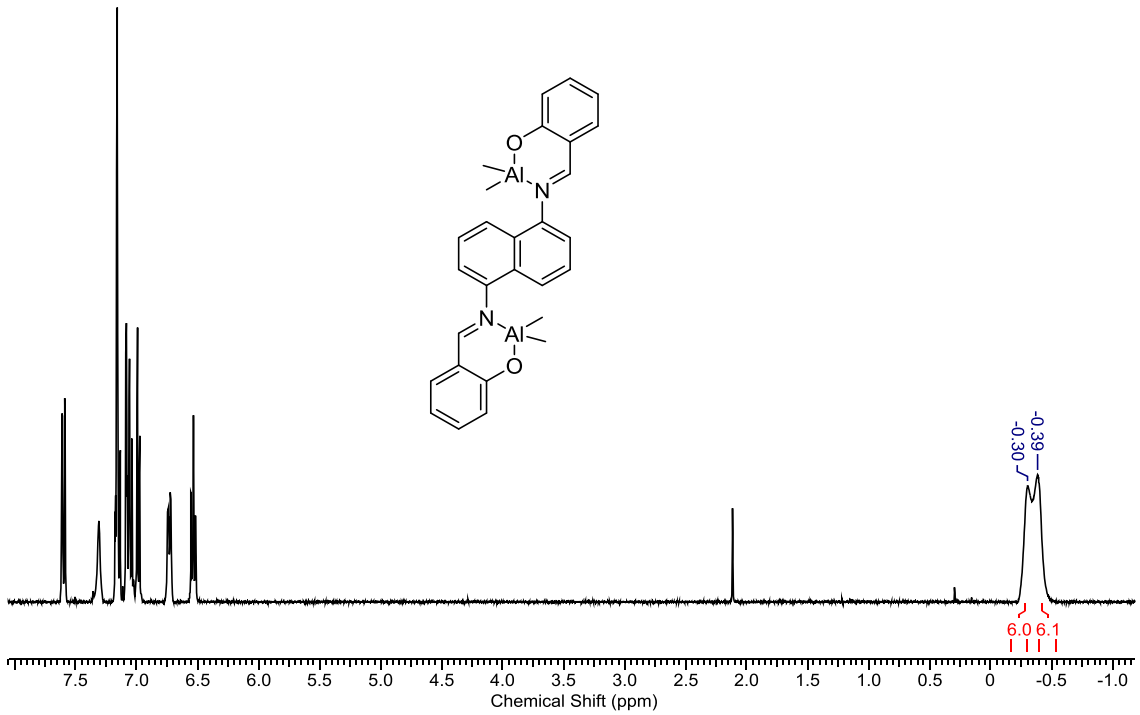


**Figure 2.06: $^{1}$H NMR spectrum of $Al_2$(1)$Me_4$ in $C_6D_5CD_3$**

To follow on from this research, further investigation was carried out using initiators with only one aluminium centre, to compare activities and polymerisation results of mononuclear aluminium complexes against the dinuclear examples. Figure 2.07 shows the synthetic routes to these complexes. The complexes were synthesised in the same method as the previous ligands, *via* an imine condensation between 1-aminonaphthalene and a substituted salicylaldehyde, followed by complexation by addition of trimethylaluminium. All initiators were characterised by $^{1}$H, $^{13}$C{$^{1}$H} NMR spectroscopy, elemental analysis and where possible, X-ray crystallography. The monomeric ligands will have the same steric and electronic effects around the aluminium centre as the dimers, the only difference between them will be the number of Schiff-base aluminium moieties. This will facilitate an investigation into the difference between the monomeric and dimeric complexes.

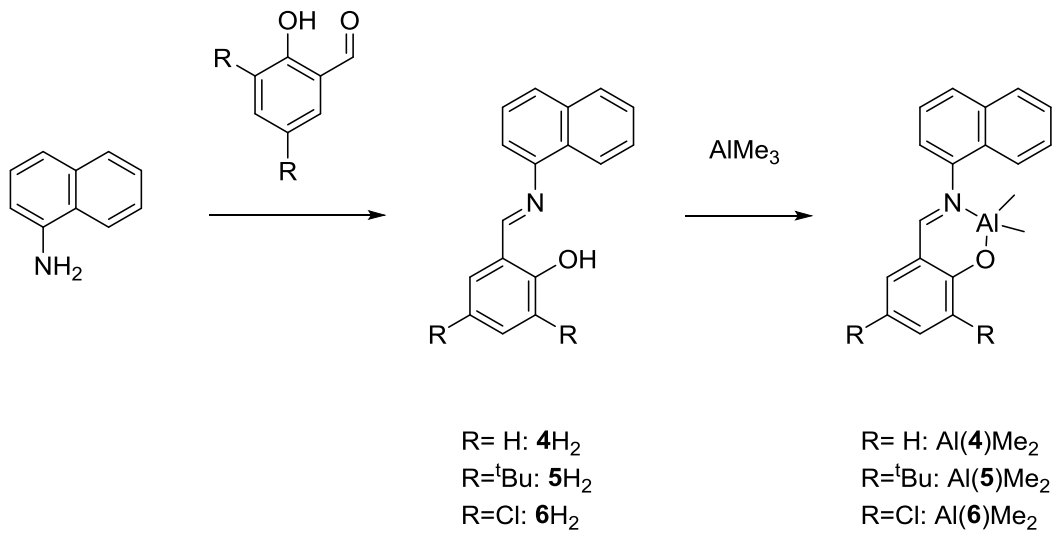


**Figure 2.07: Synthesis of Al(4-6)Me$_2$.**

Figure 2.08 shows the proton NMR spectrum of ligand **4**H$_2$. Due to the aromaticity of the ligand, the resonances all appear above 6.5 ppm. The evidence for ligand formation is the characteristic N=CH imine singlet resonance at 8.72 ppm. The Ar-OH resonance can be seen at 13.40 ppm as a broad singlet.

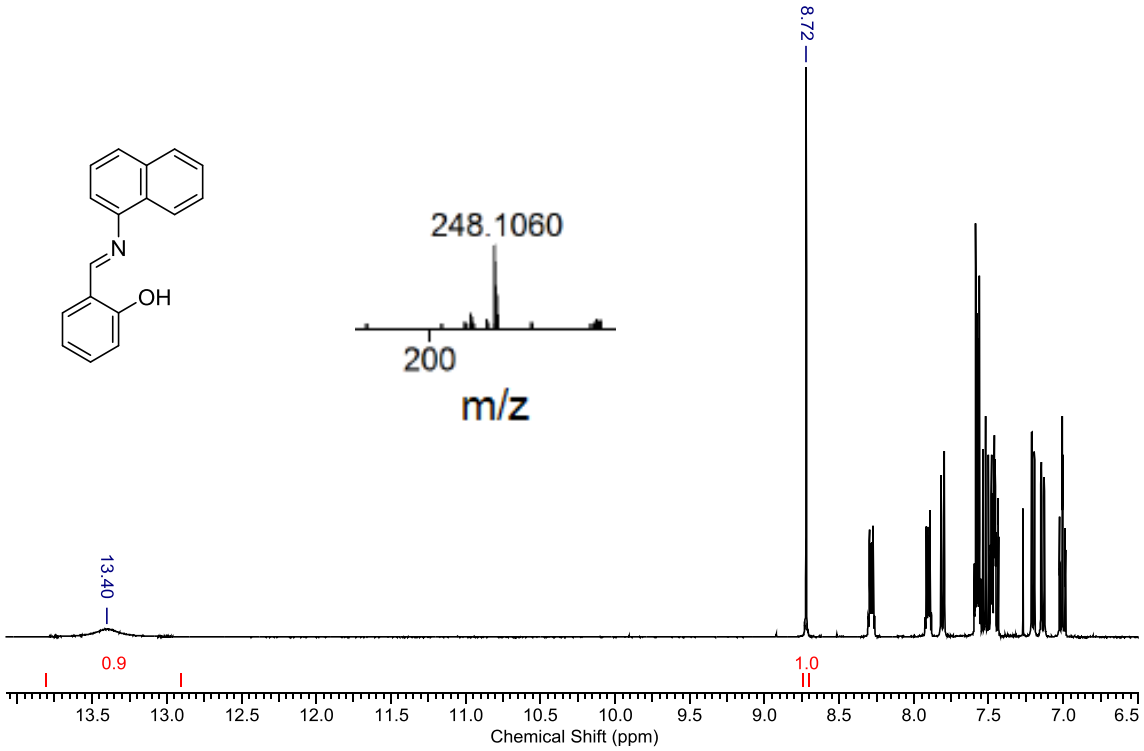


**Figure 2.08: $^1$H NMR and mass spectrum of 4H$_2$ in CDCl$_3$**

Figures 2.09 and 2.10 show the solid-state structures of Al(**4**)$Me_2$ and Al(**6**)$Me_2$ respectively, and selected bond angles and lengths are found in Table 2.02. Alongside is the data for a similar Schiff base aluminium complex **II** reported by Lewinski *et al.*, shown in Figure 2.11.[7] This is a comparable structure to Al(**4**)$Me_2$, the only difference is the naphthyl group is replaced by a phenyl.

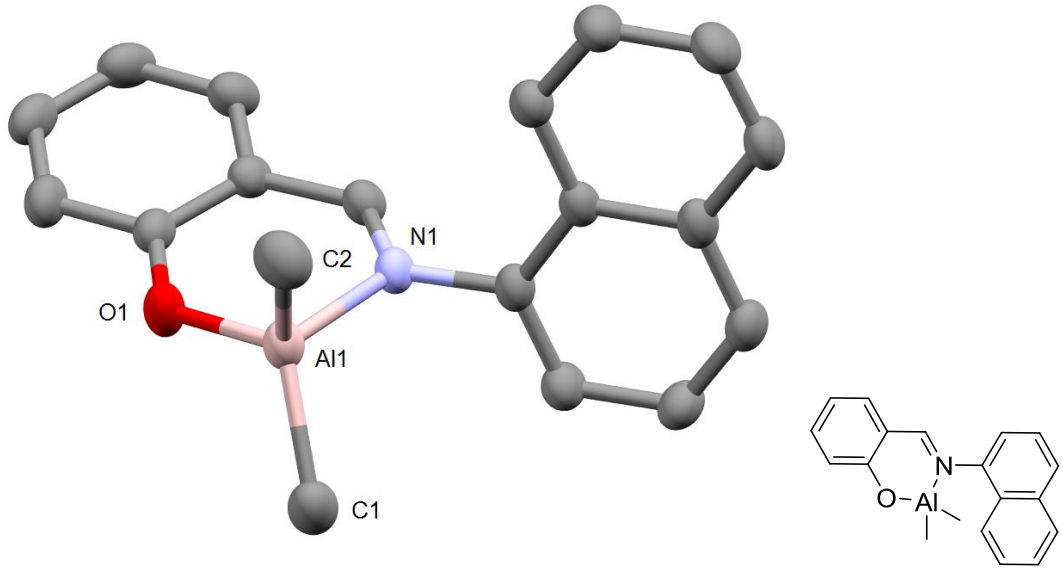


**Figure 2.09: Solid-state crystal structure for Al(4)$Me_2$. Hydrogen atoms have been omitted for clarity. Ellipsoids are shown at the 30 % probability level.**

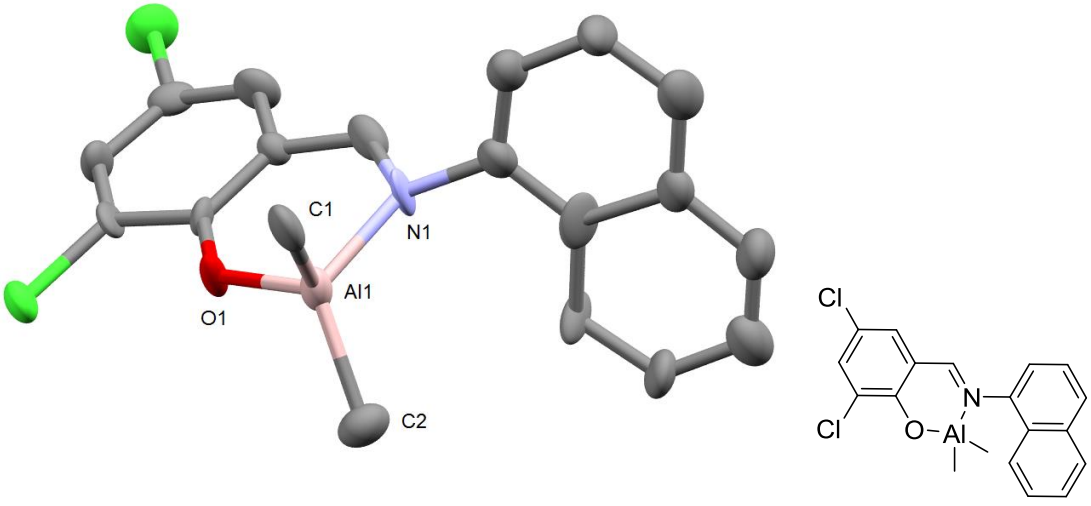


**Figure 2.10: Solid-state crystal structure for Al(6)$Me_2$. Hydrogen atoms have been omitted for clarity. Ellipsoids are shown at the 30 % probability level.**

**Table 2.02: Selected bond angles (°) and lengths (Å) for Al(4)$Me_2$ and Al(6)$Me_2$**

| | Al(4)$Me_2$ | Al(6)$Me_2$ | **II** |
|---|---|---|---|
| **Al-O** | 1.7719(12) | 1.778(8) | 1.7724(19) |
| **Al-N** | 1.9591(14) | 1.994(10) | 1.963(2) |
| **Al-C1** | 1.953(2) | 1.939(15) | 1.943(3) |
| **Al-C2** | 1.956(2) | 1.945(14) | 1.946(3) |
| **N-Al-O** | 95.20(6) | 94.6(4) | 95.14(9) |
| **N-Al-C1** | 109.87(8) | 105.9(5) | 110.1(1) |
| **O-Al-C1** | 112.80(8) | 111.1(5) | 109.6(1) |
| **O-Al-C2** | 111.07(8) | 109.8(6) | 112.5(1) |

The bond lengths and angles observed in these complexes are typical for aluminium salen complexes,[6,7] for example the N-Al-O bond is 95.14(9) for **II**, 95.20(6) for Al(**4**)$Me_2$ and 94.6(4) for Al(**6**)$Me_2$. The metal centres have distorted tetrahedral geometry ($\tau_4$ = 0.90 for Al(**4**)$Me_2$, $\tau_4$ = 0.91 for Al(**6**)$Me_2$), exemplified by the bond angles N-Al-C1 which are 109.87(8)° for Al(**4**)$Me_2$ and 105.9(5)° for Al(**6**)$Me_2$ and the angles O-Al-C1, which are 112.80(8)° and 111.1(5)° respectively. Once again, some strain occurs at the N-Al-O angles, 95.20(6)° and 94.6(4)° due to ligand rigidity. The bond distances for Al-O and Al-N correspond with literature values mentioned in Table 2.02.[7] There is some minor elongation on the Al-N bond for Al(**6**)$Me_2$ which is 1.994(10) Å, an increase of 0.035 Å compared to the Al-N bond length for Al(**4**)$Me_2$. The bond angle N-Al-C1 is approximately 4° smaller in Al(**6**)$Me_2$, which suggests that the chloro groups contribute to the distortion away from an ideal tetrahedral geometry.

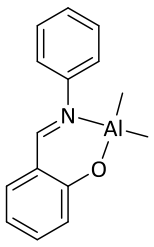


**II**

**Figure 2.11: Literature compound II[7]**

In summary, all the solid-state structures described above are similar to one another, each featuring one or two distorted tetrahedral aluminium centres, coordinated to two alkyl groups, one imine nitrogen and one phenolate oxygen.

Figure 2.12 and 2.13 shows the $^{1}$H NMR spectra of Al(**5**)$Me_2$ and Al(**6**)$Me_2$ respectively, the solid-state structure, is retained in solution for both complexes. The resonance at -0.37 ppm in Figure 2.12 has an integration of 6H and corresponds to the Al-$(Me)_2$ protons, which shows that the salen-aluminium complex has indeed successfully been formed. Interestingly, only one Al-Me resonance is present, which shows that the two methyl groups on the same aluminium atom are chemically equivalent. In the spectrum for $Al_2$(**1**)$Me_4$, two aluminium methyl resonances appeared, which suggests that the methyls on the two metal centres in the dinuclear complex are in slightly different chemical environments. The complexes were also characterised by elemental analysis, results were all found to be in agreement with the expected values, indicating high purity.

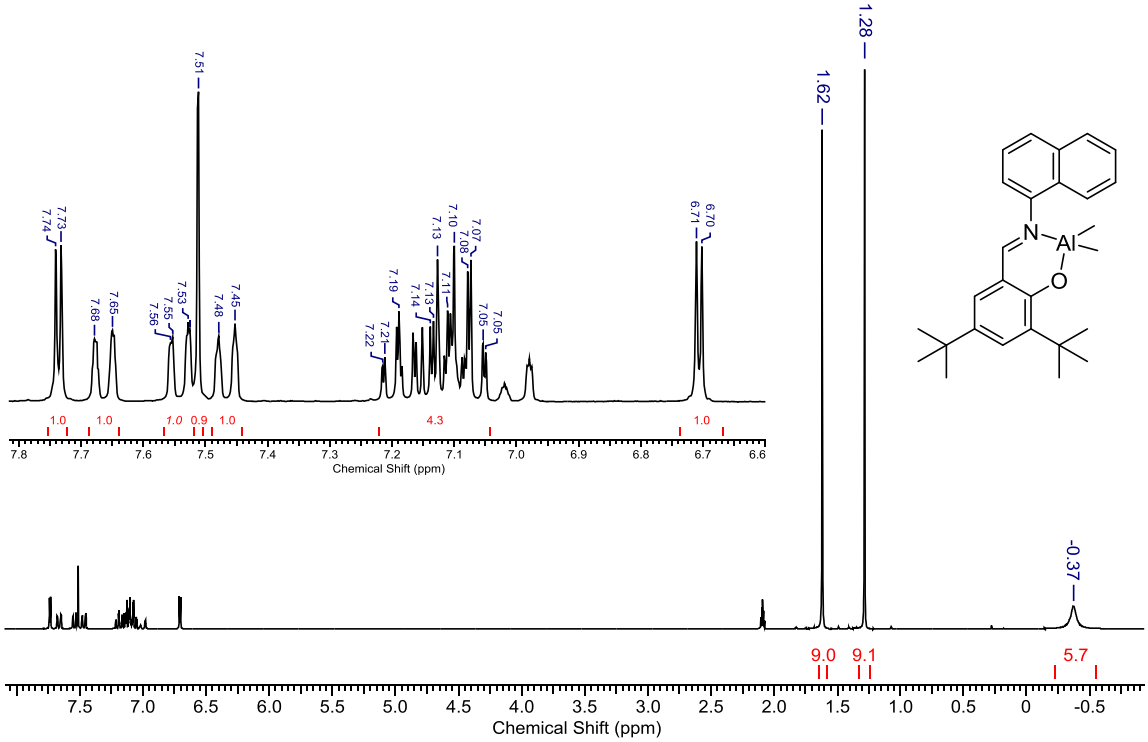


**Figure 2.12: $^{1}$H NMR spectrum of Al(5)$Me_2$ in $C_6D_5CD_3$. Inset: zoom of aromatic region.**

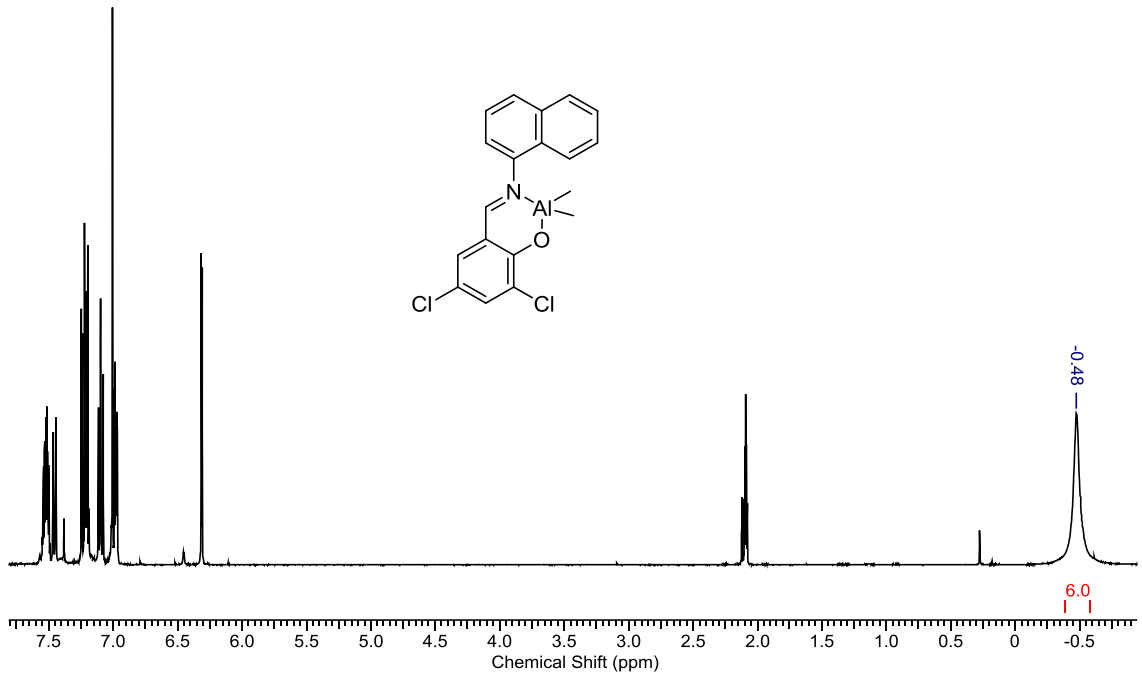


**Figure 2.13: $^{1}$H NMR spectrum of Al(6)Me$_2$ in $C_6D_5CD_3$**

In summary, a series of dinuclear and mononuclear aluminium salen complexes with a naphthalene backbone were successfully synthesised and fully characterised by $^{1}$H, $^{13}$C{$^{1}$H} NMR spectroscopy, elemental analysis and where possible, X-Ray crystallography. These complexes were taken forward for polymerisation studies to investigate the effect of the ligand on metal centre cooperative effects.

## 2.3 Polymerisation results

Table 2.03 shows initial data for polymerisations carried out using initiators Al(**4-6**)$Me_2$. Each polymerisation was carried out in toluene at 80 °C, with benzyl alcohol (BnOH) used as a co-initiator.

$$Calculated\ M_n = (conversion * 144 * Lactide{:}Initiator{:}BnOH) + 108$$

**Equation 2.2**

Equation 2.2 is used to calculate an expected value for the number average molecular weight. The 144 $gmol^{-1}$ value refers to the molecular mass of lactide and 108 $gmol^{-1}$ is the molecular mass of benzyl alcohol, which is expected to be incorporated as the end group if the reaction proceeds *via* a coordination-insertion mechanism. In column 10, a correction factor has been applied to the observed $M_n$. This is due to the GPC analysis by refractive index, which is calibrated against a polystyrene external standard. As polystyrene and polylactide have different viscosities and different hydrodynamic radii, the value measured for $M_n$ by refractive index requires correction for this difference. This is done by multiplying the observed value by 0.58 (see column labelled $M_n$ corr for the corrected values).[8]

**Table 2.03: Polymerisation data for Al(4-6)$Me_2$ in toluene at 80 °C. (1) determined by homonuclear decoupled NMR (2) determined by equation 2.2 (3) determined by GPC**

| Entry | Initiator | LA:I | BnOH | Conversion (%) | Time (h) | $P_r$[1] | $M_n$ calc[2] ($gmol^{-1}$) | $M_n$[3] ($gmol^{-1}$) | $M_n$ corr ($gmol^{-1}$) | PDI[3] |
|---|---|---|---|---|---|---|---|---|---|---|
| **1** | Al(**4**)$Me_2$ | 50:1 | 1 | 94 | 3 | 0.50 | 6,900 | 9,600 | 5,550 | 1.26 |
| **2** | | 100:1 | 1 | 97 | 6 | 0.50 | 14,100 | 18,650 | 10,800 | 1.57 |
| **3** | | 200:1 | 1 | 96 | 24 | 0.48 | 27,800 | 37,350 | 21,650 | 1.61 |
| **4** | | 300:1 | 1 | 79 | 24 | 0.50 | 34,200 | 40,500 | 23,500 | 1.21 |
| **5** | | 400:1 | 1 | 97 | 48 | 0.50 | 56,100 | 90,950 | 52,750 | 1.44 |
| **6** | | 200:1 | 2 | 95 | 24 | 0.48 | 13,850 | 23,650 | 13,700 | 1.37 |
| **7** | | 200:1 | 4 | 95 | 24 | 0.48 | 6,950 | 12,350 | 7,150 | 1.33 |
| **8** | Al(**5**)$Me_2$ | 100:1 | 1 | 92 | 24 | 0.44 | 13,350 | 16,800 | 9,750 | 1.48 |
| **9** | Al(**6**)$Me_2$ | 100:1 | 1 | 98 | 24 | 0.45 | 14,200 | 18,700 | 10,850 | 1.94 |

Al(**4**)$Me_2$ has not shown any selectivity for the ROP of *rac*-lactide, as the $P_r$ values are close to or exactly 0.50, indicating atacticity. Figure 2.14 shows the proton homonuclear decoupled NMR spectrum of the methine region for the polymer from entry 3 in Table 2.03. The atacticity is evident from the 1:1:1:3:2 distribution of the tetrad resonances. The PDI values of the polymers indicate relatively poor molecular weight control for these mononuclear complexes, when compared to results using $Al_2$(**1**)$Me_4$, where the PDIs were 1.10 or less.[4] When looking at the corrected molecular weight value for the polymerisations, they correlate well with the calculated molecular weight. This is good evidence for polymerisation *via* a coordination-insertion mechanism. When the amount of benzyl alcohol is doubled, it is expected that the molecular weight would halve, as there are twice as many alkoxide groups available for insertion into lactide. This appears to be the case, exemplified in entries 6 and 7 in Table 2.03 where the corrected molecular weights align with the expected molecular weight. For Al(**5**)$Me_2$ and Al(**6**)$Me_2$, longer reaction times (24 hours) were required to reach high conversions at 100:1 loading. This is due to the substituents on the ligand providing steric bulk to coordination of the metal centre to the lactide. The $P_r$ values were lower than seen for Al(**4**)$Me_2$, 0.44 for Al(**5**)$Me_2$ and 0.45 for Al(**6**)$Me_2$, but not significantly so. Ultimately, no stereoselectivity is seen for any of these initiators, regardless of the *ortho* and *para* substituents. This is unsurprising, as previous research utilising dinuclear aluminium initiators for the ROP of *rac*-lactide also showed no selectivity. For example, aluminium(III) imine bis(phenolate) complexes reported by Forder and Jones were found to produce atactic PLA, with $P_r$ values between 0.45-0.56.[9]

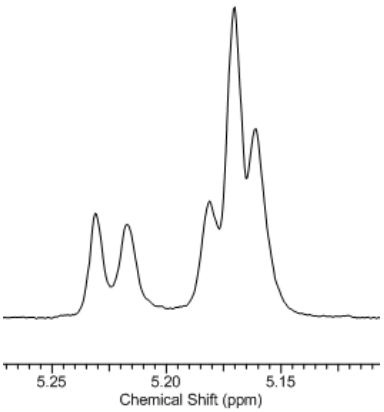


**Figure 2.14: $^1$H homonuclear decoupled NMR spectrum of polymer in Table 2.03 Entry 3, zoomed into methine proton region**

Previous work on the initiator $Al_2$(**1**)$Me_4$ had shown that the polymerisation reaction was well controlled, producing atactic PLA ($P_r$ = 0.5) with narrow PDI values (1.05-1.10) when using two equivalents benzyl alcohol as a coinitiator.[4] To investigate this mechanism further, polymerisations were carried out with only one equivalent benzyl alcohol, and also without any

coinitiator at all, to determine the effect of the coinitiator. The results can be found in Table 2.04. For comparison, the previously reported polymerisation data has been included in entries 1-3.

**Table 2.04: Polymerisation data for $Al_2(1)Me_4$ in toluene at 80 °C. (1) Reported previously by Jones *et al.*[4] (2) determined by homonuclear decoupled NMR (3) determined by equation 2.2 (4) determined by GPC**

| Entry | LA:I | BnOH | Conversion (%) | Time (h) | $P_r$[2] | $M_n$ calc[3] ($gmol^{-1}$) | $M_n$[4] ($gmol^{-1}$) | $M_n$ corr ($gmol^{-1}$) | PDI[4] |
|---|---|---|---|---|---|---|---|---|---|
| 1[1] | 100 | 2 | 97 | 2 | 0.50 | 7,097 | 6,450 | 3,750 | 1.10 |
| 2[1] | 200 | 2 | 98 | 24 | 0.50 | 14,158 | 11,700 | 6,800 | 1.07 |
| 3[1] | 400 | 2 | 25 | 24 | 0.50 | 7,313 | 5,100 | 2,950 | 1.05 |
| 4 | 100 | 1 | 57 | 2 | 0.47 | 4,193 | 9,100 | 5,300 | 1.08 |
| 5 | 200 | 1 | 79 | 6 | 0.51 | 11,521 | 34,350 | 19,900 | 1.15 |
| 6 | 400 | 1 | 93 | 22 | 0.51 | 26,767 | 94,750 | 54,950 | 1.45 |
| 7 | 100 | 0 | 32 | 24 | 0.47 | 2,378 | 27,600 | 16,000 | 1.20 |
| 8 | 200 | 0 | 29 | 24 | 0.49 | 4,215 | 57,100 | 33,100 | 1.12 |
| 9 | 400 | 0 | 21 | 24 | 0.47 | 6,045 | 39,650 | 23,000 | 1.16 |

The results in Table 2.04 show that the addition of benzyl alcohol, as expected, has a significant effect on the reaction. For polymerisations using one equivalent of the coninitiator, the observed $M_n$ values are higher than the calculated values, which is likely to be caused by only one metal centre 'activated' to the Al-OBn required for a coordination insertion, effectively halving the initiator concentration. Although lower, even the corrected values still remain higher than the calculated values, in particular for entry 6, Table 2.04 where the corrected value is approximately half the expected molecular weight. For the polymerisations carried out with no BnOH (entries 7-9), the molecular weights were much higher than predicted. This suggests that the $k_{prop} >> k_{init}$, indicating an uncontrolled polymerisation. Initiation is presumably achieved by trace water or lactic acid impurities in the monomer, leading to unpredictable $M_n$ values. This highlights the need for an aluminium alkoxide in this system for a well-controlled polymerisation. More evidence for this is the requirement for greatly extended reaction times with poorer conversions. However, the PDI values for entries 7-9 remain relatively narrow, indicating that on initiation the polymerisation runs smoothly. Figure 2.15 shows the MALDI-ToF

spectrum of the polymer from Table 2.04, entry 1, as previously reported by Jones *et al*.[4] The repeat unit is 72 gmol$^{-1}$, which indicates that the polymer has transesterified. Figure 2.16 shows the theoretical and observed isotope pattern for the sodiated ion of a lactide chain with 26 units, with a benzyl end group. The observed pattern correlates well with the expected pattern, indicating that benzyl alcohol is the end group. This indicates that the initiator undergoes a coordination-insertion mechanism.

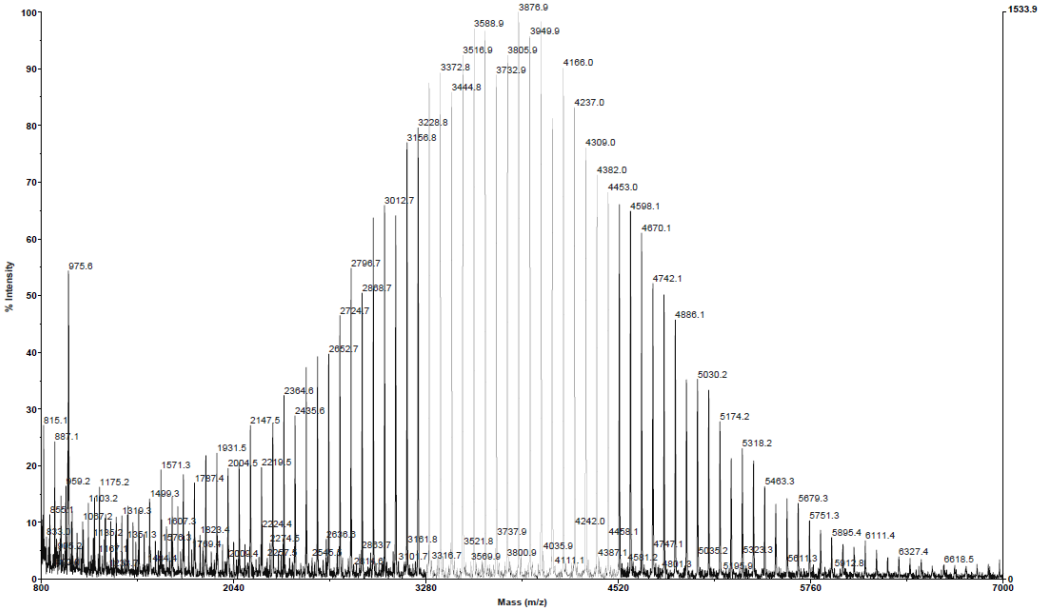


**Figure 2.15: MALDI-ToF spectrum of polymer from Table 2.04, entry 1.[4]**

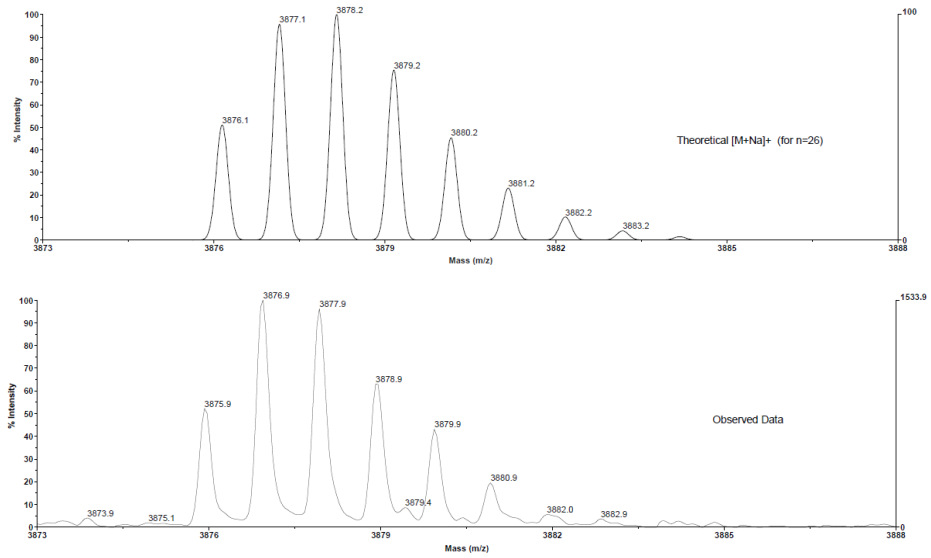


**Figure 2.16: Theoretical and observed isotope pattern for benzyl alcohol end group of polymer from Table 2.04, entry 1.[4]**

## 2.4 Kinetic study of dinuclear and mononuclear complexes

A kinetic study was carried out to compare the activity of the monometallic species to the bimetallic structures. $Al_2$(**1**)$Me_4$ has previously showed high activity, with a $k_{app}$ of 8.3 x $10^{-3}$ $min^{-1}$ at 100:1:2 lactide to initiator to BnOH loading. A kinetic study was carried out on the monometallic complex, Al(**4**)$Me_2$. The ring-opening polymerisation is expected to be a pseudo first order reaction, as the initiator takes part in the reaction. Equation 2.3 shows how to calculate $k_{app}$, the rate constant. In this case, [A] is the concentration of monomer, and $k_{app}$ is equal to k[cat].

$$rate = \frac{-d[A]}{dt} = k[cat][A]$$

$$k[cat] = k_{app}, thus:$$

$$\boldsymbol{rate = k_{app}[A]}$$

**Equation 2.3**

The kinetic experiment was carried out in an NMR tube equipped with a Young's tap, heated to 80 °C inside the spectrometer, recording spectra at regular intervals. The benefit to this method is that it is consistent and allows for a good comparison between the $k_{app}$ values determined using this method. This method has some flaws, as the solution cannot be stirred and the tube is narrow. As the polymer chains propagate the viscosity of the solution increases, which affects the reaction rate as it becomes increasingly difficult for the initiator to coordinate with lactide. There is also a delay between sample preparation (at room temperature) and loading of sample into the spectrometer. As such, the lines may appear to intersect the y-axis, when in reality they should intersect at the origin (0 % conversion at t = 0).

Figure 2.17 shows the conversion of 0.58 M *rac*-lactide in $d_8$-toluene with time, using 50:1:1 loading of lactide to Al(**4**)$Me_2$ to benzyl alcohol. As the conversion reaches 100 %, the curve levels. This is due to the increasing viscosity of the sample impeding coordination of lactide to initiator, and also due to the rate decreasing as the lactide concentration increases. Figure 2.18 shows the first order rate plot for this polymerisation, which can be used to calculate $k_{app}$ as shown by Equation 2.3. From the gradient of the graph, the $k_{app}$ value is 0.0081 $min^{-1}$.

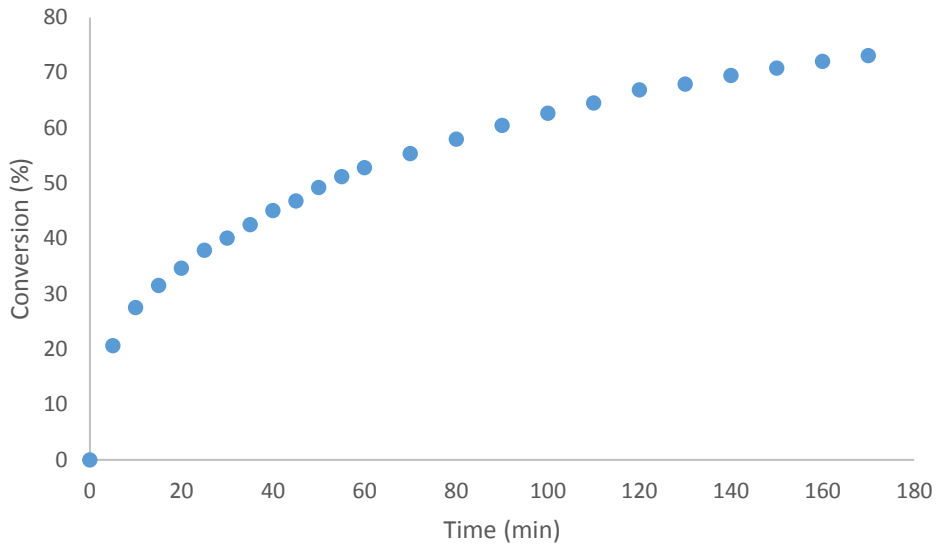


**Figure 2.17: Conversion of *rac*-lactide (0.58 M) into polylactide at 80 °C in toluene against time, with 50:1:1 lactide to Al(4)Me$_2$ to benzyl alcohol.**

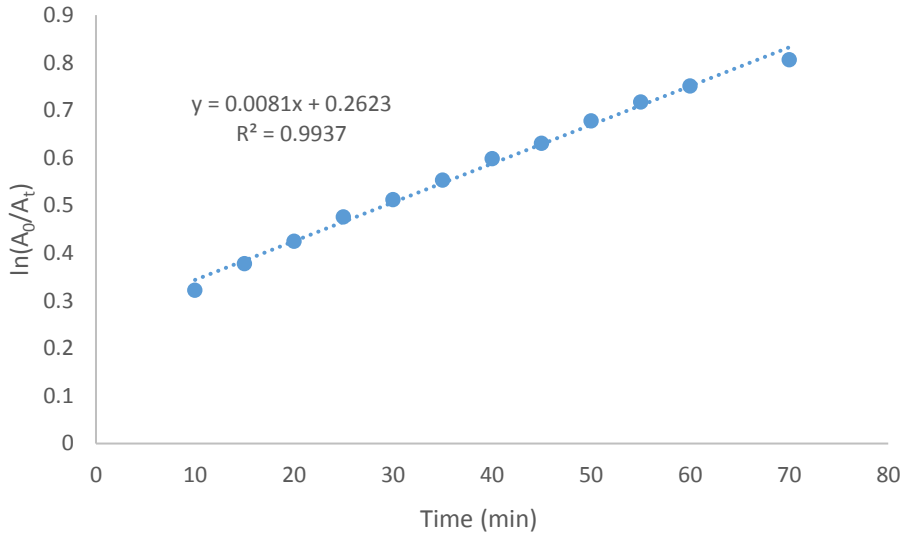


**Figure 2.18: First order rate plot for ring-opening polymerisation of 0.58 M *rac*-lactide in toluene at 80 °C using 50:1:1 lactide to Al(4)Me$_2$ to benzyl alcohol.**

As the dinuclear complexes contain two aluminium centres, the polymerisation mixture effectively contains twice the concentration of initiating centres than the concentration of initiator. As such, it would be more appropriate to compare the activity of Al(**4**)Me$_2$ at half the loading of Al$_2$(**1**)Me$_4$, as the aluminium concentration is the same. The $k_{app}$ for Al$_2$(**1**)Me$_4$ at 100:1:2 is 0.0083 min$^{-1}$, which is the same (within error) as the value of 0.0081 min$^{-1}$ found for Al(**4**)Me$_2$ a 50:1:1. The fact that the $k_{app}$ values are so close differs from the observation made by Normand *et al.*, who found that bimetallic aluminium salen complexes had $k_{app}$ values that

were 5-10 fold more active than equivalent mononuclear complexes. For example, they found that at 110 °C the mononuclear complex had a $k_{app}$ of 0.15 $min^{-1}$, and the dinuclear complex had a $k_{app}$ of 0.732 $min^{-1}$ under the same conditions.[3] They argue that the flexibility of the backbone allows the metal centres to approach each other closely and cooperate in the ROP of lactide. However in the case of complexes $Al_2$(**1-3**)$Me_4$ there is no flexibility or rotation about the naphthalene backbone, so the aluminium metal centres cannot come into close proximity of one another, thus preventing a cooperative effect. The results herein therefore support those of Normand *et al.*, that the flexibility of the ligand in a dinuclear system is of paramount importance.

Figure 2.19 shows a series of kinetic experiments using $Al_2$(**1**)$Me_4$ run at different monomer to initiator concentrations, 100:1, 200:1 and 400:1, and with one or two equivalents of benzyl alcohol. As would be expected, the activity and thus the first order rate constant increases with increasing initiator concentration.

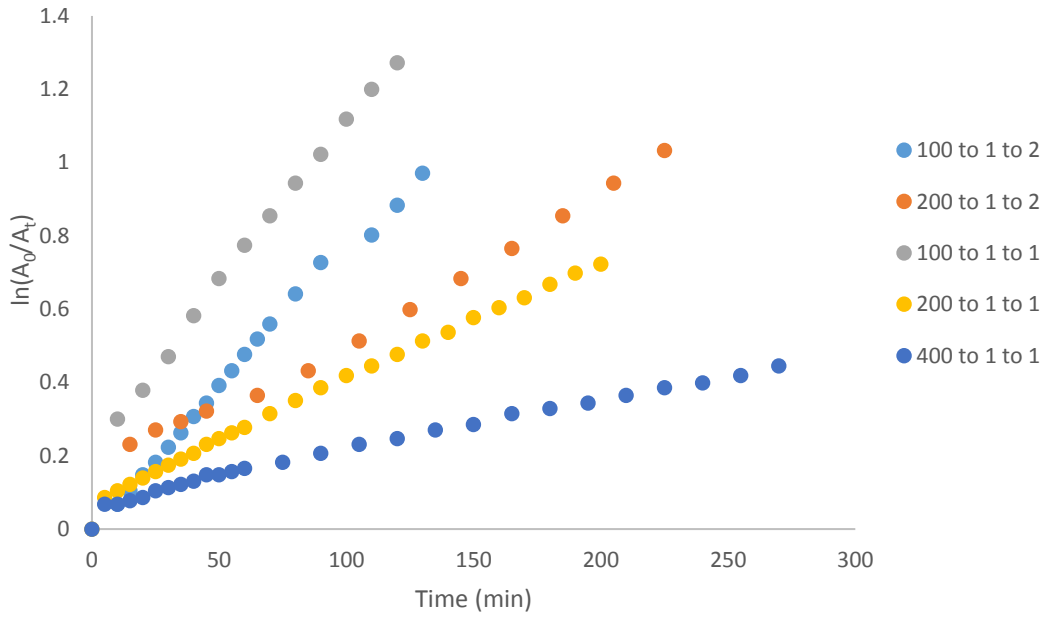


**Figure 2.19: Dinuclear kinetic series of the ROP of *rac*-lactide (0.58 M) at 80 °C in toluene against time using $Al_2$(1)$Me_4$ at different lactide:initiator:BnOH loadings**

Table 2.05 shows the $k_{app}$ values for these kinetic experiments. The rate constants at the same initiator loading but different benzyl alcohol amounts are comparable, showing that this does not have a profound effect on the activity. For example, at 200:1:1 the $k_{app}$ is 3.3 x $10^{-3}$ $min^{-1}$ and at 200:1:2 it is 3.8 x $10^{-3}$ $min^{-1}$. The ratio of lactide to aluminium is effectively half of the lactide to initiator ratio, this has been included in the table for clarity.

**Table 2.05: $k_{app}$ values for the ROP of *rac*-lactide (0.58 M) at 80 °C in toluene using $Al_2(1)Me_4$ at different initiator concentrations, including standard error by linear regression and $R^2$ values.**

| LA:I:BnOH | Lactide:Al | $k_{app}$ (x $10^{-3}$ $min^{-1}$) | Standard error | $R^2$ |
|---|---|---|---|---|
| 100:1:1 | 50 | 9.0 | 1.18 x $10^{-4}$ | 0.998 |
| 200:1:1 | 100 | 3.3 | 2.10 x $10^{-5}$ | 0.999 |
| 400:1:1 | 200 | 1.4 | 2.19 x $10^{-5}$ | 0.983 |
| 50:1:2 | 25 | 17.0 | 3.57 x $10^{-4}$ | 0.995 |
| 100:1:2 | 50 | 8.3 | 4.45 x $10^{-5}$ | 0.994 |
| 200:1:2 | 100 | 3.8 | 1.04 x $10^{-4}$ | 0.991 |

Figure 2.20 shows the ln(k) vs ln[I] plot for $Al_2$(**1**)$Me_4$ with one and two equivalents of benzyl alcohol. In each case, the gradient of the line of best fit is approximately one, indicating a first-order reaction with respect to initiator, as expected.

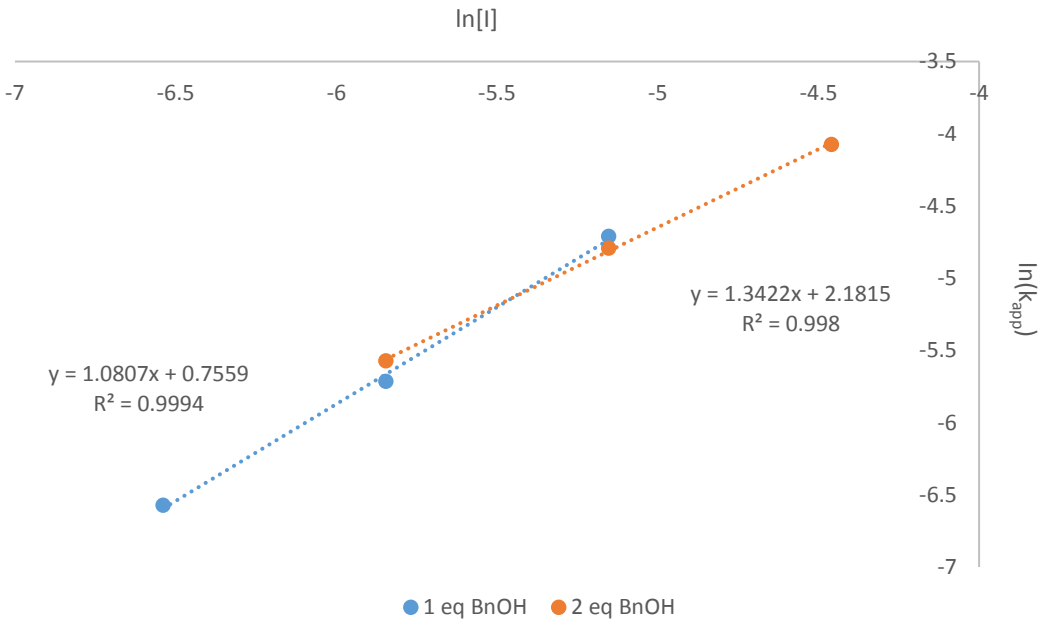


**Figure 2.20: Logarithmic order plot for ROP of lactide using $Al_2(1)Me_4$**

Figure 2.21 shows the series of kinetic experiments using Al(**4**)$Me_2$ performed at different monomer to initiator concentrations, 50:1, 100:1, 200:1 and 400:1. In every case, one equivalent of benzyl alcohol was used as there is only one metal centre per initiator. Any additional benzyl alcohol is expected to act only as a chain transfer agent.

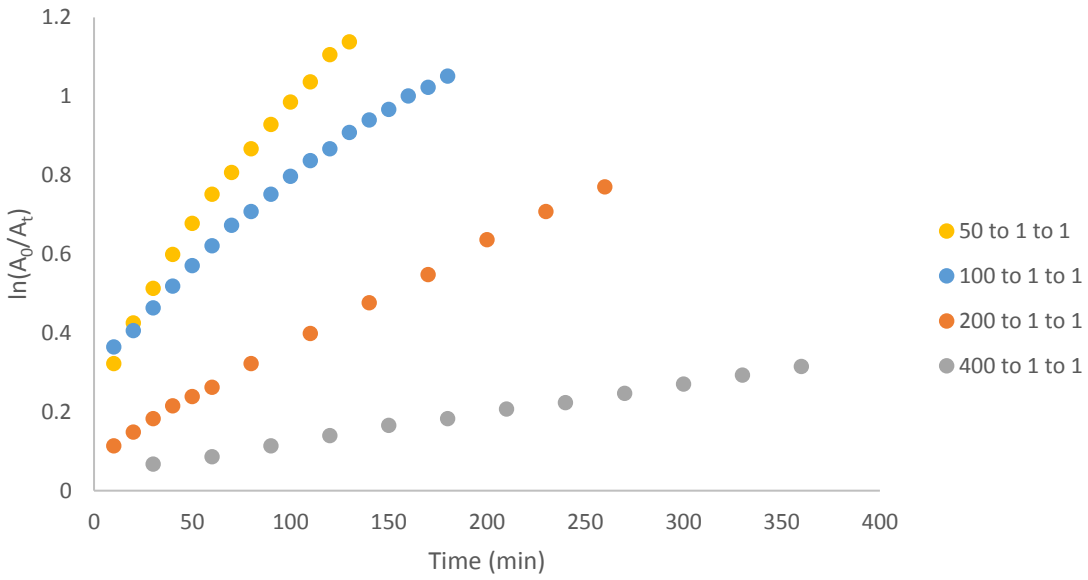


**Figure 2.21: Mononuclear kinetic series of the ROP of *rac*-lactide (0.58 M) at 80 °C in toluene against time using Al(4)Me$_2$ at different lactide:initiator:BnOH loadings**

The $k_{app}$ values for the kinetic experiments run using Al(**4**)Me$_2$ are shown in Table 2.06. For the mononuclear complexes, the monomer to initiator loading is equal to the aluminium to initiator loading. As expected, the first order rate constant $k_{app}$ reduces as the concentration of initiator decreases. If we compare the values in this table to those of the dinuclear system there is a degree of similarity, suggesting that no cooperative effect occurs for the dinuclear system. For example $k_{app}$ = 3.3 x $10^{-3}$ $min^{-1}$ at 200:1:2 using Al$_2$(**1**)Me$_4$ and 4.1 x $10^{-3}$ $min^{-1}$ at 100:1:1 using Al(**4**)Me$_2$. These values are very close to one another, albeit not statistically equivalent. This rules out synergy between the aluminium centres in the dinuclear complex, as seen in previous research with complexes of this type.

**Table 2.06: $k_{app}$ values for the the ROP of *rac*-lactide (0.58 M) at 80 °C in toluene using Al(4)Me$_2$ at different initiator concentrations, including standard error by linear regression and $R^2$ values.**

| LA:I | BnOH | $k_{app}$ (x $10^{-3}$ $min^{-1}$) | Standard Error | $R^2$ |
|---|---|---|---|---|
| 50 | 1 | 8.1 | 2.04 x $10^{-4}$ | 0.997 |
| 100 | 1 | 4.1 | 1.16 x $10^{-4}$ | 0.987 |
| 200 | 1 | 2.6 | 2.60 x $10^{-5}$ | 0.999 |
| 400 | 1 | 0.7 | 4.59 x $10^{-6}$ | 0.998 |

The graph in Figure 2.22 is the ln(k) vs ln[I] plot for the ring opening polymerisation of lactide using Al(**4**)Me$_2$, for which the gradient is approximately 1, i.e. a first order reaction with respect to initiator, as expected.

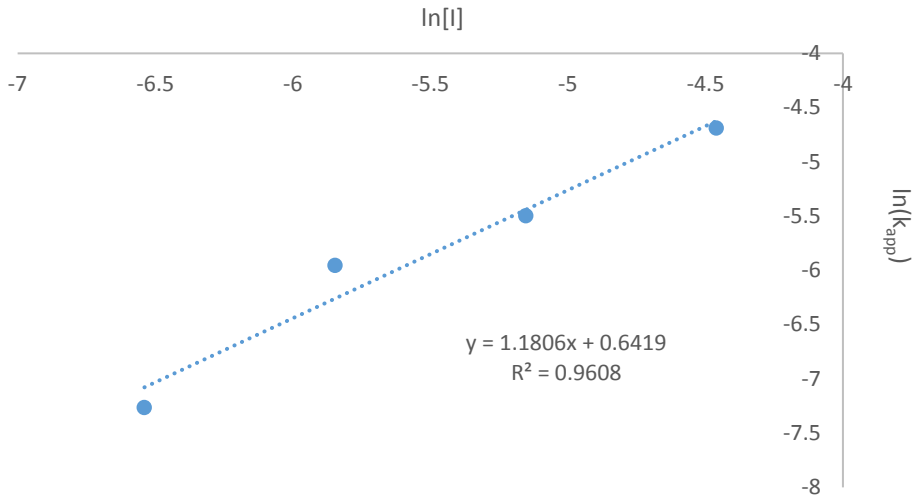


**Figure 2.22: Logarithmic order plot for ROP of lactide using Al(4)Me$_2$**

To summarise, it was found that dinuclear naphthalene Schiff base complexes show no heightened activity over their mononuclear equivalents, when comparing reaction rates at the same concentration of aluminium centres. This contrasts with the work carried out by Normand *et al.* where the dinuclear complexes showed heightened activity.[3] This difference can be attributed to the inflexible naphthalene backbone of initiators Al$_2$(**1**)Me$_4$, which cannot rotate in any way to allow the aluminium metal centres to come within proximity of one another, thus cannot engage in any cooperative mechanisms for the ROP of lactide.

## 2.5 Polymerisation of ε-caprolactone

ε-Caprolactone is a 7-membered cyclic ester which is liquid at room temperature. When polymerised it forms poly(caprolactone), a straight-chained aliphatic polyester. Table 2.07 shows the polymerisation results for the ROP of caprolactone using $Al_2$(**1**)$Me_4$ at two different temperatures. No satisfactory correction factor was available in the literature, so $M_n$ is reported as determined by GPC.

**Table 2.07: Polymerisation results for the ROP of caprolactone using $Al_2$(1)$Me_4$ at 80 °C and 40 °C**

| LA:I | BnOH | Conversion (%) | Time (min) | $M_n$ calc ($gmol^{-1}$) | $M_n$ ($gmol^{-1}$) | PDI | Temp (°C) |
|---|---|---|---|---|---|---|---|
| 100 | 2 | 100 | 20 | 5813 | 8800 | 1.25 | 80 |
| 100 | 2 | 95 | 60 | 5528 | 8700 | 1.09 | 40 |

The molecular weights correlate reasonably with the expected values, and PDI values are narrow, particularly at lower temperature, indicating a controlled polymerisation. Only 20 minutes was required for full conversion at 80 °C and even at lower temperature (40 °C) high conversion was reached within an hour. A kinetic study was run in order to determine the $k_{app}$ of the polymerisation of caprolactone at 40 °C.

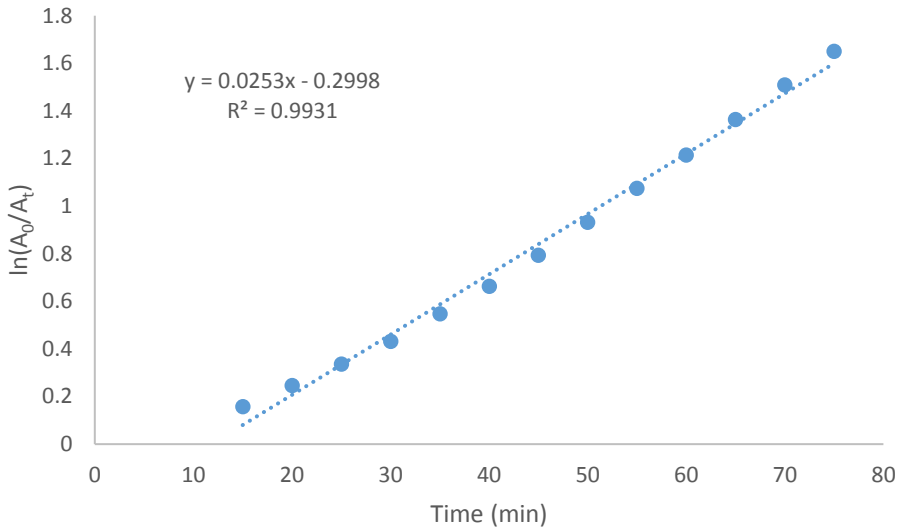


**Figure 2.23: First order rate plot for the ROP of 0.58 M caprolactone in toluene at 40 °C using $Al_2$(1)$Me_4$ at 100:1 loading with 2 equivalents benzyl alcohol**

Figure 2.22 shows the first order rate plot for the ROP of caprolactone using $Al_2$(**1**)$Me_4$. From this graph the calculated $k_{app}$ value is 0.0253 $min^{-1}$. This is an order of magnitude faster than for the ROP of *rac*-lactide at 80 °C under higher temperature, showing that this initiator is more

active for the ROP of ε-caprolactone. This value corresponds well with the observations made by Chen *et al.*, who utilised a dinuclear aluminium salen complex for the ROP of caprolactone and found that the reaction had a $k_{app}$ of ca. 14 x $10^{-3}$ $min^{-1}$ under the same conditions at 200:1 monomer loading.[2]

## 2.6 Copolymerisation of lactide and caprolactone

There is great interest in studying copolymerisation reactions of lactide with other lactones, as incorporating a second monomer has the potential to greatly influence the properties of the polymer. In the case of poly-lactide-co-caprolactone, not only do the physical properties differ to that of the homopolymers, but the degradation profiles of the copolymers varies according to the ratio of each monomer in the polymer.[10] The high activity of the unsubstituted dialuminium complex for the ring-opening polymerisations of both lactide and caprolactone made it a candidate for copolymerisation reactions of the two monomers. Figure 2.24 shows the $^1$H NMR spectrum of the crude copolymerisation mixture produced with $Al_2$(**1**)$Me_4$ as the initiator, using an equal feed of lactide and caprolactone in a one-pot reaction.

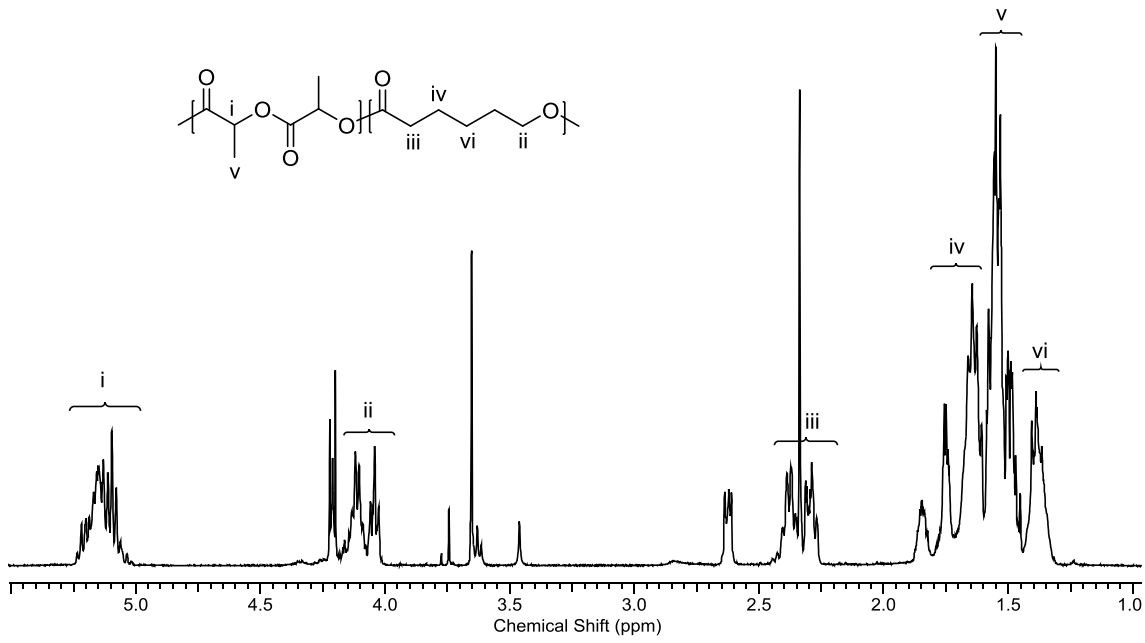


**Figure 2.24: $^1$H NMR spectrum of poly(lactide-co-caprolactone) produced using 50:50 feed of *rac*-lactide and ε-caprolactone**

Figure 2.25 shows the region between 4.0 and 5.4 ppm in the spectrum. This region of the spectrum is used to calculate the conversion of each monomer by the relative integration of the monomer and polymer resonances.

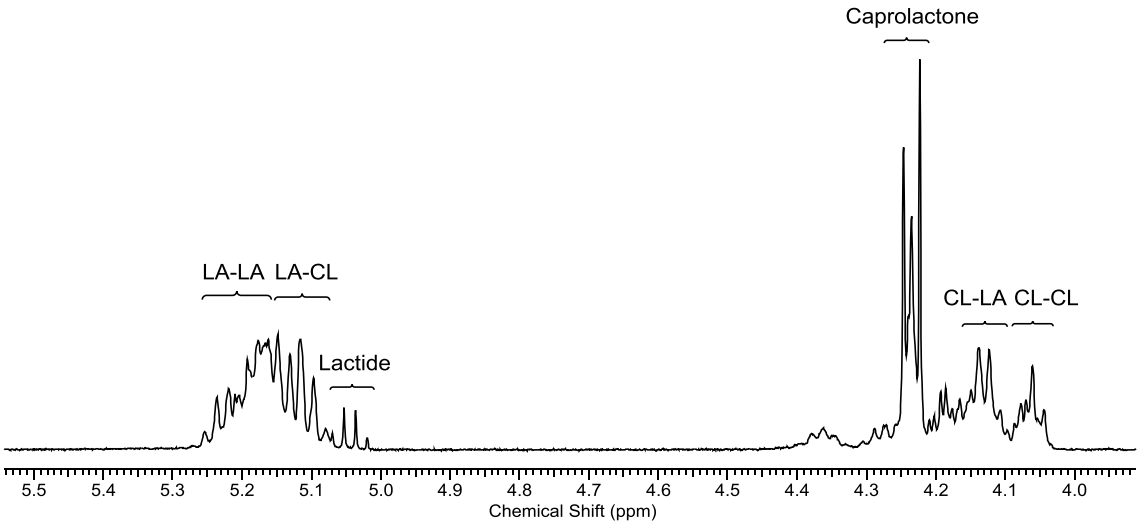


**Figure 2.25: Zoomed region of $^{1}$H NMR spectrum of poly(lactide-co-caprolactone)**

Information regarding the average block length can be obtained by Equation 2.4. Equation 2.5 shows the method of calculating the expected average block length for a random copolymer. The closer the value obtained from Equation 2.4 matches that of Equation 2.5, the more likely the polymer is to be random. A much higher block length indicates a block copolymer, and a much lower block length value indicates an alternating copolymer.

$$L_{LA} = \frac{[\text{PLA}]}{[\text{LA-CL}]} \qquad L_{CL} = \frac{[\text{PCL}]}{[\text{LA-CL}]}$$

**Equation 2.4**

$$L_{LA}\,(\text{random}) = \frac{1}{[\text{PCL}]} \qquad L_{CL}\,(\text{random}) = \frac{1}{[\text{PLA}]}$$

**Equation 2.5**

Equation 2.6 shows the calculation that provides the randomness factor, another method of quantifying the randomness of a copolymer.[11] For a block copolymer, R tends towards zero (at R = 0 the polymer is a homopolymer), whereas for an alternating copolymer, R = 1. A random copolymer has a randomness factor of 0.5.

$$\text{R} = \frac{[\text{LA-CL}]}{[\text{PLA}][\text{PCL}]}$$

**Equation 2.6**

Table 2.08 shows the copolymerisation results for the ring-opening polymerisation of *rac*-lactide and ε-caprolactone using $Al_2$(**1**)$Me_4$ at varying feed ratios and initiator loadings. For these copolymers, no suitable correction factor exists, so the $M_n$ value determined by RI only is shown

uncorrected. The eleventh and twelfth column show the percentage of polylactide and polycaprolactone in the final polymer respectively. The last four columns on the right break down the ratio of different linkages in the polymer, either homolinkages (lactide-lactide or LA-LA and caprolactone-caprolactone, CL-CL) and heterolinkages (lactide-caprolactone and vice-versa, LA-CL and CL-LA). For every entry in Table 2.08, the conversion of lactide was high or even 100%, whereas the conversion of caprolactone never reached such high conversions. This suggests that the initiator is preferentially consuming the lactide feed first. In every instance with the exception of entry 1, the observed $M_n$ is lower than the calculated $M_n$. The PDI values are narrow for entries 2-6, which is at 100:1:2 loading of monomer to initiator to benzyl alcohol, showing that $Al_2$(**1**)$Me_4$ can have good molecular weight control for this copolymerisation. However, the PDI values broaden when higher monomer loadings are used e.g. PDI = 2.21 in entry 10.

The second section of Table 2.08 (page 69) shows the observed and calculated average lactide and caprolactone block lengths, as calculated by Equations 2.4 and 2.5. In most cases the values are very close to one another, or even exactly the same (entry 1), indicating that these copolymers are random in nature. Further evidence for this is the randomness factors (R) for most of these copolymers, which are near or exactly 0.5, the expected value for a random copolymerisation (e.g. R = 0.50 for entry 1). The instances where this is not the case is entry 7 and 8. In the case of entry 7, the feed ratio and conversion of caprolactone is low. As such, there are fewer CL-CL linkages than would be expected in a random copolymer, therefore the polymer is more ‘blocky’ in character.

**Table 2.08: Copolymerisation data for *rac*-lactide and ε-caprolactone using $Al_2(1)Me_4$ at 80 °C in toluene**
**(1) obtained by $^1$H NMR spectroscopy (2) obtained by GPC (3) calculated by equation 2.4 (4) calculated by equation 2.5 (5) calculated by equation 2.6.**

| Entry | M:I | BnOH | LA:CL | Time (h) | Conv LA (%)[1] | Conv CL (%)[1] | $M_n$ calc ($gmol^{-1}$) | $M_n$ [2] ($gmol^{-1}$) | PDI[2] | [PLA] | [PCL] | [LA-LA] | [CL-CL] | [LA-CL] | [CL-LA] |
|---|---|---|---|---|---|---|---|---|---|---|---|---|---|---|---|
| 1 | 100 | 1 | 50:50 | 2 | 100 | 85 | 12,153 | 19,450 | 1.37 | 0.52 | 0.48 | 0.29 | 0.21 | 0.25 | 0.25 |
| 2 | 100 | 2 | 50:50 | 2 | 96 | 60 | 10,440 | 7,200 | 1.11 | 0.58 | 0.42 | 0.40 | 0.13 | 0.24 | 0.22 |
| 3 | 100 | 2 | 50:50 | 3 | 100 | 69 | 11,241 | 8,800 | 1.13 | 0.60 | 0.40 | 0.41 | 0.13 | 0.21 | 0.25 |
| 4 | 100 | 2 | 50:50 | 4 | 100 | 75 | 11,583 | 9,200 | 1.11 | 0.57 | 0.43 | 0.38 | 0.16 | 0.21 | 0.25 |
| 5 | 100 | 2 | 75:25 | 2 | 87 | 46 | 10,815 | 6,850 | 1.10 | 0.85 | 0.15 | 0.73 | 0.02 | 0.12 | 0.12 |
| 6 | 100 | 2 | 25:75 | 2 | 100 | 88 | 12,324 | 8,200 | 1.16 | 0.38 | 0.62 | 0.12 | 0.37 | 0.25 | 0.26 |
| 7 | 100 | 2 | 90:10 | 4 | 99 | 68 | 11,112 | 8,950 | 1.26 | 0.92 | 0.08 | 0.86 | 0.01 | 0.06 | 0.06 |
| 8 | 100 | 2 | 10:90 | 4 | 100 | 98 | 12,894 | 9,500 | 1.67 | 0.11 | 0.89 | 0.00 | 0.76 | 0.12 | 0.12 |
| 9 | 200 | 2 | 50:50 | 5 | 90 | 49 | 18,654 | 16,150 | 1.19 | 0.62 | 0.38 | 0.37 | 0.13 | 0.26 | 0.23 |
| 10 | 400 | 2 | 50:50 | 24 | 100 | 89 | 49,200 | 23,500 | 2.21 | 0.52 | 0.48 | 0.30 | 0.23 | 0.23 | 0.24 |
| 11 | 800 | 2 | 50:50 | 24 | 100 | 77 | 92,820 | 55,200 | 1.79 | 0.53 | 0.47 | 0.31 | 0.24 | 0.23 | 0.22 |

**Table 2.08, continued from page 68**

| Continued from entry | $L_{LA}$[3] | $L_{CL}$[3] | $L_{LA}$ (random)[4] | $L_{CL}$ (random)[4] | R[5] |
|---|---|---|---|---|---|
| 1 | 2.1 | 1.9 | 2.1 | 1.9 | 0.50 |
| 2 | 2.4 | 1.8 | 2.4 | 1.7 | 0.49 |
| 3 | 2.9 | 1.9 | 2.5 | 1.7 | 0.44 |
| 4 | 2.7 | 2.0 | 2.3 | 1.8 | 0.43 |
| 5 | 7.1 | 1.3 | 6.7 | 1.2 | 0.47 |
| 6 | 1.5 | 2.5 | 1.6 | 2.6 | 0.53 |
| 7 | 15.3 | 1.3 | 12.5 | 1.1 | 0.41 |
| 8 | 0.9 | 7.4 | 1.1 | 9.1 | 0.61 |
| 9 | 2.4 | 1.5 | 2.6 | 1.6 | 0.55 |
| 10 | 2.3 | 2.1 | 2.1 | 1.9 | 0.46 |
| 11 | 2.3 | 2.0 | 2.1 | 1.9 | 0.46 |

The block length data have been plotted in graphical form (Figures 2.25 and 2.26) to illustrate the relationship between the theoretical and observed block lengths of lactide and caprolactone. In Figure 2.26, the correlation between theoretical and observed block length of lactide is very close at lower lactide feed, but at very high feed (90 %) the observed block length is higher than the expected value for a random copolymer. This effect is not seen for caprolactone average block length (Figure 2.27), where at highest caprolactone feed (90 %) the observed value is actually lower than the theoretical value. This is most likely due to the initiator preferentially polymerising lactide in the first instance. The number of lactide-lactide linkages at this feed ratio is zero (entry 8, Table 2.08), meaning every lactide is adjacent to a caprolactone in the polymer, hence the shorter caprolactone block length. For every other monomer feed ratio, the theoretical and observed values for caprolactone block length correlate closely, indicating a random copolymer.

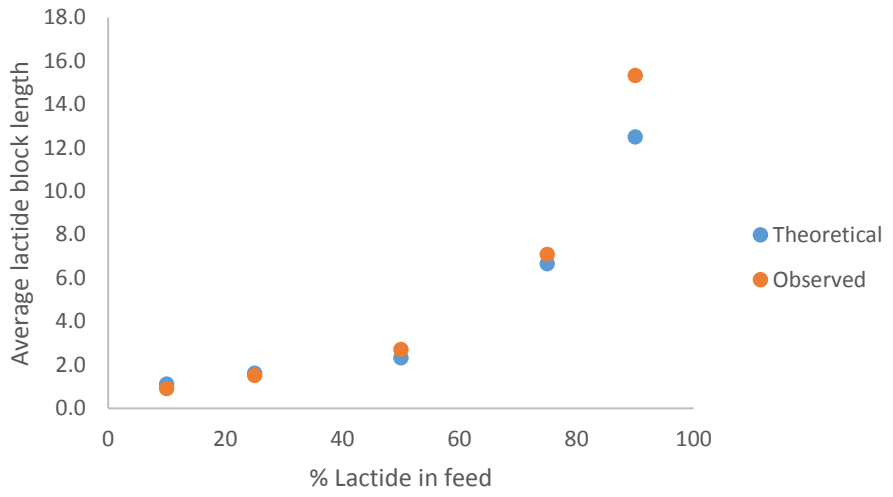


**Figure 2.26: Theoretical vs observed average lactide block length with increasing lactide feed**

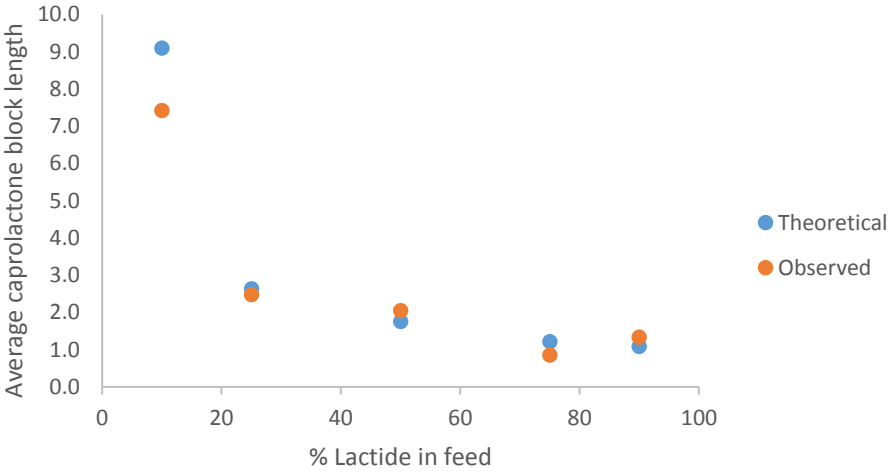


**Figure 2.27: Theoretical vs observed average caprolactone block length with increasing lactide feed**

For all copolymerisations, the lactide feed was consumed prior to the caprolactone feed. This is most evident in entries 2-4 in Table 2.08, where with increasing reaction times (under the same conditions), lactide reaches 100 % conversion first, followed by increasingly high caprolactone conversion. This is counterintuitive to the reaction rates seen for the homopolymerisations of each monomer, where lactide has a smaller $k_{app}$ than caprolactone (0.0083 $min^{-1}$ for LA *vs* 0.0253 $min^{-1}$ for CL). To investigate this, kinetic experiments were carried out to determine the activities with respect to each monomer in the one-pot copolymerisation of lactide and caprolactone.

Figure 2.28 shows the conversion with time for a 50:50 polymerisation of lactide and caprolactone using $Al_2$(**1**)$Me_4$ as the initiator, at a 100:1:2 ratio of overall monomer to initiator to benzyl alcohol. From this data, $k_{app}$ values were calculated as 11.2 x $10^{-3}$ $min^{-1}$ for lactide and 3.2 x $10^{-3}$ $min^{-1}$ for caprolactone.

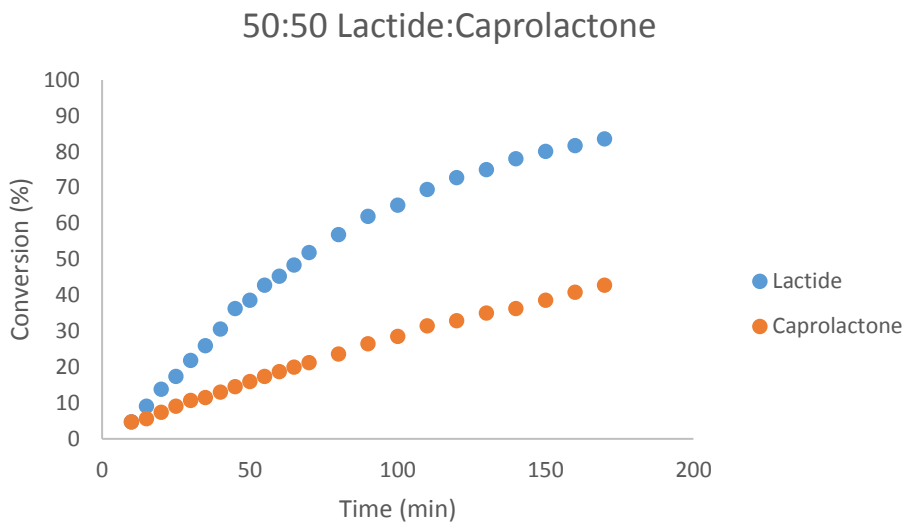


**Figure 2.28: Conversion of lactide and caprolactone with time, using 50:50 caprolactone:lactide feed ratio, at 100:1:2 monomer:initiator:BnOH at 80 °C in toluene**

Figure 2.29 shows the conversion with time of 25:75 lactide and caprolactone using $Al_2$(**1**)$Me_4$ as the initiator at a 100:1:2 ratio of overall monomer to initiator to benzyl alcohol. It appears, even with a higher ratio of caprolactone present, that lactide is polymerised faster and as such is favoured over caprolactone by the initiator. The $k_{app}$ values calculated from this data are 15.2 x $10^{-3}$ $min^{-1}$ for lactide and 4.4 x $10^{-3}$ $min^{-1}$ for caprolactone. Interestingly, at the same concentration of initiator, the $k_{app}$ for ROP of lactide is higher for a lower lactide concentration.

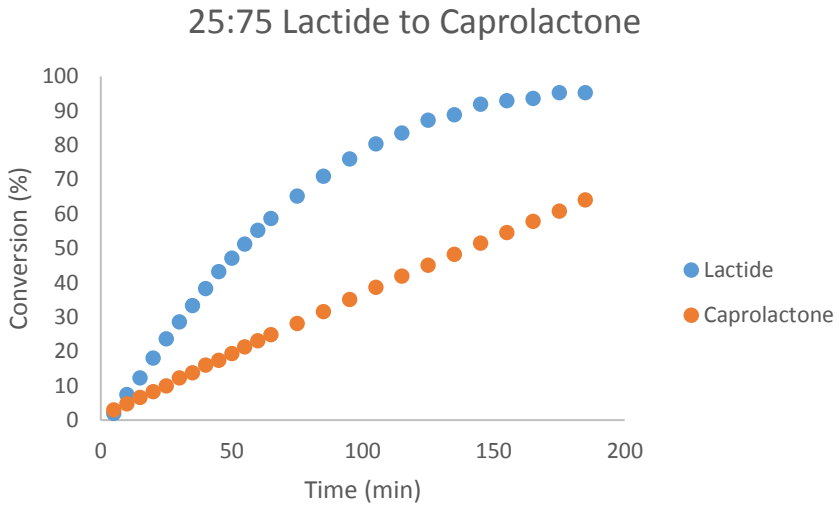


**Figure 2.29: Conversion of lactide and caprolactone with time, using 75:25 caprolactone:lactide feed ratio at 100:1:2 monomer:initiator:BnOH at 80 °C in toluene**

In conclusion, it appears that the initiator is more selective for lactide than caprolactone, despite the elevated $k_{app}$ value for the homopolymerisation of caprolactone. One explanation for this is

that the insertion into a lactide monomer by an initiator with a lactide-ended chain is faster than insertion into caprolactone. Figure 2.30 illustrates how an equilibrium favouring lactide insertion could occur.

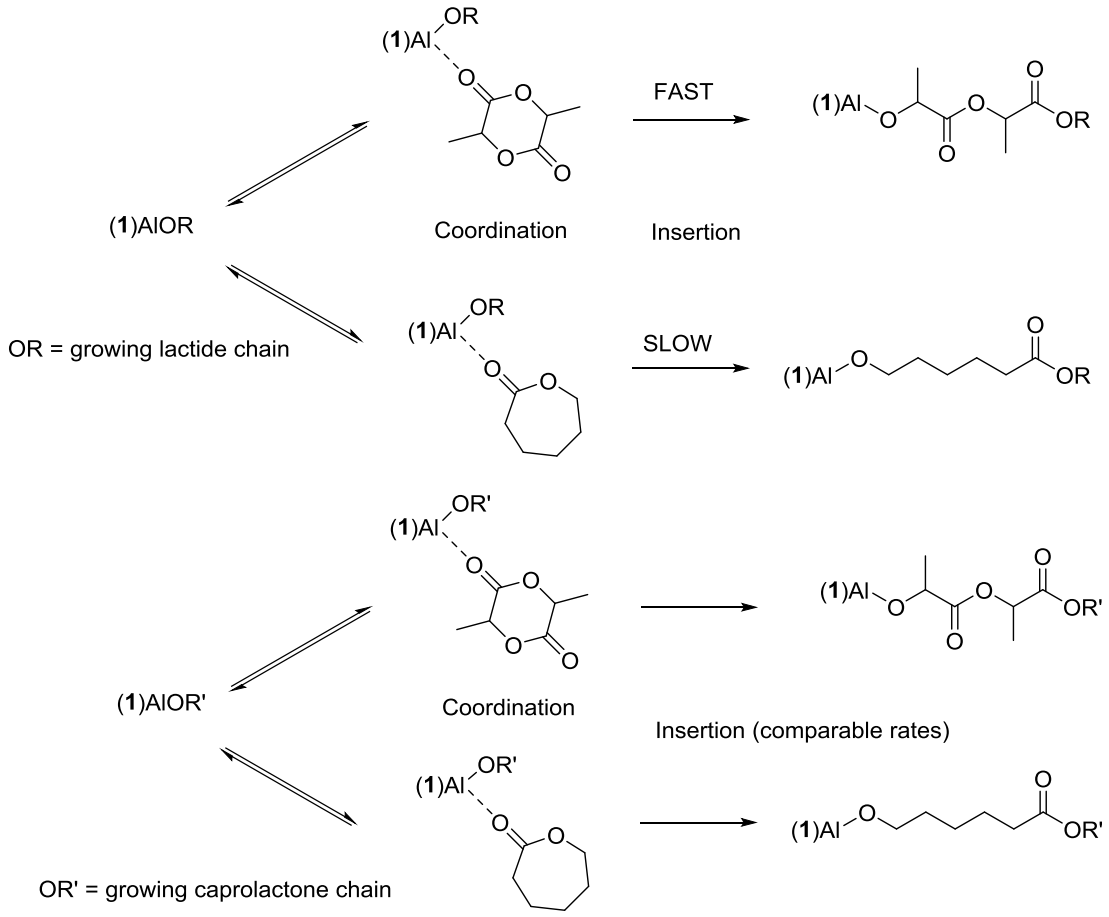


**Figure 2.30: Coordination insertion of lactide and caprolactone into growing copolymer chain**

Copolymerisations were also carried out using L-lactide and caprolactone, with the intention of producing a crystalline polymer for investigation *via* DSC. The copolymerisation data are reported in Table 2.09. However, no thermal events were seen for these copolymers in the DSC, presumably due to the short block length observed in these copolymers, leading to amorphous polymers. The molecular weight agreement between theoretical and observed appears reasonable, suggesting a well-controlled polymerisation. The PDI values are very narrow, which was also seen at 100:1 loading when *rac*-lactide was employed. As was observed with *rac*-lactide, the copolymerisation of L-lactide and caprolactone is seemingly random in nature, with R factor values for the resulting polymers between 0.40-0.59.

**Table 2.09: Copolymerisation data for L-lactide and ε-caprolactone using $Al_2(1)Me_4$ at 80 °C in toluene**
**(1) obtained by $^1$H NMR spectroscopy (2) obtained by GPC (3) calculated by equation 2.4 (4) calculated by equation 2.5 (5) calculated by equation 2.6.**

| Entry | M:I | BzOH | LA:CL | Time (h) | Conv LA (%)[1] | Conv CL (%)[1] | $M_n$ calc ($gmol^{-1}$) | $M_n$ [2] ($gmol^{-1}$) | PDI[2] | [PLLA] | [PCL] | [LA-LA] | [CL-CL] | [LA-CL] | [CL-LA] |
|---|---|---|---|---|---|---|---|---|---|---|---|---|---|---|---|
| 1 | 100 | 2 | 50:50 | 4 | 94 | 49 | 9,669 | 9,000 | 1.08 | 0.64 | 0.36 | 0.43 | 0.12 | 0.22 | 0.23 |
| 2 | 100 | 2 | 75:25 | 4 | 87 | 35 | 8,367 | 9,900 | 1.05 | 0.84 | 0.16 | 0.74 | 0.02 | 0.12 | 0.12 |
| 3 | 100 | 2 | 25:75 | 4 | 100 | 75 | 11,583 | 9,850 | 1.13 | 0.32 | 0.68 | 0.10 | 0.43 | 0.22 | 0.25 |
| 4 | 200 | 2 | 50:50 | 24 | 100 | 88 | 24,540 | 34,600 | 1.30 | 0.49 | 0.51 | 0.30 | 0.27 | 0.20 | 0.24 |
| 5 | 400 | 2 | 50:50 | 48 | 60 | 17 | 21,264 | 18,300 | 1.04 | 0.75 | 0.25 | 0.58 | 0.04 | 0.22 | 0.16 |

| Continued from entry | $L_{LA}$[3] | $L_{CL}$[3] | $L_{LA}$ (random)[4] | $L_{CL}$ (random)[4] | R[5] |
|---|---|---|---|---|---|
| 1 | 2.9 | 1.6 | 2.8 | 1.6 | 0.48 |
| 2 | 7.0 | 1.3 | 6.3 | 1.2 | 0.45 |
| 3 | 1.5 | 3.1 | 1.5 | 3.1 | 0.51 |
| 4 | 2.5 | 2.6 | 2.0 | 2.0 | 0.40 |
| 5 | 3.4 | 1.1 | 4.0 | 1.3 | 0.59 |

Copolymerisation reactions were also performed using Al(**4**)$Me_2$ in order to compare the effect of a dinuclear *vs* a mononuclear system on the copolymers. The data can be found in Table 2.10. The reaction times were doubled (of that for the homopolymerisation of lactide) in order to achieve high conversions, which will give the best representation of average block lengths in the polymer. The copolymerisations in this table carried out at 50:1:2 monomer to initiator to benzyl alcohol loading are best compared to the 100:1:2 loadings using $Al_2$(**1**)$Me_4$, as these have the same concentration of initiating metal centres as one another. For all of the copolymerisations in this table, the molecular weight agreement between the calculated and observed values is reasonably good, suggesting that the reaction is more controlled than the copolymerisation using the dinuclear initiator. However, the PDIs are broad, which suggests the opposite.

When looking at the block length data, the observed block length is always slightly shorter than the theoretical random block length, with the exception of the polymer from entry 4. All of the calculated R values are close to or slightly above 0.5 (again with the exception of entry 4, R = 0.46). This indicates that the copolymers are random in nature, with some alternating character in some cases (e.g. entry 3, R = 0.67). In summary, Al(**4**)$Me_2$ produces poly-lactide-co-caprolactone which is, on-the-whole, random in its distribution. The dinuclear complex $Al_2$(**1**)$Me_4$ produces copolymers with block lengths very close to the expected value for a random copolymer. Comparing entry 2 from Table 2.08 with entry 1 from Table 2.10, which have the same monomer to aluminium concentration and same monomer feed ratio, the former has a randomness factor R closer to 0.5, and the observed lactide block length is identical to the expected block length for a random copolymer. This suggests greater randomness than the polymer from entry 1 Table 2.10, where R = 0.60. In conclusion, employing a dinuclear system appears to produce a copolymer that is more random in nature.

**Table 2.10: Copolymerisation data for *rac*-lactide and ε-caprolactone using Al(4)$Me_2$ at 80 °C in toluene**
**(1) obtained by $^1$H NMR spectroscopy (2) obtained by GPC (3) calculated by equation 2.4 (4) calculated by equation 2.5 (5) calculated by equation 2.6.**

| Entry | M:I | LA:CL | Time (h) | Conv LA (%)[1] | Conv CL (%)[1] | $M_n$ calc ($gmol^{-1}$) | $M_n$ [2] ($gmol^{-1}$) | PDI[2] | [PLA] | [PCL] | [LA-LA] | [CL-CL] | [LA-CL] | [CL-LA] |
|---|---|---|---|---|---|---|---|---|---|---|---|---|---|---|
| 1 | 50 | 50:50 | 8 | 100 | 95 | 6,416 | 5,950 | 1.61 | 0.50 | 0.50 | 0.22 | 0.19 | 0.30 | 0.30 |
| 2 | 50 | 75:25 | 8 | 100 | 91 | 6,302 | 6,550 | 1.85 | 0.76 | 0.24 | 0.56 | 0.05 | 0.19 | 0.19 |
| 3 | 50 | 25:75 | 8 | 100 | 98 | 6,501 | 6,750 | 1.59 | 0.25 | 0.75 | 0.02 | 0.49 | 0.25 | 0.25 |
| 4 | 50 | 90:10 | 8 | 100 | 87 | 6,188 | 7,150 | 1.51 | 0.89 | 0.11 | 0.80 | 0.01 | 0.09 | 0.09 |
| 5 | 50 | 10:90 | 8 | 100 | 100 | 6,558 | 8,200 | 1.27 | 0.13 | 0.87 | 0.00 | 0.74 | 0.13 | 0.13 |
| 6 | 100 | 50:50 | 16 | 100 | 95 | 12,723 | 14,300 | 1.51 | 0.50 | 0.50 | 0.23 | 0.22 | 0.28 | 0.28 |
| 7 | 100 | 75:25 | 16 | 100 | 93 | 12,609 | 13,750 | 1.52 | 0.76 | 0.24 | 0.57 | 0.06 | 0.19 | 0.19 |
| 8 | 100 | 25:75 | 16 | 100 | 97 | 12,837 | 7,850 | 2.49 | 0.24 | 0.76 | 0.02 | 0.51 | 0.23 | 0.23 |

| Continued from entry | $L_{LA}$[3] | $L_{CL}$[3] | $L_{LA}$ (random)[4] | $L_{CL}$ (random)[4] | R[5] |
|---|---|---|---|---|---|
| 1 | 1.7 | 1.7 | 2.0 | 2.0 | 0.60 |
| 2 | 4.0 | 1.3 | 4.2 | 1.3 | 0.52 |
| 3 | 1.0 | 3.0 | 1.3 | 4.0 | 0.67 |
| 4 | 9.9 | 1.2 | 9.1 | 1.1 | 0.46 |
| 5 | 1.0 | 6.7 | 1.1 | 7.7 | 0.57 |
| 6 | 1.8 | 1.8 | 2.0 | 2.0 | 0.56 |
| 7 | 4.0 | 1.3 | 4.2 | 1.3 | 0.52 |
| 8 | 1.0 | 3.3 | 1.3 | 4.2 | 0.63 |

### 2.6.1 $^{13}$C NMR spectroscopic analysis of copolymers

Whilst the $^{1}$H NMR data can provide ratios of different monomer linkages (LA-LA, CL-CL, LA-CL), $^{13}C\{^{1}H\}$ NMR allows more insight into the nature of the copolymer, in particular any transesterification that has occurred, by inspection of the carbonyl region in the spectrum. It is also possible to determine block length by relative integration of inverse-gated $^{13}$C NMR spectra, but this technique was not utilised for this chapter due to long experiment times and satisfactory block length data already being obtained from $^{1}$H NMR spectra.

Figure 2.31 shows the $^{13}C\{^{1}H\}$ NMR spectra of poly-lactide-co-caprolactone produced using $Al_2$(**1**)$Me_4$ at different monomer feed ratios, assigned according to the literature.[12,13] The presence of additional resonances in this spectrum indicates some transesterification has occurred in the copolymers.

A small resonance appears at around 170.7 ppm in each of the spectra. This corresponds to the carbonyl carbon on a half lactide unit sandwiched between two caprolactone units. This resonance is only possible if transesterification reactions have happened, as only whole lactide units are incorporated from the ring-opening polymerisation. This provides further evidence that transesterification has occurred, which may partly explain the random nature of the copolymers despite a clear preference for lactide in the consumption rates of the monomers. Transesterification would have randomised the monomers in the chain to give a random copolymer, this also explains some of the high PDI values seen. Inspection of the $^{13}C\{^{1}H\}$ NMR spectra of the copolymers produced using Al(**4**)$Me_2$ also showed these characteristic transesterification resonances.

In conclusion, $Al_2$(**1**)$Me_4$ is highly active for the copolymerisation of lactide and caprolactone. The copolymers produced are random in character, which is likely caused by transesterification on quenching of the reaction with methanol, randomising the chains.

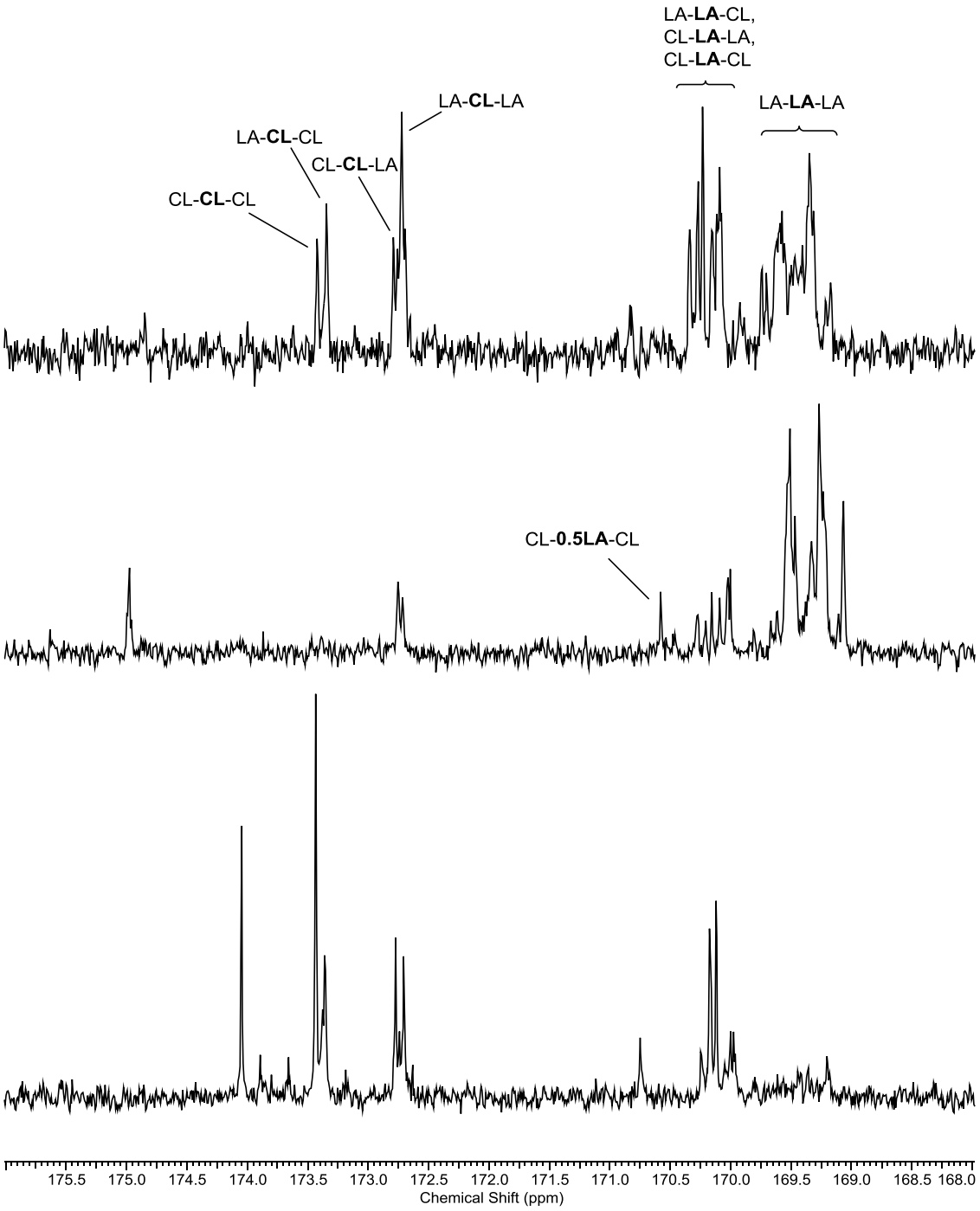


**Figure 2.31: $^{13}C\{^{1}H\}$ NMR spectrum of copolymer synthesised with $Al_2(1)Me_4$ using i) 50:50 LA:CL monomer feed ii) 75:25 LA:CL monomer feed and iii) 25:75 LA:CL monomer feed.**

## 2.7 Conclusions

Firstly, novel salen ligands featuring a naphthalene backbone were synthesised and complexed with one or two equivalents aluminium to form either a mononuclear or dinuclear aluminium salen complex. The solid-state crystal structures of $Al_2$(**1,2**)$Me_4$ and Al(**4,6**)$Me_2$ were obtained. It was found that all of these compounds retained their solid-state structure in solution.

Subsequent utilisation of these initiators for the investigation of the ROP of lactide in toluene at 80 °C found that the mononuclear set of initiators Al(**4-6**)$Me_2$ had poor molecular weight control and no stereoselectivity under these conditions. When compared to studies of a bimetallic aluminium salen complex $Al_2$(**1**)$Me_4$, the dinuclear system also shows no stereoselectivity for the ROP of *rac*-lactide, but has better molecular weight control, with PDI values of 1.05-1.10 when employing 2 equivalents of benzyl alcohol as a co-initiator.

The initiators $Al_2$(**1**)$Me_4$ and Al(**4**)$Me_2$ were investigated to compare the activities of the dinuclear and mononuclear systems to determine if the dinuclear complex shows elevated activity. It was shown that the activity is similar for the dinuclear compared to the analogous mononuclear compound when comparing concentration of initiating metal centres. This is because the metal centres have no way of coming in proximity of one another, due to the highly rigid and inflexible naphthalene backbone. As such, no cooperative effect occurs between the metal centres in the dinuclear complex $Al_2$(**1**)$Me_4$.

Both $Al_2$(**1**)$Me_4$ and Al(**4**)$Me_2$ were trialled for the copolymerisation of *rac*-lactide and ε-caprolactone. Interestingly, the lactide monomer feed was always consumed first, despite $Al_2$(**1**)$Me_4$ exhibiting a larger $k_{app}$ value for the ROP of caprolactone. This is thought to be caused by the presence of two carbonyls in the lactide, creating favourable coordination towards this monomer. It was found that both the initiators produced random copolymers, which is thought to be due to transesterification of the polymer, evidenced by a half lactide unit in the copolymer which was observed by $^{13}C\{^1H\}$ NMR spectroscopy.

## 2.8 Future Work

In this chapter the relationship between mononuclear and dinuclear complexes with rigid backbone systems was explored. Whilst previous studies on the effect of flexible ligands in dinuclear complexes on the ROP of lactide, this was the first study on a ligand system where the metal centres cannot come within proximity of one another. Future work in this vein could include investigation of other rigid mono- and dinuclear systems. Examples of such complexes are shown in Figure 2.32. This is based on the dinuclear complex reported by Normand *et al.*,[3] however with this structure the Schiff base aluminium moieties are *trans* to the phenyl-phenyl bond, so rotation about this bond would not allow the metal centres to approach one another.

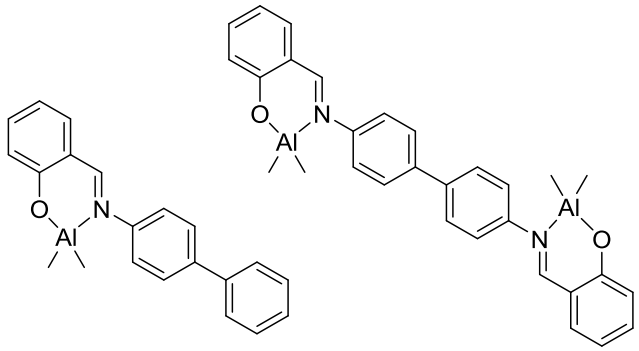


**Figure 2.32: Possible mono- and dinuclear complexes for future research**

The copolymerisation reactions of lactide and caprolactone using $Al_2$(**1**)$Me_4$ and Al(**4**)$Me_2$ were investigated in this work. However, whilst caprolactone is biodegradable it is not bio-based, which means part of the polymer has to be sourced from crude oil. An entirely bio-derived copolymer would be ideal. Previous work has been carried out on functionalising natural products in order to convert them into monomers that can undergo ROP (example in Figure 2.33).[14,15] Future copolymerisation research using these complexes could include monomers from terpene derived feedstocks such as these in place of caprolactone (Figure 2.34).

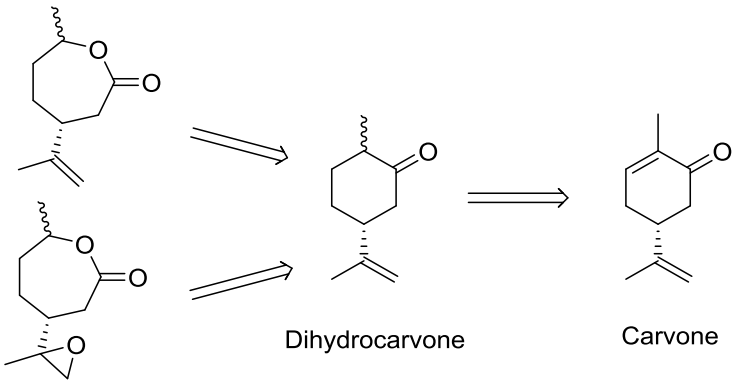


**Figure 2.33: Retrosynthetic pathway from cyclic lactones to carvone.**

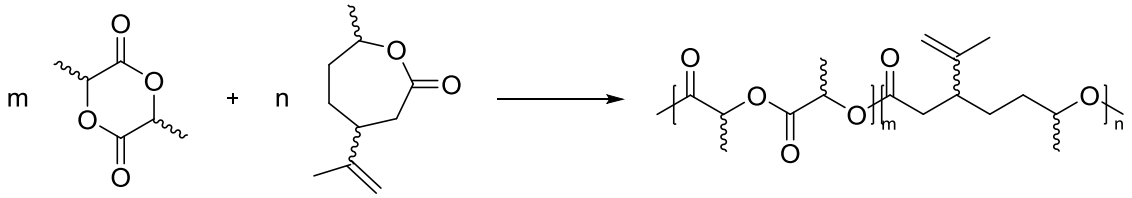

**Figure 2.34: Copolymerisation of lactide and oxidised dihydrocarvone**

Preliminary work has shown that a carvone-derived monomer can be successfully synthesised using the synthetic methodology set out by Hillmyer *et al*.[16] This method does not use sustainable reagents, so new preparations should be investigated. Furthermore, the oxidation is not selective and results in epoxidation of the alkene. The $^{13}C\{^{1}H\}$ NMR spectrum of the monomer is shown in Figure 2.35.

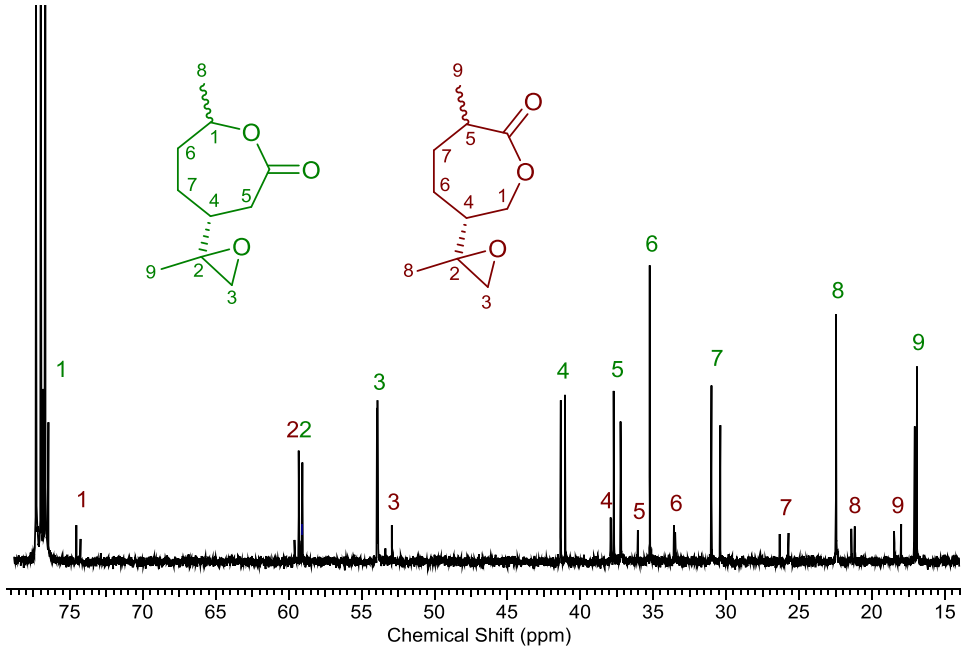


**Figure 2.35: $^{13}C\{^{1}H\}$ NMR of oxidised dihydrocarvone. Two regioisomers are present.**[16]

## 2.9 References


1. N. Spassky, M. Wisniewski, C. Pluta and B. A. Le, *Macromol. Chem. Phys.*, 1996, **197**, 2627-2637.
2. X. Pang, R. Duan, X. Li and X. Chen, *Polym. Chem.*, 2014, **5**, 3894-3900.
3. M. Normand, T. Roisnel, J. F. Carpentier and E. Kirillov, *Chem. Commun.*, 2013, **49**, 11692-11694.
4. S. M. Kirk, H. C. Quilter, A. Buchard, L. H. Thomas, G. Kociok-Kohn and M. D. Jones, *Dalton Trans.*, 2016, **45**, 13846-13852.
5. L. Yang, D. R. Powell and R. P. Houser, *Dalton Trans.*, 2007, 955-964.
6. L. Li, B. Liu, D. Liu, C. Wu, S. Li and D. Cui, *Organometallics*, 2014, **33**, 6474-6480.
7. J. Lewinski, J. Zachara, K. B. Starowieyski, Z. Ochal, I. Justyniak, T. Kopec, P. Stolarzewicz and M. Dranka, *Organometallics*, 2003, **22**, 3773-3780.
8. A. Kowalski, A. Duda and S. Penczek, *Macromolecules*, 1998, **31**, 2114-2122.
9. T. R. Forder and M. D. Jones, *New J. Chem.*, 2015, **39**, 1974-1978.
10. B. D. Ulery, L. S. Nair and C. T. Laurencin, *J. Polym. Sci., Part B: Polym. Phys.*, 2011, **49**, 832-864.
11. M. Tessier and A. Fradet, *e-Polymers*, 2003, **3**, 391.
12. N. Nomura, A. Akita, R. Ishii and M. Mizuno, *J. Am. Chem. Soc.*, 2010, **132**, 1750-1751.
13. D. Pappalardo, L. Annunziata and C. Pellecchia, *Macromolecules*, 2009, **42**, 6056-6062.
14. M. A. Hillmyer and W. B. Tolman, *Acc. Chem. Res.*, 2014, **47**, 2390-2396.
15. H. C. Quilter, M. Hutchby, M. G. Davidson and M. D. Jones, *Polym. Chem.*, 2017, **8**, 833-837.
16. J. R. Lowe, W. B. Tolman and M. A. Hillmyer, *Polym. Prepr.*, 2009, **50**, 220.

# 3. Zinc and aluminium complexes of novel Schiff base ligands

## 3.1 Preamble

Previous work by Jones *et al.* has shown that complexes with asymmetric ligands such as salalens can yield high molecular weight polymer with tuneable tacticities, as discussed in chapter 1.[1-3] Kol *et al*. also observed that chiral aluminium salalen complexes, featuring imine and amine moieties, can yield either heterotactic or isotactic PLA, depending on the substituents on the phenolate rings.[4] For example, an initiator with steric bulk ($R_2$ = adamantyl) on the salen moiety produced of isotactic PLA (42 % conversion within 24 hours), with a $P_r$ value of 0.18.

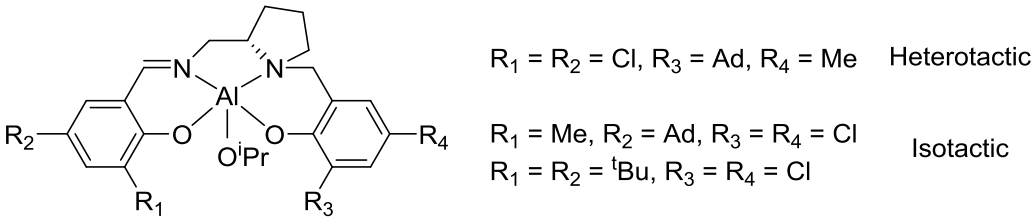


**Figure 3.01: Chiral aluminium salalen complexes as reported by Kol *et al*.[4]**

Zinc complexes with {ONN} motifs have also proved selective for the ROP of *rac*-lactide. The zinc complexes shown in Figure 3.02 synthesised by Darensbourg and Karroonnirun was found to produce heterotactic PLA at ambient temperature in chloroform within 24 hours.[5] For R = 2-(methylthio)ethyl, the $P_r$ value achieved was 0.83 at 22 °C, with 95 % conversion after 24 hours.

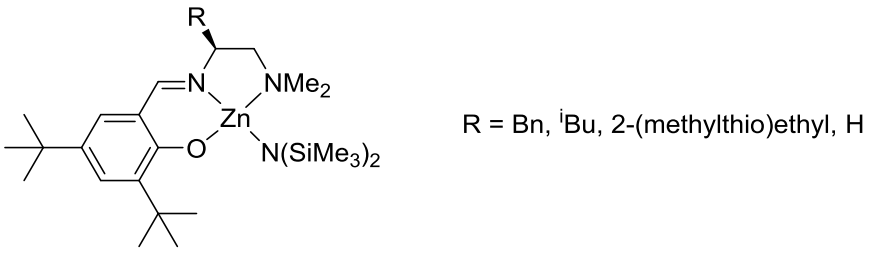


**Figure 3.02: Zinc tridentate complex as reported by Darensbourg and Karroonnirun[5]**

This chapter aims to further investigate structural relationships and the outcome in lactide polymerisation by preparing ligands that feature both amine and imine moieties and complexing them to aluminium and zinc metal centres and utilising them for the ROP of *rac*-lactide.

## 3.2 Synthesis of ligands

Figure 3.03 shows the first steps of the synthetic route to asymmetric ligands. First, *trans*-diaminocyclohexane is monoprotected using di-*tert*-butyl-dicarbonate (Boc anhydride). It is possible to remove the di- and unprotected diamine side products by a series of extractions, isolating the monoprotected species. The mono protected amine is then reacted with one equivalent of a substituted salicylaldehyde to form a mono-salen ligand featuring a NHBoc group.

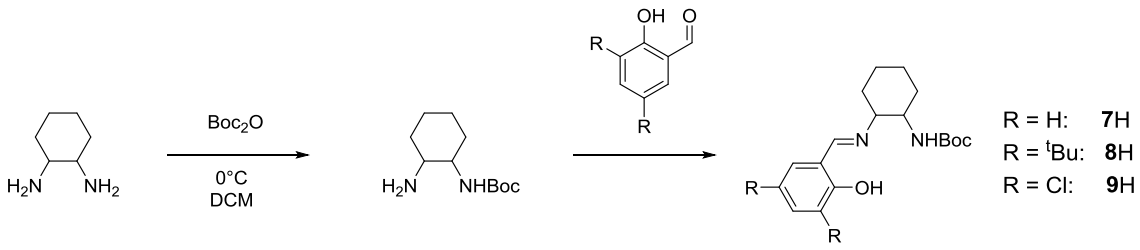


**Figure 3.03: Synthesis of ligands 7-9H**

These ligands were easily precipitated or crystallised from methanol at room temperature. A solid-state crystal structure for **8**H was obtained (Figure 3.04). Selected bond angles and lengths for this structure can be found in Table 3.01, on page 86. The crystal data shows the compound to have formed as expected, with an imine bond C15-N2 of length 1.274(3) Å. More discussion of the structure can be found under Table 3.01.

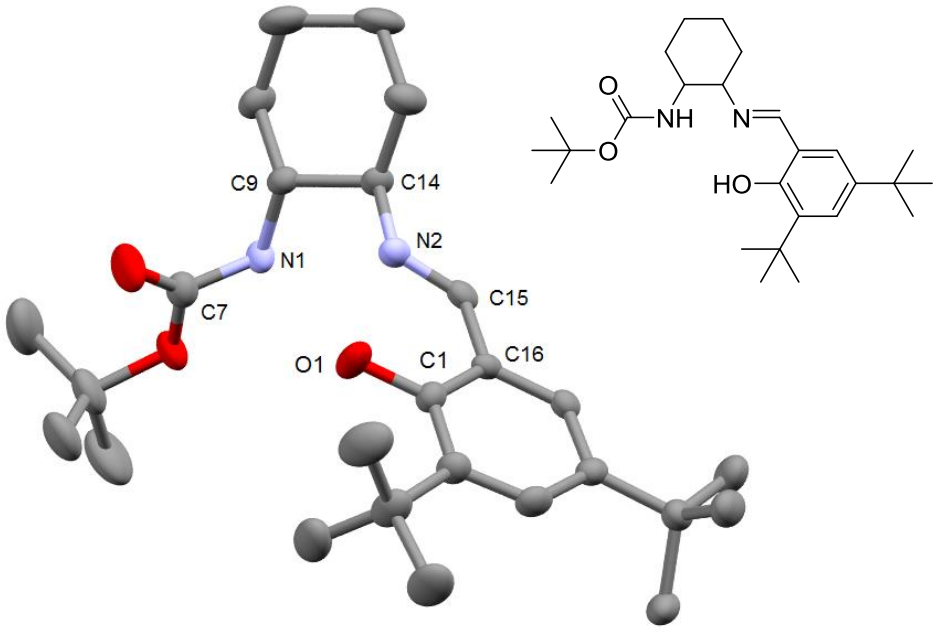


**Figure 3.04: Solid-state crystal structure of 8H. Ellipsoids are shown at the 30 % probability level, all hydrogen atoms have been removed for clarity.**

Figure 3.05 shows the proton NMR spectrum of **8**H. The most intense resonances at 1.31 ppm and 1.44 ppm originate from tert-butyl group on the NHBoc and the aryl substituents respectively. At 8.24 ppm is the N=CH proton, indicating this ligand has been successfully formed and retains the solid-state structure in solution. The N-H proton of the NHBoc moiety can be seen at 4.39 ppm as a broad singlet. Also depicted in Figure 3.05 is the mass spectrum of **8**H, the major peak at 453.3088 m/z corresponds to the sodiated ion of the ligand, and the peak to the left of it (at 431.3268 m/z) corresponds to the protonated ion.

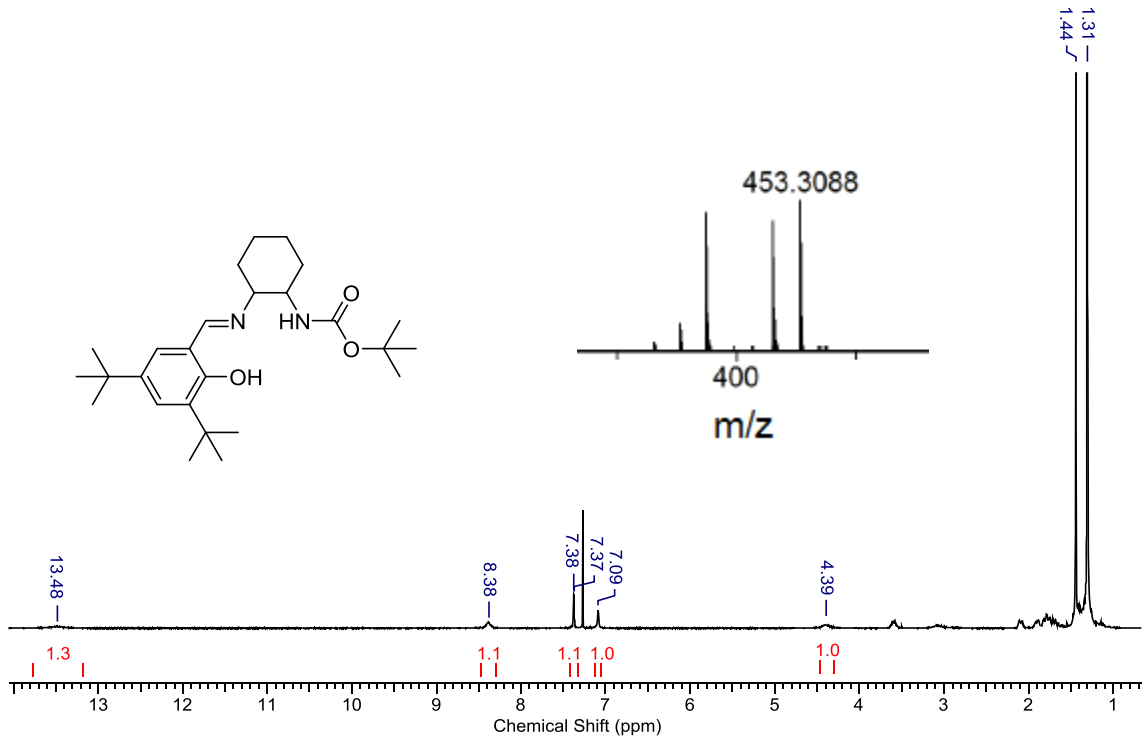


**Figure 3.05: $^{1}$H NMR spectrum in $CDCl_3$ of 8H and mass spectrum, the major labelled peak is the sodium ion**

These proligands were taken forward to synthesise further tridentate {ONN} ligands (Figure 3.06). This was achieved by reduction and subsequent methylation of the imine moiety to an amine, using sodium borohydride and formaldehyde. The Boc protective group was then removed using concentrated hydrochloric acid and the resulting free amine reacted with benzaldehyde to form the monophenolate ligands **10-12**H.

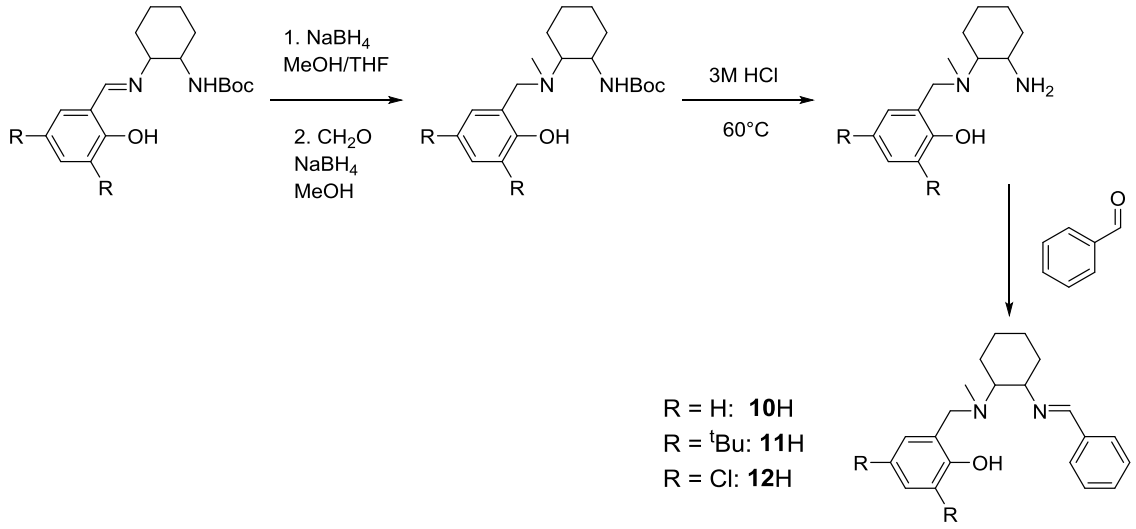


**Figure 3.06: Synthesis of 10-12H**

Ligand **12**H was successfully recrystallised from methanol and the solid-state crystal structure obtained, shown in Figure 3.07. Table 3.01 on the following page shows selected bond lengths and angles for **8**H, **12**H and a comparable literature structure **I**, synthesised by Sun *et al*.[6] The chemical skeleton of **I** is depicted in Figure 3.08.

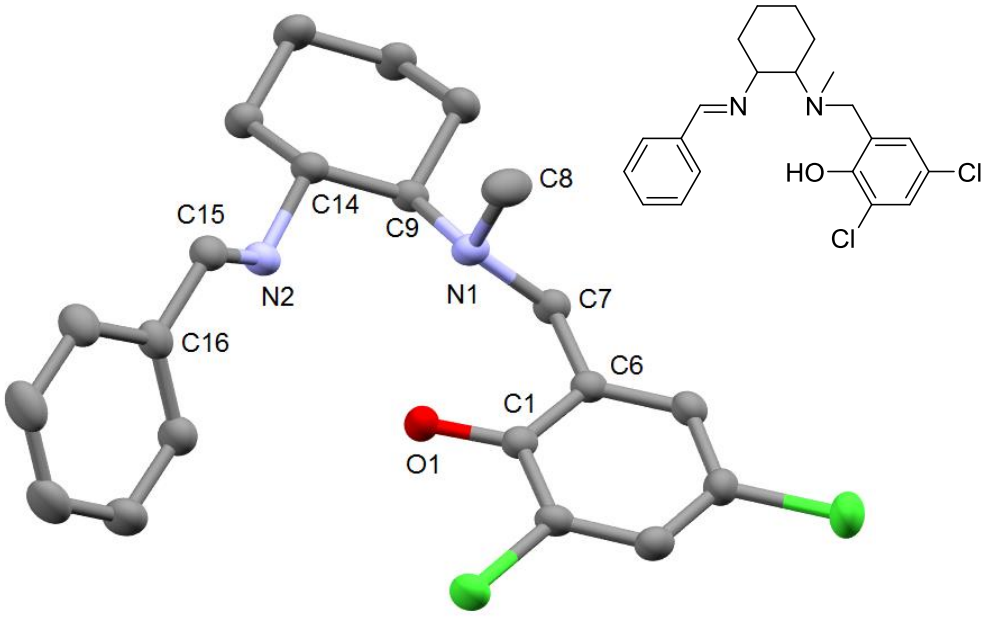


**Figure 3.07: Solid-state crystal structure of 12H. Ellipsoids are shown at the 50 % probability level, hydrogen atoms have been removed for clarity.**

**Table 3.01: Selected bond lengths (Å) and angles (°) for 12H**

| | **8**H | **12**H | **I** |
|---|---|---|---|
| N1-C8 | - | 1.469(2) | - |
| N1-C7 | 1.336(3) | 1.469(3) | 1.337(3) |
| N2-C15 | 1.274(3) | 1.265(3) | 1.303(3) |
| O1-C1 | 1.364(3) | 1.345(3) | 1.350(3) |
| N1-C7-C6 | - | 110.9(2) | 119.4(2) |
| N2-C15-C16 | 123.5(2) | 122.5(2) | 123.0(2) |
| C14-N2-C15 | 119.0(2) | 118.3(2) | 126.6(2) |
| C7-N1-C9 | 121.2(2) | 112.6(2) | 120.7(2) |
| N1-C9-C14-N2 | -64.43 | -56.0(2) | 63.2(2) |

As expected for bonds of these types, in each ligand the amine bond N1-C7 is longer than the imine bond N2-C15. For example, in **8**H the amine bond N1-C7 is 1.336(3) Å and the imine N2-C15 is 1.274(3) Å, significantly shorter. This is expected for these bond types (i.e. single vs double), as seen in literature compound **I** where the amine bond N1-C7 is 1.337(3) Å and the imine bond N2-C15 is 1.303(3) Å. The difference in imine/amine bond length distance is most pronounced in **12**H, with a difference of approx. 0.2 Å, whereas the other two examples have shorter C-N bond lengths due to the electron-withdrawing effect of the adjacent carbonyl. The angle C7-N1-C9 is reduced for **12**H, 112.6(2)° compared to 121.2(2)° for **8**H and 120.7(2)° for **I**, which is due to the methyl group introducing steric repulsion, whereas in **8**H and **I** the proton on the nitrogen atom does not give this effect.

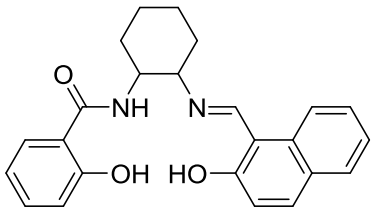


**I**

**Figure 3.08: Compound I, as reported by Sun *et al.*[6]**

Figure 3.09 shows the $^{1}$H NMR spectrum and mass spectrum of **12**H. The NMR spectrum features the expected imine resonance at 8.35 ppm and the N-methyl protons at 2.20 ppm, indicating

this ligand has been successfully synthesised. This is confirmed by the mass spectrum data showing a peak at 391.1434 m/z with the necessary isotope pattern for a ligand containing chlorine atoms.

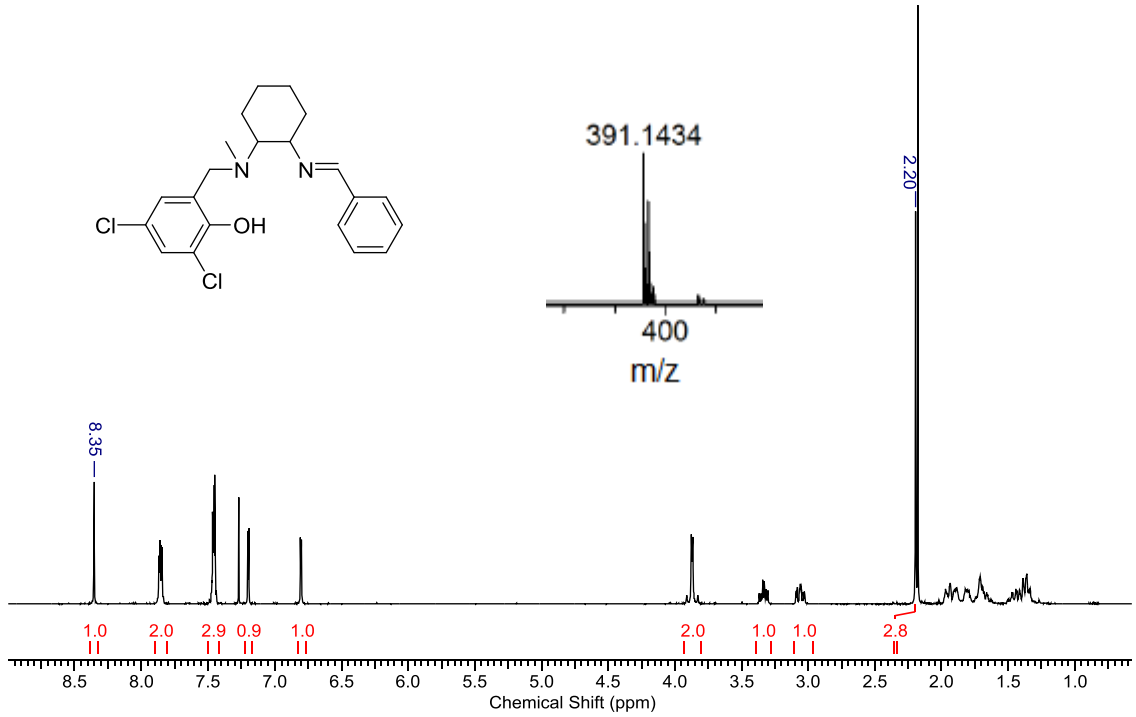


**Figure 3.09: $^{1}$H NMR spectrum in $CDCl_3$ and mass spectrum of 12H**

## 3.3 Synthesis of metal complexes

### 3.3.1 Aluminium complexes

As the ligand intermediates **7-9**H have not yet been investigated for possible complexes as an initiator for lactide polymerisation, studies were performed using these as ligands to investigate their potential to control the ROP of lactide. It was hypothesised that the free NHBoc group could have some interaction (e.g. *via* hydrogen bonding) with lactide during the process, possibly encouraging stereoselectivity *via* potential stabilisation of transition states. Trimethylaluminium ($AlMe_3$) was added stoichiometrically to **8**H in an attempt to form the 1:1 complex, Al(**8**)$Me_2$ (Figure 3.10).

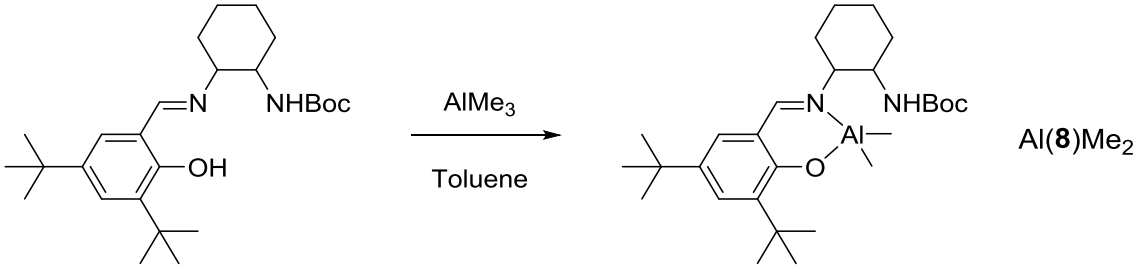


**Figure 3.10: Synthesis of Al(8)$Me_2$**

Figure 3.11 shows the solid-state structure of Al(**8**)$Me_2$. Selected bond angles and lengths can be found in Table 3.02 on page 95. The aluminium centre in this structure has a distorted tetrahedral geometry ($\tau_4$ = 0.91). Interestingly, the aluminium does not coordinate with the nitrogen on the NHBoc group, which remains protonated. As such, the ligand acts in a bidentate fashion. As with all the salen complexes, the O1-Al-N1 bond is strained, 94.23(13)° in this case, due to the rigid ligand structure which is the cause of the distortion to the tetrahedral geometry.

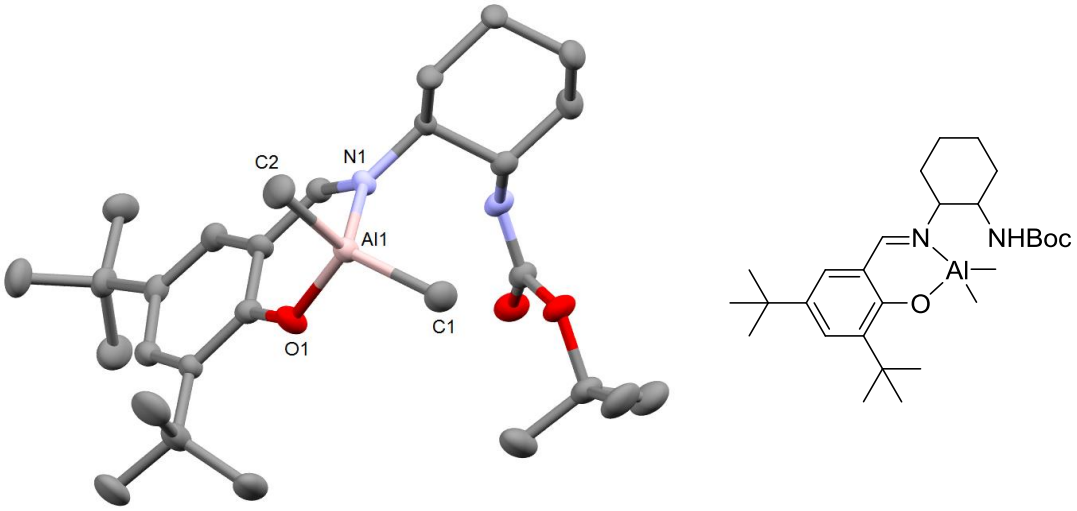


**Figure 3.11: Solid-state crystal structure of Al(8)Me$_2$. Hydrogen atoms have been omitted for clarity. Ellipsoids are shown at the 30 % probability level.**

Figure 3.12 shows the $^1$H NMR spectrum for Al(**8**)Me$_2$. The resonances at -0.22 and -0.36 ppm correspond to the Al-Me resonances (with an integral of 3H each), which confirms that the structure is retained in solution. The two aluminium methyl groups are not in identical chemical environments, as demonstrated by the two separate singlet resonances. This indicates that the structure is "locked" in place once coordinated. The resonance for the NH proton can be seen at 3.91 ppm as a doublet, supporting the observation that the amine is not deprotonated and does not bond with the aluminium centre.

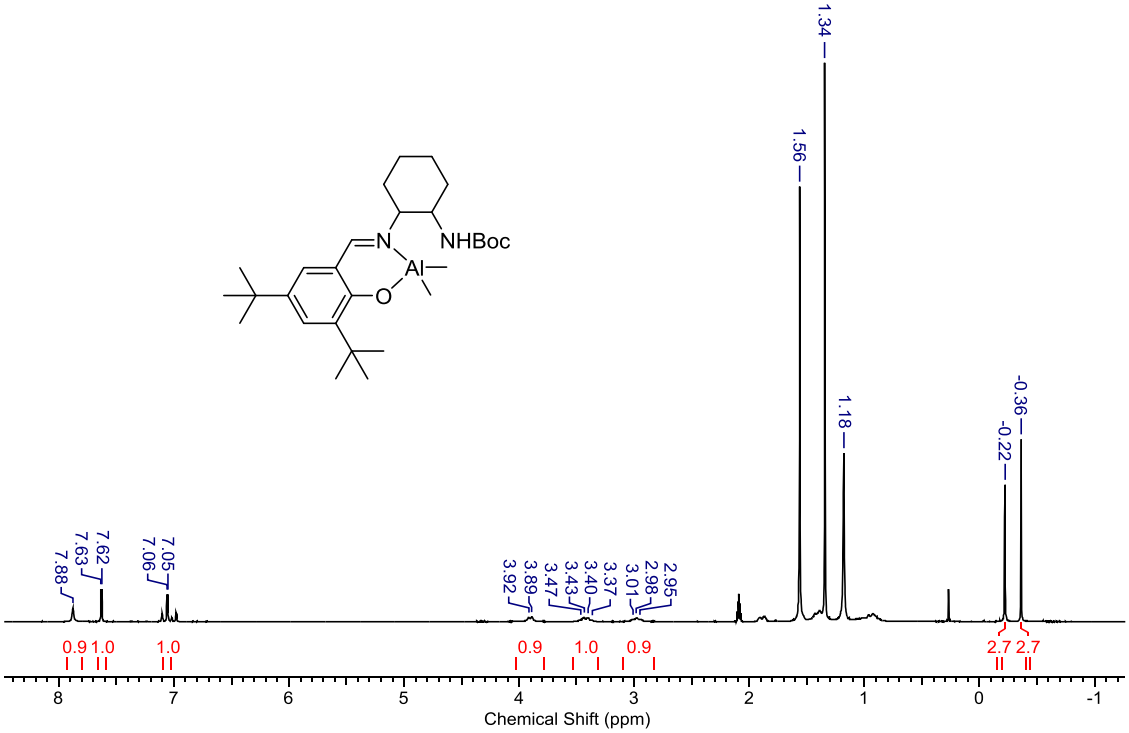


**Figure 3.12: $^1$H NMR spectrum of Al(8)Me$_2$ in d$_8$ toluene**

Interestingly, when $AlMe_3$ was added to **7**H at a stoichiometry of 1:1, a 2:1 ligand to metal complex formed, shown in Figure 3.13. Despite repeated attempts, it was not possible to isolate a 1:1 complex with **7**H, with the biligated system always being favoured. This is likely due to the reduced steric demand of **7**H compared to **8**H. The complex Al(**7**)$_2$Me could be prepared in high yield when the appropriate molar ratio of $AlMe_3$ was used.

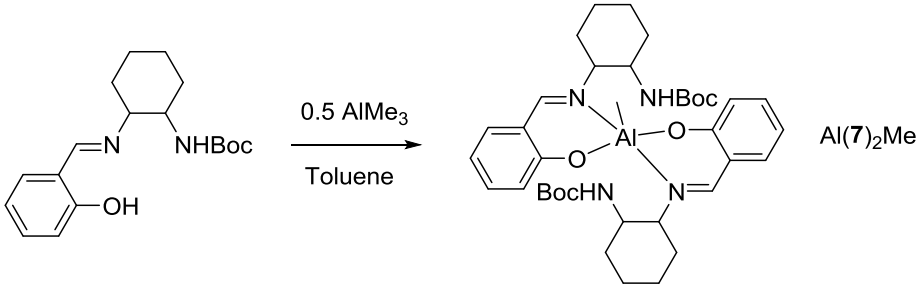


**Figure 3.13: Synthesis of Al(7)$_2$Me**

The solid-state crystal structure for Al(**7**)$_2$Me was obtained, shown in Figure 3.14. The $\tau_5$ value for five-coordinate structures is given in equation 3.1, where β is the largest basal angle and α is the second largest basal angle.[7] When $\tau_5$ = 0, perfect square pyramidal geometry is observed and conversely when $\tau_5$ = 1, perfect trigonal bipyramidal geometry is observed. Al(**7**)$_2$Me has a distorted trigonal bipyramidal geometry ($\tau_5$ = 0.85), evidenced by bond angles O1-Al-C1: 119.20(7)°, O1-Al-N1: 89.92(5)°, N1-Al-C1: 92.48(7)°.

$$\tau_5 = \frac{\beta - \alpha}{60}$$

**Equation 3.1: Degree of trigonality[7]**

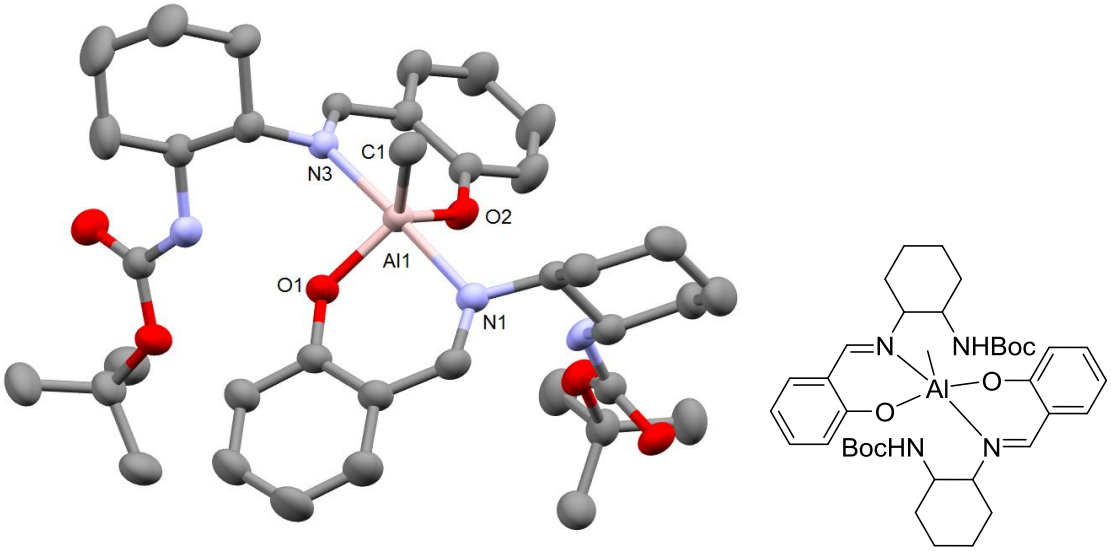


**Figure 3.14: Solid-state crystal structure of Al(7)$_2$Me. Hydrogen atoms and solvent of recrystallisation have been removed for clarity. Ellipsoids are shown at the 30 % probability level.**

Figure 3.15 shows the $^{1}$H NMR spectrum of Al(**7**)$_2$Me, which has two small resonances (rather than one, which is expected) in the aluminium-methyl region around -0.5 ppm. Combined these have an integral of less than 1H, thus there must be more than one species in solution as the expected Al-Me integration would be 3H. Due to the insolubility of the compound, the sample had to be heated to dissolve the solid into $d_8$-toluene. On first inspection, this appears to be similar to the ligand NMR, featuring the Ar-OH resonance at 13.26 ppm, suggesting that the reaction did not go to completion. The appearance of the Ar-OH resonance suggests that this complex has degraded back to ligand. Most likely, heating of the complex to solubilise it sufficiently for NMR analysis caused it to degrade. The NMR sample still contained solid suspended in the solvent despite heating, which could have been non-degraded or non-dissociated complex that is entirely insoluble. Unfortunately, this insolubility makes the complex difficult to fully characterise. Elemental analysis of Al(**7**)$_2$Me confirmed the solid-state structure and showed high purity of complex, which supports the hypothesis that only in solution upon heating does the complex degrade or dissociate.

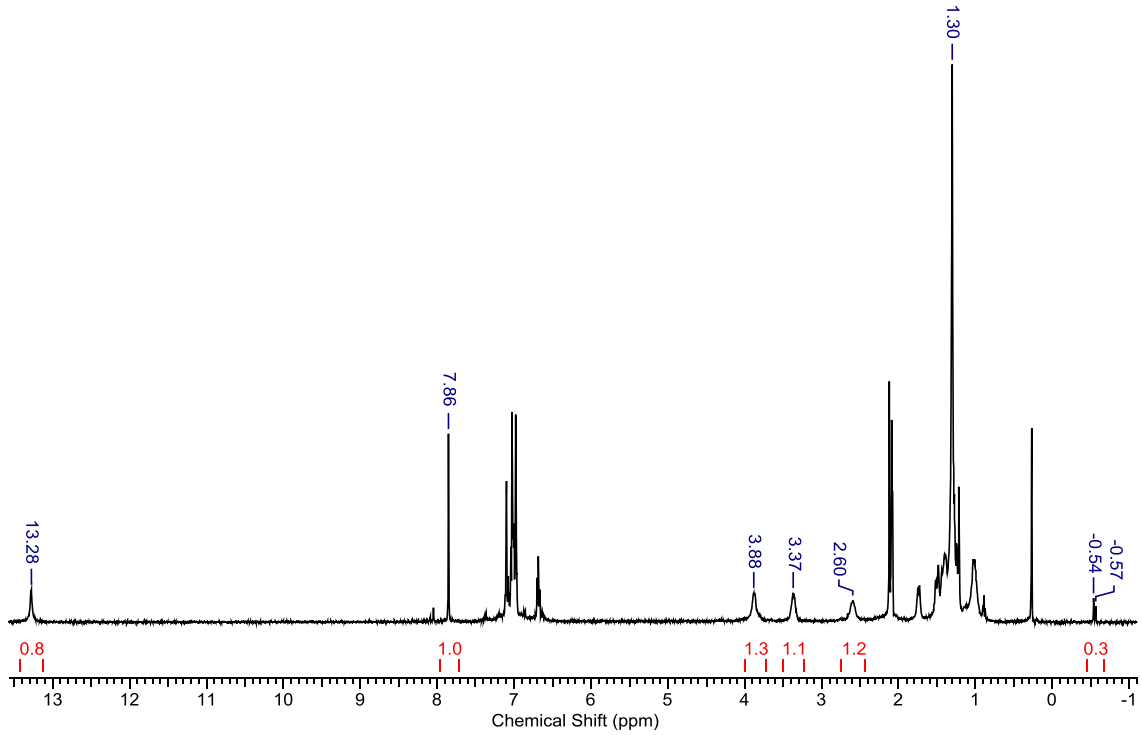


**Figure 3.15: $^{1}$H NMR spectrum of Al(7)$_2$Me in $d_8$ toluene. Solid-state structure is not retained in solution, possibly due to degradation of complex. The complex was sparingly soluble, even in $C_6D_5CD_3$ at 100 °C.**

In the case of ligand **9**H, it is possible to form a 2:1 and 1:1 ligand to aluminium complex, depending on the stoichiometry used for the reaction (Figure 3.16). In both these reactions the conditions were the same, namely room temperature in toluene. The reaction outcome is

controlled by equivalence of $AlMe_3$ added to the ligand solution. Both of these compounds were isolated by crystallisation in a hexane/toluene mixture.

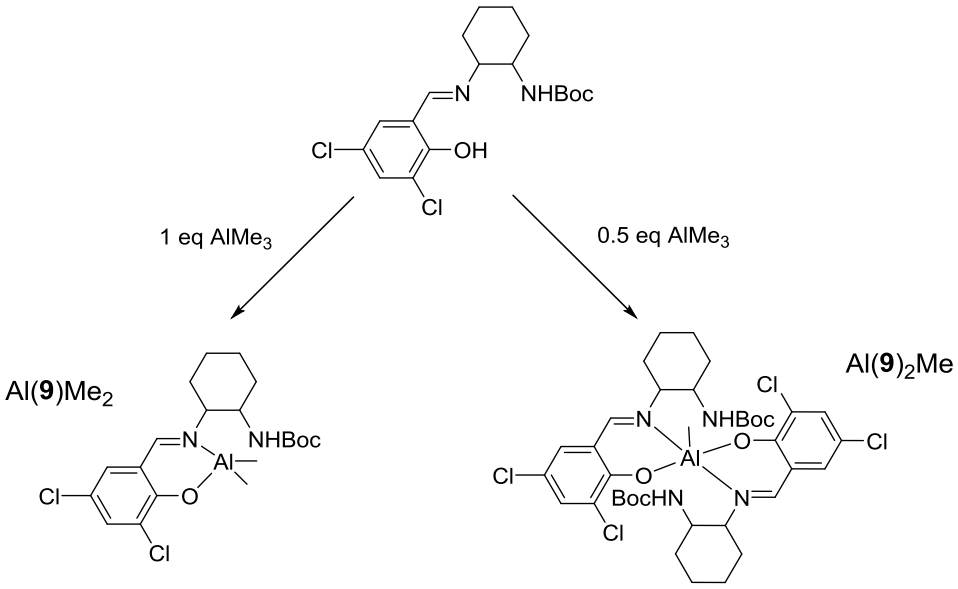


**Figure 3.16: Syntheses of Al(9)$Me_2$ and Al(9)$_2$Me**

Figures 3.17 and 3.18 show the crystal structures for Al(**9**)$Me_2$ and Al(**9**)$_2$Me respectively. As previously seen with the 1:1 complex, the aluminium centre in Al(**9**)$Me_2$ has a tetrahedral geometry ($\tau_4$ = 0.92). The structure is comparable with the *tert*-butyl substituted complex, with the strained O-Al-N bond, the angle being 94.67(5)°. The aluminium centre in Al(**9**)$_2$Me has a highly distorted trigonal bipyramidal geometry ($\tau_5$ = 0.65). Bond angles and lengths of these complexes are presented in Table 3.02, along with further discussion of the structures.

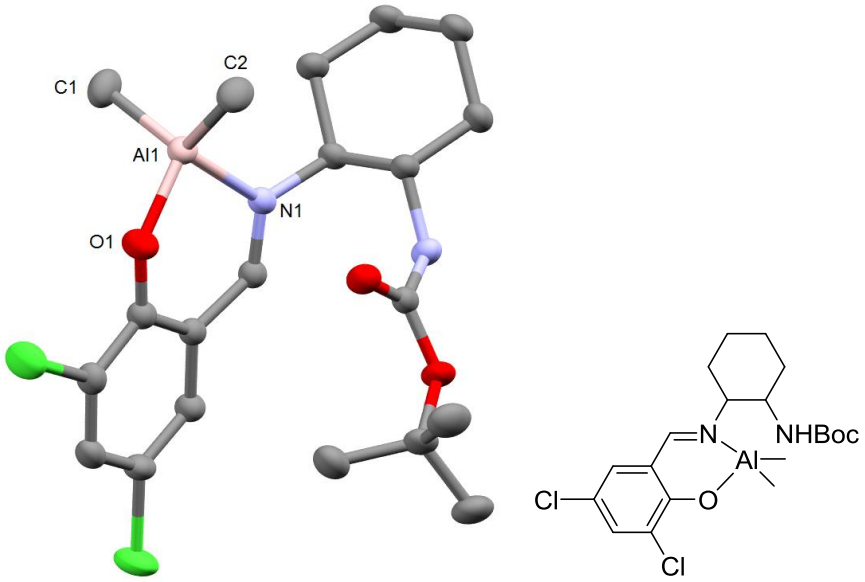


**Figure 3.17: Solid-state crystal structure of Al(9)$Me_2$. Hydrogen atoms have been removed for clarity. Ellipsoids are shown at the 30 % probability level.**

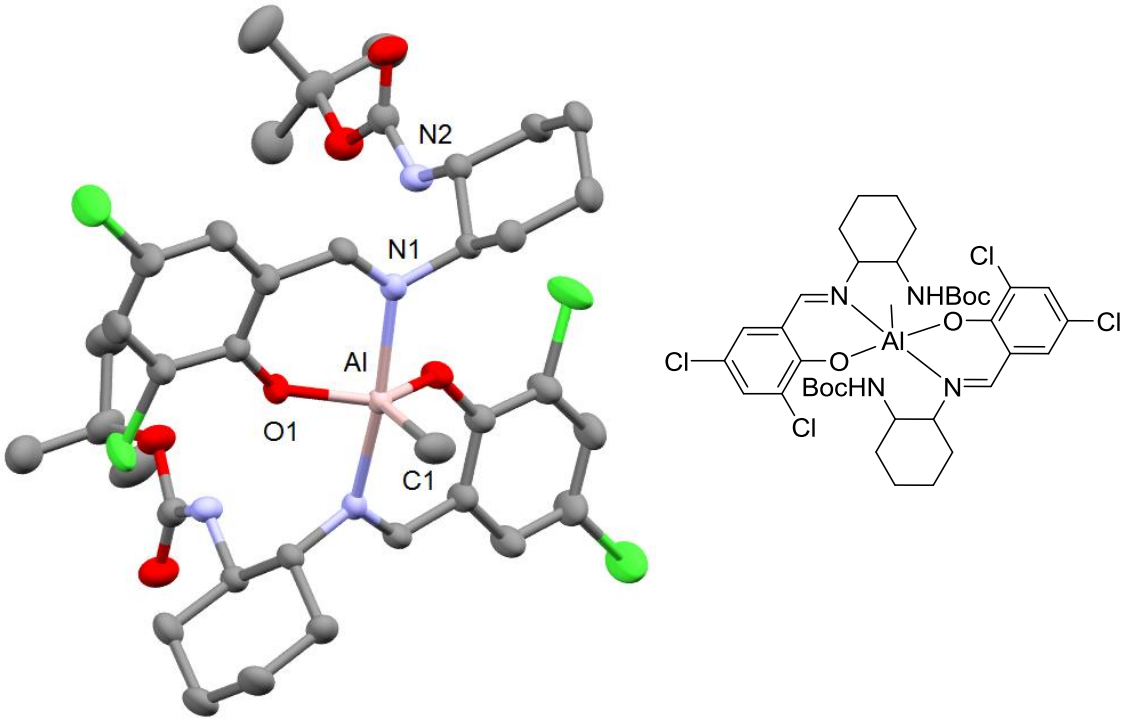


**Figure 3.18: Solid-state crystal structure of Al(9)$_2$Me. All hydrogen atoms have been removed for clarity. Ellipsoids are shown at the 30 % probability level. A molecule of toluene is present in the unit cell which has been removed for clarity.**

Figure 3.19 shows the $^1$H NMR spectrum of Al(**9**)Me$_2$. As seen with Al(**8**)Me$_2$, the two aluminium methyl resonances are distinct (seen at -0.43 and -0.33 ppm), indicating that the structure is 'locked' into position with the methyl groups in different environments, implying the solid-state structure is retained in solution. The nitrogen of the NHBoc moiety is not deprotonated by the aluminium centre, evidenced by the N-H proton seen as the doublet at 3.86 ppm. This was also observed for Al(**8**)Me$_2$, showing that the structures are similar and that the change of aryl substituent does not greatly affect the bonding nature of the aluminium centre.

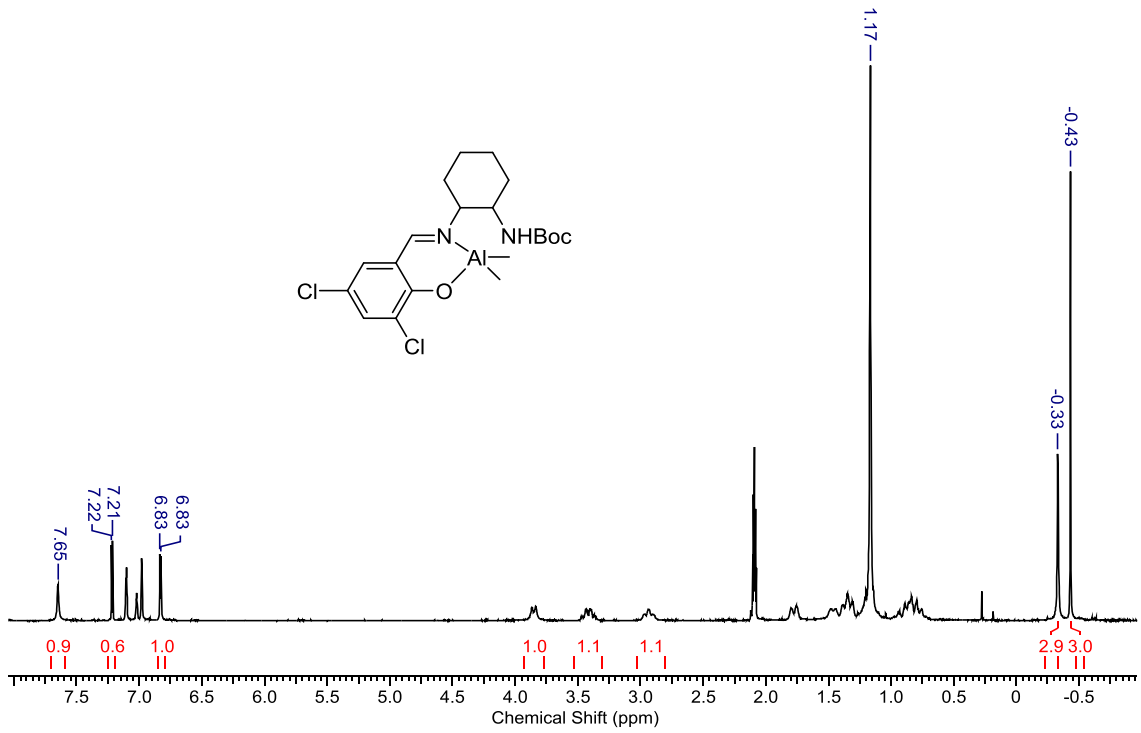


**Figure 3.19: $^{1}$H NMR spectrum of Al(9)Me$_2$ in $C_6D_5CD_3$**

The 2:1 complex Al(**9**)$_2$Me was found to be extremely insoluble in common deuterated solvents, as was found with the other complex Al(**7**)$_2$Me. As such, no reliable NMR spectroscopic data was obtained and the complex was characterised by X-ray crystallography and elemental analysis. The elemental analysis results showed the complex to be of high purity and is in agreement with the solid-state formula obtained.

Table 3.02 shows selected bond lengths and angles for the four aluminium structures discussed above. Figure 3.20 shows structure **II**, which has a comparable structure to the 2:1 structures, and has been included in Table 3.02 for comparison.

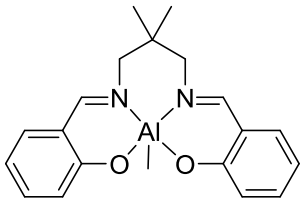


**II**

**Figure 3.20: Structure II**[8]

**Table 3.02: Selected bond angles (°) and lengths (Å) for structures described above**

| | Al(**7**)$_2$Me | Al(**8**)Me$_2$ | Al(**9**)$_2$Me | Al(**9**)Me$_2$ | **II**[9] |
|---|---|---|---|---|---|
| **Al-O1** | 1.802(1) | 1.771(3) | 1.803(2) | 1.784(1) | 1.836(2) |
| **Al-O2** | 1.800(1) | - | 1.803(2) | - | 1.797(2) |
| **Al-N1** | 2.053(1) | 1.982(3) | 2.090(2) | 1.980(1) | 2.008(2) |
| **Al-N3** | 2.048(1) | - | 2.090(2) | - | 2.078(2) |
| **Al-C1** | 1.976() | 1.952(4) | 1.969(4) | 1.961(2) | 1.982(3) |
| **Al-C2** | - | 1.963(4) | - | 1.952(2) | - |
| **O1-Al-C1** | 119.20(7) | 109.82(16) | 116.76(6) | 111.26(7) | 97.2(1) |
| **O1-Al-N1** | 89.92(5) | 94.23(13) | 88.36(7) | 94.67(5) | 89.38(8) |
| **N1-Al-C1** | 92.48(7) | 113.24(16) | 95.54(5) | 108.40(6) | 118.0(1) |
| **N1-Al-N3** | 174.53(6) | - | 168.91(11) | - | 83.74(8) |
| **O1-Al-O2** | 117.18(6) | - | 126.47(12) | - | 89.36(8) |

Comparing Al(**7**)$_2$Me and Al(**9**)$_2$Me, the Al-O1 bond lengths are within error of one another and as such can be considered analogues; 1.802(1) Å for Al(**7**)$_2$Me and for 1.803(2) Å Al(**9**)$_2$Me. Interestingly this is not the case for the Al-N1 and Al-N3 bonds, which are shorter for Al(**7**)$_2$Me, 2.053(1) Å and 2.048(1) Å respectively, than in Al(**9**)$_2$Me, 2.090(2) Å for both Al-N1 and Al-N3. This lengthening of these bonds may be attributed to the chloro groups in Al(**9**)$_2$Me creating steric repulsion between the ligands, elongating the axial Al-N bonds. Further, electronic effects could also be coming into play, with the electron-withdrawing nature of the chloro groups potentially reducing the nucleophilicity of the imine, which again could contribute to the lengthening of these bonds. Presumably, sterics also goes some way to explain why the 2:1 ligand complex could not be formed using **8**H, as the tert-butyl groups would cause a steric clash along this axis, preventing a second ligand from bonding with the aluminium centre. The bond lengths in these two complexes are similar to those in the literature compound **II**, despite this structure featuring a single tetradentate ligand as opposed to two bidentate ligands as seen in Al(**7**)$_2$Me and Al(**9**)$_2$Me. This is due the aluminium centre in structure **II** having a distorted trigonal bipyramidal geometry. The bond angles in the structures Al(**7**)$_2$Me and Al(**9**)$_2$Me are typical for this geometry, exemplified in Al(**7**)$_2$Me by the planar equatorial bond angle O1-Al-C1 at 119.20(7) °, the axial-equatorial bond angle O1-Al-N1 at 89.92(5) ° and the slightly distorted

planar axial bond angle N1-Al-N3 at 174.53(6) °. The bond angles in structure **II** are not directly comparable as in this complex the two nitrogen atoms are situated *cis* to one another (as are the oxygen atoms), whereas they are *trans* in Al(**7**)$_2$Me and Al(**9**)$_2$Me. As such, the aluminium methyl is situated around 90 ° from N1 in the complexes in this chapter: N1-Al-C1 = 92.48(7) ° in Al(**7**)$_2$Me and 95.54 ° in Al(**9**)$_2$Me. For **II**, N1-Al-C1 is 118.0(1) ° as this is an equatorial bond. In both Al(**7**)$_2$Me and Al(**9**)$_2$Me the axial bond angle is reduced from 180 °, due to the rigid ligand structure forcing the nitrogen atoms slightly out of plane, seen in the angle N1-Al-N3, which is 174.53(6) ° for Al(**7**)$_2$Me and 168.91(11) ° for Al(**9**)$_2$Me.

With the mono ligated complexes, in Al(**8**)Me$_2$ and Al(**9**)Me$_2$ the Al-N1 bond lengths are statistically the same, 1.982(3) Å and 1.980(1) Å respectively. The other bond lengths with the aluminium are close in value between these two complexes, indicating that the change of the phenyl substituent has little effect upon the metal centre. For example, Al-O1 is 1.771(3) Å in Al(**8**)Me$_2$ and 1.784(1) Å in Al(**9**)Me$_2$. Both of these structures have distorted tetrahedral geometries about the aluminium centre, as evidenced by the bond angles approaching 109.5 °. For example, O1-Al-C1 in Al(**8**)Me$_2$ is 109.82(16) ° and in Al(**9**)Me$_2$ N1-Al-C1 is 108.40(6) °. The rigidity of the salen moiety of the ligand causes some distortion in the geometry, best evidenced by the O1-Al-N1 bond angles in these complexes.

To summarise, it is possible to prepare 2:1 ligand to metal centre complexes using **7**H and **9**H as the ligand, but **8**H can only form a 1:1 complex, due to the steric environment of the *tert*-butyl groups preventing another ligand from associating with the aluminium centre. The ligand **7**H cannot form a 1:1 complex with aluminium, suggesting that without any steric hindrance the biligated structure is the most favourable.

### 3.3.2 Zinc complexes

To provide a comparison, zinc complexes were also formed using these ligands. It was found that the ligand **7**H could form both a 2:1 and 1:1 complex with zinc (Figure 3.21). Ligand **9**H successfully formed a 2:1 complex but no 1:1 complex was isolated. Solid-state crystal structures of Zn(**7**)$_2$ and Zn(**9**)$_2$ were obtained and are shown in Figures 3.24 and 3.25 on page 99. Unfortunately, no zinc compounds were successfully isolated using **8**H as a ligand.

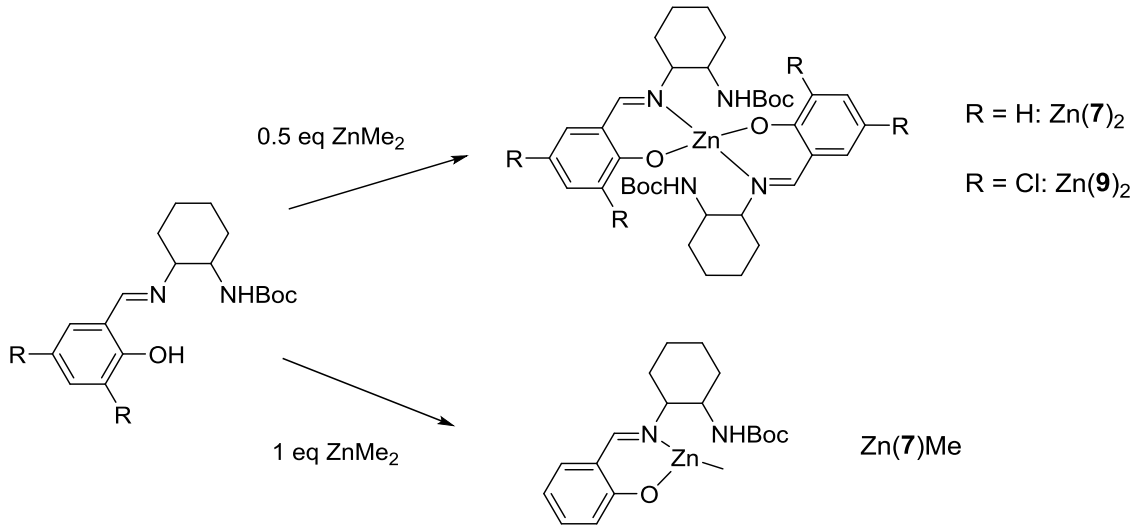


**Figure 3.21: Syntheses of zinc complexes Zn(7)$_2$ and Zn(7)Me**

A single crystal structure was not obtained from compound Zn(**7**)Me, however analysis of the $^1$H NMR spectrum (Figure 3.22) confirmed that the 1:1 ligand to zinc complex had been formed, evidenced by the Zn-Me resonance at -0.07 ppm, which integrates to 3H. $^{13}$C{$^1$H} NMR shown in Figure 3.23 also confirmed the expected solution state structure, with the resonance at -13.9 ppm corresponding to the zinc methyl carbon moiety. Moreover, elemental analysis of the solid showed it to be of high purity.

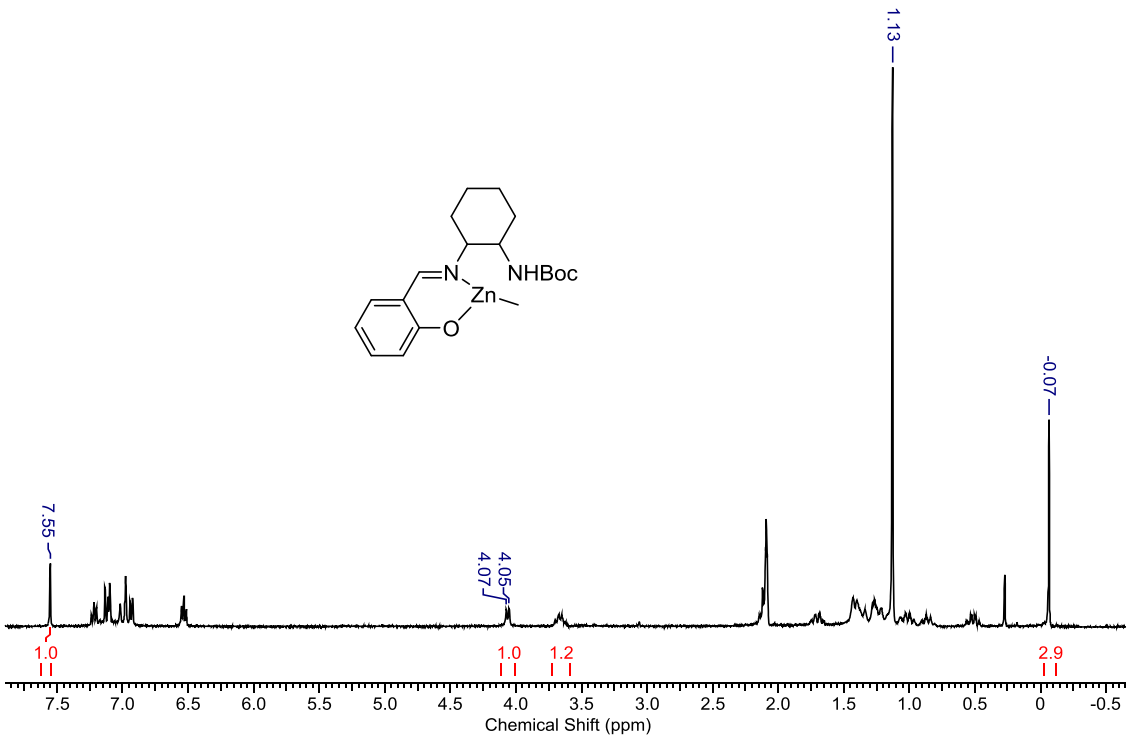


**Figure 3.22: $^{1}$H NMR spectrum of Zn(7)Me in $d_8$ toluene**

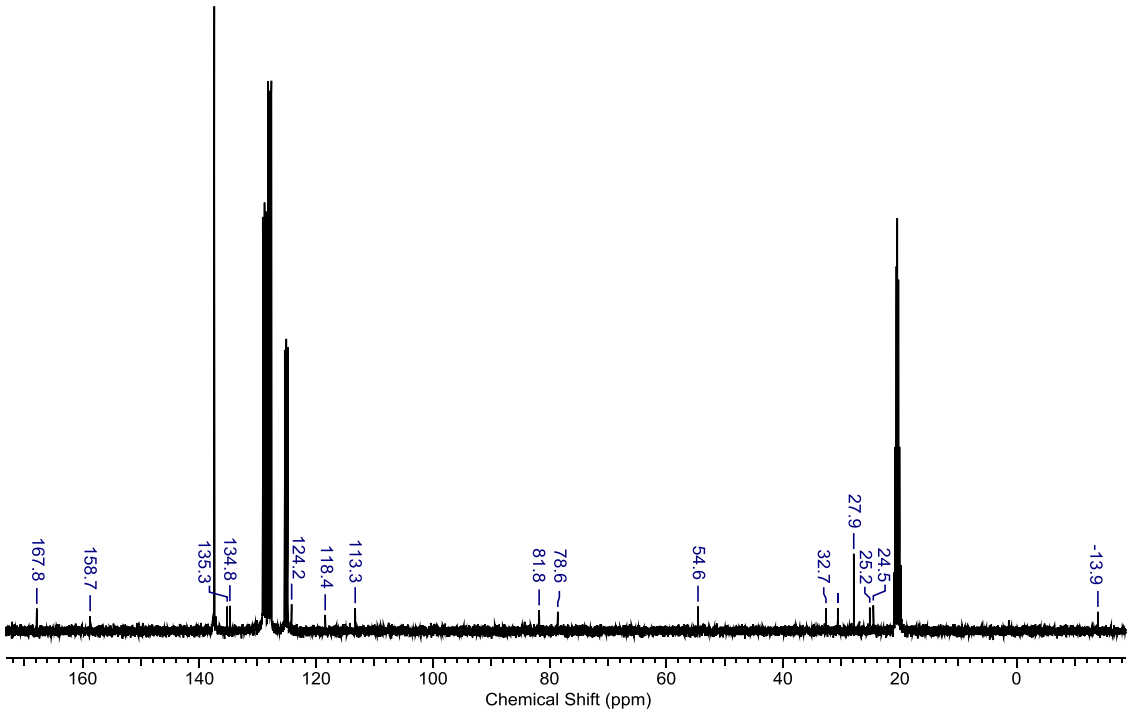


**Figure 3.23: $^{13}C\{^{1}H\}$ NMR spectrum of Zn(7)Me in $d_8$ toluene**

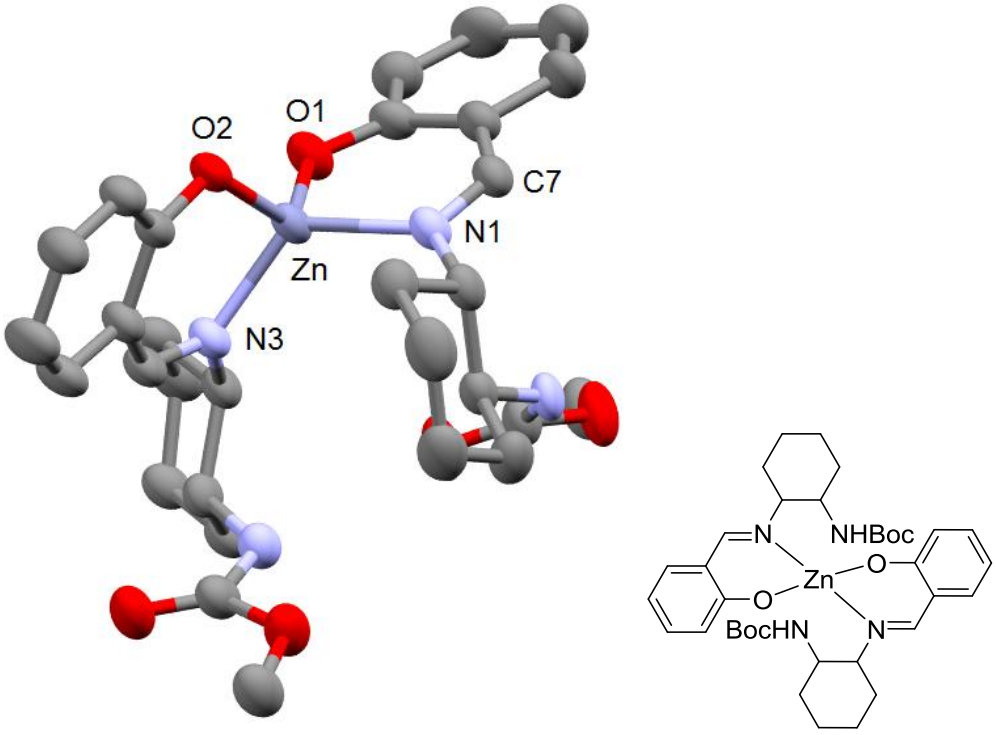


**Figure 3.24: Solid-state crystal structure of Zn(7)$_2$. The methyl groups of the Boc, all hydrogen atoms and two molecules of toluene have been removed for clarity. Ellipsoids are shown at the 30 % probability level.**

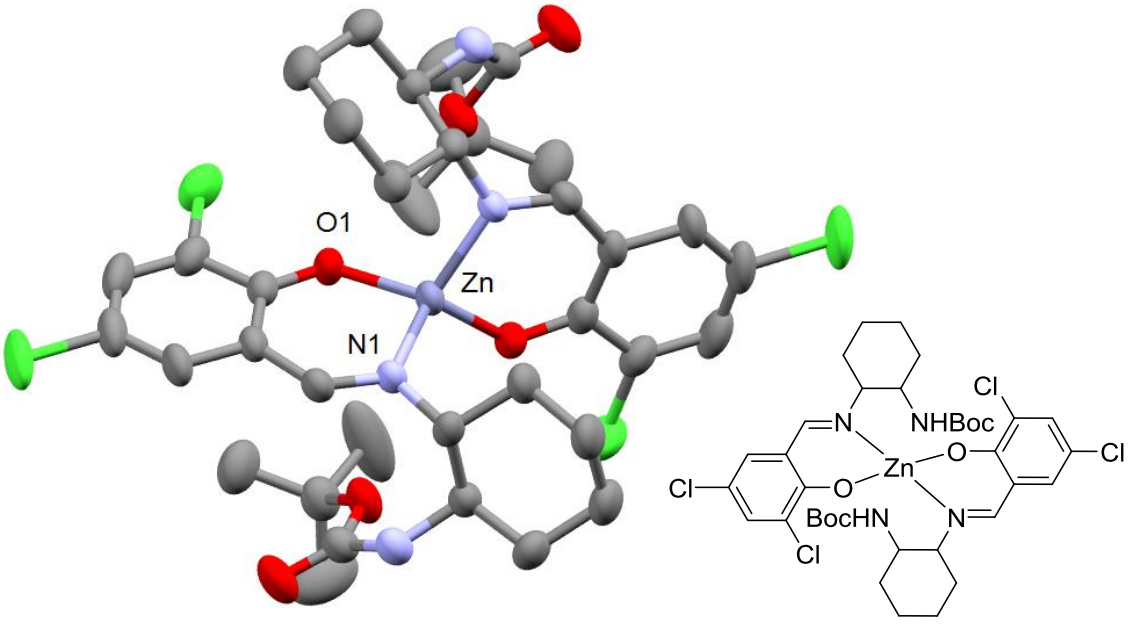


**Figure 3.25: Solid-state crystal structure of Zn(9)$_2$. Ellipsoids are shown at the 30 % probability level and all hydrogen atoms have been removed for clarity.**

Zn(**7**)$_2$ and Zn(**9**)$_2$ both have distorted tetrahedral structure, with $\tau_4$ = 0.80 for the former and $\tau_4$ = 0.85 for the latter. The bond lengths and angles in these complexes have been compared to a zinc compound in the literature (**III**, Figure 3.26), which is similar to Zn(**9**)$_2$ but does not have the NHBoc moiety on the cyclohexane or a chloro group *ortho* to the phenoxy oxygen.[10] The

bond lengths for Zn-N1 are statistically equivalent in Zn(**9**)$_2$ and **III**, which is not surprising as the complexes are so structurally similar. Similarly, the Zn-O1 bond is statistically equivalent in Zn(**7**)$_2$ and **III**, 1.921(2) Å and 1.922(2) Å respectively. This is most likely due to the fact that they both lack a substituent *ortho* to the phenoxy oxygen, whereas Zn(**9**)$_2$ has a chloro group *ortho* to the phenoxy oxygen. The bond N1-Zn-N3 is 116.34(18) ° for Zn(**9**)$_2$, which is much smaller than in Zn(**7**)$_2$ or **III**, at 124.72(12) ° and 122.35(9) ° respectively. Once again, this can be attributed to the chloro group that is *ortho* to the phenoxy oxygen in Zn(**9**)$_2$, causing the bis- ligand to twist slightly to avoid steric clashes, thus altering the bond angles about the zinc metal centre.

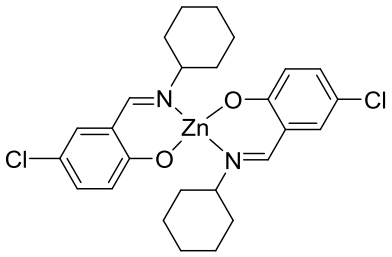


**III**

**Figure 3.26: Complex III, as reported by Hou[10]**

**Table 3.03: Selected bond angles (°) and lengths (Å) for Zn(7)$_2$, Zn(9)$_2$ and III**

| | **Zn(7)$_2$** | **Zn(9)$_2$** | **III** |
|---|---|---|---|
| **Zn-O1** | 1.921(2) | 1.905(2) | 1.922(2) |
| **Zn-O2** | 1.941(2) | 1.905(2) | 1.910(2) |
| **Zn-N1** | 2.004(3) | 2.016(3) | 2.019(2) |
| **Zn-N3** | 1.982(3) | 2.016(3) | 2.015(2) |
| **O1-Zn-O2** | 122.35(11) | 124.21(18) | 120.24(9) |
| **O1-Zn-N1** | 97.73(11) | 96.67(12) | 94.72(9) |
| **O1-Zn-N3** | 95.73(11) | 112.17(12) | 112.72(9) |
| **N1-Zn-N3** | 124.72(12) | 116.34(18) | 122.35(9) |

Figure 3.27 shows the proton NMR spectrum of Zn(**9**)$_2$. The solid-state structure appears to be retained in solution. As was observed with the aluminium complexes of these ligands, the nitrogen on the NHBoc group does not bond with the metal centre and remains protonated, evidenced by the N-H resonance at 5.56 ppm. As the zinc metal centre is coordinatively saturated and has no methyl groups, the spectrum appears very similar to that of the ligand, as

the distinctive Zn-Me resonance is not present. Evidence that this is indeed the complex rather than ligand is the lack of Ar-OH resonance in the 13 ppm region.

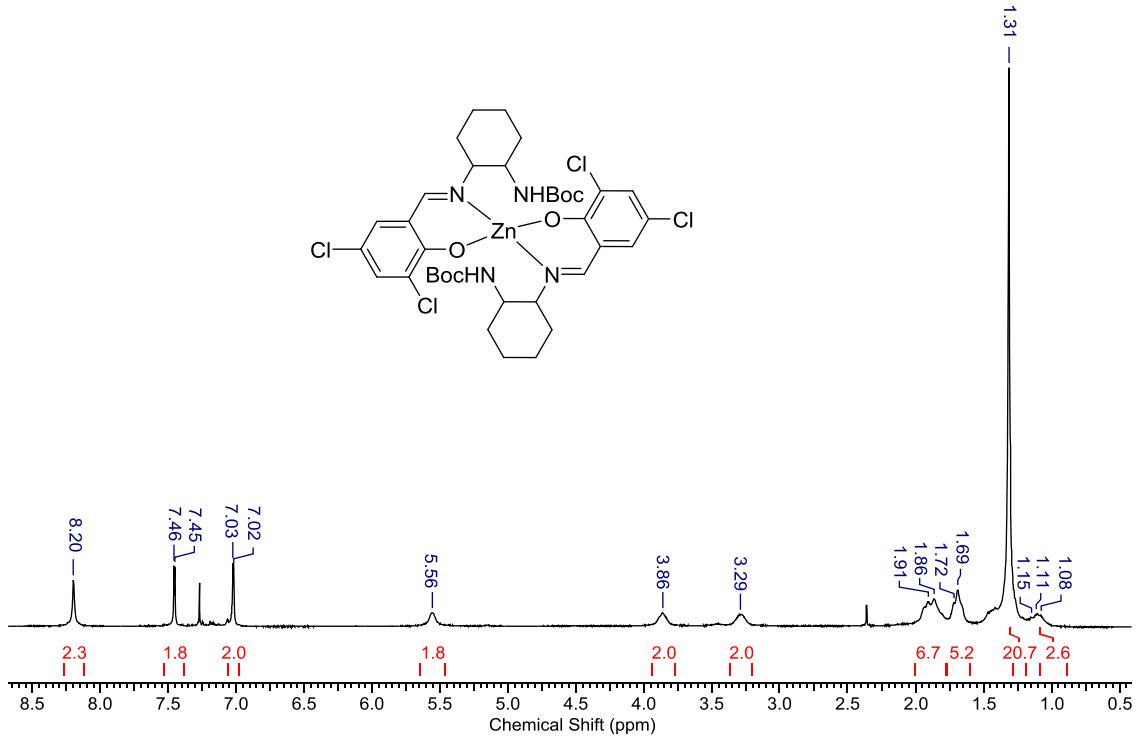


**Figure 3.27: $^{1}$H NMR spectrum of Zn(9)$_2$ in CDCl$_3$**

The asymmetric tridentate ligands **10**H and **12**H were reacted with one equivalent dimethylzinc in toluene at room temperature to form complexes Zn(**10**)Me and Zn(**12**)Me (Figure 3.28). No zinc complex using ligand **11**H was successfully isolated, due to high solubility of the complex which was not conducive to crystallisation. Where possible, the complexes were successfully recrystallised from toluene and the solid-state crystal structures obtained, Zn(**10**)Me shown in Figure 3.29 and Zn(**12**)Me shown in Figure 3.30 on page 102.

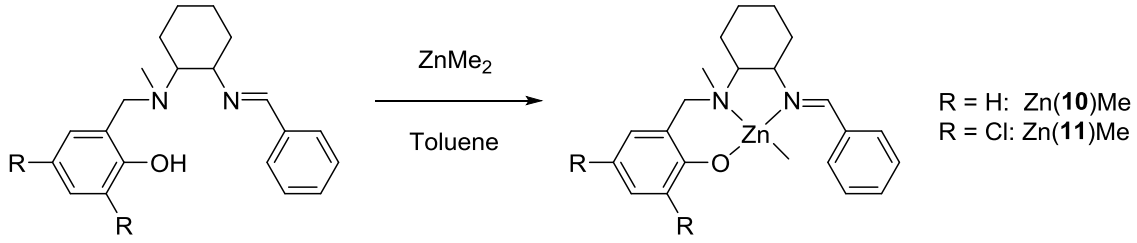


**Figure 3.28: Synthesis of Zn(10,12)Me**

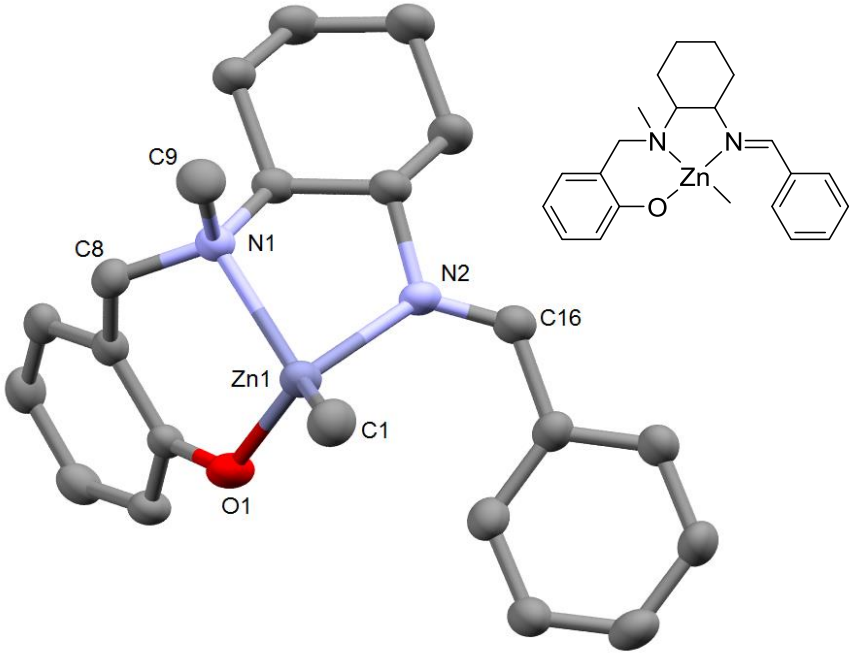


**Figure 3.29: Solid-state crystal structure for Zn(10)Me. Hydrogen atoms have been removed for clarity. Ellipsoids are shown at the 30 % probability level. Twinning (14 %) by virtue of a 180 degree rotation about the 1 0 0 reciprocal lattice direction was accounted for in the model presented.**

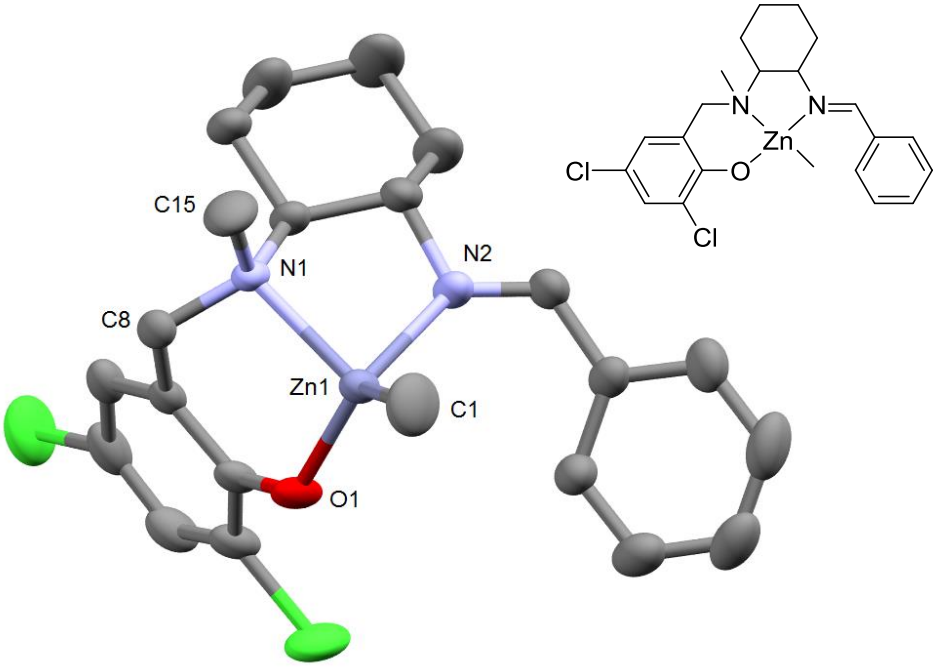


**Figure 3.30: Solid-state crystal structure for Zn(12)Me. Ellipsoids are shown at the 30 % probability level and all hydrogen atoms have been removed for clarity.**

For both complexes the metal centre has a distorted tetrahedral geometry, with $\tau_4$ = 0.81 for Zn(**10**)Me and $\tau_4$ = 0.80 for Zn(**12**)Me. The bond angles and lengths for both structures can be found in Table 3.04 and compared to a literature zinc compound, **IV** (depicted in Figure 3.31).

Between all three structures, the zinc bond lengths are very similar to one another. For example, bond length Zn-O1 is 1.942(2) Å in Zn(**10**)Me, 1.951(2) Å in Zn(**12**)Me and 1.975(1) Å in **IV**. In particular, the zinc bond lengths between Zn(**10**)Me and Zn(**12**)Me show little difference, as the two complexes are structurally similar. For **IV**, the nitrogen adjacent to the phenolate is part of an imine group rather than an amine, so some differences occur. For example, the bond length Zn-N1 in **IV** is 2.292(1) Å, which is significantly longer than in Zn(**10**)Me or Zn(**12**)Me, where it is 2.130(2) Å and 2.140(3) Å respectively. The bond angles in each complex exemplify the distorted nature of the tetrahedral geometry of the zinc metal centres. For example, the N1-Al-N2 angle of 81.86(8) ° in Zn(**10**)Me is far lower than the theoretical value of 109.5 °, indicating strain as a result of the ligand structure.

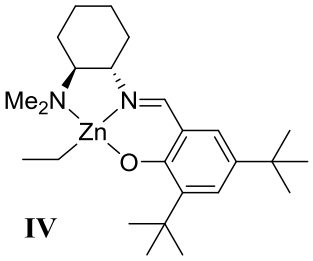


**IV**

**Figure 3.31: Literature compound IV**[11]

**Table 3.04: Selected bond angles (°) and lengths (Å) for Zn(10)Me, Zn(12)Me and IV**

| | Zn(10)Me | Zn(12)Me | IV |
|---|---|---|---|
| **Zn-O1** | 1.942(2) | 1.951(2) | 1.975(1) |
| **Zn-N1** | 2.130(2) | 2.140(3) | 2.292(1) |
| **Zn-N2** | 2.135(2) | 2.169(3) | 2.042(1) |
| **Zn-C1** | 1.959(3) | 1.978(5) | 1.991(1) |
| **N1-C8** | 1.490(4) | 1.489(4) | 1.289(1) |
| **N2-C16** | 1.273(4) | 1.282(5) | 1.476(2) |
| **N1-Zn-N2** | 81.86(8) | 81.2(1) | 76.86(4) |
| **N1-Zn-O1** | 96.54(9) | 94.7(1) | 89.55(4) |
| **N1-Zn-C1** | 123.70(12) | 123.8(2) | 139.75(5) |
| **N2-Zn-C1** | 117.04(12) | 112.3(2) | 106.31(5) |

Figure 3.32 shows the $^{1}$H NMR spectrum for Zn(**10**)Me. The spectrum shows expected resonances for the Zn-ligand complex, along with a smaller secondary series. The Zn-Me resonance at -0.64 ppm was observed to split into two, suggesting that either more than one isomer is present, or that impurities are present in the compound.

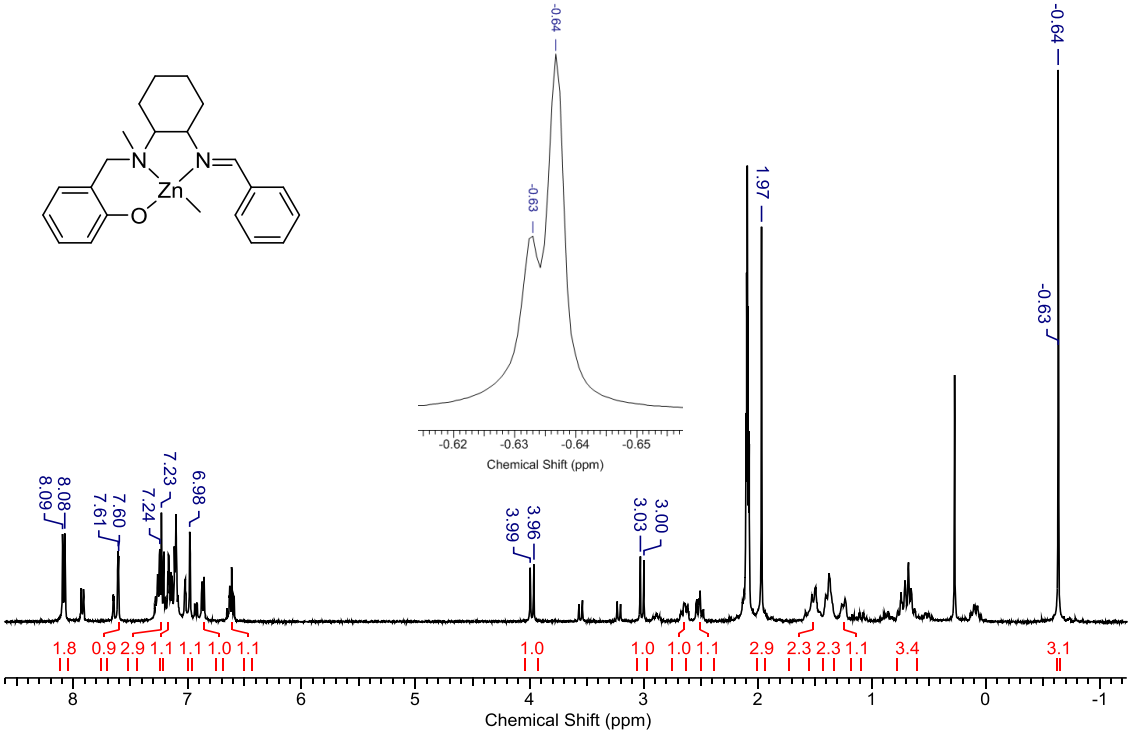


**Figure 3.32: $^{1}$H NMR spectrum of Zn(10)Me. Inset: enlarged Zn-methyl region.**

To verify that there are diastereomers present, and that these resonances do not originate from impurities (such as unreacted ligand, or a 2:1 complex), a DOSY (diffusion-ordered spectroscopy) NMR was acquired, Figure 3.33 shows the spectrum. Visual inspection of the spectrum shows that the major and minor species present diffuse at the same rate, which implies that the different resonances are representative of species of similar volume (such as isomers), rather than ligand, impurities or a 2:1 species. The diffusion rate of Zn(**10**)Me is ca. 8.9 x $10^{-10}$ $m^2s^{-1}$. Figure 3.34 illustrates the possible stereoisomers that could exist for Zn(**10**)Me. Highlighted in blue is the stereochemistry that is observed with the solid-state crystal structure of this compound, which could be the major isomer seen in the NMR spectrum.

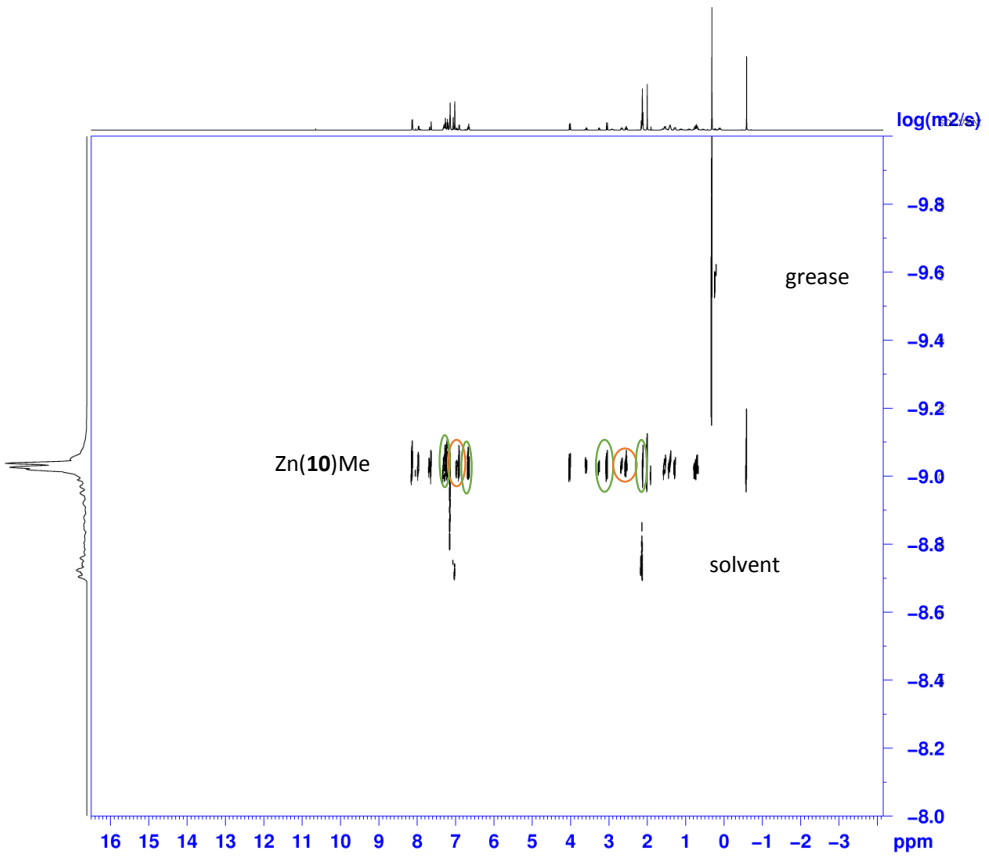


**Figure 3.33: DOSY NMR spectrum of Zn(10)Me. Some major (green) and minor (orange) resonances have been highlighted.**

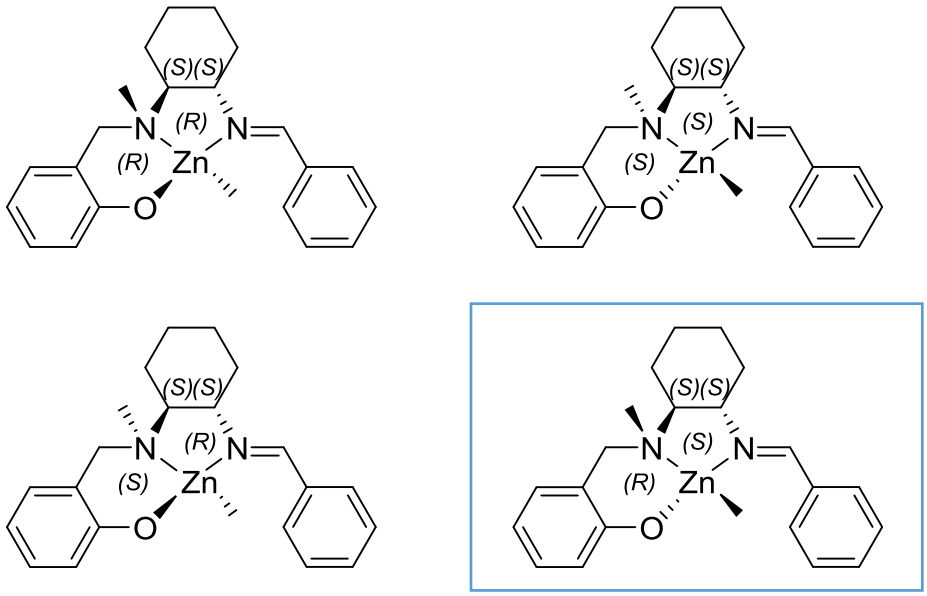


**Figure 3.34: Possible stereoisomers of Zn(10)Me. The highlighted isomer shows the stereochemistry observed by X-ray crystallography. Not pictured are the enantiomers of each stereoisomer above, which are also possible isomers of Zn(10)Me.**

Figure 3.35 shows the $^{1}$H NMR spectrum of Zn(**12**)Me. A series of minor resonances is also visible in this spectrum, indicating that there are various isomers present in the solution. The integrals shown are that for the most abundant isomer. The major and minor isomer visible in this spectrum are present in an approximate 4:1 ratio. Relative integration of the minor series of resonances indicates a 1:1 ratio of Zn-Me to ligand, further confirming that these resonances belong to a stereoisomer of Zn(**12**)Me rather than an impurity.

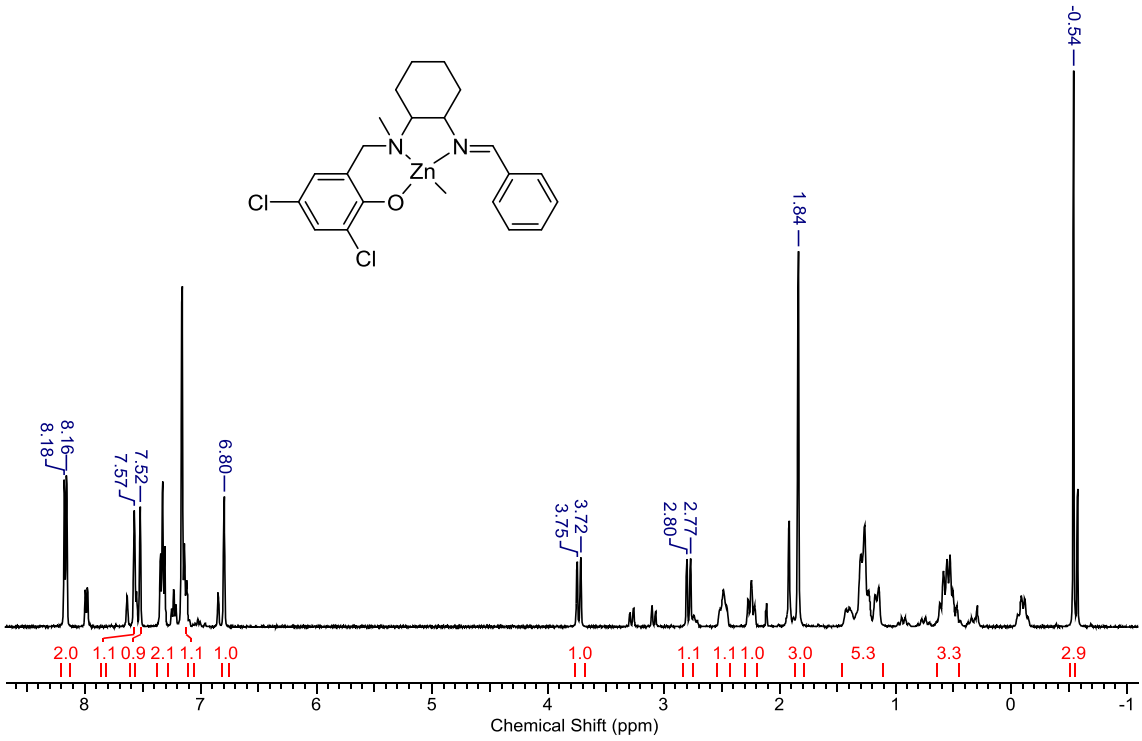


**Figure 3.35: $^{1}$H NMR spectrum of Zn(12)Me in $d_8$ toluene**

The ligand **12**H was also reacted with one equivalent trimethylaluminium to form a metal complex, Al(**12**)$Me_2$, shown in Figure 3.36.

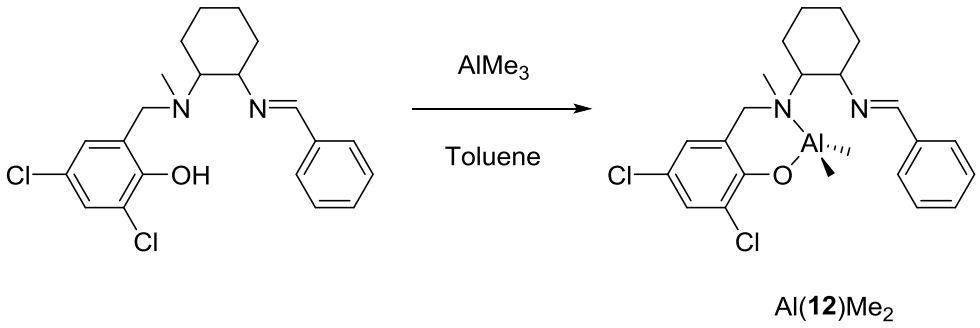


**Figure 3.36: Synthesis of Al(12)Me$_2$**

The solid-state crystal structure of Al(**12**)$Me_2$ is shown in Figure 3.37. Selected bond angles and lengths for this structure can be found in Table 3.05. Interestingly, there is no bond between the

aluminium metal centre and the nitrogen of the imine (N2). This was not observed with the zinc complexes with these ligands. The aluminium centre in this complex has slightly distorted tetrahedral geometry with a $\tau_4$ value of 0.91.

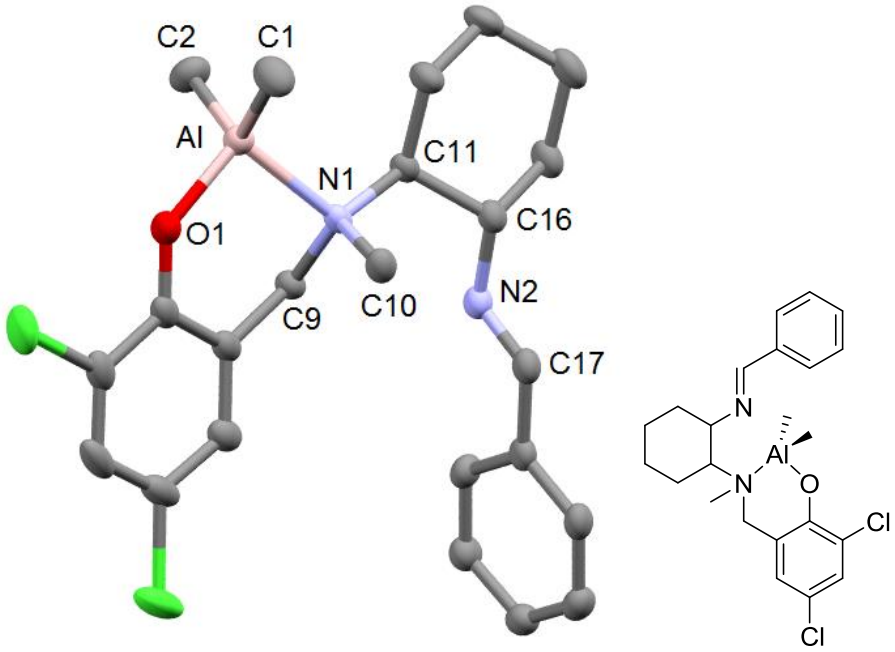


**Figure 3.37: Solid-state crystal structure of Al(12)Me$_2$. Ellipsoids are shown at the 30 % probability level and hydrogen atoms have been removed for clarity.**

When reacted with one equivalent of trimethylaluminium (reaction scheme in Figure 3.38), the ligand **11**H behaved in a different manner to **12**H. A methyl group from the aluminium centre has migrated to the carbon of the imine bond, creating a formal negative charge on the nitrogen atom, which is bonded to the aluminium centre. This methyl migration behaviour on complexation with trimethylaluminium has been previously observed in the literature, for example by Solan *et al.* when utilising 2-(phenyl-2-olate)-6-iminopyridine ligands.[12]

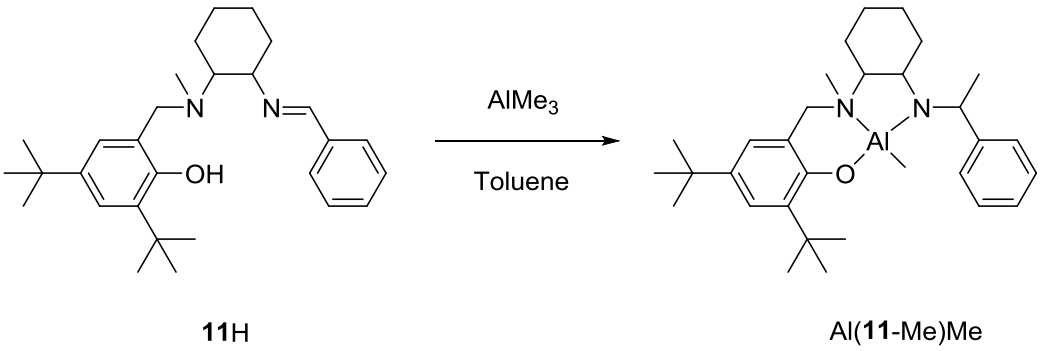


**11**H Al(**11**-Me)Me

**Figure 3.38: Synthesis of Al(11-Me)Me**

Figure 3.39 shows the solid-state crystal structure of Al(**11**-Me)Me, which depicts the migrated methyl group on the carbon atom C24. The aluminium centre has distorted tetrahedral

geometry, with a $\tau_4$ value of 0.86. This is more distorted than the metal centre in Al(**12**)$Me_2$ ($\tau_4$ = 0.91), due to the extra coordinating atom of ligand **11** imposing steric confinement.

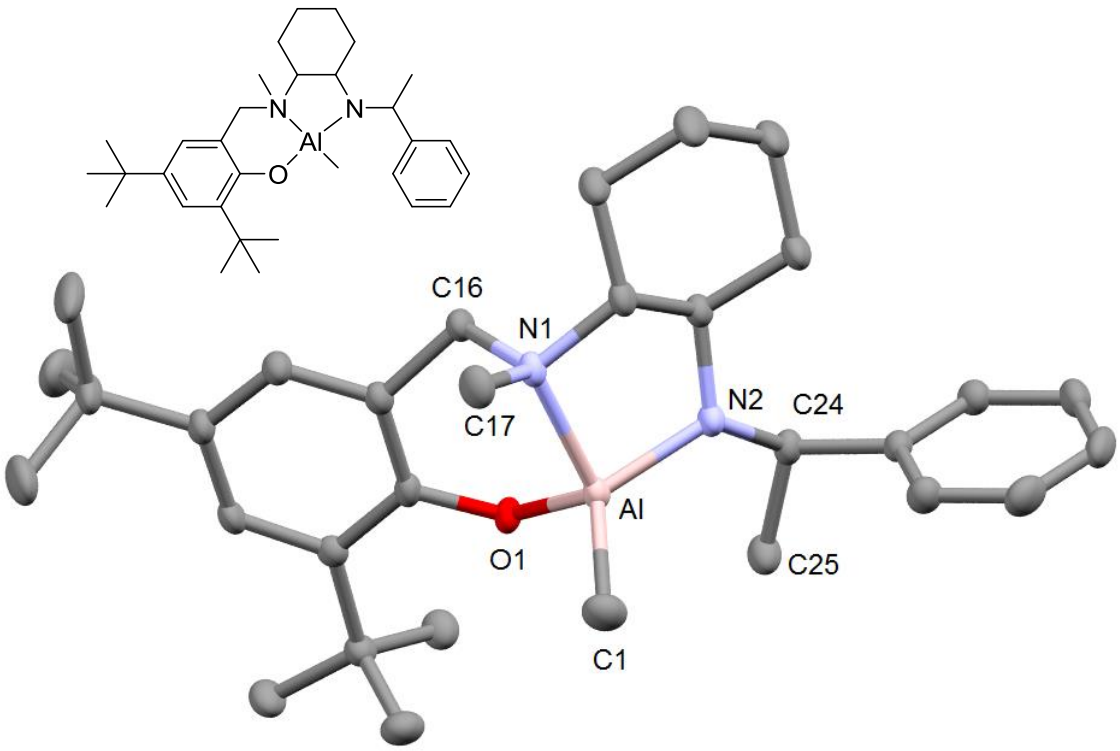


**Figure 3.39: Solid-state crystal structure of Al(11-Me)Me. Ellipsoids are shown at the 30 % probability level and hydrogen atoms have been removed for clarity.**

Table 3.05 shows bond angles and lengths in structures Al(**11**-Me)Me, Al(**12**)$Me_2$, and Al(**9**)$Me_2$ as reported earlier in this chapter, which has a very similar structure to Al(**12**)$Me_2$. Despite the differences in ligand coordination, the aluminium bond lengths in Al(**11**-Me)Me and Al(**12**)$Me_2$ are comparable. For example, Al-O1 is 1.766(1) Å in the former and 1.775(1) Å in the latter. A notable difference in bond lengths between Al(**12**)$Me_2$ and Al(**9**)$Me_2$ is seen with Al-N1, which is 2.035(2) Å in Al(**12**)$Me_2$ and 1.980(1) Å in Al(**9**)$Me_2$. This bond lengthening can be attributed to the nature of the N1 atom in Al(**12**)$Me_2$ which is an amine instead of an imine nitrogen as seen in Al(**9**)$Me_2$. Some bond angles around the tetrahedral aluminium in these complexes are comparable. For example, all complexes exhibit the strained O1-Al-N1 bond, 99.17(4) ° for Al(**11**-Me)Me, 95.94(6) ° for Al(**12**)$Me_2$ and 94.67(5) ° for Al(**9**)$Me_2$, which is far lower in all cases than the theoretical bond angle of 109.5 °. In Al(**11**-Me)Me, the Al-N2 bond is significantly shorter than the Al-N1 bond, at 1.820(1) Å and 2.001(1) Å respectively. This can be attributed to the negative charge on the N2 atom, forming a stronger bond with the Lewis acidic aluminium centre.

**Table 3.05: Selected bond lengths (Å) and angles (°) for Al(11-Me)Me, Al(12)$Me_2$ and Al(9)$Me_2$**

| | Al(**11**-Me)Me | Al(**12**)$Me_2$ | Al(**9**)$Me_2$ |
|---|---|---|---|
| Al-O1 | 1.766(1) | 1.775(1) | 1.784(1) |
| Al-N1 | 2.001(1) | 2.035(2) | 1.980(1) |
| Al-N2 | 1.820(1) | - | - |
| Al-C1 | 1.951(1) | 1.958(2) | 1.961(2) |
| Al-C2 | - | 1.955(2) | 1.952(2) |
| O1-Al-C1 | 110.30(5) | 109.07(8) | 111.26(7) |
| O1-Al-N1 | 99.17(4) | 95.94(6) | 94.67(5) |
| N1-Al-C1 | 115.03(5) | 111.83(7) | 108.40(6) |
| O1-Al-N2 | 118.21(4) | - | - |
| N1-Al-N2 | 90.15(5) | - | - |

Figure 3.40 shows the $^1$H NMR spectrum of Al(**11**-Me)Me. The singlet resonance at -0.94 ppm corresponds to the single aluminium methyl group. The spectrum lacks an imine proton resonance, usually observed above 8 ppm as a singlet, thus supporting the observation that a methyl has migrated onto the imine carbon atom. Further evidence is the doublet at 1.68 ppm (shown in zoomed region) with an integral of 3H, which corresponds to the migrated methyl group. The quartet resonance at 4.22 ppm corresponds to the N-CH proton adjacent to this migrated methyl group.

Figure 3.41 shows the $^1$H NMR spectrum of Al(**12**)$Me_2$. The solid-state structure is retained in solution. The spectrum appears weak due to the complex only being partially soluble in $d_8$ toluene. The two distinct Al-Me resonances at -0.30 and -0.37 ppm show that the methyls are chemically inequivalent, likely due to one of them being situated adjacent to the N-methyl group. The two protons on the methylene bridge are also inequivalent, appearing as two doublets at 4.01 and 4.59 ppm. This spectrum indicates that the complex is structurally 'locked' into place. There are no stereoisomers as was seen with the zinc complexes due to the different coordination of the aluminium centre.

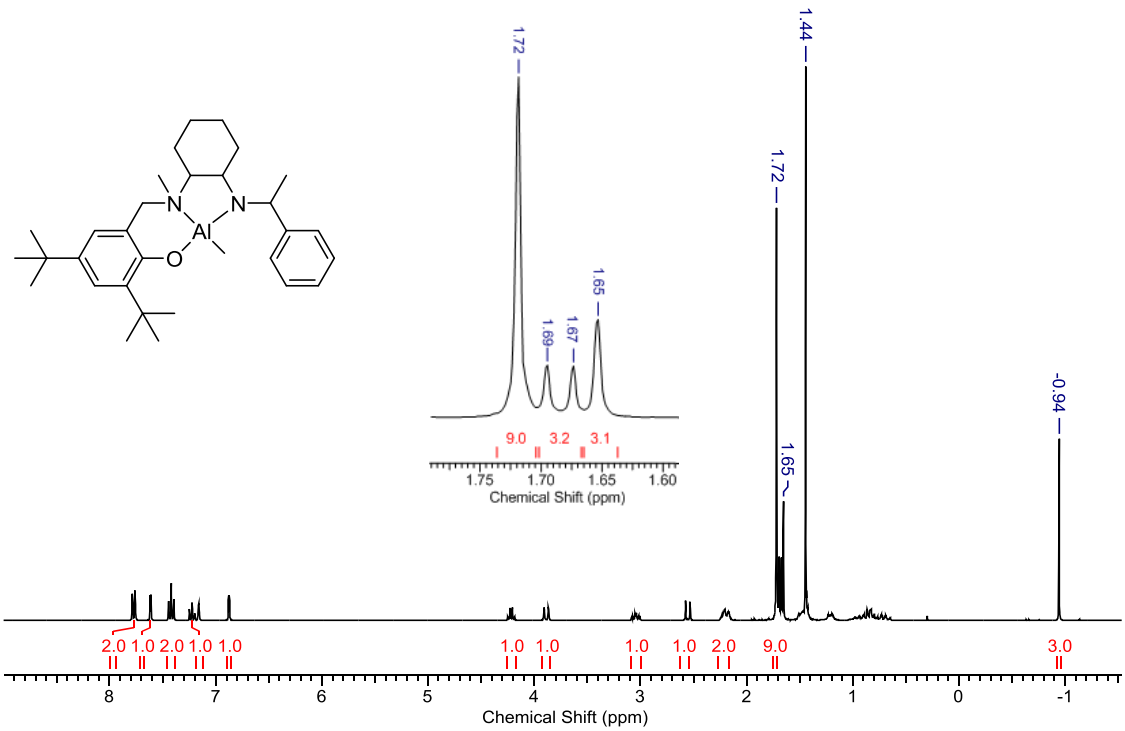


**Figure 3.40: $^{1}$H NMR spectrum of Al(11-Me)Me in $C_6D_6$ with zoomed region inset**

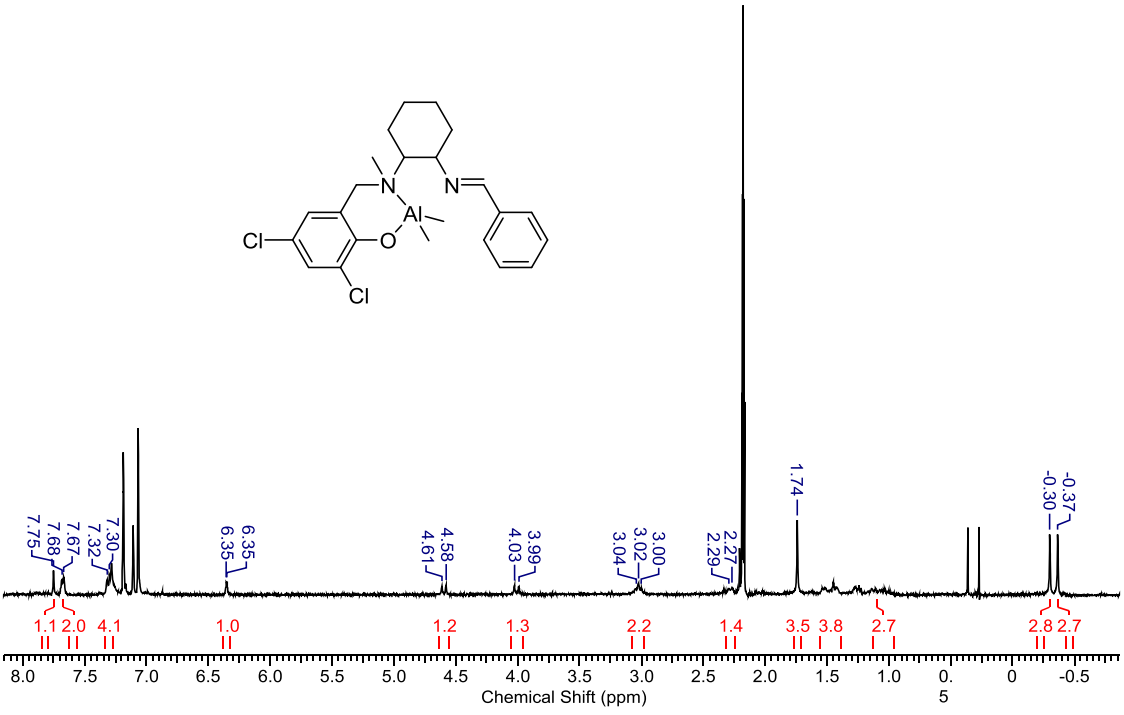


**Figure 3.41: $^{1}$H NMR spectrum of Al(12)$Me_2$ in $d_8$ toluene**

## 3.4 Polymerisation Results

The initiators were used for the ring-opening polymerisation of *rac*-lactide. In this chapter, a GPC with only single detection by refractive index was utilised, as such, corrected $M_n$ values are shown in the tables. These values are obtained by multiplication of $M_n$ by 0.58, as discussed in section 2.3 on page 50. Table 3.06 shows the polymerisation data using the aluminium complexes synthesised using ligand **7-9**H. All polymerisations in this table were carried out using a using one equivalent of benzyl alcohol as a co-initiator. At this ratio, one benzyl alcohol molecule should theoretically displace a methyl group on the aluminium centre, generating a metal alkoxide initiator *in situ*. To investigate the living and controlled nature of these initiators, polymerisations were carried out using different ratios of lactide to initiator.

**Table 3.06: Polymerisation results for the ROP of rac-lactide using aluminium initiators in toluene at 80°C. (1) determined by homonuclear decoupled NMR (2) determined by equation 2.2 (3) determined by GPC (4) corrected by a factor of 0.58**

| Entry | Initiator | LA:I | Conversion (%) | Time (days) | $P_r$[1] | $M_n$ calc[2] ($gmol^{-1}$) | $M_n$ obs[3] ($gmol^{-1}$) | $M_n$ corr[4] ($gmol^{-1}$) | PDI[3] |
|---|---|---|---|---|---|---|---|---|---|
| 1 | Al(**8**)$Me_2$ | 100:1 | 75 | 2 | 0.50 | 10,900 | 12,800 | 7,400 | 1.24 |
| 2 | | 200:1 | 80 | 4 | 0.53 | 23,150 | 34,400 | 19,950 | 1.24 |
| 3 | | 400:1 | 76 | 8 | 0.51 | 43,914 | 30,100 | 17,450 | 1.11 |
| 4 | Al(**9**)$Me_2$ | 100:1 | 97 | 2 | 0.49 | 14,100 | 7,600 | 4,400 | 1.08 |
| 5 | | 200:1 | 96 | 2 | 0.50 | 27,750 | 30,950 | 17,950 | 1.31 |
| 6 | | 400:1 | 95 | 4 | 0.52 | 54,866 | 39,200 | 22,750 | 1.42 |
| 7 | Al(**7**)$_2$Me | 100:1 | 87 | 1 | 0.46 | 12,650 | 10,800 | 6,250 | 1.20 |
| 8 | | 200:1 | 85 | 2 | 0.47 | 24,600 | 16,150 | 8,250 | 1.14 |
| 9 | | 400:1 | 88 | 4 | 0.47 | 50,800 | 19,900 | 15,100 | 1.11 |
| 10 | Al(**9**)$_2$Me | 100:1 | 94 | 1 | 0.49 | 13,650 | 9,700 | 5,650 | 1.16 |
| 11 | | 200:1 | 96 | 2 | 0.48 | 27,775 | 14,000 | 8,100 | 1.43 |
| 12 | | 400:1 | 95 | 4 | 0.49 | 54,866 | 29,000 | 16,800 | 1.34 |

Across all the initiators in Table 3.06 no stereoselectivity is observed, each complex produced atactic polylactide, with $P_r$ values between 0.46 and 0.53. They also require prolonged reaction times (2-8 days) to achieve high conversions. For polymerisations at the higher loading of 400:1,

the molecular weights ($M_n$) were far below the calculated values. There appears to be no remarkable difference in polymerisation data between the monoligated complexes Al(**8**-**9**)$Me_2$ and the diligated complexes Al(**7**,**9**)$_2$Me, with the primary difference being the longer reaction times required (roughly double) for Al(**8**)$Me_2$ to achieve similar conversions to Al(**7**)$_2$Me. This is more likely due to the effect of the substituents than the number of ligands coordinated to the aluminium centre, as the reaction times are similar for Al(**9**)$Me_2$ and Al(**9**)$_2$Me to reach the same conversion.

Table 3.07 shows the polymerisation results for the ROP of lactide using the zinc complexes described in this chapter, at 200:1 initiator loading unless otherwise stated. For the melt polymerisations at 130 °C, both Zn(**7**)$_2$ and Zn(**9**)$_2$ reached high molecular weights within an hour (see entries 1 and 7). Zn(**7**)$_2$ was slightly faster, with high conversion after just 15 minutes. For both complexes the molecular weights are much greater than the expected values, which suggests that the $k_{init}$ is much lower than the $k_{prop}$, or that not all sites are initiating a PLA chain. Even after applying the correction factor, the $M_n$ values are in great excess of the calculated values. The $P_r$ of 0.65 indicates some heterotactic bias of Zn(**7**)$_2$. No benzyl alcohol was added for these melt polymerisations and the initiator itself does not feature an alkoxide bond, so it is not clear how these initiate polymerisation. The initiation could be facilitated by trace impurities in the monomer, which would account for the low degree of initiation and hence high molecular weight. This could be confirmed by end-group analysis, however due to the high molecular weight of the polymer, it is not possible to carry out end-group analysis *via* MALDI-ToF or NMR spectroscopy.

When the polymerisations are carried out in toluene at 80 °C with one equivalent benzyl alcohol as a co-initiator (entries 2 and 8), the initiators have far better molecular weight control, with a narrow PDI of 1.12 for both Zn(**7**)$_2$ and Zn(**9**)$_2$ under these conditions. When the reaction temperature is reduced to 40 °C (entries 3-5) for Zn(**7**)$_2$, the corrected molecular weights agree well with the calculated ones, which shows that good molecular weight control can be achieved with the initiators. The PDI values are in agreement with this, with narrow values of 1.10-1.11 for entries 3-5. With increasing equivalents of benzyl alcohol, the molecular weight decreases.

**Table 3.07: Polymerisation results for the ROP of *rac*-lactide using zinc complexes, all at 200:1 monomer to initiator loading unless otherwise specified. (1) determined by homonuclear decoupled NMR (2) determined by equation 2.2 (3) determined by GPC (4) corrected by a factor of 0.58 (5) 100:1 lactide to initiator loading**

| Entry | Initiator | BnOH | Time (h) | Conversion (%) | $P_r$[1] | $M_n$ calc[2] ($gmol^{-1}$) | $M_n$ obs[3] ($gmol^{-1}$) | $M_n$ corr[4] ($gmol^{-1}$) | PDI[3] | Conditions |
|---|---|---|---|---|---|---|---|---|---|---|
| 1 | Zn(**7**)$_2$ | 0 | 0.25 | 53 | 0.65 | 15,275 | 90,500 | 52,500 | 1.36 | Melt, 130°C |
| 2 | | 1 | 1 | 61 | 0.58 | 17,688 | 8,700 | 5,050 | 1.12 | Tol, 80 °C |
| 3 | | 1 | 18 | 75 | 0.66 | 21,723 | 38,900 | 22,550 | 1.10 | Tol, 40 °C |
| 4 | | 2 | 18 | 93 | 0.64 | 13,509 | 21,700 | 12,600 | 1.11 | Tol, 40 °C |
| 5 | | 4 | 18 | 92 | 0.67 | 6,737 | 15,350 | 8,900 | 1.11 | Tol, 40 °C |
| 6[5] | Zn(**7**)Me | 1 | 120 | 77 | 0.60 | 11,204 | 5,400 | 3,150 | 1.19 | Tol, 80 °C |
| 7 | Zn(**9**)$_2$ | 0 | 1 | 46 | 0.56 | 13,257 | 149,100 | 86,500 | 1.28 | Melt, 130°C |
| 8[5] | | 1 | 1 | 85 | 0.64 | 12,249 | 16,350 | 9,500 | 1.12 | Tol, 80 °C |

Entry 6 *vs* 2 shows that the 1:1 complex, Zn(**7**)Me, was found to be far slower for the ROP of lactide at 80 °C in toluene than the 2:1 complex Zn(**7**)$_2$, the former achieving good conversion in 5 days and the latter only requiring one hour. The polymerisations in entries 2 and 6 were carried out under the same conditions and have similar outcomes in terms of selectivity. For example, $P_r$ = 0.58 in entry 2 and 0.60 in entry 6, and in each case the $M_n$ is lower than the calculated value. This suggests that on addition of benzyl alcohol the outcome in stereochemistry imposed by the ligand is similar, however Zn(**7**)Me requires a longer polymerisation period. The primary difference between these initiators is that Zn(**7**)Me features a zinc methyl bond and Zn(**7**)$_2$ is coordinatively saturated by the coordinating ligands. A possible explanation for this is that Zn(**7**)$_2$ undergoes the activated monomer mechanism (illustrated in Figure 3.42), whereby the initiator interacts with the monomer, facilitating the insertion of the free alcohol into the monomer in the case of initiation, or the insertion of the alcohol-end of the polymer chain into the monomer for subsequent propagation steps. This mechanism has been previously observed when using zinc complexes for the ROP of lactide, for example, it was reported by Gowda and Chakraborty using zinc acetate as an initiator.[13] In the case of Zn(**7**)Me it may be that formation of the alkoxide *in situ* is the rate limiting step in entry 6.

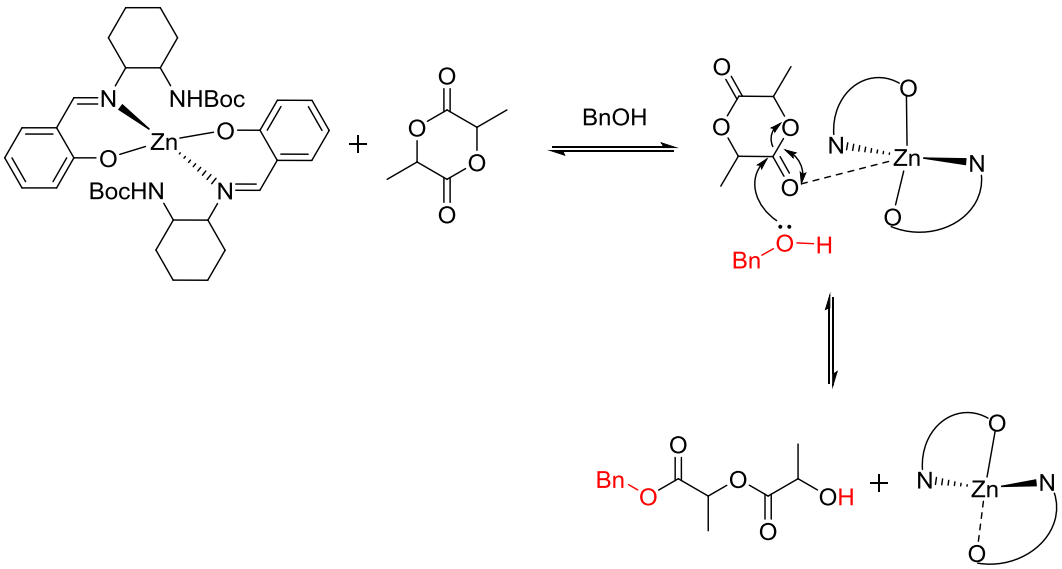


**Figure 3.42: Proposed mechanism for the ROP of lactide using Zn(7)$_2$ and benzyl alcohol *via* an activated monomer mechanism**

To determine whether the ligand itself was having an effect on the polymerisation or acting as an initiator, ligands **7**H-**9**H were used as initiators for polymerisations in the melt. After 24 hours, conversions were very low (0-16 %). This shows that the metal centre plays a vital role in the initiation of the polymerisation, as well as the activity, and that the ligand itself does not initiate the polymerisation. The resulting oligomers from these polymerisations were not further characterised.

Table 3.08 on the following page shows the results of the polymerisation of *rac*-lactide using Zn(**10**)Me, Zn(**12**)Me and Al(**12**)Me$_2$ in solution. In every case, one equivalent of benzyl alcohol was added as a co-initiator to form the zinc alkoxide *in situ*.

The zinc initiators are highly active for the ROP of lactide, as evidenced by the high conversions achieved within hours. These complexes both appear to produce PLA with a mild heterotactic bias, with $P_r$ values between 0.60 and 0.66. The initiator Zn(**10**)Me did not achieve a $P_r$ greater than 0.63 whereas Zn(**12**)Me did not produce any PLA with a $P_r$ lower than 0.64, showing a slight increase in heteroselectivity between H and Cl substituted complexes. Unfortunately, the substituent effect could not be explored further with a *tert*-butyl as this complex was not successfully isolated. Future work would include synthesis of bulkier ligands (e.g. R = Ph) to further investigate the effect of the R group on heterotactic bias. The polymerisation using Zn(**10**)Me was also carried out in THF, to observe any solvent effect. The primary difference appears to be reduced activity, with the same conversion obtained in one day instead of one hour. This could be caused by the solvent coordinating with the metal centre, hindering the lactide from coordination. In every case with the zinc complexes the observed $M_n$ is much lower

than the calculated value, even more so for the corrected values. Alongside this, the PDI values are broad, which suggests that transesterification reactions are occurring. This is likely caused by the addition of methanol to terminate the polymerisation, where the excess alcohol behaves as a chain transfer agent, catalysed by the zinc complexes to break up the polymer chains.

**Table 3.08: Solution polymerisation results for the ROP of rac-lactide at room temperature (20 °C) in solution using tridentate zinc and aluminium complexes (1) determined by homonuclear decoupled NMR (2) determined by equation 2.2 (3) determined by GPC (4) corrected by a factor of 0.58**

| Entry | Initiator | LA:I | Conversion (%) | Time (h) | $P_r$[1] | $M_n$ calc[2] (gmol$^{-1}$) | $M_n$ obs[3] (gmol$^{-1}$) | $M_n$ corr[4] (gmol$^{-1}$) | PDI[3] | Solvent |
|---|---|---|---|---|---|---|---|---|---|---|
| 1 | Zn(**10**)Me | 100 | 98 | 1 | 0.63 | 14,230 | 11,950 | 6,950 | 1.35 | Tol |
| 2 | | 200 | 99 | 1 | 0.62 | 28,928 | 11,600 | 6,750 | 1.41 | Tol |
| 3 | | 400 | 99 | 4 | 0.61 | 57,172 | 27,550 | 16,000 | 1.44 | Tol |
| 4 | | 800 | 99 | 24 | 0.60 | 114,235 | 34,300 | 19,900 | 1.66 | Tol |
| 5 | | 100 | 99 | 24 | 0.61 | 14,374 | 3,750 | 2,200 | 1.55 | THF |
| 6 | Zn(**12**)Me | 100 | 97 | 1 | 0.66 | 14,086 | 16,950 | 9,850 | 1.15 | Tol |
| 7 | | 200 | 97 | 1 | 0.64 | 14,086 | 11,100 | 6,450 | 1.03 | Tol |
| 8 | | 400 | 99 | 24 | 0.65 | 14,374 | 18,550 | 10,750 | 1.52 | Tol |
| 9 | | 800 | 99 | 24 | 0.65 | 14,374 | 67,650 | 39,250 | 1.21 | Tol |
| 10 | Al(**12**)$Me_2$ | 100 | 83 | 24 | 0.56 | 12,050 | 19,050 | 11,050 | 1.05 | Tol |

The initiator Al(**12**)$Me_2$ was found to be far less active for the ROP of lactide but with better molecular weight control, with a narrow PDI of 1.05. The corrected $M_n$ value 11,050 gmol$^{-1}$ lies very close to the expected value which is 12,050 gmol$^{-1}$ and the $P_r$ value is 0.56, tending towards atactic PLA. This initiator is less selective than the zinc analogue. With poor initiator yields and lack of stereoselectivity, no further polymerisations were carried out for Al(**12**)$Me_2$.

Zn(**12**)Me was trialled for the copolymerisation of *rac*-lactide and ε-caprolactone, however after 24 hours of reaction at room temperature lactide conversion had reached 100 % and caprolactone had achieved 0 % conversion, despite being the more readily soluble monomer at this temperature. Indeed, for the homopolymerisation of caprolactone only 11 % conversion was reached with this initiator after heating at 80 °C for 24 hours. It can be concluded that this initiator is not active for caprolactone polymerisation, therefore no more copolymerisation reactions were attempted.

## 3.5 Conclusions

Salen ligands featuring an NHBoc moiety were complexed with aluminium, forming a range of 2:1 and 1:1 ligand to aluminium compounds. Ligand **7**H, which is based on the parent salicylaldehyde, formed a complex with two ligands associated with the metal centre. This also occurred for **9**H, which has chloro substituent groups, on addition of 0.5 equivalents of trimethylaluminium. The compounds Al(**7**)$_2$Me and Al(**9**)$_2$Me had poor solubility in $d_8$-toluene and required heating to dissolve into solution, making solution characterisation problematic for these complexes. It was found that ligand **8**H with sterically demanding $^t$Bu groups on the phenyl ring prevented formation of a 2:1 complex with the metal centre. The compounds Al(**8**)Me$_2$ and Al(**9**)Me$_2$ retained their solid-state structure in solution. When employed for the solution ROP of lactide in toluene, these initiators exhibited no stereoselectivity, producing only atactic polymer ($P_r$ = 0.46-0.53) and reasonable molecular weight control (PDI = 1.08-1.31).

Ligand **7**H was complexed with zinc metal centres, forming both a 2:1 and 1:1 complex, depending on the stoichiometry employed in the synthesis. Ligand **9**H also formed a 2:1 complex with zinc. The most promising initiator in this set was Zn(**7**)$_2$, which shows very high activity in the melt and in solution, with conversion in as little as 5 minutes for melt polymerisation, as well as some selectivity, shown by the moderate heterotacticity of the polymer ($P_r$ = 0.65). Molecular weight control was poor in the melt but moderate in the solution with benzyl alcohol as a coinitiator, producing polymer with a PDI of 1.12 in toluene at 80 °C.

Finally, tridentate ligands were synthesised and complexed with zinc, the product of which was a mixture of stereoisomers which indicated a loss of conformational freedom in the metal centre. These were employed for the ROP of lactide, producing mildly heterotactic PLA ($P_r$ = 0.6-0.66). The molecular weight control was poor, indicating that some transesterification reactions were occurring. The ligand **12**H was also reacted with trimethylaluminium to form an aluminium complex which did not exhibit the stereoisomerism seen with the equivalent zinc complexes. When employed for the ROP of lactide, the complex Al(**12**)Me$_2$ showed poor stereoselectivity but good molecular weight control.

## 3.6 Future Work

In this work it was found that chloro-substituted tridentate zinc complexes showed greater heteroselectivity than unsubstituted complexes. To further investigate this effect, ligands with bulkier groups on the phenolate ring could be reacted with zinc metal centres (Figure 3.43). The purpose of this would be to observe if the extra steric bulk could further enhance the heterotactic selectivity of initiators of this type.

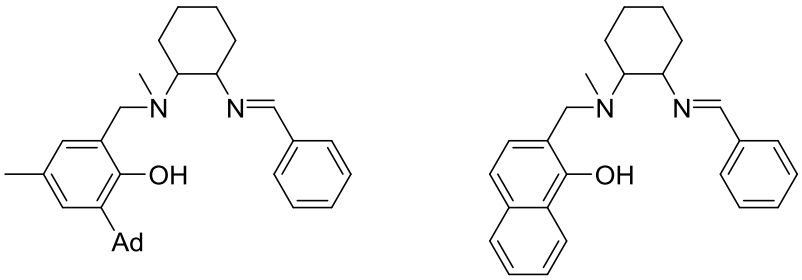


**Figure 3.43: Possible variants on ligands synthesised in this chapter**

A racemic mixture of *trans*-diaminocyclohexane was used as the starting material as the backbone for the ligands in this chapter. Future work would involve isolating the R,R- and S,S-forms of the diaminocyclohexane and using this as the backbone for these ligands, in order to individually synthesise the different isomers of the zinc complexes (Figure 3.44). This would allow for studies into the effect, if any, of the different chirally pure isomers on the selectivity of the initiator.

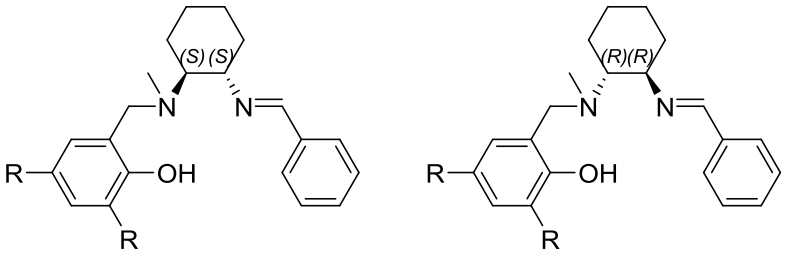


**Figure 3.44: Different enantiomers of ligands**

## 3.7 References


1. E. L. Whitelaw, G. Loraine, M. F. Mahon and M. D. Jones, *Dalton Trans.*, 2011, **40**, 11469-11473.
2. E. L. Whitelaw, M. D. Jones and M. F. Mahon, *Inorg. Chem.*, 2010, **49**, 7176-7181.
3. S. L. Hancock, M. F. Mahon and M. D. Jones, *Dalton Trans.*, 2013, **42**, 9279-9285.
4. A. Pilone, K. Press, I. Goldberg, M. Kol, M. Mazzeo and M. Lamberti, *J. Am. Chem. Soc.*, 2014, **136**, 2940-2943.
5. D. J. Darensbourg and O. Karroonnirun, *Inorg. Chem.*, 2010, **49**, 2360-2371.
6. H.-Q. Hao, X. Lin and J. Sun, *Chin. J. Inorg. Chem.*, 2013, **29**.
7. A. W. Addison, T. N. Rao, J. Reedijk, J. Van Rijn and G. C. Verschoor, *J. Chem. Soc., Dalton Trans.*, 1984, 1349-1356.
8. P. Hormnirun, E. L. Marshall, V. C. Gibson, R. I. Pugh and A. J. P. White, *Proc. Natl. Acad. Sci.*, 2006, **103**, 15343-15348.
9. M. A. Van Aelstyn, T. S. Keizer, D. L. Klopotek, S. Liu, M.-A. Munoz-Hernandez, P. Wei and D. A. Atwood, *Organometallics*, 2000, **19**, 1796-1801.
10. H. N. Hou, *Acta Crystallogr., Sect. E: Struct. Rep. Online*, 2005, **61**, m1197-m1198.
11. T. Ebrahimi, E. Mamleeva, I. Yu, S. G. Hatzikiriakos and P. Mehrkhodavandi, *Inorg. Chem.*, 2016, **55**, 9445-9453.
12. W. Alkarekshi, A. P. Armitage, O. Boyron, C. J. Davies, M. Govere, A. Gregory, K. Singh and G. A. Solan, *Organometallics*, 2013, **32**, 249-259.
13. R. R. Gowda and D. Chakraborty, *J. Mol. Catal. A: Chem.*, 2010, **333**, 167-172.

# 4. Aluminium and Group 4 Salen and Salalen Complexes

## 4.1 Preamble

Salalen ligands have been an area of recent interest for the ring-opening polymerisation of lactide.[1-5] They are ONNO type ligands that feature both a salan (amine) and a salen (imine) moiety. Previous work has shown the ligands can be tailored to different selectivities by subtle changes of the phenyl substituents (Figure 4.01). For example, the aluminium complex with the ethylene backbone ligand produces mildly isotactic PLA when R=Me and R'=R''=$^{t}$Bu, whereas heterotactic PLA is produced when R'=R''=H.[2] For the aluminium benzoxy complex with the cyclohexyl backbone, heterotactic PLA was formed where R'=R''=Cl, and isotactic PLA produced for R'=H, R''=$^{t}$Bu.[3]

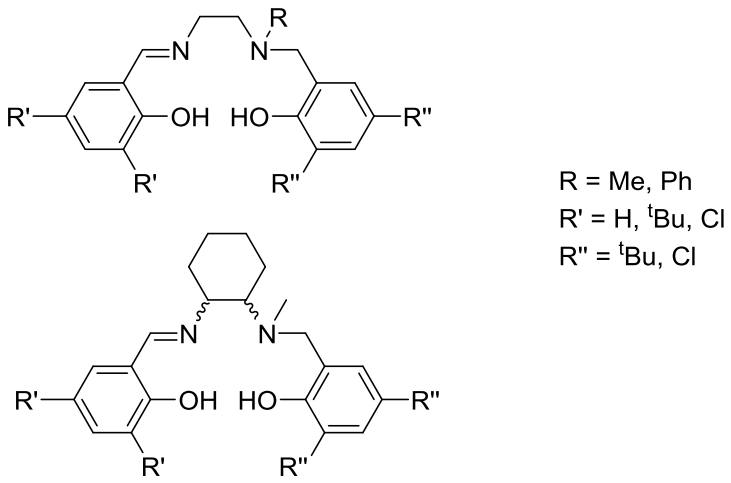


**Figure 4.01: Salalen ligands previously produced by Jones *et al*.[2, 3]**

Salalen ligands with a chiral pyrrolidine backbone (illustrated in Figure 4.02, left) were synthesised by Kol *et al.* and complexed with aluminium isopropoxide.[5] It was found that the *S*-isomers of these complexes produced either heterotactic or isotactic PLA depending on the substituents on the phenoxy rings. Another publication by this group reported that a chiral aluminium salalen complex with an ethylene backbone and bulky groups on the salen moiety (Figure 4.02, right) yielded isotactic PLA.[4] When these initiators were employed for the copolymerisation of L-lactide and ε-caprolactone, the resulting copolymers tended towards randomness (as determined by block length and reactivity ratio).

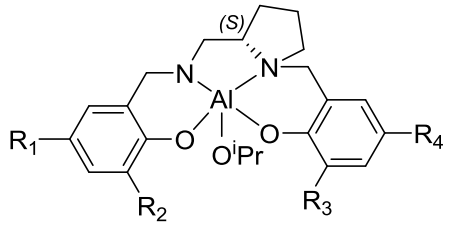


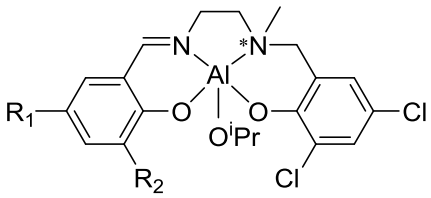


$R_1 = R_2 = Cl$, $R_3 = Ad$, $R_4 = Me$ Heterotactic

$R_1 = Me$, $R_2 = Ad$, $R_3 = R_4 = Cl$
$R_1 = R_2 = {}^t$Bu, $R_3 = R_4 = Cl$ Isotactic

$R_1 = R_2 = {}^t$Bu
$R_1 = Me$, $R_2 = Ad$ Isotactic

**Figure 4.02: Chiral salalen complexes as reported by Kol *et al*.[4, 5]**

While these studies have provided insight into the effect of phenoxy substituents, little is understood about the effect of the ligand backbone on the selectivity and activity of these complexes. In order to understand what effect a more rigid and inflexible backbone would have on the polymer microstructure, a series of ligands with a phenylene backbone have been prepared. These were then complexed with aluminium and group 4 metals and utilised for the ring-opening polymerisation of lactide, and the copolymerisation of lactide and caprolactone. The induced stereoselectivity is compared, including the differences between group 4 and aluminium initiators. Furthermore, the differences between salen and salalen ligands in discussed herein.

## 4.2 Synthesis and characterisation of salen, salalen and salan ligands

An aromatic salophen ligand was synthesised *via* an imine condensation of *ortho*-phenylenediamine and 3,5-di-*tert*-butylsalicylaldehyde (Figure 4.03). Unlike some other salen syntheses which are complete at room temperature in minutes, this required an overnight reflux,[6] presumably due to a combination of the high rigidity of the backbone and the steric bulk of the *tert*-butyl phenoxy substituents.

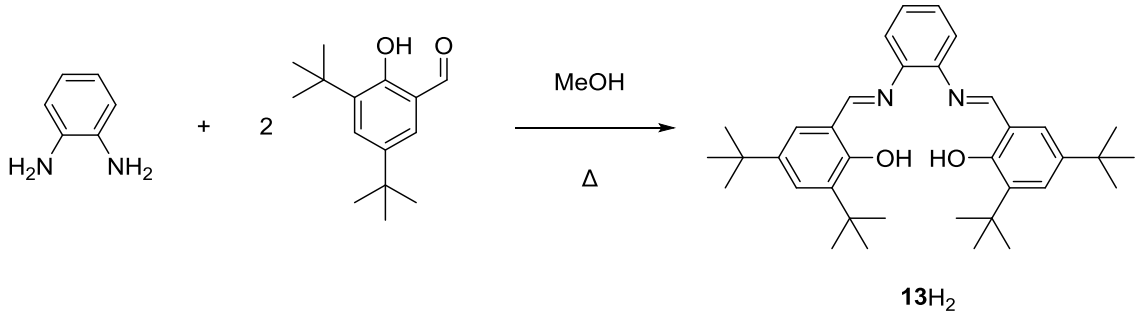


**13**$H_2$

**Figure 4.03: Synthesis of the salen ligand with a phenyl backbone**

The ligand **13**$H_2$ has been previously used for the synthesis of polymerisation catalysts. Zintl *et al*. complexed this ligand with chromium for use as a catalyst in the ring-opening polymerisation of racemic β-butyrolactone, and found that isotactic PHB was produced.[7] Wang *et al.* also utilised this ligand in a titanium complex for the production of polycarbonates.[8] For the purposes of this study the salen complexes will be used as a comparison to the salalen complexes. Figure 4.04 shows the $^1$H NMR spectrum for **13**$H_2$, which highlights the highly symmetrical nature of this ligand. The protons from each functional group on either side of the ligand are chemically equivalent, for example the imine proton resonance at 8.68 ppm which integrates to 2H. The phenol protons can be observed as the resonance at 13.54 ppm and the tert-butyl resonances at 1.34 and 1.46 ppm. The mass spectrum of **13**$H_2$ is also shown in Figure 4.04, confirming the expected formula for the ligand ion at 541.3873 m/z.

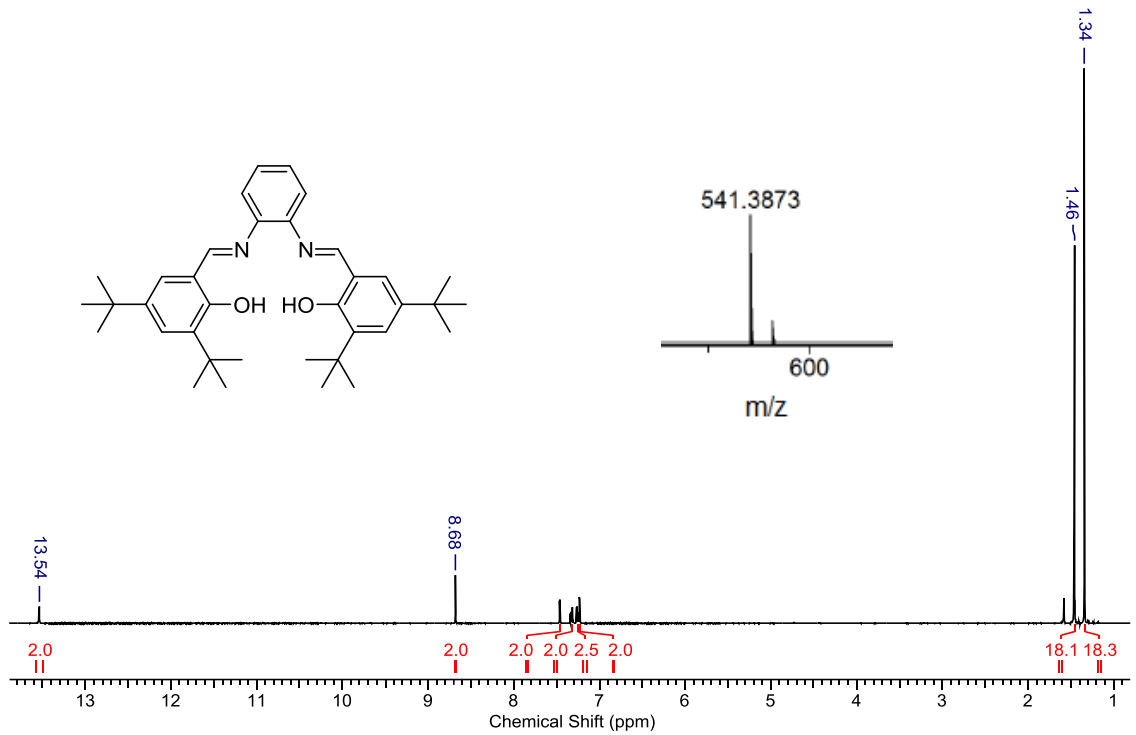


**Figure 4.04: $^{1}$H NMR spectrum for 13H$_2$ in CDCl$_3$ and mass spectrum**

Salalen ligands featuring an *ortho*-phenylene backbone were synthesised to examine the effect of the rigid aromatic system on the complexes prepared and, ultimately, polymer microstructure. This was achieved by synthesising an asymmetric precursor, again *via* an imine condensation in methanol (Figure 4.05).

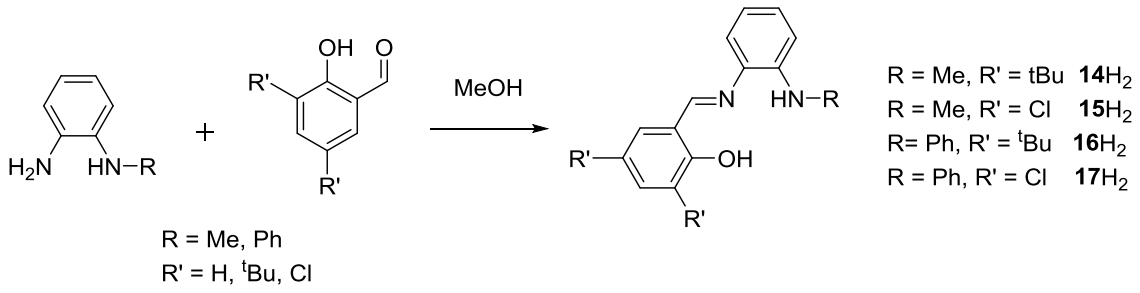


**Figure 4.05: Synthesis of salalen ligand precursors**

Surprisingly, on the addition of salicylaldehyde to the N-substituted (methyl or phenyl) phenylenediamine, a cyclised product formed (proton NMR spectrum of N-phenyl substituted ligand **19**H shown in Figure 4.06). The evidence for this is the lack of an imine singlet resonance in the proton NMR spectrum. Further to this, no peak of the imine product is observed at 289.1341 m/z in the mass spectrum of the purified product. As a result of this, the subsequent step of the synthesis to form the salalen could not be performed using these precursors.

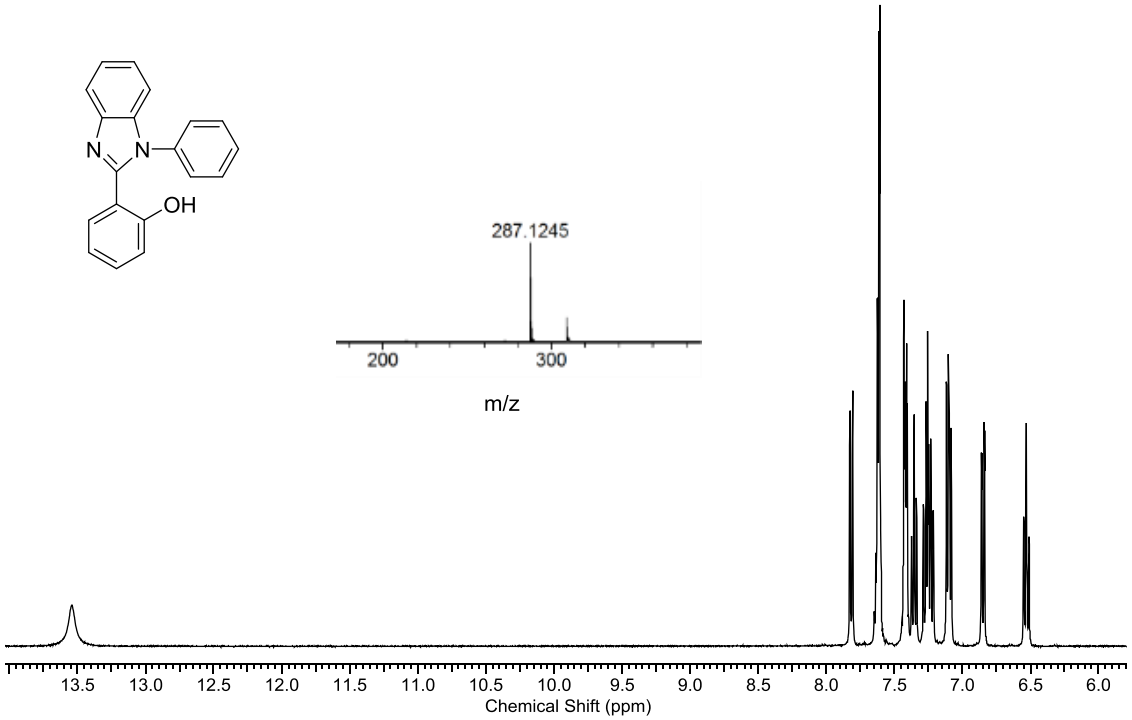


**Figure 4.06: $^{1}$H NMR spectrum in $CDCl_3$ and mass spectrum of cyclised precursor, 19H**

A mechanism for the formation of this cyclised product is proposed in Figure 4.07. A resonance form the imine undergoes a 5-*exo*-*trig* ring-closure resulting in the isolated product. This is not observed for the substituted precursors, perhaps due to steric effects between the substituents and the amine. In addition, the extended reaction times employed in order to produce a precipitate from the solution provided an opportunity for this cyclisation to occur. These long reaction times (16 hours) are not required for the less soluble chloro- substituted imines which precipitated quickly (less than 1 hour).

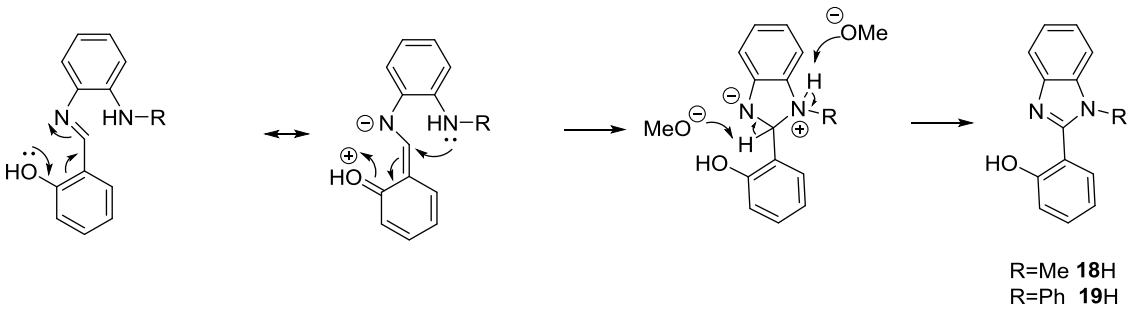


**Figure 4.07: Proposed mechanism of ligand cyclisation**

The proposed mechanism suggests that the cyclisation of the ligand occurs after the formation of the imine bond. This is supported by the $^{1}$H NMR spectrum of the incomplete reaction for the synthesis of **19**H, highlighting the imine proton as indicated by the resonance at 8.7 ppm (Figure 4.08).

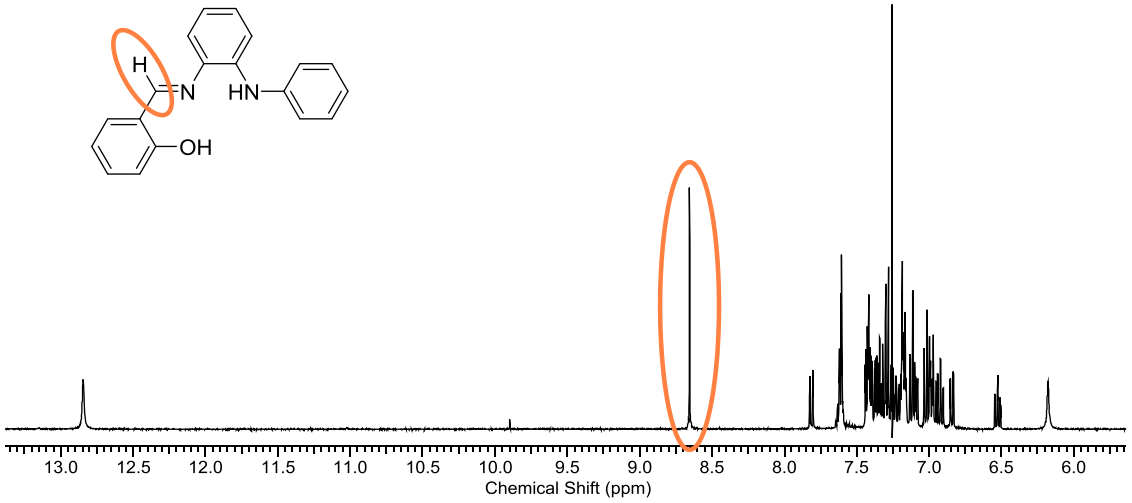


**Figure 4.08: Aromatic region of $^{1}$H NMR spectrum of incomplete cyclisation step for 19H in $CDCl_3$**

Interestingly, Li *et al*. also reported the synthesis of **18**H using a Rhodium(III) catalyst.[9] This is a resource-intensive preparation involving multiple reagents, utilising DMF as the solvent at 140 °C, whereas the method described above follows several Green Chemistry principles - it is atom efficient and uses less energy and less harmful solvents.[10] Consequently, **19**H was taken forward for preliminary complexation and polymerisation studies.

To form the salalen ligand, the precursors were refluxed for 3 hours with 3,5-di-tert-butyl-2-hydroxybenzylbromide and one equivalent of trimethylamine (Figure 4.09). Only the *tert*-butyl substituted precursor was used for this reaction. This salalen synthesis is straightforward and can be carried out using industrially available precursors with a simple work up, as opposed to the previously investigated cyclohexane backbone salalen ligand, which requires protection chemistry and lengthy work up procedures.[3]

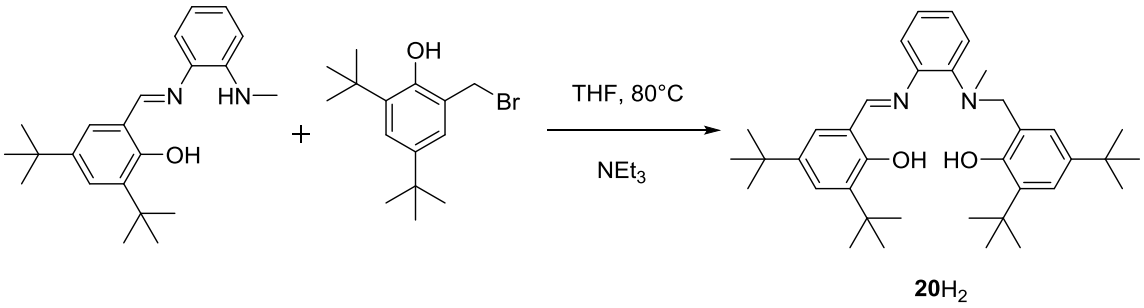


**20**$H_2$

**Figure 4.09: Synthesis of the salalen ligand 20$H_2$**

The ligand **20**$H_2$ was produced easily after a 3 hour reaction and work up. The product was recrystallised in hexane and the solid-state structure obtained by single crystal X-ray diffraction studies (Figure 4.10). In ca. 24 hours, multiple grams of this ligand can be readily prepared in high purity.

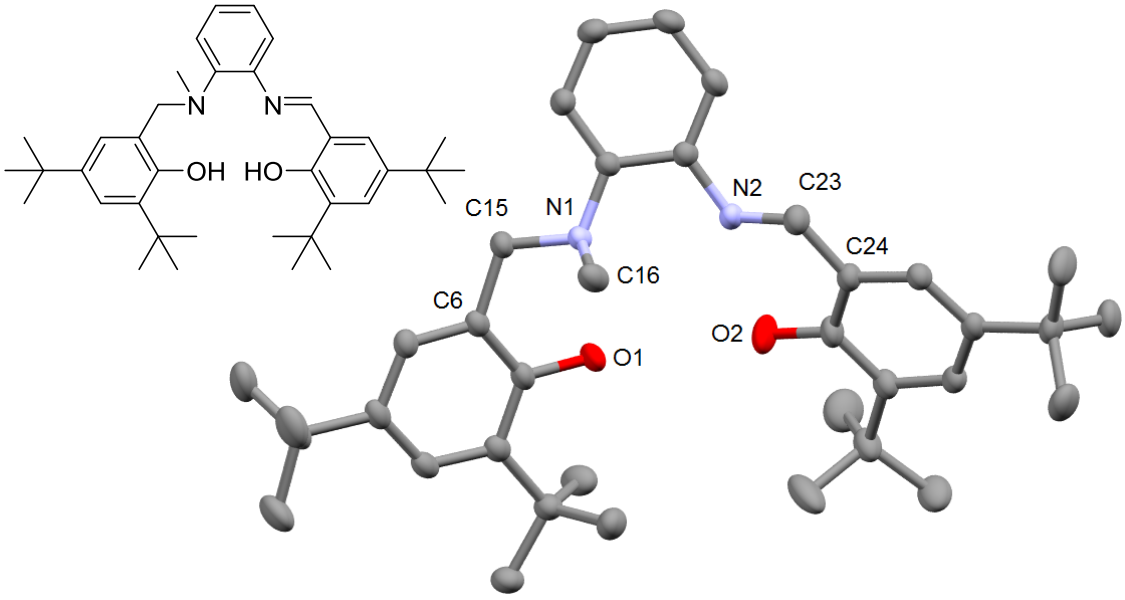


**Figure 4.10: Solid-state structure of $20H_2$. Ellipsoids are shown at the 30 % probability level. Hydrogen atoms have been removed for clarity.**

Table 4.01 shows some important bond lengths and angles from this structure. The imine bond N2-C23 is 1.286(2) Å, much shorter than the amine bond N1-C15 at 1.458(2) Å. This is expected for these bond types, as the former has a double bond and the latter a single bond only. This also manifests itself in the bond angles, with the bond of N1-C15-C6 at 113.80(14) ° which slightly larger than the theoretical angle of 109.5 °, whereas the N2-C23-C24 bond of the imine is 122.82(17) ° which is slightly larger than the theoretical bond angle of 120 °.

**Table 4.01: Selected bond lengths (Å) and angles (°) for $20H_2$**

| | **20**$H_2$ |
|---|---|
| C15-N1 | 1.458(2) |
| C16-N1 | 1.489(2) |
| C23-N2 | 1.286(2) |
| C1-O1 | 1.365(2) |
| C25-O2 | 1.344(2) |
| N1-C15-C6 | 113.80(14) |
| N2-C23-C24 | 122.82(17) |

The $^{1}H$ and $^{13}C\{^{1}H\}$ NMR spectra conformed to the observed solid-state structure ($^{1}H$ NMR spectrum shown in Figure 4.11). It features four distinct *tert*-butyl resonances in the 1.32-

1.49 ppm region and two Ar-OH proton resonances at 10.07 and 13.00 ppm, indicating that these protons are in different chemical environments, as would be expected for an asymmetric ligand. The methylene bridge protons (-$CH_2$-) can be observed as the singlet at 4.32 ppm.

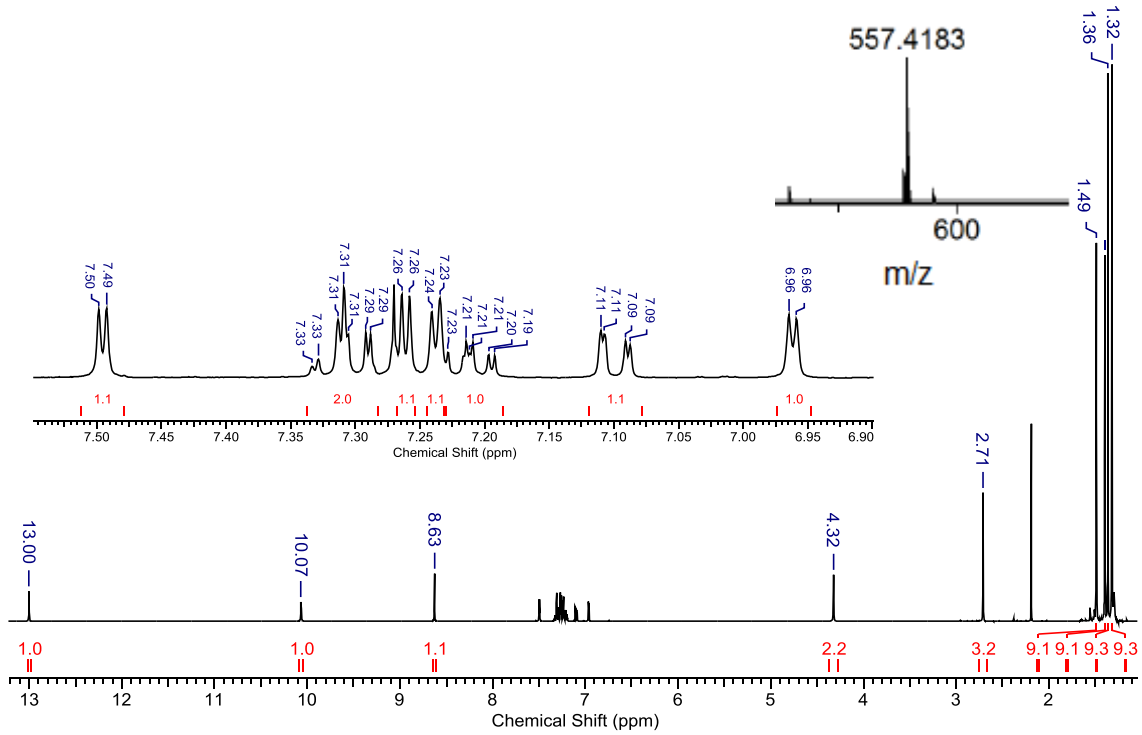


**Figure 4.11: $^1$H NMR spectrum in $CDCl_3$ and mass spectrum of $20H_2$, with $^1$H NMR aromatic region zoom**

Attempts to synthesise the N-phenyl substituted salalen ligand (Figure 4.12) proved unsuccessful. This could be due to the combined steric bulk of the N-phenyl, phenyl backbone and *tert*-butyl substituents hindering the nucleophilic attack on the incoming bromo compound.

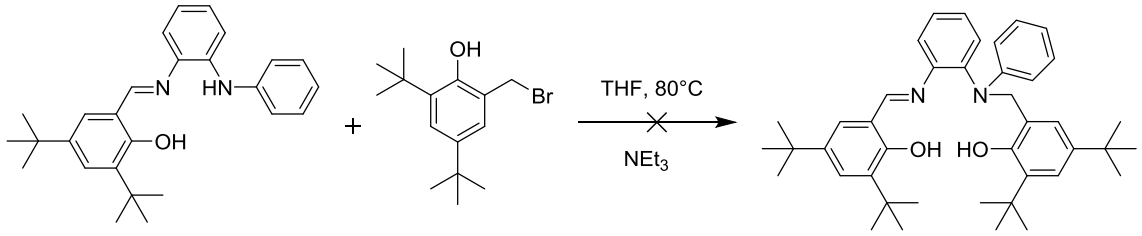


**Figure 4.12: Unsuccessful N-phenyl salalen synthesis**

It was found that increasing the reaction time had no effect on the conversion; Figure 4.13 shows the near identical spectra of the products formed from this reaction after 3 and 16 hours. The spectra are unclear and do not feature the desired -$CH_2$- resonance expected of the salalen product. No product could be purified out of this mixture by recrystallisation, as such this was not followed up as a potential salalen route.

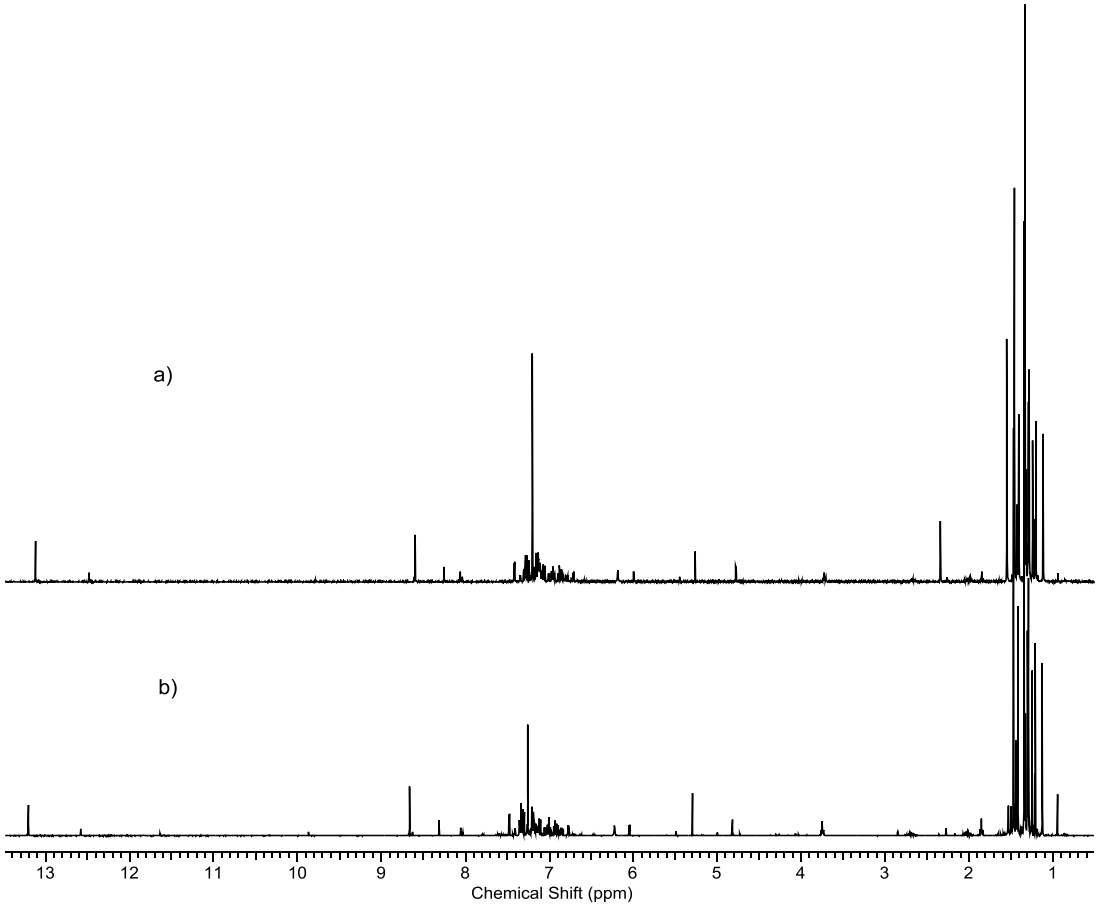


**Figure 4.13: $^1$H NMR spectrum of reaction mixture after attempted synthesis of N-phenyl salalen ligand after a) 3 hours b) 16 hours reflux**

Finally, a salan ligand, **21**$H_2$, with the same motif (phenyl backbone, tert-butyl substituents) as the ligands above was synthesised (Figure 4.14). This ligand type is symmetrical, containing two amine moieties. This is intended to act as a comparison between the salen and salalen ligands.

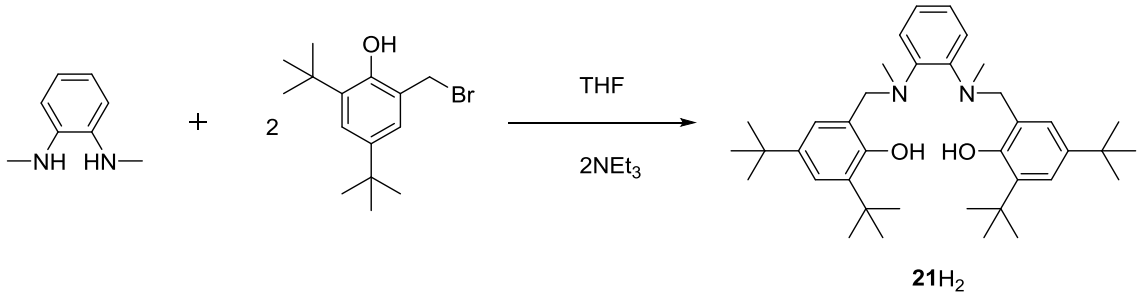


**Figure 4.14: Synthesis of 21$H_2$, a symmetrical salan ligand**

This ligand has been previously used by Kol *et al.* to synthesise titanium isopropoxide and zirconium *tert*-butoxide and benzyl salan complexes, which were utilised for the polymerisation of 1-hexene.[11] The proton NMR spectrum of this ligand is shown in Figure 4.15.

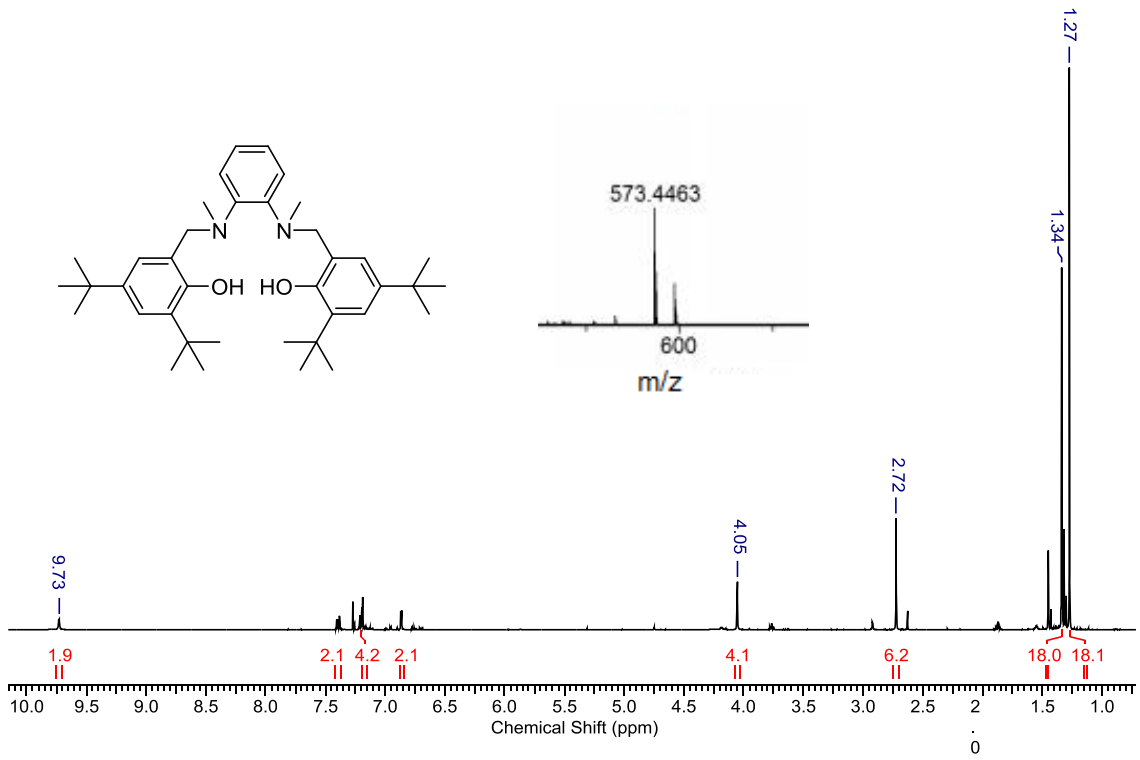


**Figure 4.15: $^{1}$H NMR spectrum in $CDCl_3$ and mass spectrum of $21H_2$**

The proton NMR spectrum confirms the expected structure of this ligand. There are 6 N-methyl protons (2.72 ppm) and 4 methylene protons (4.05 ppm) present. The symmetrical nature of this ligand can be seen in this spectrum, with protons on either side being chemically equivalent, e.g. the two phenol protons at 9.73 ppm. The ion of the ligand was observed in the mass spectrum at 573.4463 m/z along with the sodiated ion at 595.4257 m/z.

## 4.3 Synthesis and characterisation of metal complexes

### 4.3.1 Complexation with salen ligand **13**$H_2$

The ligands described in section 4.2 were taken forward and complexed with aluminium, zirconium and hafnium. The complexations of the salen ligand **13**$H_2$ in toluene are shown below in Figure 4.16. For the zirconium and hafnium complexation, gentle heating was employed whereas the aluminium reaction was carried out at room temperature (heating not required due to the highly reactive nature of trimethylaluminium). In all cases, a bimetallic complex was formed. This occurred even after initial attempts to form mononuclear complexes using only one equivalent of metal precursor.

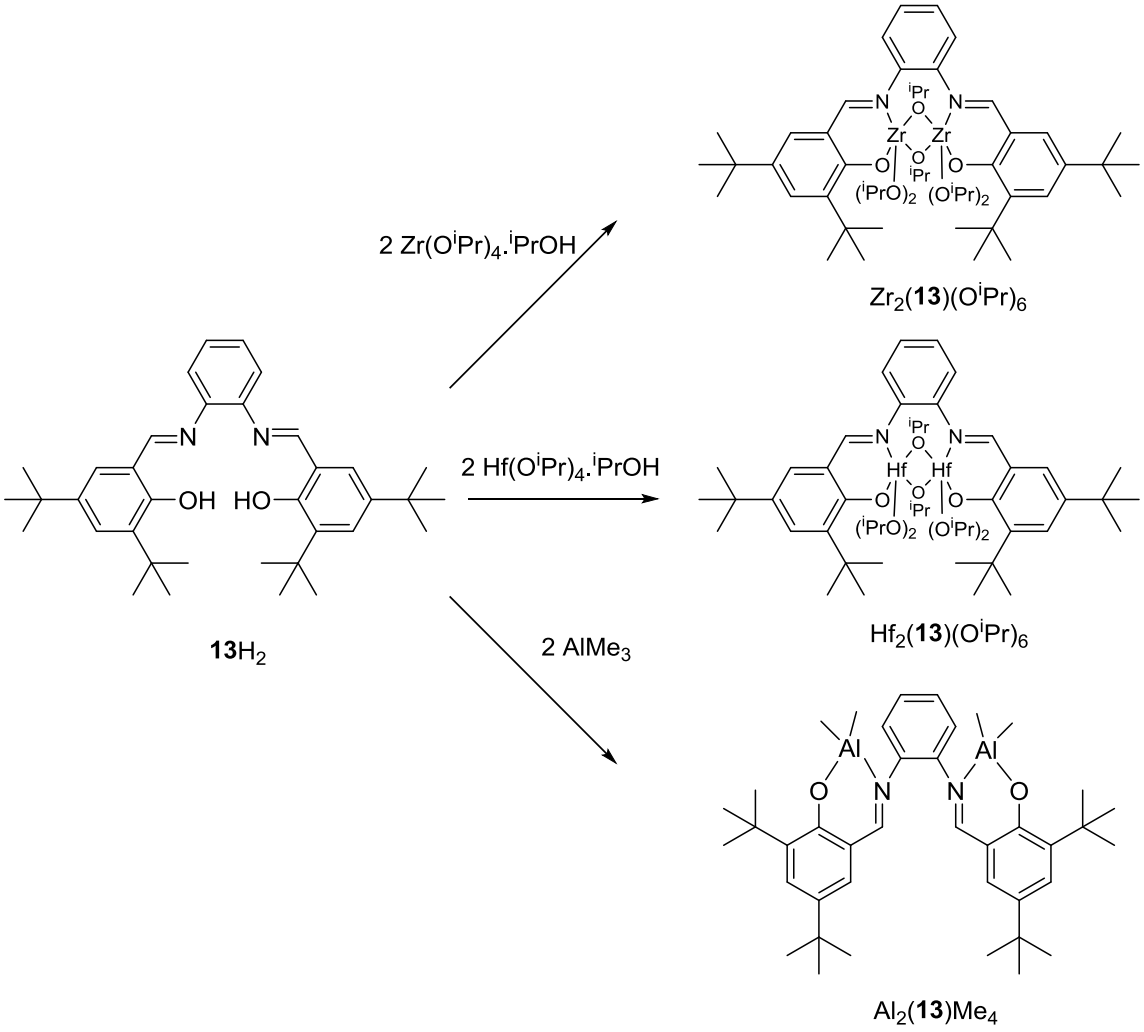


**Figure 4.16: Synthesis of dinuclear salen complexes**

Interestingly, Jing *et al.* found that upon reaction of **13**$H_2$ with one equivalent of triethylaluminium, a monomeric tetradentate complex was formed.[12] In our case, the dimeric complex was formed in toluene regardless of stoichiometry of trimethylaluminium used. This

appears to be due to the aluminium precursor, as Jing used the bulkier triethylaluminium, whereas trimethylaluminium was used in our case. Jing reported that Al(**13**)Et induced a slight isotacticity ($P_m$ = 0.62) in PLA produced at 70 °C in solution at 56:1 monomer to initiator ratio, with 65% conversion after 72 hours.[12] Regarding group 4 complexes, a similar observation was made by Kol *et al.*, who formed dimers when complexing a symmetrical {ONNO} ligand (depicted in Figure 4.17) with zirconium isopropoxide.[13] It was found in this publication that the monomeric complex could be formed by using the bulkier zirconium *tert*-butoxide precursor. Interestingly, the dinuclear complex produced entirely atactic PLA whereas the mononuclear initiator produced heterotactic PLA, $P_r$ = 0.87.

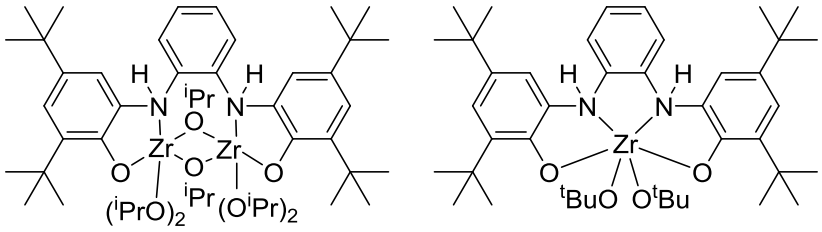


**Figure 4.17: Dinuclear and mononuclear complexes reported by Kol *et al.*[13]**

Figures 4.18 and 4.19 show the solid-state crystal structures of $Zr_2$(**13**)($O^iPr$)$_6$ and $Hf_2$(**13**)($O^iPr$)$_6$ respectively. These two complexes are extremely similar in structure, both featuring two bridging and four terminal isopropoxide ligands around two 6-coordinate octahedral metal centres.

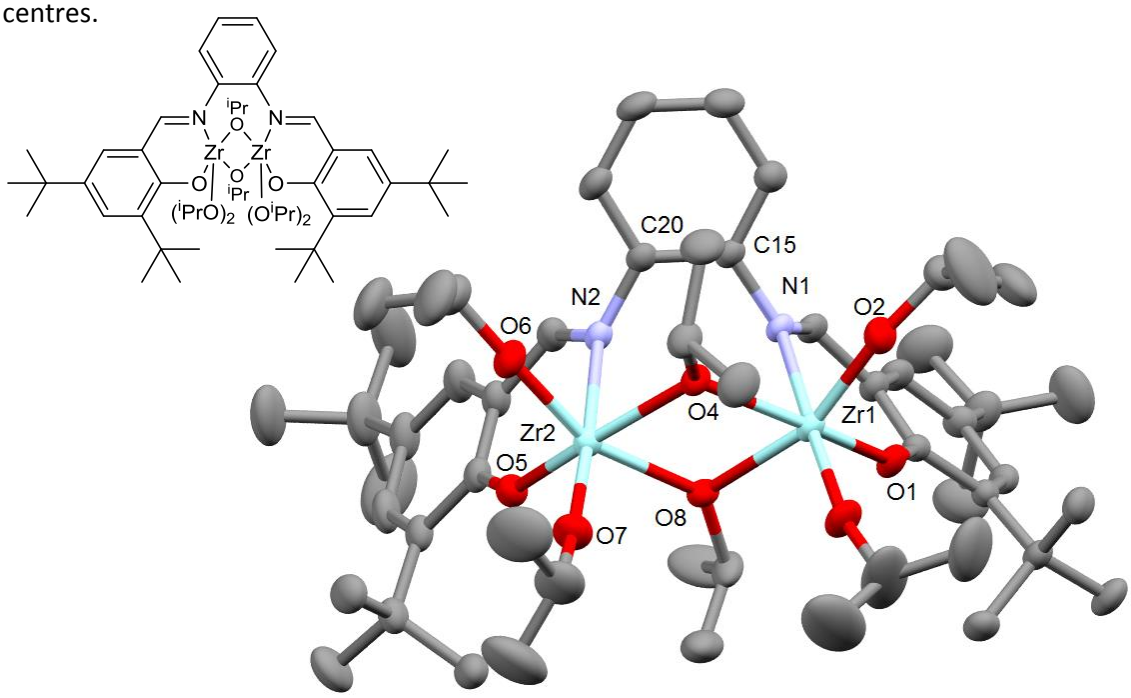


**Figure 4.18: Solid-state crystal structure of $Zr_2$(13)($O^iPr$)$_6$. Ellipsoids are shown at the 30 % probability level. Hydrogen atoms, disordered Me groups and several molecules of disordered toluene have been removed for clarity.**

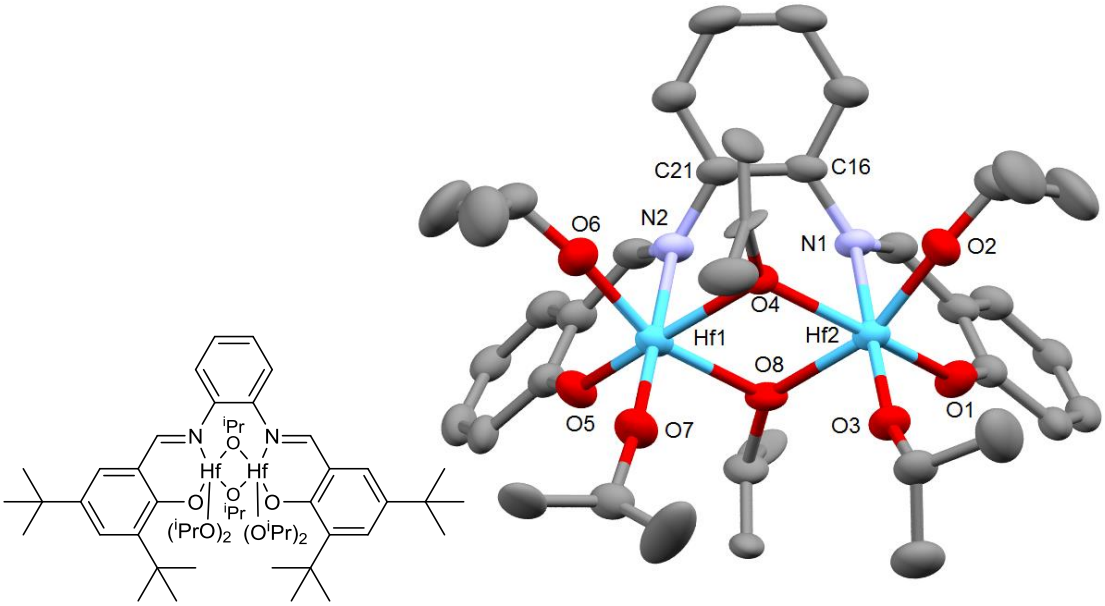


**Figure 4.19: Solid-state crystal structure of $Hf_2$(13)($O^iPr$)$_6$. Ellipsoids are shown at the 30 % probability level. Hydrogen atoms, disordered solvent, tert-butyl groups and disordered isopropoxide carbons have been removed for clarity.**

Table 4.02 on page 132 shows selected bond lengths and angles for these bimetallic complexes. In addition, crystal data from a similar complex **I,** as reported by Chakraborty and coworkers is shown for comparison (chemical structure shown in Figure 4.20).[14]

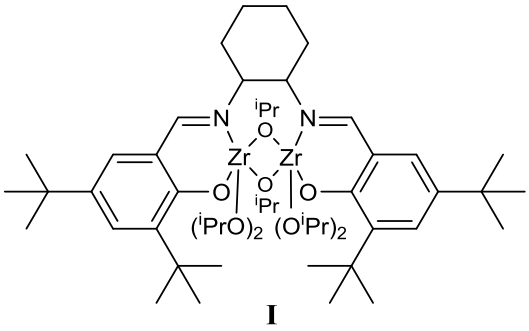


**I**

**Figure 4.20: Previously reported dinuclear zirconium salen complex, I[14]**

A notable bond length difference in the literature compound *vs* the salen complexes described in this chapter is the variation between the M1-N and M2-N bond lengths in complex **I**, which are 2.504(9) Å and and 2.393(7) Å respectively, a difference of approx. 0.1 Å. Such a drastic difference in M1-N and M2-N bonds is not observed for $Zr_2$(**13**)($O^iPr$)$_6$ and $Hf_2$(**13**)($O^iPr$)$_6$. For example, M1-N in $Hf_2$(**13**)($O^iPr$)$_6$ is 2.407(1) Å and M1-N is 2.421(3) Å. This heightened difference in nitrogen-metal bond lengths for **I** is caused by twisting of the backbone, which does not occur with the more rigid phenyl backbone, as such no significant change in bond length is observed. For each of the complexes in Table 4.02, the M-O1 bond is longer than the M-O2 bond. For example, in $Zr_2$(**13**)($O^iPr$)$_6$, Zr1-O1 is 2.051(1) Å and Zr1-O2 is 1.936(2) Å, a difference of approx.

0.1 Å. The reason for this is that in each case O1 is the phenoxy oxygen atom, whereas O2 is a free terminal isopropoxide ligand. Note that in all complexes the M-O2 bond lengths are statistically equivalent. In each complex the M-O4 bonds are further elongated due to the bridging nature of the O4 isopropoxide ligand. For example, in $Zr_2$(**13**)($O^iPr$)$_6$, Zr1-O4 is 2.157(1) Å, more than 0.2 Å longer than Zr1-O2.

Each metal centre in the three complexes has a distorted octahedral geometry. Due to the rigid structure some bond angles are more strained than the theoretical values. For example, in $Hf_2$(**13**)($O^iPr$)$_6$, the bond angle O1-Hf2-N1 is 76.27(9) °, far lower than 90 °. Particularly "pinched" is the O4-M1-O8 bond angle, which is very strained in each complex, as it is the angle between the metal and the two bridging ligands. For example, in $Zr_2$(**13**)($O^iPr$)$_6$ this bond angle is 71.24(5) °. The bond angles for M1-O4-M2 are close or equivalent to the theoretical value for tetrahedral geometry, at 109.63(6) °, 108.77(8) ° and 109.5(3) ° for $Zr_2$(**13**)($O^iPr$)$_6$, $Hf_2$(**13**)($O^iPr$)$_6$ and **I** respectively.

**Table 4.02: Selected bond lengths (Å) and angles (°) for $Zr_2$(13)($O^iPr$)$_6$, $Hf_2$(13)($O^iPr$)$_6$**

| | $Zr_2$(**13**)($O^iPr$)$_6$ | $Hf_2$(**13**)($O^iPr$)$_6$ | **I** |
|---|---|---|---|
| M1-N | 2.431(2) | 2.407(3) | 2.504(9) |
| M2-N | 2.443(2) | 2.421(3) | 2.393(7) |
| M-O1 | 2.051(1) | 2.027(2) | 2.045(8) |
| M-O2 | 1.936(2) | 1.936(2) | 1.942(8) |
| M1-O4 | 2.157(1) | 2.129(2) | 2.175(6) |
| M1-O4-M2 | 109.63(6) | 108.77(8) | 109.5(3) |
| O4-M1-O8 | 71.24(5) | 72.15(8) | 71.5(2) |
| N2-M-O6 | 81.64(6) | 85.17(10) | 83.9(3) |
| N1-M-O3 | 168.87(6) | 169.95(9) | 168.2(3) |
| O1-M-N1 | 75.38(6) | 76.27(9) | 75.6(3) |

Figure 4.21 shows the $^1$H NMR spectrum for $Zr_2$(**13**)($O^iPr$)$_6$. All isopropoxide protons are accounted for and the spectrum confirms that the solid-state structure is maintained in solution.

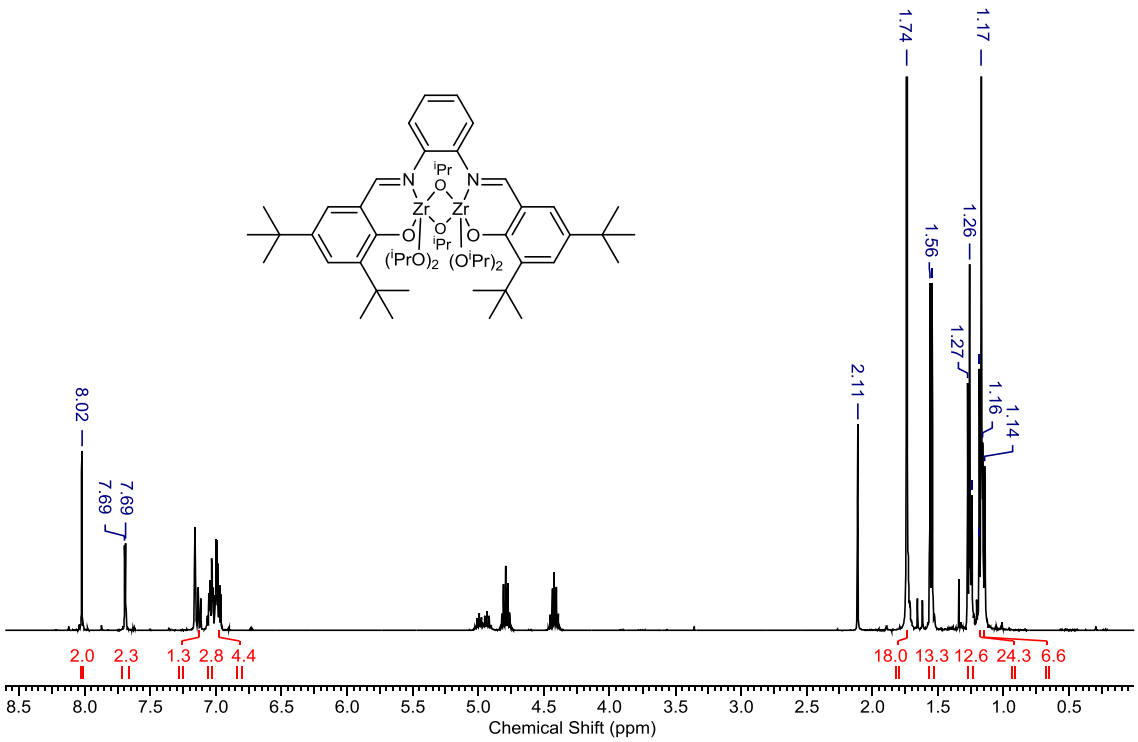


**Figure 4.21: $^{1}$H NMR spectrum of $Zr_2$(13)($O^iPr$)$_6$ in $CDCl_3$**

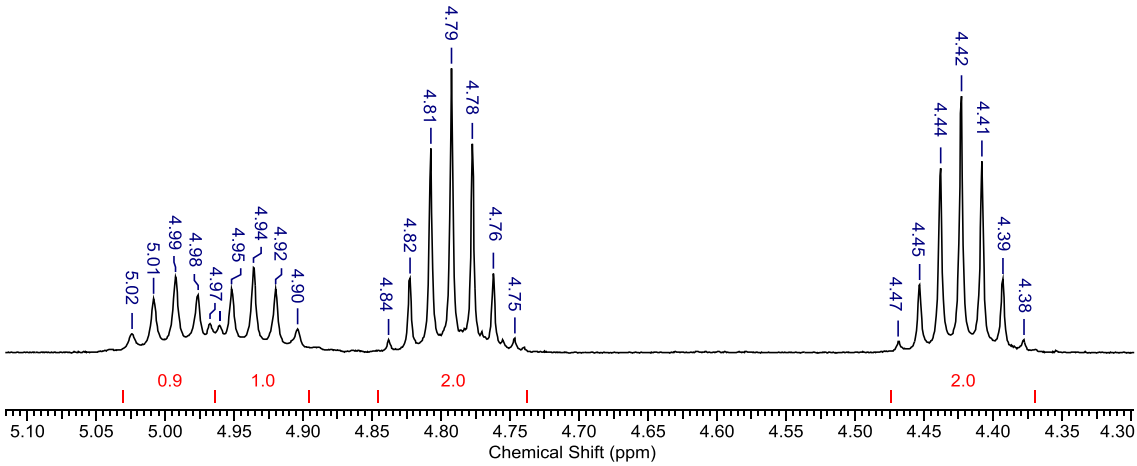


**Figure 4.22: Spectrum of $Zr_2$(13)($O^iPr$)$_6$, zoomed isoproxide region**

Figure 4.22 shows the isopropoxide proton region for $Zr_2$(**13**)($O^iPr$)$_6$. The terminal isopropoxides (2 x 2 protons) are found as septets at 4.42 and 4.79 ppm, and the bridging isopropoxides (2 x 1 proton) at 4.94 and 4.99 ppm, not showing as septets as they are overlapping one another. The different chemical shifts displayed by the bridging isopropoxides can be explained by the subtly different environments brought about by O8 being *cis* to the adjacent phenoxides, whereas O4 is situated *trans* to the phenoxides. The spectrum for $Hf_2$(**13**)($O^iPr$)$_6$ is near identical, exhibiting all of these traits which support the solid-state structure.

When the dinuclear salen complexes were initially synthesised, it was hoped that they would be mononuclear, so they could be used as a comparison to the mononuclear salalen complexes. As this was not the case, further attempts at a zirconium mononuclear complex were carried out, using zirconium *tert*-butoxide instead of isopropoxide (Figure 4.23). The rationale was that the bulkier substituents would prevent a second metal centre fitting in the ligand, as observed by Kol *et al.* after unsuccessful attempts of synthesising a mononuclear zirconium isopropoxide complex using a phenylenediamine bis(phenolate) ligand.[13]

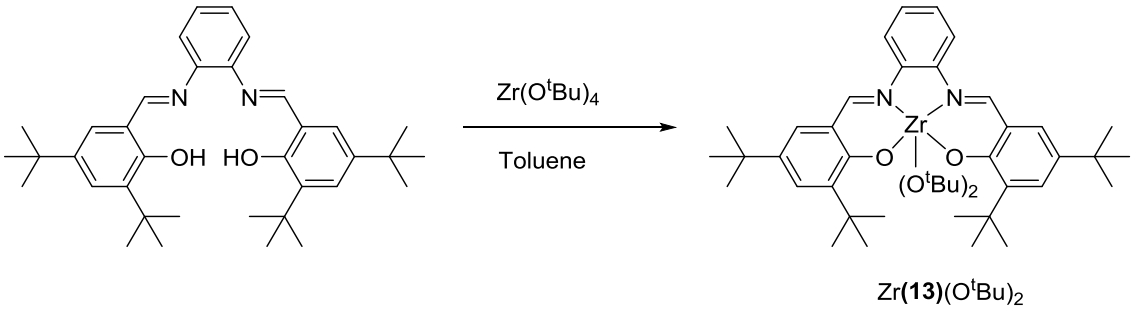


**Figure 4.23: Synthesis of Zr(13)(O$^t$Bu)$_2$**

Due to the high solubility of Zr(**13**)(O$^t$Bu)$_2$, crystals suitable for X-ray diffraction were not forthcoming. The crude reaction mixture was taken forward for use in polymerisation reactions. Figure 4.24 shows the $^1$H NMR spectrum of Zr(**13**)(O$^t$Bu)$_2$. Whilst the aromatic protons are all accounted for, some unusual splitting occurs in the tert-butyl region of the spectrum. This could be caused by isomerism, for example, two species with the isobutyl groups either *cis* or *trans* to one another. To investigate further, a DOSY experiment was run (Figure 4.26, page 122).

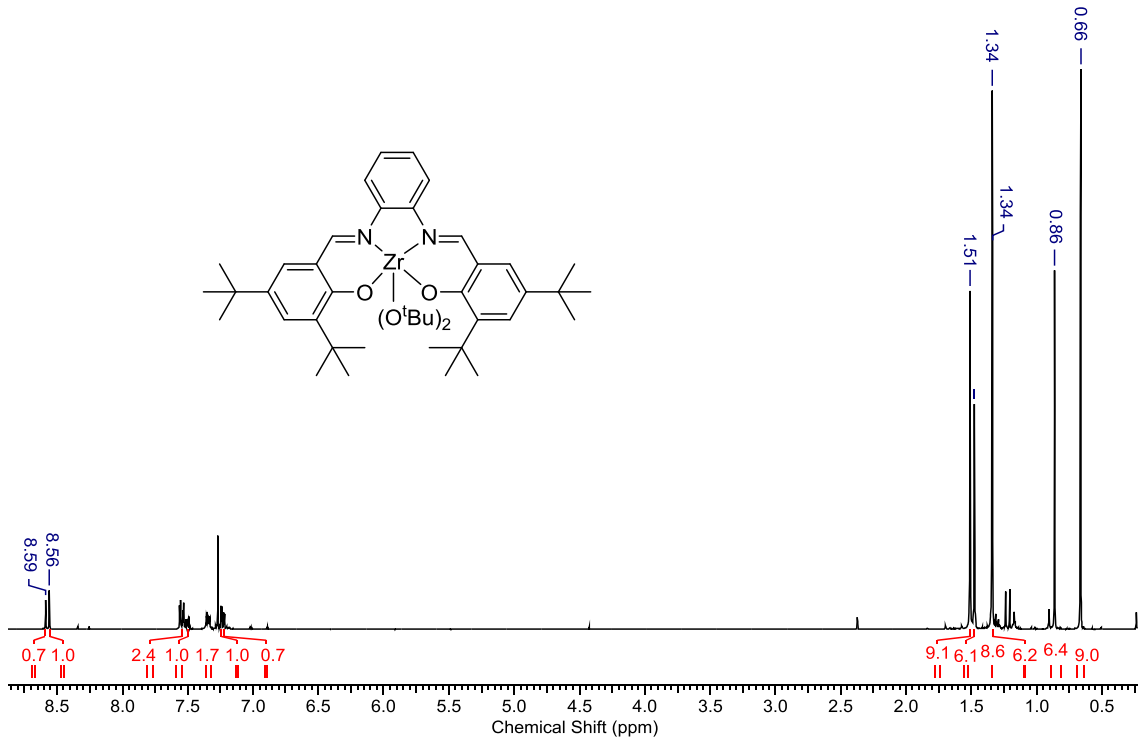


**Figure 4.24: $^{1}$H NMR spectrum of Zr(13)(O$^{t}$Bu)$_2$ in $CDCl_3$**

The $^{13}C\{^{1}H\}$ NMR spectrum of Zr(**13**)(O$^{t}$Bu)$_2$ in Figure 4.25 accounts for all the carbons present and confirms the expected structure, with two distinct Zr-O$^{t}$Bu resonances at 72.9 and 74.6 ppm.

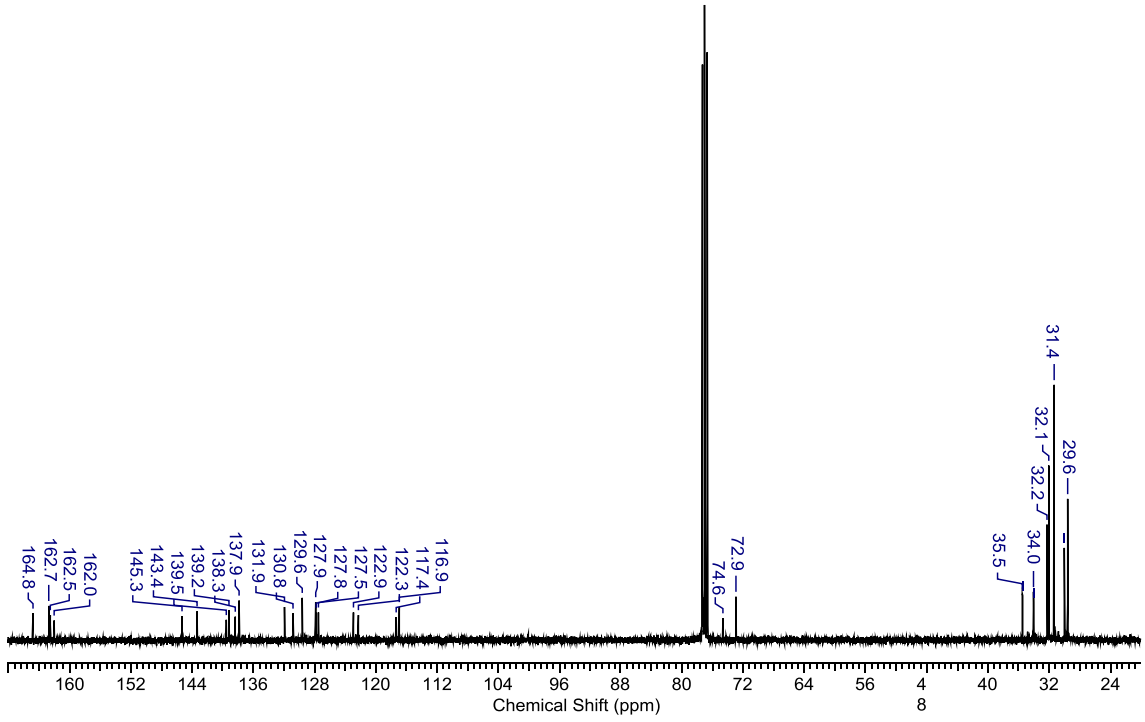


**Figure 4.25: $^{13}C\{^{1}H\}$ NMR spectrum of Zr(13)(O$^{t}$Bu)$_2$ in $CDCl_3$**

Figure 4.26 shows the DOSY NMR spectrum of Zr(**13**)(O$^{t}$Bu)$_2$. On visual inspection the main *tert*-butyl resonances appear to diffuse at the same rate. On examination of the diffusion

coefficients of resonances 1, 4-6, 10-13, they all diffuse at approximately 6 x $10^{-10}$ $m^2s^{-1}$, indicating that these resonances belong to the same molecule. From this evidence, it can be concluded that Zr(**13**)($O^tBu$)$_2$ has been successfully synthesised. Exact diffusion constant values for all resonances in this spectrum can be found in the appendix, page 209. The smaller series of peaks that have a different diffusion constant are attributed to ligand.

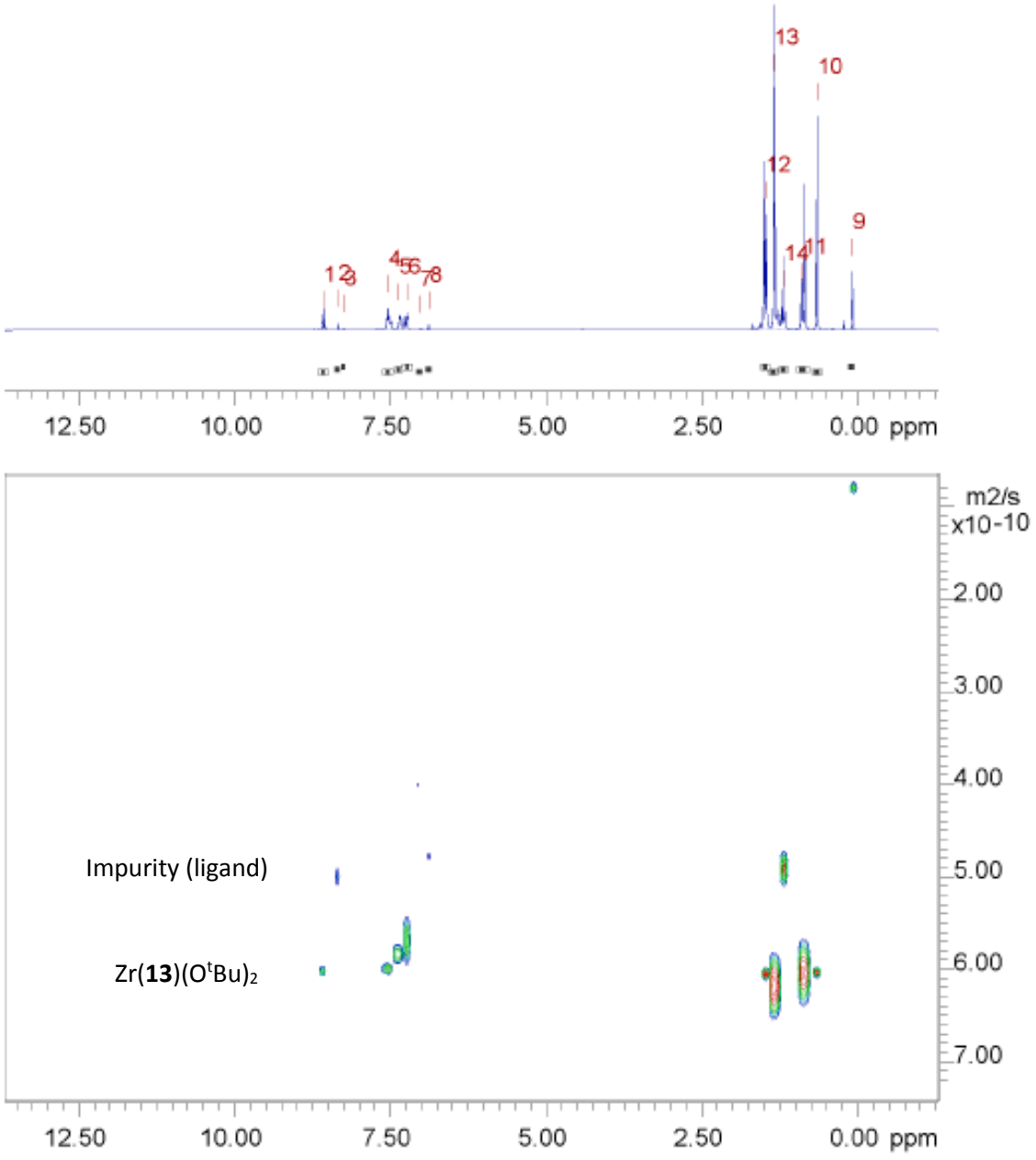


**Figure 4.26: DOSY spectrum of Zr(13)($O^tBu$)$_2$**

Figure 4.27 shows the solid-state crystal structure for $Al_2$(**13**)$Me_4$ (reaction scheme in Figure 4.16). Unlike the group 4 complexes with this ligand, the metal centres have no bridging ligands and are oriented away from one another, in order to avoid aluminium-methyl steric clashes.

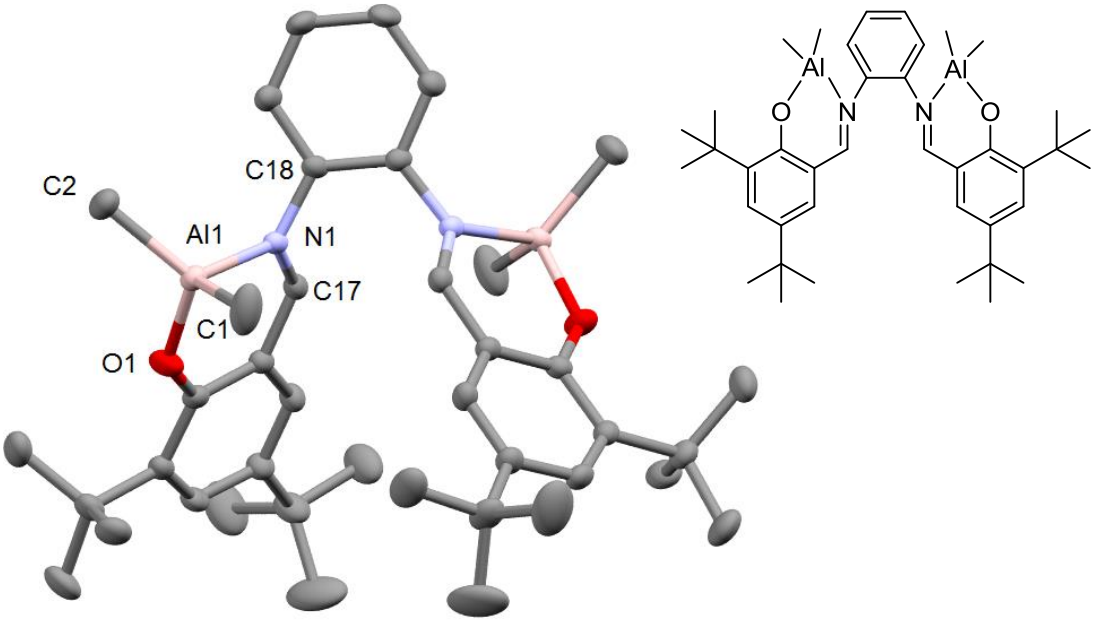


**Figure 4.27: Solid-state crystal structure of $Al_2$(13)$Me_4$. Ellipsoids are shown at the 30 % probability level, hydrogen atoms have been removed for clarity.**

Table 4.03 shows selected bond lengths and angles for $Al_2$(**13**)$Me_4$, as well as a similar dialuminium salen complex featuring a cyclohexyl backbone (**II**), published by Atwood *et al.* (Figure 4.28).[15]

**Table 4.03: Selected bond lengths (Å) and angles (°) for $Al_2$(13)$Me_4$ and II**

| | $Al_2$(**13**)$Me_4$ | **II** |
|---|---|---|
| Al-O1 | 1.766(1) | 1.757(3) |
| Al-N1 | 1.980(1) | 1.980(4) |
| Al-C1 | 1.948(1) | 1.946(5) |
| Al-C2 | 1.941(1) | 1.946(4) |
| N1-C17 | 1.303(2) | 1.229(5) |
| N1-C18 | 1.439(2) | 1.483(4) |
| O1-Al-N1 | 93.92(4) | 94.0(1) |
| N1-Al-C1 | 109.16(5) | 111.0(2) |
| O1-Al-C2 | 109.97(6) | 112.0(2) |
| C1-Al-C2 | 118.37(7) | 119.0(2) |
| N1-C18-C18a-N1a | -0.5 | -65.6 |

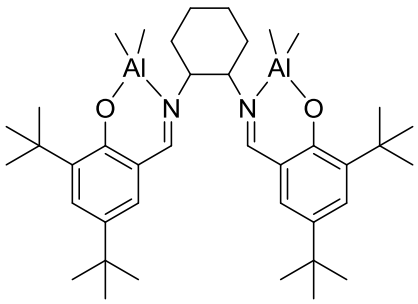


**II**

**Figure 4.28: Literature dialuminium salen complex as reported by Atwood *et al.*[15]**

When comparing these structures, it appears that the backbone has little effect on the geometry and bond lengths about the aluminium metal centre, indeed most of the lengths are within error of one another and can therefore be described as statistically equivalent. For example, Al-N1 is 1.980(1) Å for $Al_2$(**13**)$Me_4$ and 1.980(4) Å for **II**. The bond angles in both complexes differ, but not dramatically. The most notable difference between the structures is the N1-C18-C18a-N1a torsion angle, which is -0.5° for $Al_2$(**13**)$Me_4$ and -65.6° for **II**. The inflexibility of the phenyl backbone in $Al_2$(**13**)$Me_4$ is the cause of this. The Al-Al distances in the complexes are similar, 6.224 Å for **II** and 6.231 Å for $Al_2$(**13**)$Me_4$.

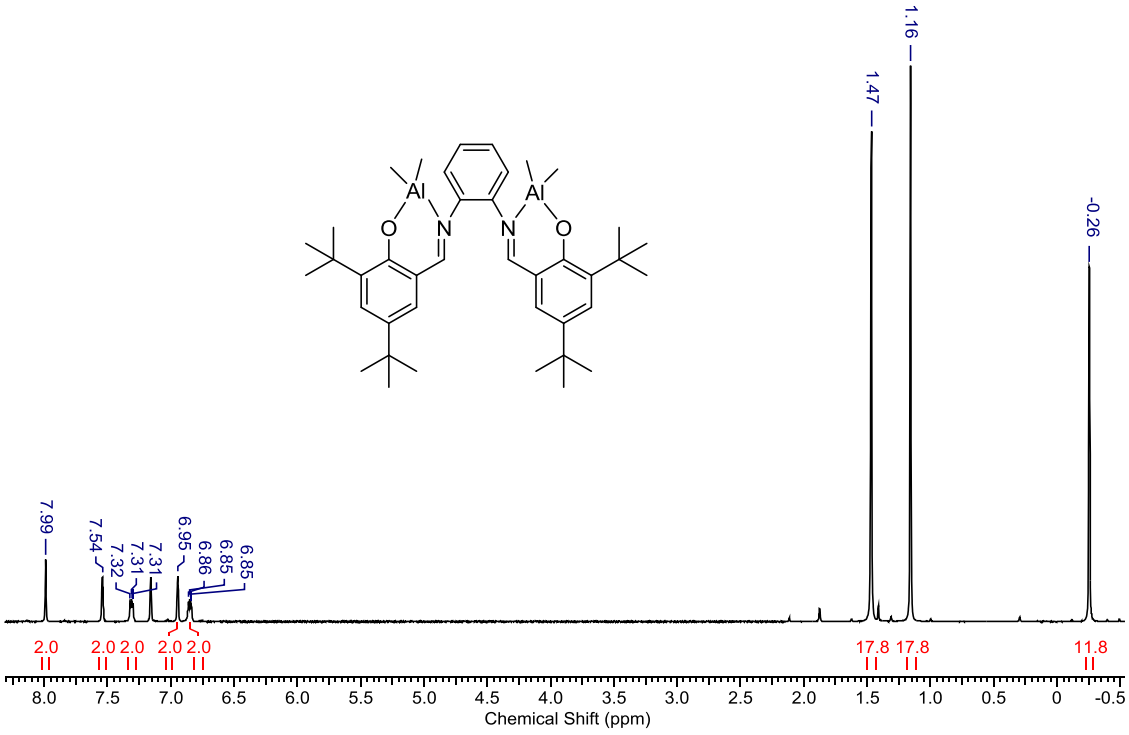


**Figure 4.29: $^1$H NMR spectrum of $Al_2$(13)$Me_4$ in $C_6D_6$**

The proton NMR spectrum of $Al_2$(**13**)$Me_4$ is shown in in Figure 4.29, indicating that the solid-state structure is retained in solution. All aluminium methyl groups appear to be chemically equivalent, shown by a single resonance at -0.26 ppm which integrates to 12 protons. The

symmetry of the complex is typified by the chemical equivalence of, for example, the two imine protons, found under one singlet at 7.99 ppm.

### 4.3.2 Salalen precursor complexation using **16**$H_2$, **17**$H_2$ and **19**H

The uncyclised N-phenyl precursors were reacted stoichiometrically with trimethylaluminium (Figure 4.30). Surprisingly, a highly coloured dialuminium complex with two ligands was formed. X-ray crystallography (Figure 4.31) and proton NMR spectroscopy confirmed that the amine of each ligand had been deprotonated, resulting in one coordinatively saturated aluminium centre, and another with two methyl groups. This is interesting compared to the results from the previous chapter where the nitrogen of the amine on the ligands did not coordinate to the metal centre and remained protonated (see section 3.3). The difference is that the system below is highly conjugated, and it is likely that the amine proton has a lower $pK_a$ than the ligands reported in Chapter 3. There is a precedent for this behaviour, for example, Dagorne and coworkers reported that the nitrogen atoms in aminophenol ligands were deprotonated by aluminium in toluene at 80 °C, forming a two-ligand dialuminium complex.[16]

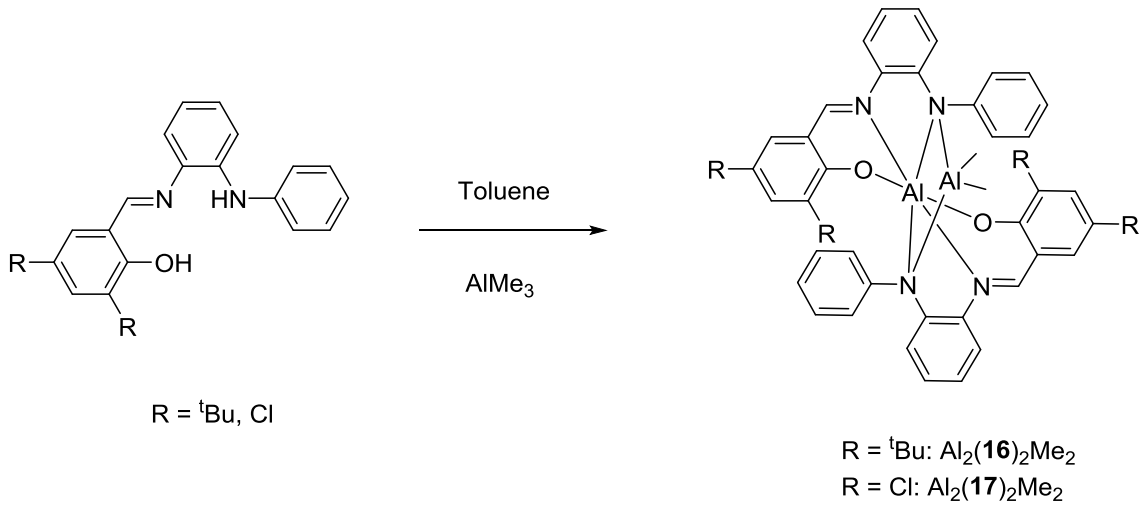


**Figure 4.30: Synthesis of diligated dialuminium complexes**

Figure 4.31 shows the solid-state crystal structure for $Al_2$(**16**)$_2Me_2$. It features one coordinatively saturated aluminium centre in octahedral geometry, and one tetrahedral aluminium centre with two bonded methyl groups. Further discussion of this structure can be found on page 141 and selected bond angles and lengths are listed in Table 4.04 on page 142.

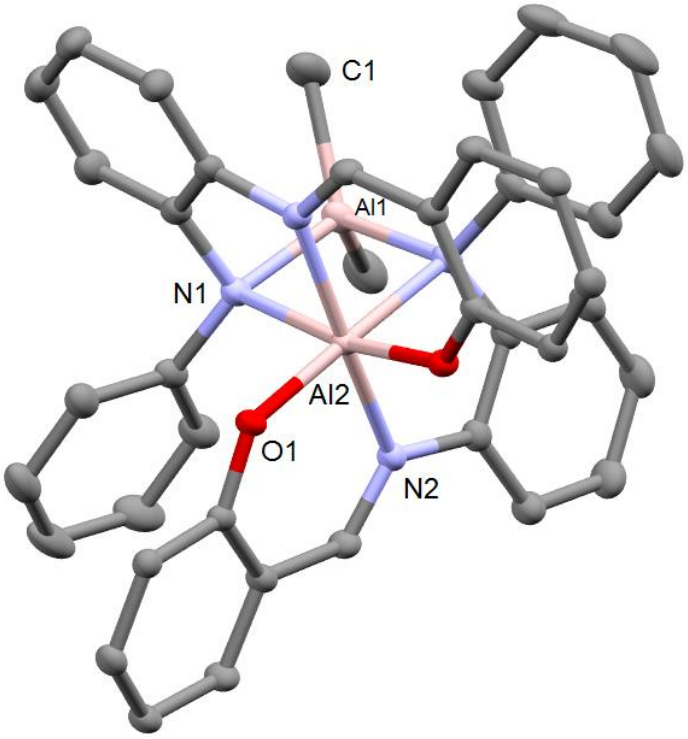


**Figure 4.31: Solid-state crystal structure of $Al_2(16)_2Me_2$. Hydrogen atoms and *tert*-butyl groups have been removed for clarity. Ellipsoids are shown at the 50 % probability level.**

The cyclised ligand **19**H was reacted with one equivalent of trimethylaluminium to form Al(**19**)$Me_2$. (Figure 4.32). The solid-state crystal structure of Al(**19**)$Me_2$ is shown in Figure 4.33.

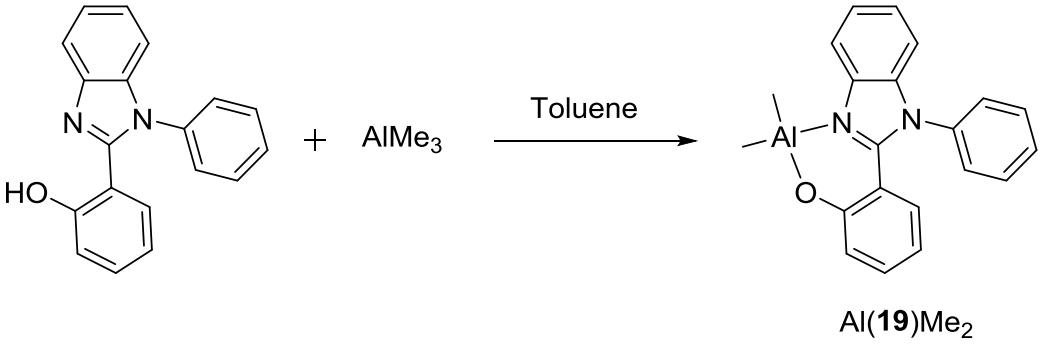


**Figure 4.32: Synthesis of Al(19)$Me_2$**

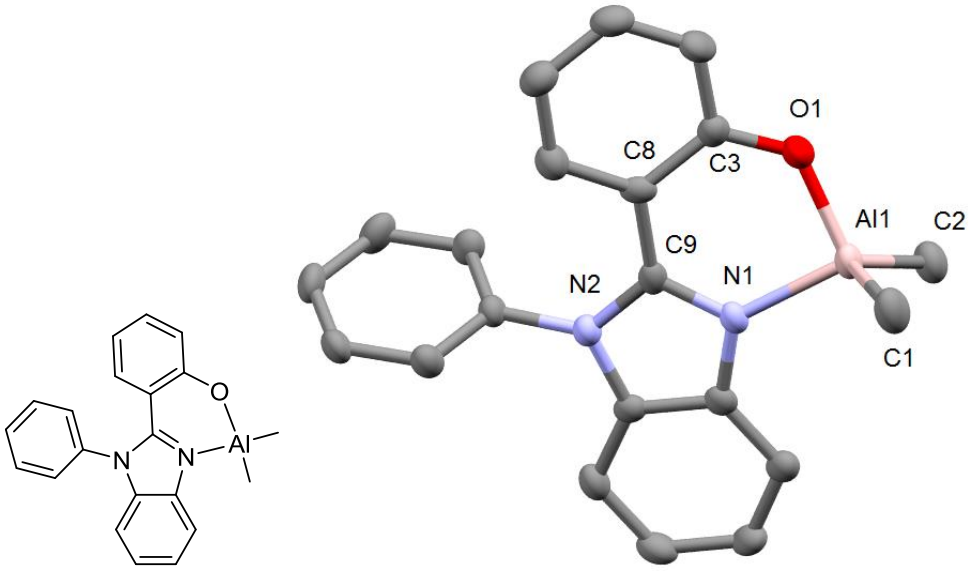


**Figure 4.33: Solid-state crystal structure of Al(19)$Me_2$. Hydrogen atoms have been removed for clarity. Ellipsoids are shown at the 50 % probability level.**

Table 4.04 shows selected bond angles and lengths for Al(**19**)$Me_2$ and $Al_2$(**16**)$_2Me_2$. The aluminium centres denoted Al1 in each complex are comparable, both being tetrahedral in geometry, with $\tau_4$ = 0.90 for both structures. The tetrahedrality is exemplified by bond angles such as N1-Al1-C1 which is 109.81(10) ° in Al(**19**)$Me_2$. In $Al_2$(**16**)$_2Me_2$, the secondary aluminium centre is distorted octahedral in geometry, with bond angles approaching 90° for groups *cis* to one another e.g. O1-Al2-N2 at 92.05(4) °, and nearing 180° for those *trans* to one another, for example N1a-Al2-O1 at 170.48(4) °.

**Table 4.04: Selected bond lengths (Å) and angles (°) for Al(19)$Me_2$ and $Al_2$(16)$_2Me_2$**

| | Al(**19**)$Me_2$ | $Al_2$(**16**)$_2Me_2$ |
|---|---|---|
| Al1-N1 | 1.944(2) | 1.994(1) |
| Al1-C1 | 1.955(2) | 1.969(1) |
| Al1-O1 | 1.775(2) | - |
| Al2-O1 | - | 1.821(1) |
| Al2-N1 | - | 2.168(1) |
| Al2-N2 | - | 1.974(1) |
| N1-Al1-O1 | 92.33(8) | - |
| N1-Al1-C1 | 109.81(10) | 116.84(5) |
| O1-Al1-C1 | 114.13(10) | - |
| N1-Al1-N1a | - | 89.06(6) |
| N1-Al2-N1a | - | 80.38(5) |
| O1-Al2-N2 | - | 92.05(4) |
| N1a-Al2-O1 | - | 170.48(4) |

No purification was carried out for $Al_2$(**16**)$_2Me_2$, instead the crude product mixture was taken forward for polymerisation in the case of these initiators. The $^1$H NMR spectrum of this product mixture shows that more than one species is present in solution (Figure 4.34). Whilst a crystal structure was obtained for what must be the major product, other minor products may have formed. The aluminium methyl region of the spectrum has been zoomed in to show the minor peaks at -0.78 and -0.28 ppm, alongside the major singlet at -0.47 ppm.

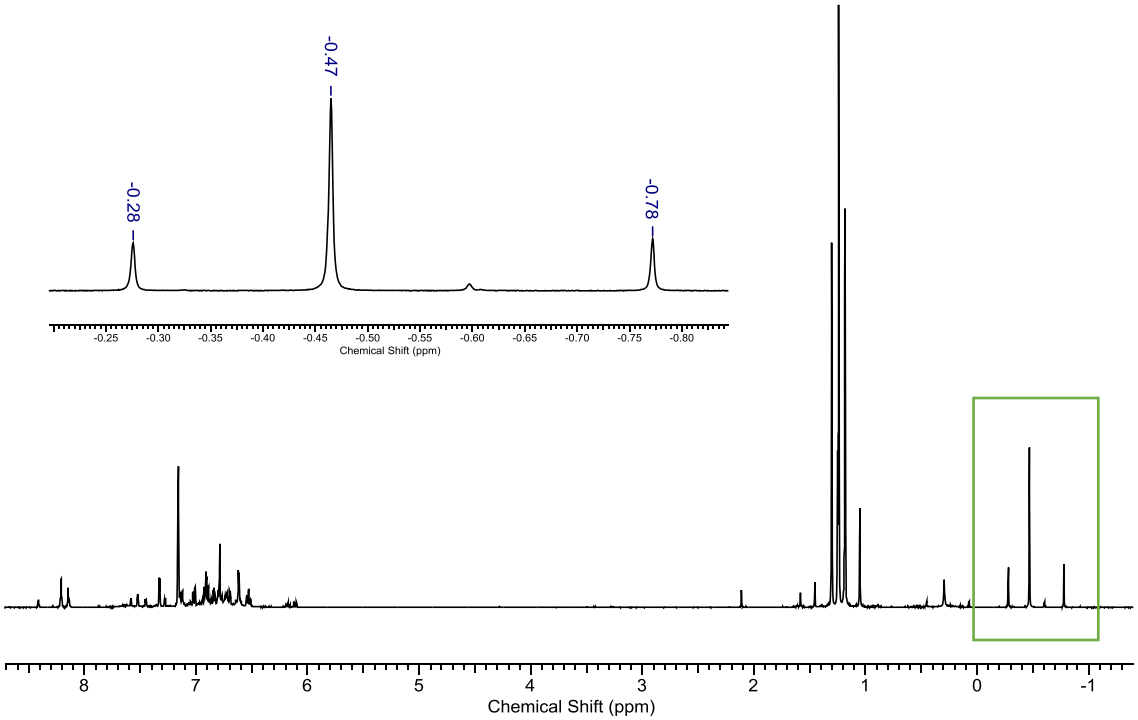


**Figure 4.34: $^{1}$H NMR spectrum of $Al_2(16)_2Me_4$ in $C_6D_6$. The Al-methyl region has been zoomed in to illustrate the presence of multiple species in the product mixture.**

An example of a potential isomer is illustrated in Figure 4.35, with one methyl per metal centre. This would account for the two chemically inequivalent Al-Me resonances seen in the spectrum. Such isomerisation has been previously observed in the literature, for example by Jones *et al*.[17]


Observed 6-4 motif  Possible 5-5 motif

**Figure 4.35: Example of possible isomer of $Al_2(16)_2Me_4$**

Figure 4.36 shows the $^{1}$H NMR of Al(**19**)$Me_2$, which shows that the solid-state structure is retained in solution. The two aluminium methyl groups are chemically equivalent and appear as a singlet at -0.02 ppm. This is surprisingly downfield, perhaps due to the electron-withdrawing effect of the highly aromatic ligand, causing the aluminium methyls to be more deshielded.

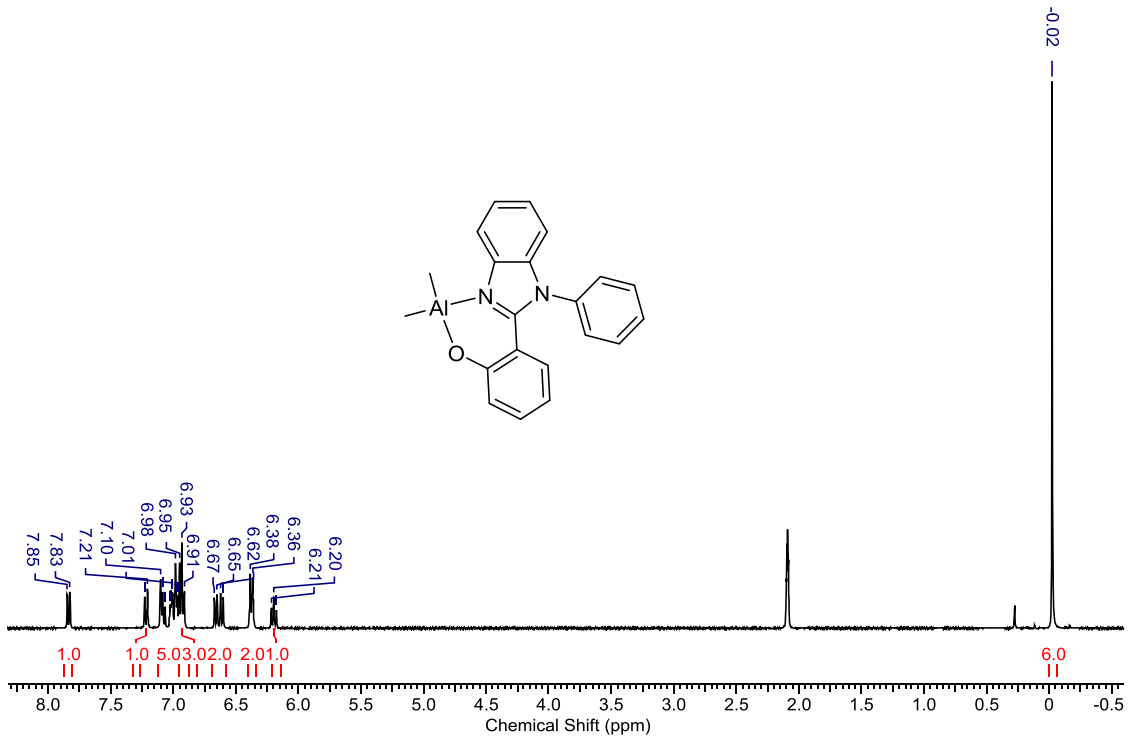


**Figure 4.36: $^{1}$H NMR spectrum of Al(19)Me$_2$ in $C_6D_5CD_3$**

4.3.3 Salalen complexes

The salalen ligand **20**$H_2$ was reacted with 2 M trimethylaluminium solution to form a tetradentate aluminium complex (Figure 4.37). This complex retained the bright yellow colour of the ligand. Crystal structure data was obtained for this complex (Figure 4.38).

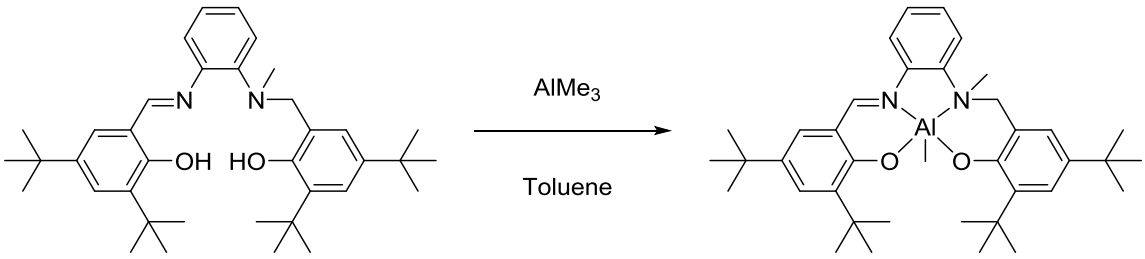


**Figure 4.37: Synthesis of Al(20)Me**

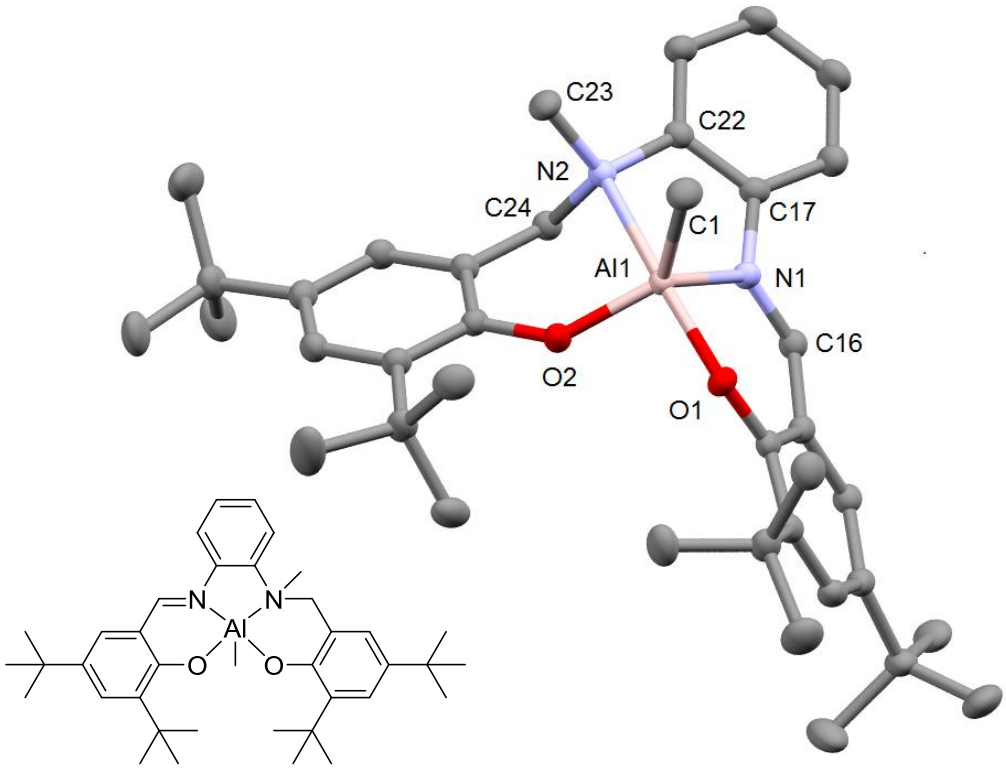


**Figure 4.38: Solid-state crystal structure of Al(20)Me. Ellipsoids are shown at the 30% probability level. Hydrogen atoms have been omitted for clarity.**

The complex formed consists of the tetradentate coordinated with the aluminium centre, which has one methyl group, resulting in a 5-coordinate complex, as expected for this complex type. The aluminium centre has a distorted trigonal bipyramidal geometry, with $\tau_5 = 0.66$. The highly distorted nature of the complex could be attributed to the inflexibility of the phenylene backbone. The N-amine and the imine phenoxy oxygen adopt the axial positions in this complex, which is consistent with previous aluminium salalen complexes.[5]

Table 4.05 shows selected bond lengths and angles from structure Al(**20**)Me and also from previous aluminium salalen complexes (labelled **III** and **IV**) prepared by Jones *et al.*, pictured in Figure 4.39.[2, 3] This will allow for comparison between three near-identical structures to discern the effect of different backbones. The increasing structural rigidity from ethylene to cyclohexyl through to phenyl backbone is exemplified through various bond lengths and angles. For example, the bond angle for N1-Al-N2 reduces from 79.10(11) ° in complex I to 75.13(3) ° in Al(**20**)Me. This is caused by the shortening of the C-C bond on the backbone (which is $sp^3$ in compound **IV** and $sp^2$ in Al(**20**)Me) from 1.523(3) Å to 1.396(2) Å. As is expected for structures of this type, the imine bond length at 1.308(1) Å is shorter than the amine at 1.502(1) Å. Bond angles which typify the trigonal bipyramidal geometry include the equatorial C1 group, at 92.86(4) ° from the axial N2, and the equatorial bond N1-Al-O2, at 120.64(4) °. The distortion of

the geometry can be best exemplified through the axial bond O1-Al-N2, which is 161.56(4) °. This distortion also occurs for the literature compounds, although to a lesser extent. This comes back to the rigidity of the backbone, whose effect on the N1-Al-N2 angle is carried through to the rest of the angles.

**Table 4.05: Selected bond lengths (Å) and angles (°) for Al(20)Me, III and IV**

| | Al(**20**)Me | **III** | **IV** |
|---|---|---|---|
| Al-C1 | 1.964(1) | 1.960(3) | 1.966(7) |
| N1-Al | 1.973(1) | 1.979(3) | 1.978(6) |
| N2-Al | 2.301(1) | 2.266(3) | 2.179(5) |
| O1-Al | 1.831(1) | 1.827(2) | 1.831(4) |
| O2-Al | 1.758(1) | 1.757(2) | 1.768(4) |
| N2-C24 | 1.502(1) | 1.496(4) | 1.478(8) |
| N1=C16 | 1.308(1) | 1.296(5) | 1.303(8) |
| C17-C22 | 1.396(2) | 1.500(6) | 1.523(3) |
| N1-Al-N2 | 75.13(3) | 79.10(11) | 77.7(2) |
| N1-Al-O2 | 120.64(4) | 120.70(12) | 117.7 |
| O1-Al-N2 | 161.56(4) | 165.46(12) | 164.4(2) |
| C1-Al-N2 | 92.86(4) | 93.82(11) | 95.1(3) |

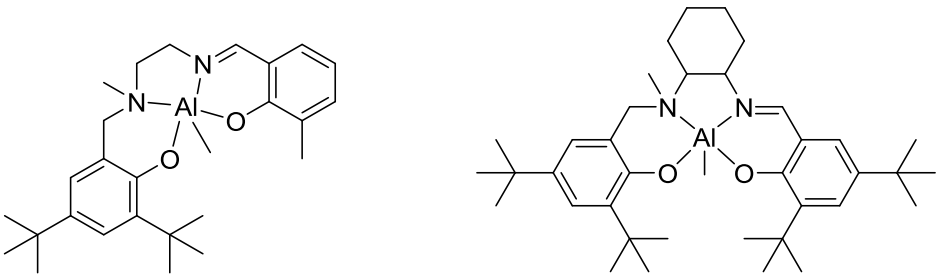


**III** **IV**

**Figure 4.39: Literature aluminium salalen complexes**

Further evidence of the greatly increased rigidity of the phenylene backbone in Al(**20**)Me is the torsion angle. Table 4.06 shows the N1-C17-C22-N2 torsion angles for Al(**20**)Me and the literature compounds discussed above. As expected, the $sp^3$ hybridised backbone shows far

greater flexibility, with torsion angles greater than 40 °, whereas the aromatic backbone has a greatly reduced angle of -3.72 °. The difference between the ethylene backbone and the cyclised cyclohexyl can also be seen, with compound **III** exhibiting the largest backbone torsion angle.

**Table 4.06: Torsion angles (°) for the N-C-C-N bond of the backbone of Al(20)Me, III and IV**

| | Al(**20**)Me | **III** | **IV** |
|---|---|---|---|
| Backbone torsion angle N-C-C-N (°) | -3.72 | 48.5(4) | -41.7(6) |

Proton and $^{13}C\{^{1}H\}$ NMR spectroscopic analysis of Al(**20**)Me showed that the solid-state crystal structure is retained in solution. Figure 4.40 shows the $^{1}H$ NMR spectrum in deuterated benzene. The four *tert*-butyl resonances are distinct due to the asymmetry of the ligand, as such they are all chemically inequivalent. Notably, the methylene bridging protons appear as two separate diastereotopic doublets, indicating that the ligand is coordinatively 'locked' upon complexation. This is not the case with the ligand, as seen in Figure 4.11, where the two equivalent methylene protons are seen as a singlet at 4.32 ppm.

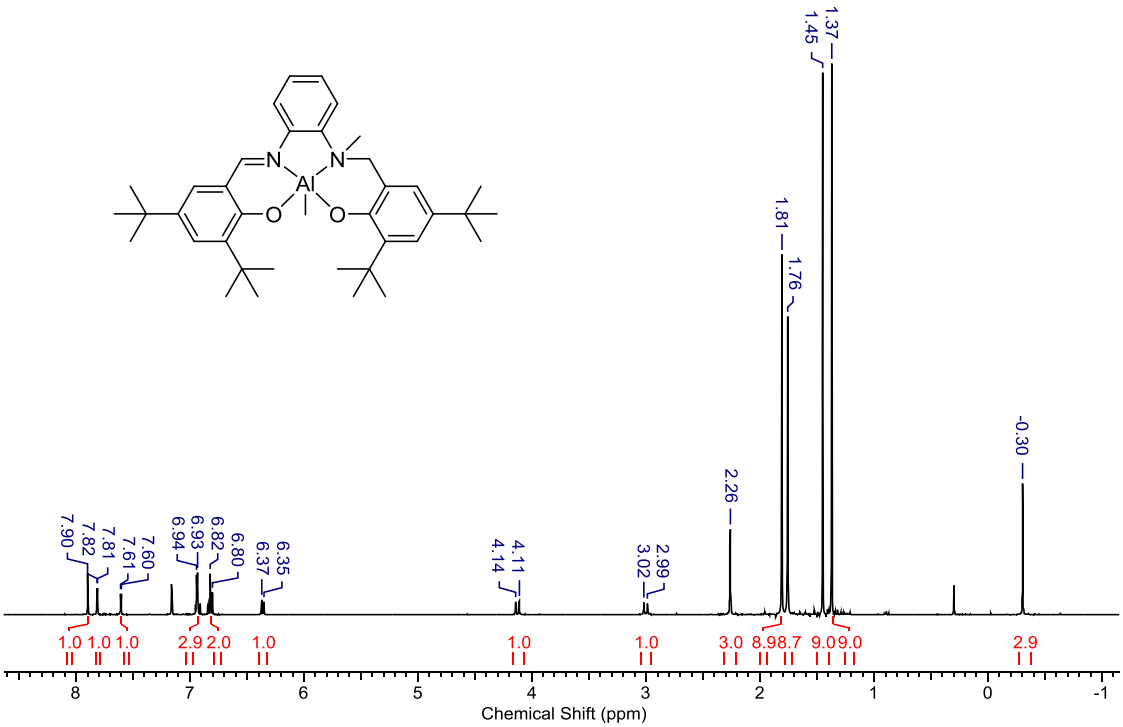


**Figure 4.40: $^{1}H$ NMR spectrum of Al(20)Me in $C_6D_6$**

The ligand **20**$H_2$ was also reacted stoichiometrically with various group 4 precursors – zirconium isopropoxide and *tert*-butoxide, and hafnium isopropoxide to form salalen complexes (Figure 4.41). These reactions were carried out in hexane/toluene with gentle heating (50 °C). The purpose of synthesising the zirconium *tert*-butoxide complex is to provide a direct comparison

between the salen and salalen ligands, as in both Zr(**13**)($O^tBu$)$_2$ and Zr(**20**)($O^tBu$)$_2$ only one zirconium metal centre is present, allowing for comparison.

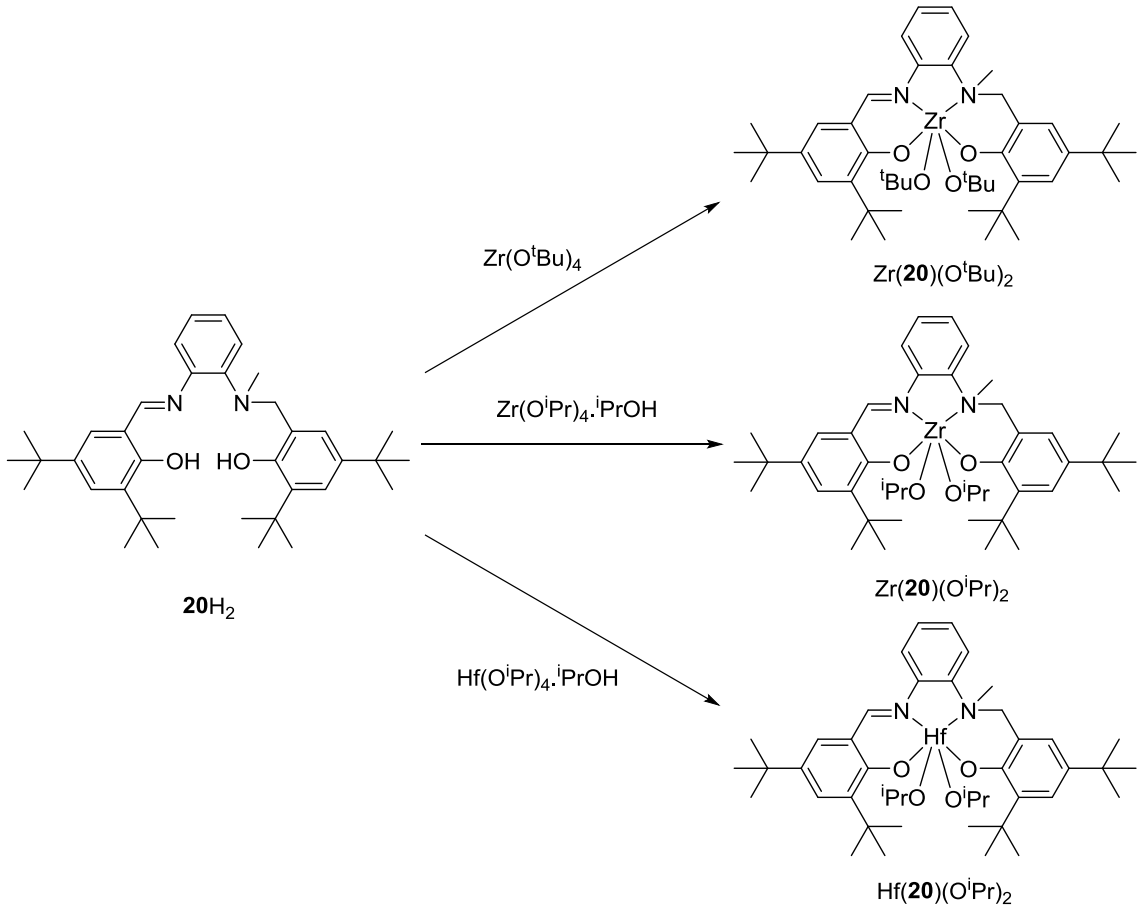


**Figure 4.41: Synthesis of zirconium and hafnium salalen complexes**

Figures 4.42, 4.43 and 4.44 show the solid-state crystal structures of Zr(**20**)($O^iPr$)$_2$, Zr(**20**)($O^tBu$)$_2$ and Hf(**20**)($O^iPr$)$_2$ respectively. The metal centres are all 6-coordinate with distorted octahedral geometry. In all complexes, the isopropoxide groups are situated *cis* to one another, and they exhibit the *fac-mer* wrapping mode (see Figure 4.46). As this is observed for all three complexes, this wrapping mode can be attributed to the structure of the ligand. In each case, it is the oxygen atom of the amine phenoxy group that resides in a different plane to the other three coordinating atoms on the ligand.

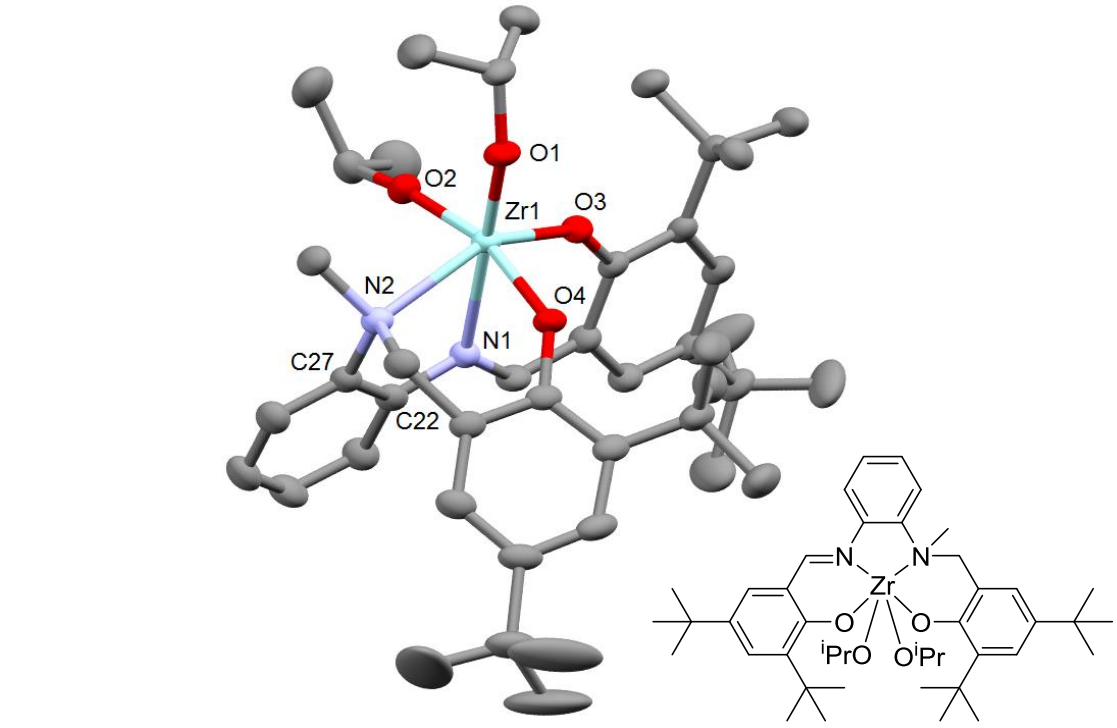


**Figure 4.42: Solid-state crystal structure of Zr(20)($O^iPr$)$_2$. Ellipsoids shown at the 50 % probability level. Hydrogen atoms and disordered tert-butyl carbons have been removed for clarity.**

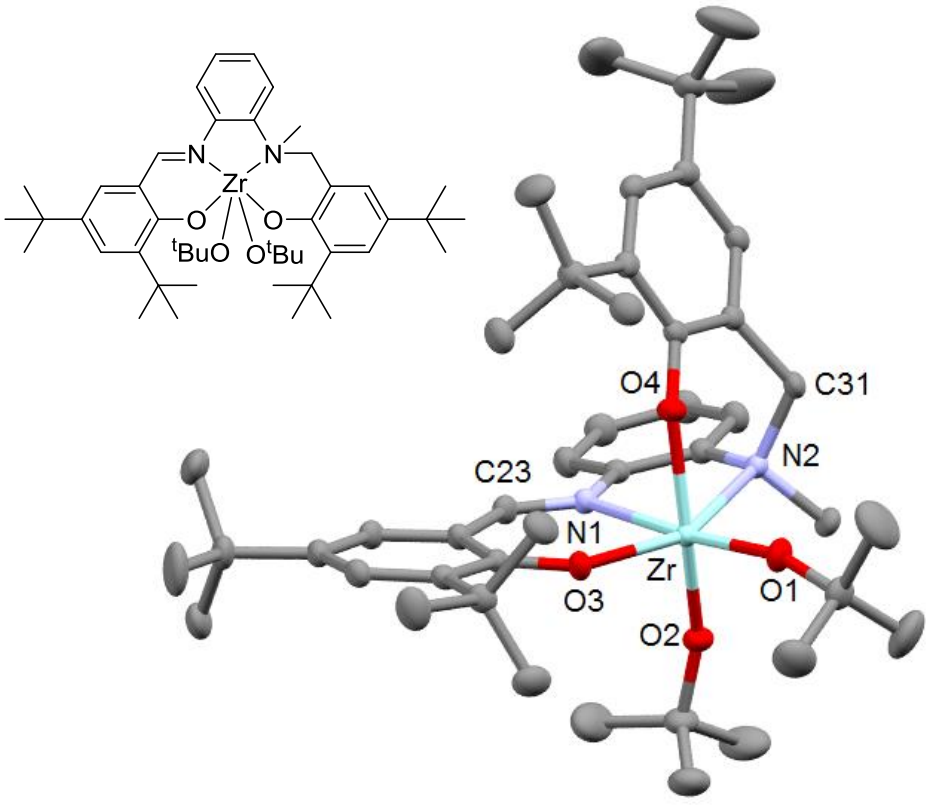


**Figure 4.43: Solid-state crystal structure of Zr(20)($O^tBu$)$_2$. Ellipsoids shown at the 30 % probability level. Hydrogen atoms and a molecule of disordered toluene have been removed for clarity.**

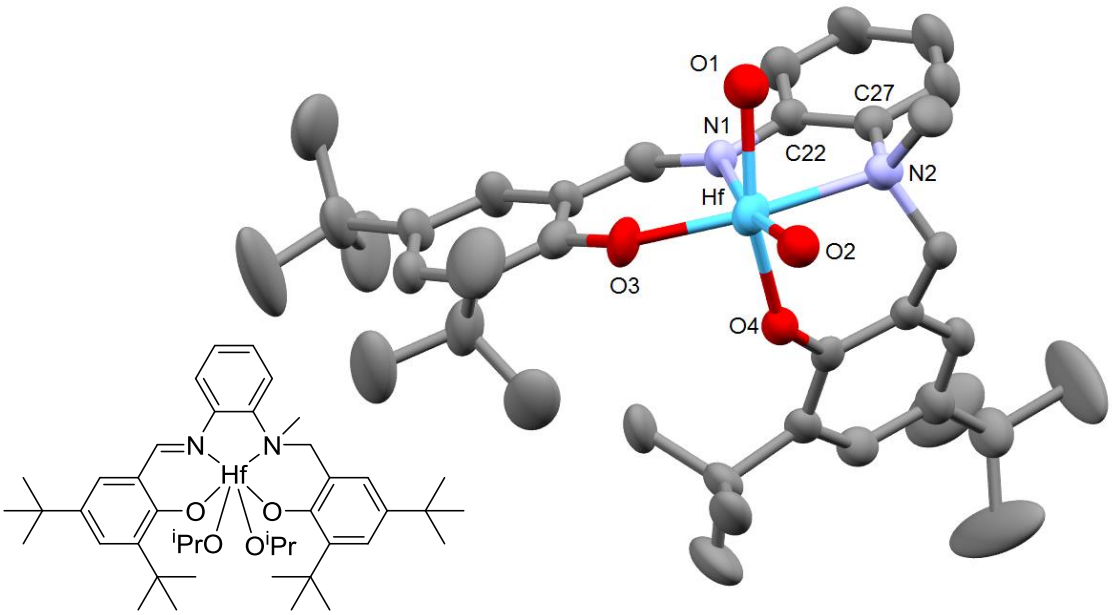


**Figure 4.44: Solid-state crystal structure of Hf(20)($O^iPr$)$_2$. Ellipsoids shown at the 50 % probability level. Hydrogen atoms, one molecule of hexane and isopropyl groups have been removed for clarity.**

Table 4.07 shows selected bond lengths and angles for each of the group 4 salalen complex, along with crystal data for a previously reported zirconium salalen complex, **V** (Figure 4.45) for comparison.

**Table 4.07: Selected bond lengths (Å) and angles (°) for Zr(20)($O^iPr$)$_2$, Zr(20)($O^tBu$)$_2$, Hf(20)($O^iPr$)$_2$ and V**

| | Zr(**20**)($O^iPr$)$_2$ | Hf(**20**)($O^iPr$)$_2$ | Zr(**20**)($O^tBu$)$_2$ | **V** |
|---|---|---|---|---|
| **M-N1** | 2.391(2) | 2.340(5) | 2.370(1) | 2.338(1) |
| **M-N2** | 2.414(2) | 2.380(5) | 2.402(1) | 2.433(1) |
| **M-O3** | 2.018(1) | 2.008(4) | 2.026(1) | 2.027(1) |
| **M-O4** | 2.073(2) | 2.049(5) | 2.078(1) | 2.053(1) |
| **N2-C (amine)** | 1.507(3) | 1.52(1) | 1.508(3) | 1.502(2) |
| **N1=C (imine)** | 1.293(3) | 1.293(8) | 1.288(2) | 1.281(2) |
| **N1-M-N2** | 70.53(6) | 71.7(2) | 71.43(4) | 71.94(5) |
| **N2-M-O4** | 79.80(6) | 80.5(2) | 79.60(4) | 78.08(5) |
| **O1-M-O2** | 97.35(6) | 95.0(6) | 96.62(4) | 93.15(5) |
| **O1-M-N1** | 175.36(6) | 79.8(4) | 173.10(4) | 168.59(5) |
| **O3-M-N2** | 148.51(6) | 152.3(2) | 150.48(4) | 148.79(5) |

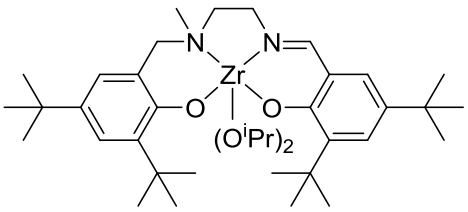


**V**

**Figure 4.45: Zirconium salalen complex previously reported by Jones *et al.*[18]**

All the structures have a distorted octahedral geometry, as exemplified by near-90 ° bond angles (e.g. 95.0(6) ° for O1-Hf-O2 in Hf(**20**)($O^iPr$)$_2$) and angles approaching 180° for groups *trans* to one another, e.g. 175.36(6) ° for O1-M-N1 in Zr(**20**)($O^iPr$)$_2$. In each case the N1-M-N2 is less than 72 °, a distortion caused by the polydentate nature of the ligand and the rigidity of the phenyl backbone, as was also seen for Al(**20**)Me. For each complex the N-C amine bond is longer for the amine than the imine N=C, which is to be expected for a single vs double bond, and typical for these ligand types. This is likely the cause of the *fac-mer* wrapping mode of each structure. Conversely, structure **V** exhibits *mer-fac* wrapping, although the reason for this subtle change in orientation cannot be obviously discerned, it could be attributed to the backbone as that is the only difference between these structures. Apart from this difference in wrapping, the structure **V** exhibits very similar bond lengths and angles as seen in the group 4 salalen complexes prepared in this chapter.

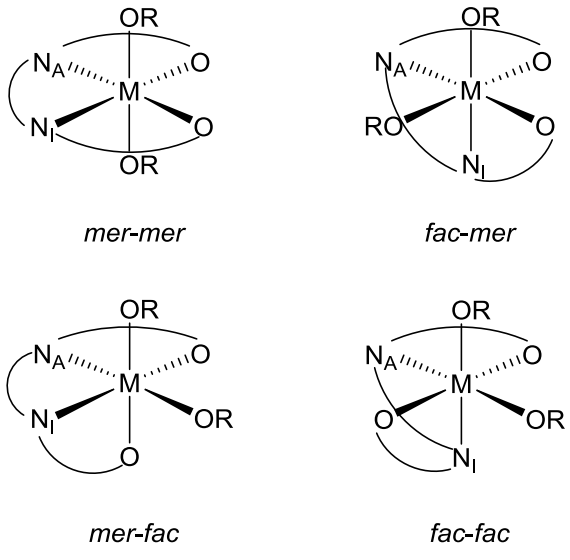


**Figure 4.46: Different ligand wrapping modes. $N_A$ = amine nitrogen, $N_I$ = imine nitrogen.**

Figure 4.47 shows the $^1$H NMR spectrum of Zr(**20**)($O^iPr$)$_2$. This solution data confirms the solid-state structure of the complex, with two isopropoxide protons around the 4 ppm region, shown zoomed in Figure 4.48. The $^1$H NMR spectrum for Hf(**20**)($O^iPr$)$_2$ is near identical to that in Figure 4.47, as would be expected. There is only one imine resonance present at 8.52 ppm, indicating

that only one structural isomer is present in solution, thus confirming the *fac-mer* wrapping in solution.

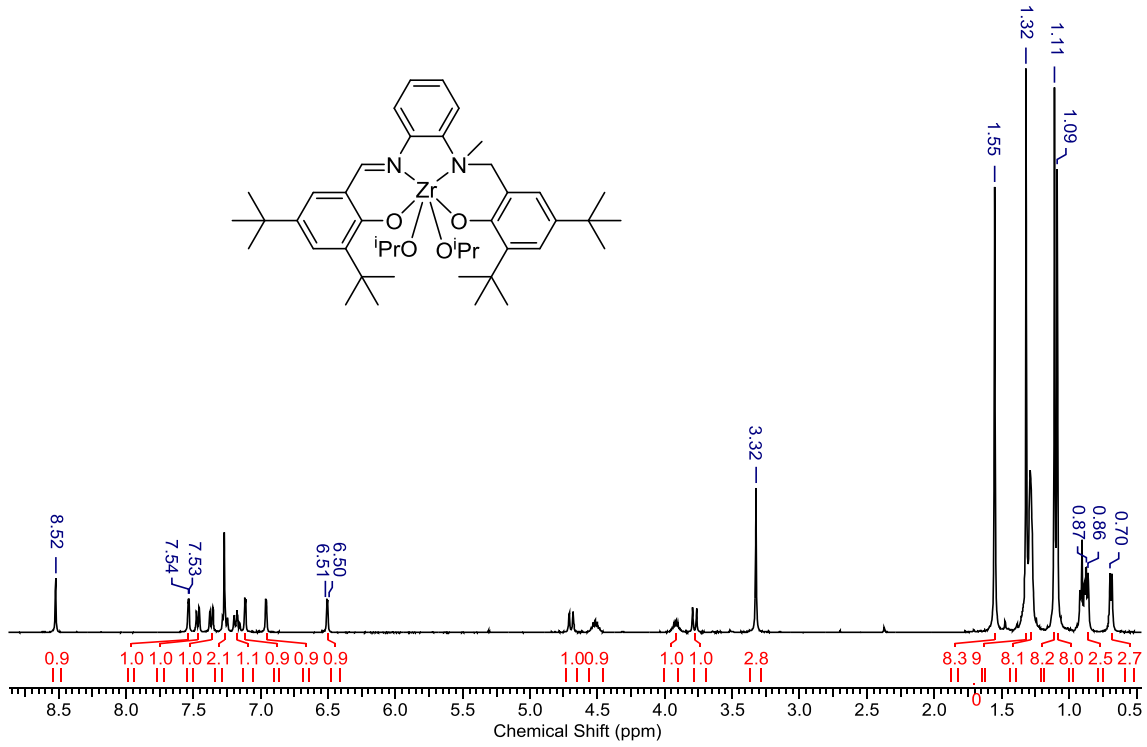


**Figure 4.47: $^{1}$H NMR spectrum of Zr(20)(O$^{i}$Pr)$_2$ in $CDCl_3$**

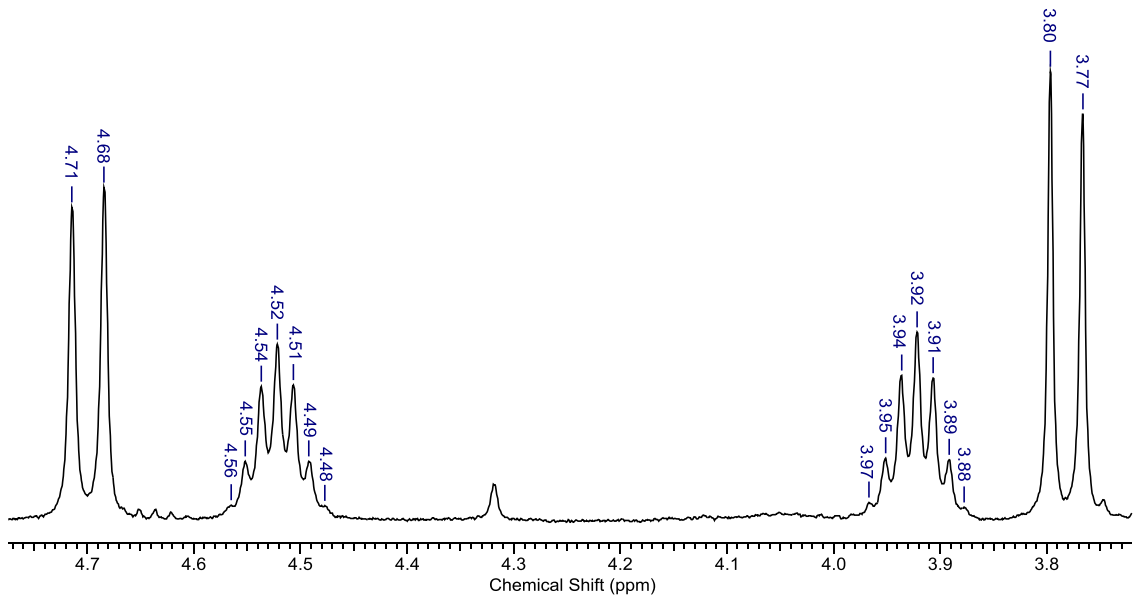


**Figure 4.48: $^{1}$H NMR spectrum of Zr(20)(O$^{i}$Pr)$_2$, zoomed in on isopropoxide region.**

Figure 4.48 shows that each proton is in a different environment, which is due to the geometry of the complex and the asymmetry of the ligand. This, along with the distinct diastereotopic -$CH_2$- doublets (as seen with the aluminium salalen), shows that the complex is coordinatively 'locked' into place.

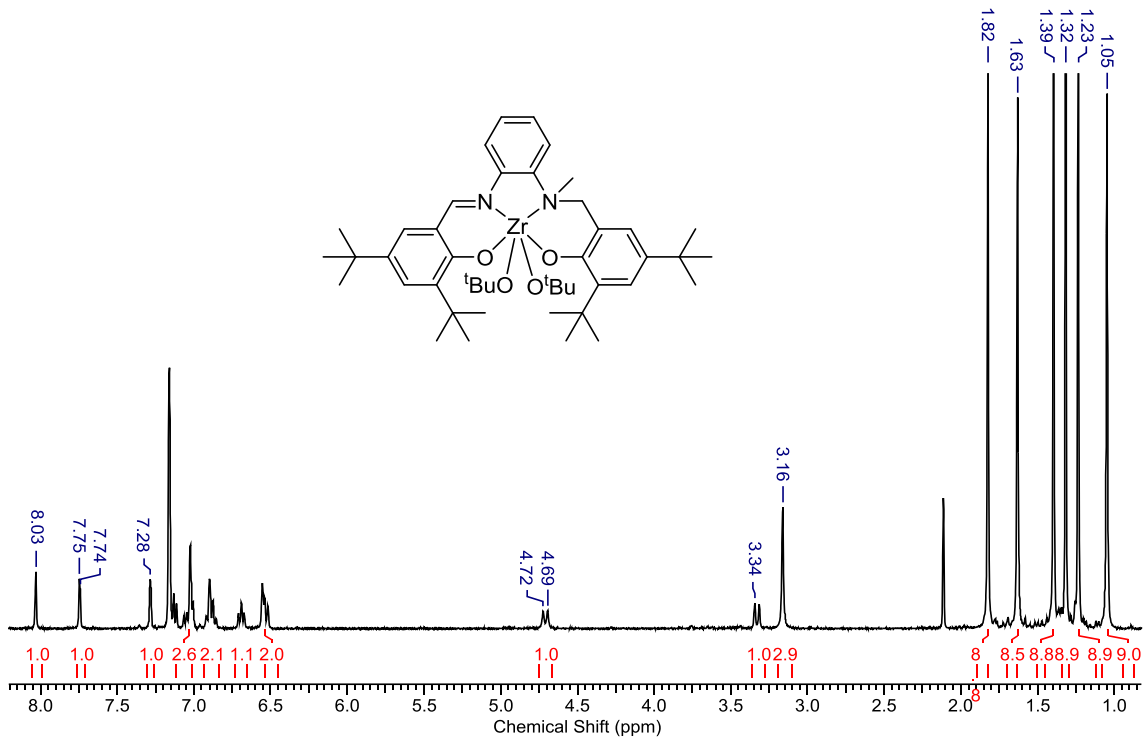


**Figure 4.49: $^{1}$H NMR spectrum of Zr(20)(O$^{t}$Bu)$_2$ in $C_6D_6$**

Figure 4.49 shows the proton NMR spectrum for Zr(**20**)(O$^{t}$Bu)$_2$, which is distinguishable from the spectrum in Figure 4.47 by the six tert-butyl resonances in the 1-2 ppm region, two of these belonging to the $^{t}$BuO ligands on the zirconium centre. Again, the -$CH_2$- protons manifest themselves as separate doublets.

## 4.3.4 Salan complex

The salan ligand **21**$H_2$ was complexed with aluminium (Figure 4.50) in order to create a comparable structure featuring only the N-methyl amine moieties. This complex was easily formed, however no crystal structure was obtained as the complex precipitated almost immediately from solution on addition of trimethylaluminium. It was not possible to isolate the zirconium analogue, due to high solubility of the complex and large amount of impurity in the crude reaction mixture.

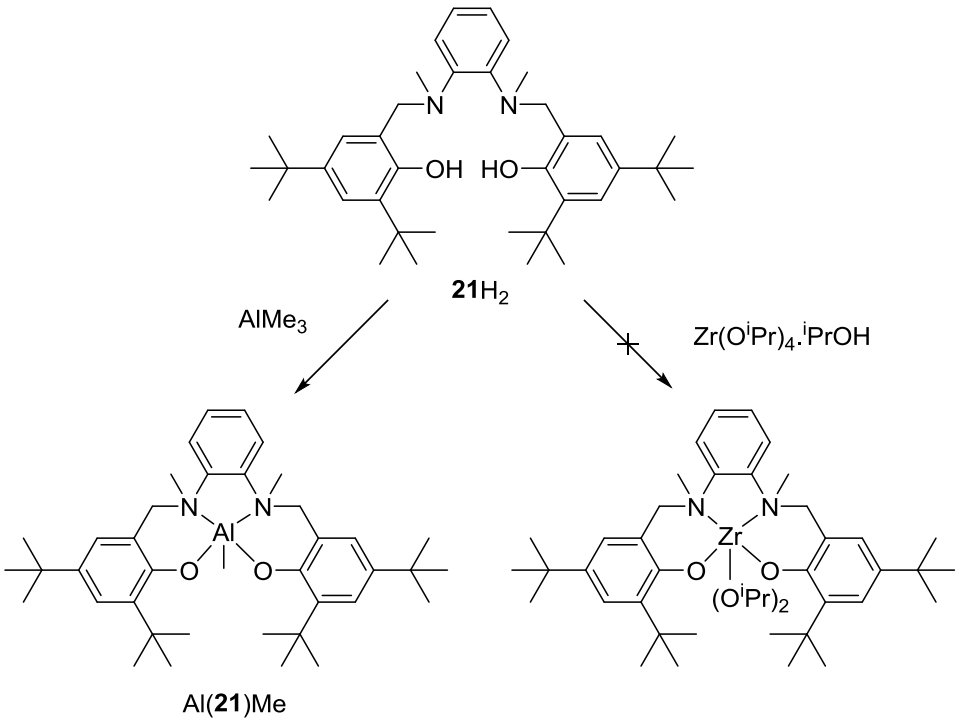


**Figure 4.50: Synthesis of salan complexes.**

The $^{1}$H NMR spectrum of Al(**21**)Me is shown in Figure 4.51. As was seen with the salalen aluminium complex, the methylene protons are not chemically equivalent and show as separate doublets, indicating that the complex is 'locked' into configuration. The aluminium methyl resonance is visible at -0.37 ppm.

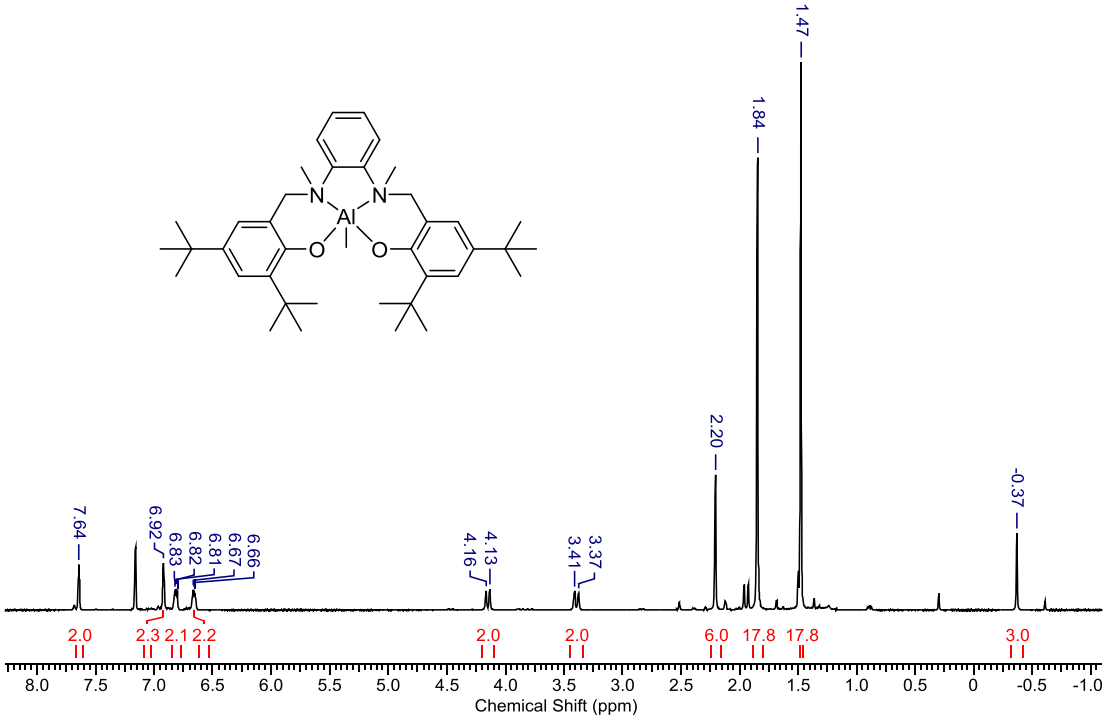


**Figure 4.51: $^{1}$H NMR spectrum of Al(21)Me in $C_6D_6$**

## 4.4 Polymerisation Results

The complexes described above were taken forward for use as initiators in the polymerisation of lactide. For all polymerisations sublimed *rac*-lactide is used, unless otherwise stated. In all cases, conversions were obtained from $^1$H NMR spectroscopic data of the crude polymerisation mixture, $P_r$ values determined by homonuclear decoupled NMR spectroscopy, theoretical molecular weights calculated using equation 2.2 and number average molecular weights ($M_n$) and polydispersities (PDI) determined by GPC. It should be noted that for this chapter a gel permeation chromatograph with triple detection (RI, light scattering, viscometry) was used, as such no correction factor has been applied to any of the molecular weights.

### 4.4.1 Ring opening polymerisation of *rac*-lactide using salalen precursor complexes

Table 4.08 shows the data for the ring-opening polymerisation of *rac*-lactide using the precursor complexes $Al_2$(**16**)$_2Me_2$ and $Al_2$(**17**)$_2Me_2$ and Al(**19**)$Me_2$ in toluene at 80 °C. Benzyl alcohol is used as a coinitiator in order to form an alkoxide *in situ*.

**Table 4.08: Solution polymerisation data using $Al_2(16)_2Me_2$, $Al_2(17)_2Me_2$ and $Al(19)Me_2$ in toluene at 80 °C. (1) determined by homonuclear decoupled NMR (2) determined by equation 2.2 (3) determined by GPC**

| Entry | Initiator | LA:I | BnOH | Conversion (%) | Time (h) | $P_r$[1] | $M_n$ Calc[2] (gmol$^{-1}$) | $M_n$[3] (gmol$^{-1}$) | PDI[3] |
|---|---|---|---|---|---|---|---|---|---|
| 1 | $Al_2$(**16**)$_2Me_2$ | 100 | 1 | 99 | 48 | 0.54 | 14,374 | 24,200<br>12,950 | 1.06<br>1.03 |
| 2 | | 100 | 2 | 100 | 24 | 0.55 | 7,313 | 8,700 | 1.14 |
| 3 | $Al_2$(**17**)$_2Me_2$ | 100 | 1 | 88 | 48 | 0.52 | 12,789 | 27,900 | 1.04 |
| 4 | | 100 | 2 | 92 | 24 | 0.52 | 6,737 | 10,000 | 1.07 |
| 5 | Al(**19**)$Me_2$ | 100 | 1 | 97 | 24 | 0.42 | 14,086 | 24,700 | 1.47 |
| 6 | | 200 | 1 | 97 | 24 | 0.42 | 28,063 | 52,450 | 1.42 |
| 7 | | 400 | 1 | 96 | 48 | 0.42 | 55,442 | 78,850 | 1.37 |

In each case the molecular weight of the polymer produced is far higher than calculated. It could be that for $Al_2$(**16**)$_2Me_2$ and $Al_2$(**17**)$_2Me_2$ the second metal centre is initiating an uncontrolled polymerisation (where $k_{prop} >> k_{init}$), thus increasing the average molecular weight. If this were the case, it would be expected that high polydispersities would be observed. Indeed, for polymers produced using Al(**19**)$Me_2$ the polydispersities are high, however this is not the case

for $Al_2$(**16**)$_2Me_2$ and $Al_2$(**17**)$_2Me_2$. Interestingly, two peaks were clearly observed in the GPC chromatogram of polymer from entry 1 (Figure 4.52). The second peak comes much closer to the expected molecular weight of polymer produced by this initiator at this loading. The presence of two peaks suggests two different initiation sites, which could occur given the two metal centres present. Counterintuitively, the two peaks occur for the polymerisation using only one equivalent of benzyl alcohol, whereas one would expect that the polymerisation with two equivalents of the coinitiator would facilitate the two initiation sites. This can be explained by the stoichiometry of the reaction – if two equivalents of coinitiator are present and the reaction is well controlled for both initiation sites, then a single peak with a narrow polydispersity is expected as both initiation sites would product polymer chains at similar rates. On the other hand, a polymerisation with two potential initiation sites but insufficient coinitiator present may have unusual results, such as two polymer chain lengths with different molecular weights, as is observed. Alternatively, it could be the presence of two different initiating species present in solution. In section 4.3.2, more than one species was observed by $^1$H NMR spectroscopy in the solution. The secondary peak in the GPC trace could be attributed to the minor species carrying out ROP of the monomer at a different rate.

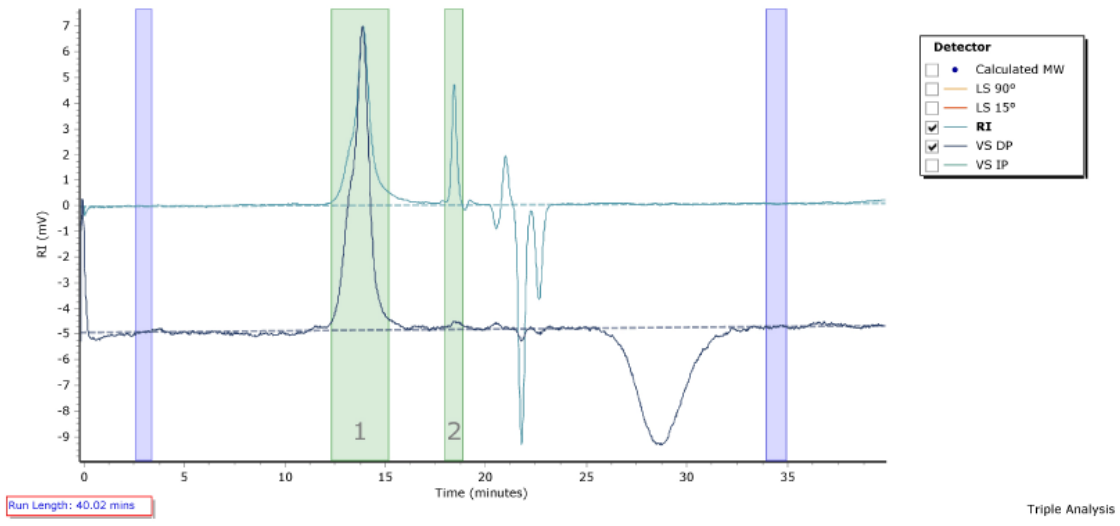


**Figure 4.52: GPC chromatogram for polymer from entry 1, Table 4.08. Triple detection used, only RI and Viscometry shown on chromatogram. Two peaks are present.**

## 4.4.2 Ring opening polymerisation of *rac*-lactide using salen complexes

Table 4.09 shows the data obtained for melt polymerisations using group 4 salen complexes, carried out at 130°C in the melt. In these polymerisations, no benzyl alcohol co-initiator was used as the alkoxide group is already incorporated into each initiator.

**Table 4.09: Melt polymerisation data for group 4 salen complexes at 130 °C. (1) determined by homonuclear decoupled NMR (2) determined by equation 2.2 (3) determined by GPC**

| Entry | Initiator | LA:I | Conversion (%) | Time (h) | $P_r$[1] | $M_n$ Calc[2] ($gmol^{-1}$) | $M_n$[3] ($gmol^{-1}$) | PDI[3] |
|---|---|---|---|---|---|---|---|---|
| 1 | $Zr_2$(**13**)($O^iPr$)$_6$ | 300 | 64 | 0.5 | 0.60 | 13,894 | 81,400 | 1.22 |
| 2 | | 600 | 58 | 0.5 | 0.58 | 25,133 | 70,800 | 2.04 |
| 3 | | 900 | 70 | 0.5 | 0.58 | 45,452 | 46,350 | 1.29 |
| 4 | Zr(**13**)($O^tBu$)$_2$ | 300 | 35 | 24 | 0.53 | 15,205 | 22,800 | 1.10 |
| 5 | $Hf_2$(**13**)($O^iPr$)$_6$ | 300 | 71 | 1 | 0.61 | 15,407 | 30,350 | 1.24 |
| 6 | | 600 | 76 | 1 | 0.58 | 32,915 | 36,750 | 1.36 |

In entries 1-3, the bulk polymerisation of *rac*-lactide using $Zr_2$(**13**)($O^iPr$)$_6$ produced high molecular weight polylactide within half an hour. The $P_r$ values tend towards heterotacticity, but only mildly. Strangely, the observed molecular weights were far higher than those calculated, with the exception of entry 3. The calculated molecular weights in Table 4.09 assume a two-metal site initiation for the dinuclear complexes, however even for a one-metal initiation the calculated molecular weights would be far below those observed (e.g. $M_n$ calc = 50,266 $gmol^{-1}$ for entry 2). For Zr(**13**)($O^tBu$)$_2$, the polymerisation only reached 35 % conversion after 24 hours. Due to this poor activity and selectivity, no further melt polymerisations were carried out using this initiator. For $Hf_2$(**13**)($O^iPr$)$_6$, high conversions are reached within an hour, with slight heterotacticity in the polymer, as seen with $Zr_2$(**13**)($O^iPr$)$_6$. However, the observed molecular weight agrees well with the calculated value at 600:1 loading (entry 6) but is nearly double the expected molecular weight at 300:1 loading (entry 5), suggesting that potentially the complex initiates only one polymer chain in the latter case and two polymer chains in the former.

Table 4.10 shows the solvent polymerisation data (in toluene at 80 °C) for the salen complexes. Benzyl alcohol is used as a coinitiator only with $Al_2$(**13**)$Me_4$ to form the metal alkoxide *in situ*. Two equivalents are used in order to activate both metal centres in the complex.

**Table 4.10: Solution polymerisation data using salen complexes at 80 °C in toluene. (1) determined by homonuclear decoupled NMR (2) determined by equation 2.2 (3) determined by GPC**

| Entry | Initiator | LA:I | BnOH | Conversion (%) | Time (h) | $P_r$[1] | $M_n$ Calc[2] ($gmol^{-1}$) | $M_n$ [3] ($gmol^{-1}$) | PDI[3] |
|---|---|---|---|---|---|---|---|---|---|
| 1 | $Al_2$(**13**)$Me_4$ | 100 | 2 | 74 | 5 | 0.53 | 5,440 | 4,450 | 1.02 |
| 2 | | 200 | 2 | 98 | 16 | 0.57 | 14,230 | 17,850 | 1.09 |
| 3 | | 400 | 2 | 98 | 24 | 0.57 | 28,352 | 33,850 | 1.27 |
| 4 | $Zr_2$(**13**)$(O^iPr)_6$ | 100 | 0 | 100 | 24 | 0.51 | 7,265 | 11,250 | 1.35 |
| 5 | | 200 | 0 | 98 | 24 | 0.54 | 14,182 | 21,300 | 1.68 |
| 6 | | 400 | 0 | 97 | 48 | 0.57 | 28,015 | 35,350 | 1.27 |
| 7 | | 800 | 0 | 97 | 72 | 0.55 | 55,971 | 25,200 | 1.30 |
| 8 | Zr(**13**)$(O^tBu)_2$ | 100 | 0 | 50 | 24 | 0.44 | 7,279 | 11,900 | 1.04 |
| 9 | $Hf_2$(**13**)$(O^iPr)_6$ | 100 | 0 | 43 | 6 | 0.57 | 3,158 | 15,300 | 1.03 |
| 10 | | 200 | 0 | 94 | 24 | 0.58 | 13,605 | 32,750 | 1.26 |

The $P_r$ values for all complexes are close to 0.5, showing that these initiators have no significant selectivity in solution. The initiator $Al_2$(**13**)$Me_4$ shows good molecular weight control, as shown by agreement of the observed molecular weights with those calculated (calculation assumes two-metal centre initiation) and narrow PDI values. For $Zr_2$(**13**)$(O^iPr)_6$, the observed molecular weights are all larger than the calculated molecular weight, as observed in the melt, with the exception of entry 7. If we assume a one metal centre initiation, the calculated molecular weight will double – if this were the case, the observed molecular weights would all be lower than expected, e.g. 15,250 $gmol^{-1}$ calculated vs 11,250 $gmol^{-1}$ observed for entry 4. All of the PDI values are broad (1.27 - 1.68) which shows that the reactions in entries 4-7 are poorly controlled. When considering that there are 6 different possible alkoxide groups to insert into the monomer, this is not surprising. Figure 4.53 shows the MALDI-ToF spectrum for the polymer in entry 4. The repeat unit between the major peaks is 72 $gmol^{-1}$, which indicates that the polymer has transesterified. The peak at 5414.0 m/z corresponds to the mass a polymer chain

featuring 37 lactide units and a -H and -O$^{i}$Pr end group. This indicates that the initiator undergoes the expected coordination-insertion mechanism.

Similar results are seen for the dinuclear hafnium complex, Hf$_2$(**13**)(O$^{i}$Pr)$_6$. It has poor stereocontrol and the molecular weights are larger than expected. This shows that these complexes have poor predictability. Furthermore, with no stereoselectivity observed, the investigation of these complexes was not taken further.

With Zr(**13**)(O$^{t}$Bu)$_2$, a very minor switch in selectivity can be seen between the isopropoxide and *tert*-butoxide zirconium complexes, from above 0.5 (i.e. tending towards heteroselectivity) for the former and below 0.5 (i.e. tending towards isoselectivity) for the latter. Most likely this subtle change is due to the dimeric vs monomeric nature of the two catalysts. In summary, it can be observed that metal complexes of the ligand **13**H$_2$ produce polylactide that is atactic.

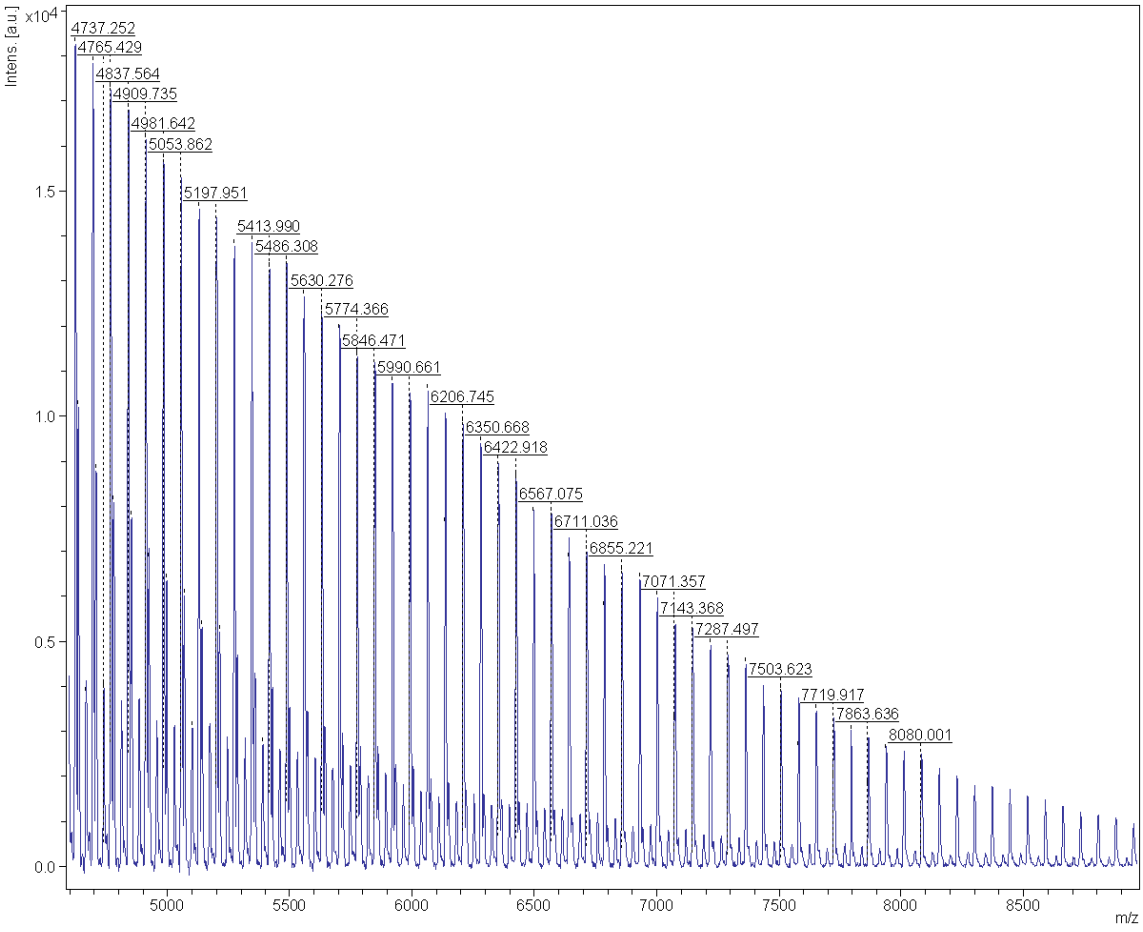


**Figure 4.53: MALDI-ToF spectrum of polylactide produced using Zr$_2$(13)(O$^{i}$Pr)$_6$ at 100:1 at 80 °C in toluene, Table 4.10, entry 4**

### 4.4.3 Ring-opening polymerisation of lactide using salalen complexes

Table 4.11 shows the melt polymerisation data for the group 4 salalen complexes, Zr(**20**)($O^iPr$)$_2$, Zr(**20**)($O^tBu$)$_2$ and Hf(**20**)($O^iPr$)$_2$. In each case the polymerisation was carried out near the melting point of the monomer and reaction stopped when stirrer bar ceased stirring, with the exception of entry 6, where industrial production temperature (180 °C) was used, above the melting point of the polymer.

**Table 4.11: Melt polymerisation data for group 4 salalen complexes. Doubly sublimed *rac*-lactide used except for (a) L-lactide (b) D-lactide (c) *rac*-lactide purified by single recystallisation only (d) 10 equivalents of benzyl alcohol were utilised. (1) determined by homonuclear decoupled NMR (2) determined by equation 2.2 (3) determined by GPC**

| Entry | Initiator | LA:I | Conversion (%) | Time (h) | $P_r$[1] | $M_n$ Calc[2] ($gmol^{-1}$) | $M_n$[3] ($gmol^{-1}$) | PDI[3] | Temp (°C) |
|---|---|---|---|---|---|---|---|---|---|
| 1 | Zr(**20**)($O^iPr$)$_2$ | 300 | 81 | 1 | 0.29 | 35,076 | 38,800 | 1.03 | 130 |
| 2 | | 900 | 53 | 16 | 0.31 | 68,796 | 34,950 | 1.44 | 130 |
| 3[a] | | 300 | 67 | 16 | - | 29,024 | 30,000 | 1.48 | 100 |
| 4[b] | | 300 | 45 | 3 | - | 19,514 | 14,250 | 1.02 | 100 |
| 5[c] | | 300 | 84 | 2 | 0.26 | 36,373 | 17,000 | 1.26 | 130 |
| 6[c,d] | | 3000 | 61 | 4 | 0.6 | 26,430 | 21,900 | 1.15 | 180 |
| 7 | Zr(**20**)($O^tBu$)$_2$ | 300 | 77 | 1.5 | 0.42 | 33,361 | 23,650 | 1.31 | 130 |
| 8 | Hf(**20**)($O^iPr$)$_2$ | 300 | 83 | 48 | 0.28 | 35,941 | 16,650 | 1.09 | 130 |

In entry 1, Zr(**20**)($O^iPr$)$_2$ shows promising isoselectivity in the melt, with a $P_r$ value of 0.29, with good molecular weight agreement and a narrow PDI. This is the most isoselective catalyst to operate under melt conditions. In most other cases the molecular weights of the polymer produced by Zr(**20**)($O^iPr$)$_2$ agree well with the calculated value. At 3000:1 loading at 180 °C the selectivity of the catalyst is lost in the melt, in fact some slight heteroselectivity is observed. The reaction was carried out using unsublimed lactide and at an elevated temperature, so this loss of selectivity is likely due to temperature effects and impurities in the monomer. In this polymerisation ten equivalents of benzyl alcohol were used to act as a chain transfer agent to control the molecular weight of the polymer. It could be that the benzyl alcohol acted as a coinitiator and coordinated with the zirconium *in situ* to form a different complex, with different selectivity. The molecular weight agreement is very good and the PDI is narrow. MALDI-ToF analysis of the polymer end group would confirm this hypothesis, however the molecular weight

of this polymer is too high for this technique to be used. The complex Zr(**20**)($O^tBu$)$_2$ is also isoselective in the melt, albeit only weakly. The reason for this is not entirely clear, but given its structural similarity with Zr(**20**)($O^iPr$)$_2$, it seems to be due to the bulkier *tert*-butoxide groups on the zirconium centre. Only one polymer chain is growing per metal centre and the presence of the extra bulk in the non-initiated alkoxide may influence the observed selectivity. The hafnium complex Hf(**20**)($O^iPr$)$_2$ in entry 8 shows similar selectivity to its zirconium analogue, however the reactivity is reduced, with high conversions reached in days, not hours.

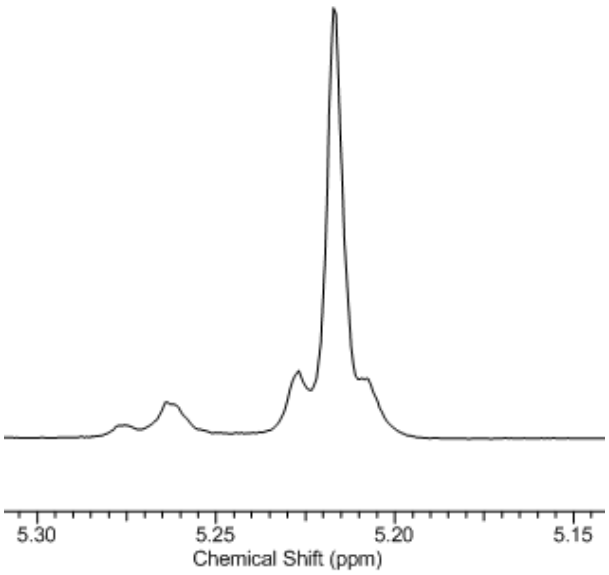


**Figure 4.54: Homonuclear decoupled $^1$H NMR spectrum of polylactide produced using 300:1 Zr(20)($O^iPr$)$_2$ under melt conditions, Table 4.11, entry 1**

Figure 4.54 shows the methine region of the $^1$H-$^1$H decoupled spectrum of the polymer from Table 4.11, entry 1. The isotacticity of the polymer is evident from the dominant *iii* tetrad resonance. The $P_r$ value was calculated from Equation 1.02 on page 14, in this case it is 0.29.

Table 4.12 shows solvent polymerisation data for the aluminium and group 4 salalen complexes in toluene. In the case of Al(**20**)Me one equivalent of benzyl alcohol is employed as the coinitiator.

**Table 4.12: Solution polymerisation data using salalen complexes in toluene. (1) determined by homonuclear decoupled NMR (2) determined by equation 2.2 (3) determined by GPC**

| Entry | Initiator | LA:I | BnOH | Conversion (%) | Time (day) | $P_r$[1] | $M_n$ Calc[2] ($gmol^{-1}$) | $M_n$[3] ($gmol^{-1}$) | PDI[3] | Temp (°C) |
|---|---|---|---|---|---|---|---|---|---|---|
| 1 | Al(**20**)Me | 100 | 1 | 73 | 4 | 0.39 | 10,627 | 13,350 | 1.04 | 80 |
| 2 | | 200 | 1 | 45 | 10 | 0.46 | 13,077 | 18,800 | 1.02 | 80 |
| 3 | | 400 | 1 | 78 | 28 | 0.45 | 45,067 | 33,750 | 1.07 | 80 |
| 4 | | 100 | 1 | 45 | 8 | 0.36 | 6,593 | 11,450 | 1.04 | 65 |
| 5 | Zr(**20**)($O^iPr$)$_2$ | 100 | 0 | 72 | 1 | 0.21 | 10,435 | 13,600 | 1.05 | 80 |
| 6 | | 200 | 0 | 100 | 2 | 0.25 | 28,880 | 29,050 | 1.13 | 80 |
| 7 | | 400 | 0 | 95 | 4 | 0.25 | 54,818 | 26,200 | 1.1 | 80 |
| 8 | | 800 | 0 | 94 | 7 | 0.29 | 108,423 | 67,650 | 1.08 | 80 |
| 9 | | 100 | 0 | 97 | 4 | 0.15 | 14,038 | 6,650 | 1.01 | 50 |
| 10 | Zr(**20**)($O^tBu$)$_2$ | 100 | 0 | 81 | 1 | 0.45 | 11,746 | 11,700 | 1.11 | 80 |
| 11 | | 100 | 0 | 23 | 6 | - | 3,388 | - | - | 50 |
| 12 | Hf(**20**)($O^iPr$)$_2$ | 100 | 0 | 92 | 2 | 0.23 | 13,317 | 8,500 | 1.02 | 80 |

The initiator Al(**20**)Me shows promising isoselectivity at 100:1 monomer to initiator ratio. This isotactic bias appears to diminish slightly at lower catalytic loadings. As expected, at a reduced temperature of 65°C (entry 4), the isoselectivity is enhanced, with a $P_r$ value of 0.36. However this requires much longer reaction times, with only 45 % conversion achieved after 8 days. This is not suitable for industrial production. Zr(**20**)($O^iPr$)$_2$ was trialled (entry 5) and showed increased isoselectivity ($P_r$ = 0.21) compared to the aluminium complex under the same conditions (entry 1). For this initiator, no benzyl alcohol was utilised as the alkoxide is already present in the complex. The temperature of this polymerisation was reduced to 50 °C and the reaction time increased to 4 days (entry 9), which yielded polymer of very high isotacticity, with a $P_r$ value of 0.15. Zr(**20**)($O^tBu$)$_2$ was trialled in the same manner, interestingly not showing the same selectivity as the isopropyl equivalent, with a $P_r$ value of 0.45 at 1 mol % loading (entry 10). At reduced temperature, the complex was less active (entry 11), only able to produce very low conversions of lactide even with prolonged reaction times, as such no molecular weight or tacticity data were obtained. This difficulty was not observed with Zr(**20**)($O^iPr$)$_2$, which managed

to achieve high conversion of lactide (entry 9), albeit with a longer reaction time, as would be expected. This difference may be related to the bulkier nature of the *tert*-butoxide groups hindering coordination of the lactide.

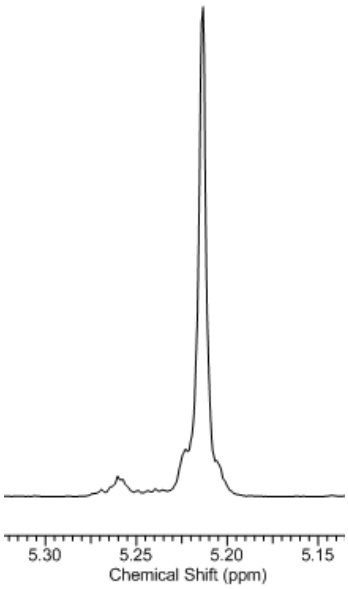


**Figure 4.55: Homonuclear decoupled $^{1}$H NMR spectrum of polylactide produced using 100:1 Zr(20)(O$^{i}$Pr)$_2$ at 50 °C in toluene, Table 4.12 entry 9**

Figure 4.55 shows the homonuclear decoupled NMR spectrum for the methine region of the polymer produced at 50 °C in toluene. The resonance corresponding to the iii triad is even more pronounced here than that of Figure 4.54, showing extremely high isotacticity, in this case a $P_r$ of 0.15. Analysis of the other resonances showed the iis, isi and sii tetrads to have roughly equal intensity, whereas the resonance corresponding to the sis tetrad is negligible. This indicates that PLA with the arrangement $(RRRR)_n(SSSS)_m$ has been produced, i.e. with consecutive blocks of D- and L- lactide.[19]

Figure 4.56 shows the MALDI-ToF spectrum of the polymer produced in entry 4 of Table 4.12, i.e. produced using Al(**20**)Me at 65 °C in solution. From visual inspection of this spectrum it can be seen that little transesterification has occurred during this polymerisation, the transesterified polymer being the smaller series of peaks. The repeat unit is 144 gmol$^{-1}$, as calculated from the largest peak, which confirms untransesterifed polymer. Figure 4.57 shows the theoretical and observed spectrum for the end group of the polymer. The observed data correlates for the expected spectrum of a benzyl alcohol end group. This confirms the coordination-insertion mechanism of the polymerisation, whereby the alkoxide of the initiator inserts into the lactide and becomes the end group of the polymer chain.

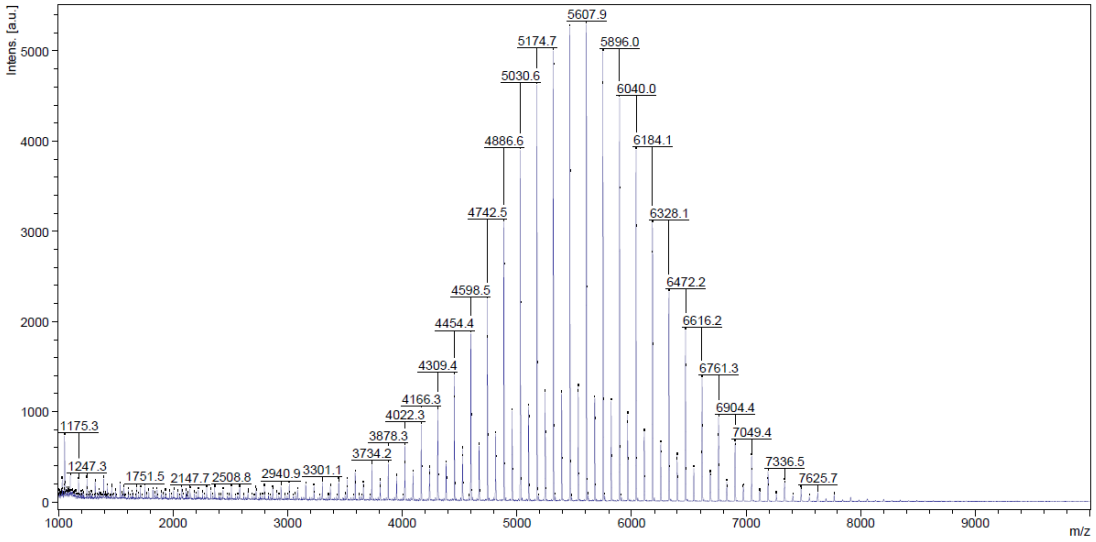


**Figure 4.56: MALDI-ToF spectrum of polymer from Table 4.12, entry 4**

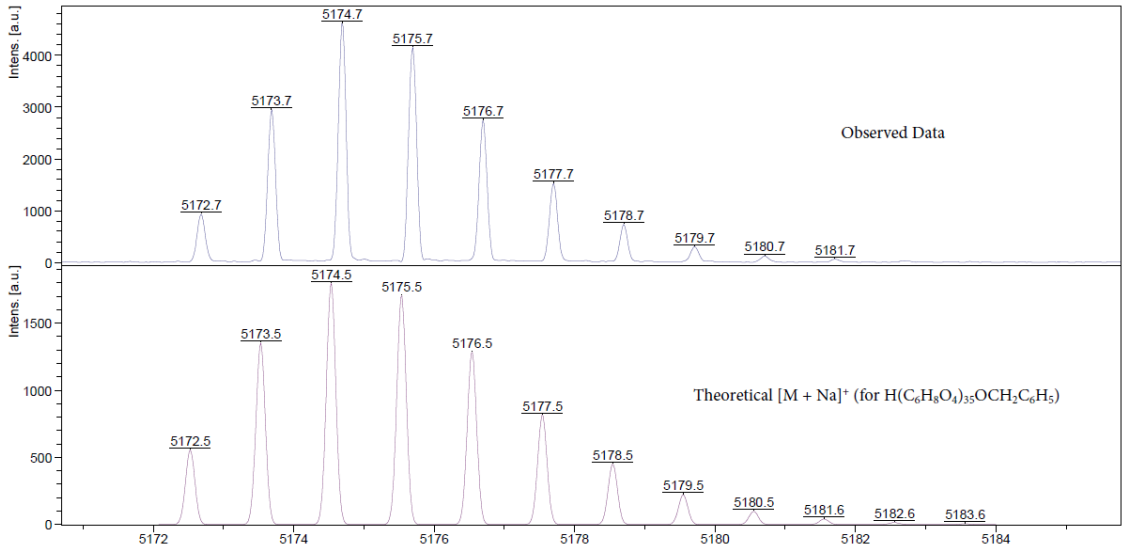


**Figure 4.57: End group analysis by MALDI-ToF spectrometry of polymer from Table 4.12, entry 4**

Figure 4.58 shows the MALDI-ToF spectrum for polymer produced using Zr(**20**)($O^iPr$)$_2$ at 50 °C in toluene. In this spectrum the repeat unit is 72 gmol$^{-1}$, indicating that transesterification reactions have occurred. In Figure 4.59, the similarity of the theoretical and observed spectra for isopropyl end group polymer confirms the presence of this end group. As such, it can be confirmed that this polymerisation occurs *via* the coordination-insertion mechanism.

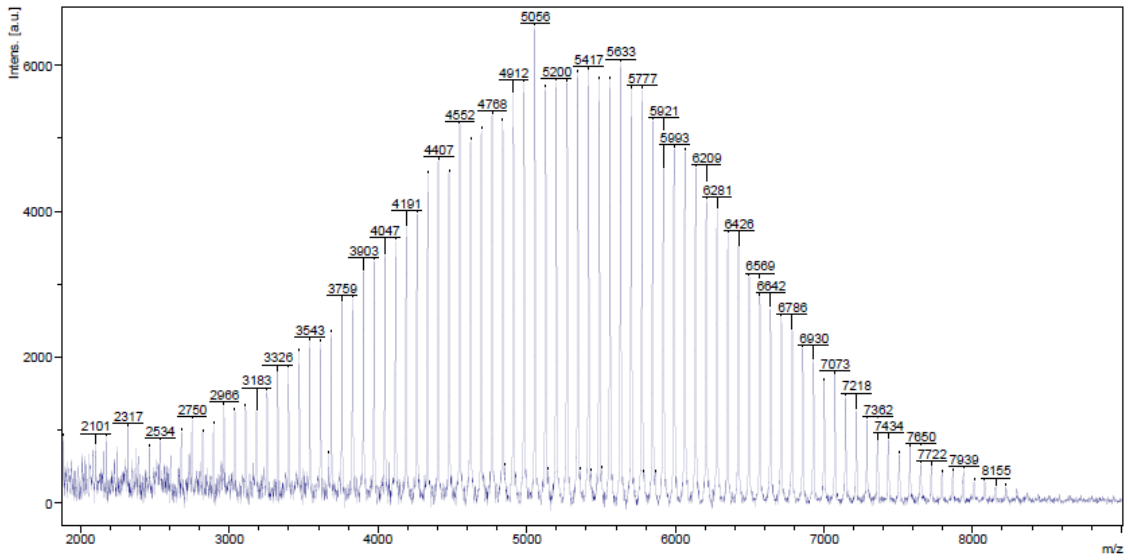


**Figure 4.58: MALDI-ToF spectrum of polymer from Table 4.12, entry 9**

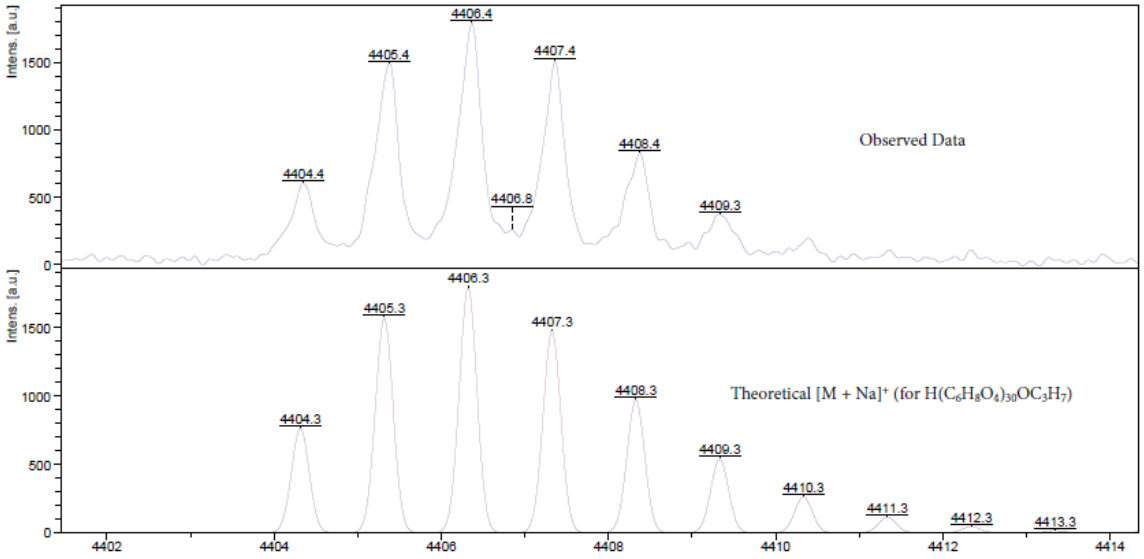


**Figure 4.59: End group analysis by MALDI-ToF spectrometry of polymer from Table 4.12, entry 9**

The DSC of the polymer from Table 4.12 entry 9 is shown in Figure 4.60. Two thermal events can be seen, the melting point and the crystallisation temperature. For this polymer, the melting point is 184°C and the crystallisation temperature is 100°C.

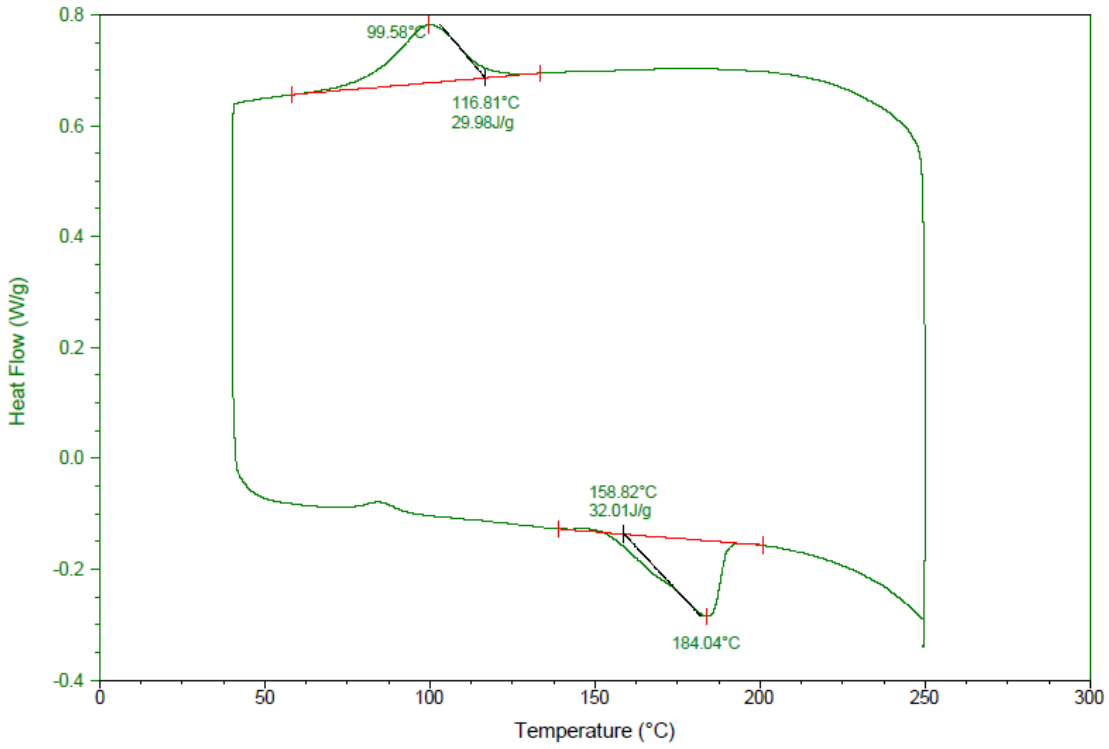


**Figure 4.60: DSC of isotactic polylactide produced using 100:1 Zr(20)($O^iPr$)$_2$ at 50 °C in toluene, from Table 4.12, entry 9**

Al(**21**)Me was trialled for the ring-opening polymerisation of *rac*-lactide at 80 °C in toluene with benzyl alcohol as a coinitiator, however it was found that this complex was not active for the polymerisation. This could be due to the excess steric bulk of both N-methyl groups preventing coordination of the lactide and thus no insertion into the monomer, or even preventing the benzyl alcohol from approaching the metal centre and forming the necessary alkoxide *in situ*.

## 4.5 Kinetic studies

The activities of initiators Zr(**20**)($O^iPr$)$_2$ and $Zr_2$(**20**)($O^iPr$)$_6$ were evaluated using solution NMR spectroscopic kinetic studies, carried out at 80 °C inside the spectrometer. Zr(**20**)($O^iPr$)$_2$ was used for this study in order to examine the reactivity with each isomer of lactide, in order to better understand the selectivity.

Figure 4.61 shows the first-order rate plot for L-, D- and *rac*-lactide in solution at 100:1 loading. It was found that the rate was considerably slower for *rac*-lactide whereas both D- and L- had similarly higher rates. This supports the polymerisation data where the complex was found to be isoselective. As the complex is achiral and shows no enhanced rate for either isomer over the other, the selectivity observed could be attributed to a chain end control mechanism.

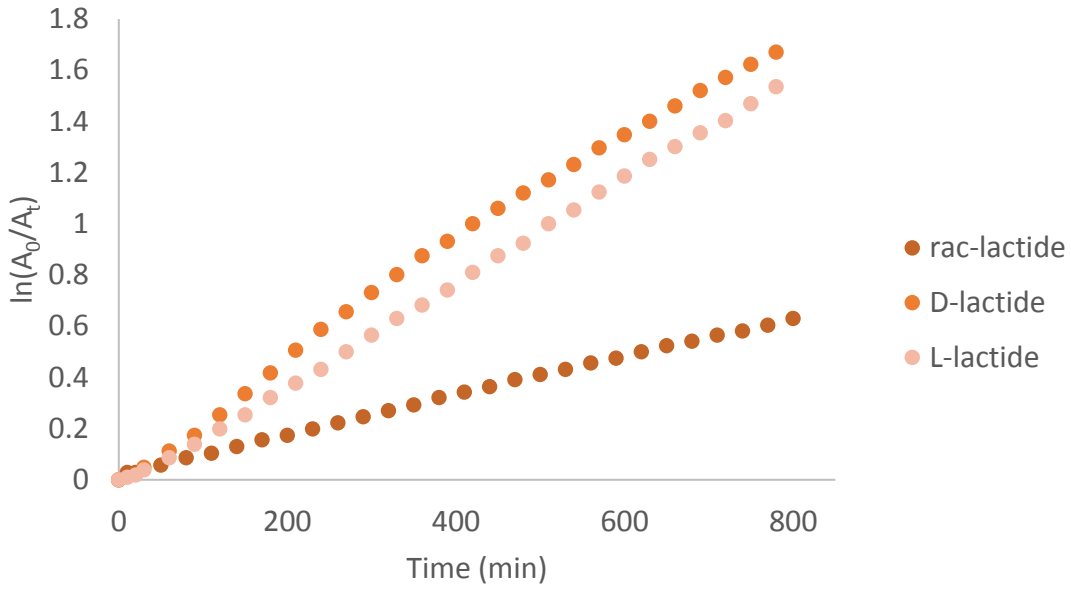


**Figure 4.61: First order rate plot in solution using Zr(20)($O^iPr$)$_2$ at 100:1 loading**

Table 4.13 shows the $k_{app}$ values as calculated from the graph in Figure 4.61. The rate constants for D- and L- lactide are over twice that of *rac*-lactide.

**Table 4.13: $k_{app}$ for the initation of each monomer of lactide using Zr(20)($O^iPr$)$_2$**

| | *rac*-lactide | L-lactide | D-lactide |
|---|---|---|---|
| $k_{app}$ (x $10^{-3}$ $min^{-1}$) | 0.8 ± 0.005 | 2.0 ± 0.01 | 2.2 ± 0.03 |

Figure 4.62 shows the first order rate plot of $Zr_2$(**13**)($O^iPr$)$_6$ at 200:1 loading. This catalyst loading was used under the assumption that the complex undergoes a two metal centre initiation, as such the initiator loading had to be halved in order to get the correct concentration of metal

centres for comparison. The $k_{app}$ from this graph is 1.1 ± 0.03 x$10^{-3}$ $min^{-1}$, indicating that this complex is slightly faster for *rac*-lactide than the mononuclear zirconium salalen complex.

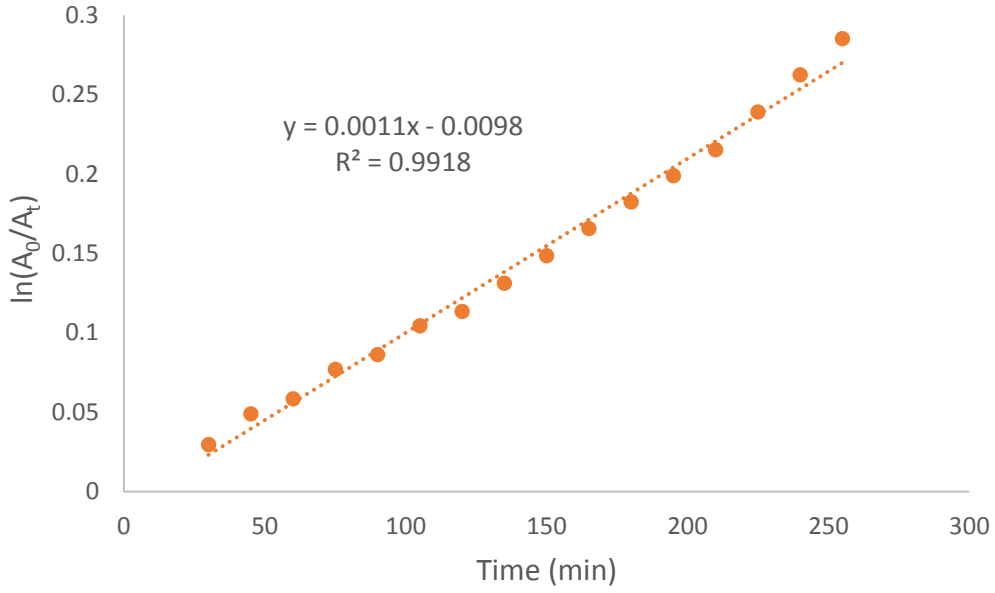


**Figure 4.62: First order rate plot in solution using $Zr_2$(13)($O^iPr$)$_6$ at 200:1 loading**

Figure 4.63 shows a plot of increasing conversion and molecular weight with time using Zr(**20**)($O^iPr$)$_2$, also, marked on each data point is the $P_r$ at this conversion. With time, the $P_r$ values decrease, this is understandable as with increasing chain length, the frequency of iii tetrads will begin to increase. The molecular weight of the polymer increases steadily with the conversion, showing that this is a controlled reaction in the melt, where $k_{init} > k_{prop}$.

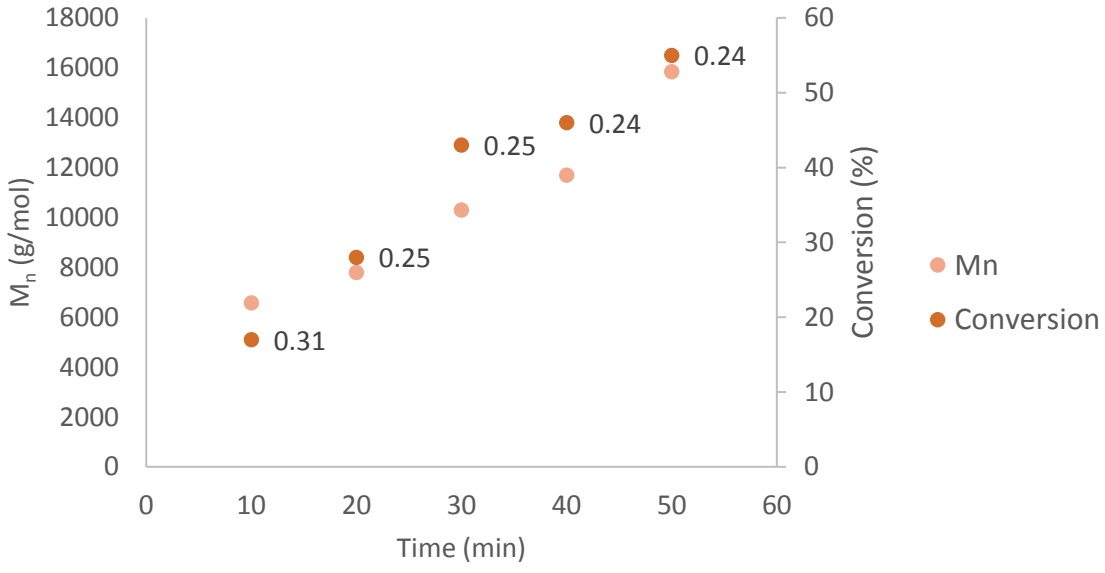


**Figure 4.63: Conversion and molecular weight with time using Zr(20)($O^iPr$)$_2$ as an initiator in the melt. $P_r$ values at each conversion are shown next to data point.**

## 4.6 Copolymerisation studies

### 4.6.1 $^{1}$H NMR spectroscopic analysis of copolymer

After exhibiting interesting stereoselectivity for the ring-opening polymerisation of *rac*-lactide, Zr(**20**)($O^{i}Pr$)$_2$ was utilised for copolymerisation reactions with ε-caprolactone. More discussion about this copolymerisation type can be found in chapter 2, including the equations used to calculate block length and copolymer randomness. Figure 4.64 shows the proton NMR spectrum of poly-lactide-co-caprolactone produced using a 50:50 feed of *rac*-lactide and ε-caprolactone.

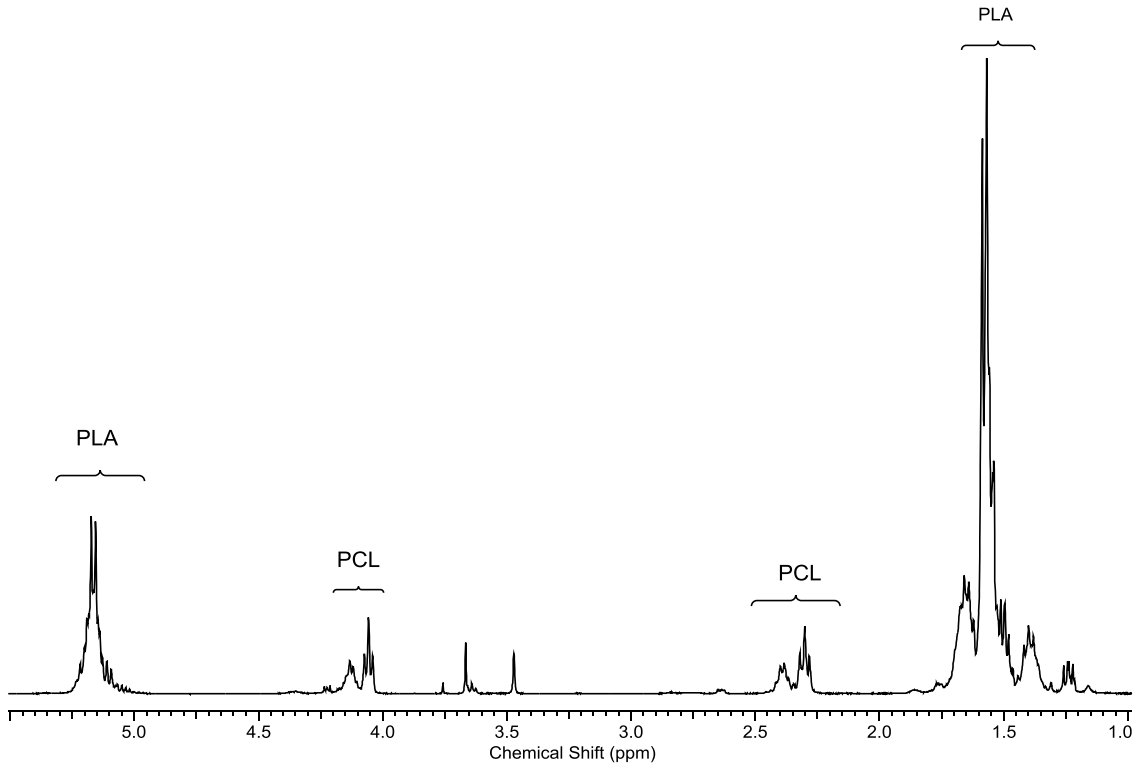


**Figure 4.64: $^{1}$H NMR spectrum of poly(lactide-co-caprolactone) produced in solution using Zr(20)($O^{i}Pr$)$_2$ with a 50:50 monomer feed ratio**

Table 4.14 shows the copolymerisation data at varying feed ratios and catalyst loadings. The ninth and tenth column show the percentage of polylactide and polycaprolactone in the final polymer respectively. The last four columns on the top-right break down the ratio of different linkages in the polymer, either homolinkages or heterolinkages. Below, on the second part of the table, are the average block lengths for polylactide and polycaprolactone in the polymer, along with the expected block lengths for a random polymer. In the final column is the randomness factor (R), as calculated by equation 2.6 on page 66.

**Table 4.14: Copolymerisation data for the ROP of *rac*-lactide and ε-caprolactone at 80 °C in toluene. Relative polymeric fractions determined by $^{1}$H NMR spectroscopy, average block lengths (L) calculated by Equation 2.5, randomness factor (R) calculated by Equation 2.6**

| Entry | M:I | LA:CL | Time (day) | Conv LA (%) | Conv CL (%) | $M_n$ calc ($gmol^{-1}$) | $M_n$ ($gmol^{-1}$) | PDI | [PLA] | [PCL] | [LA-LA] | [CL-CL] | [LA-CL] | [CL-LA] |
|---|---|---|---|---|---|---|---|---|---|---|---|---|---|---|
| 1 | 100 | 50:50 | 1 | 88 | 43 | 8,847 | 6,400 | 1.04 | 0.80 | 0.20 | 0.72 | 0.11 | 0.09 | 0.09 |
| 2 | 100 | 50:50 | 2 | 95 | 63 | 10,491 | 5,550 | 1.03 | 0.73 | 0.27 | 0.61 | 0.15 | 0.12 | 0.12 |
| 3 | 100 | 75:25 | 2 | 97 | 61 | 10,521 | 6,650 | 1.06 | 0.90 | 0.10 | 0.84 | 0.04 | 0.06 | 0.06 |
| 4 | 100 | 25:75 | 2 | 94 | 69 | 10,761 | 6,350 | 1.09 | 0.36 | 0.64 | 0.22 | 0.48 | 0.15 | 0.15 |
| 5 | 100 | 90:10 | 2 | 100 | 83 | 11,991 | 9,400 | 1.04 | 0.94 | 0.06 | 0.90 | 0.02 | 0.04 | 0.04 |
| 6 | 100 | 10:90 | 2 | 100 | 99 | 12,903 | 1,900 | 1.21 | 0.12 | 0.88 | 0.01 | 0.79 | 0.11 | 0.11 |
| 7 | 200 | 50:50 | 4 | 96 | 45 | 19,014 | 11,350 | 1.05 | 0.72 | 0.28 | 0.60 | 0.15 | 0.12 | 0.12 |

| Cont. from entry | L(LA) | L(CL) | L(LA)random | L(CL)random | R |
|---|---|---|---|---|---|
| 1 | 8.9 | 2.2 | 5.0 | 1.3 | 0.28 |
| 2 | 6.1 | 2.3 | 3.7 | 1.4 | 0.30 |
| 3 | 15.0 | 1.7 | 10.0 | 1.1 | 0.33 |
| 4 | 2.4 | 4.3 | 1.6 | 2.8 | 0.33 |
| 5 | 23.5 | 1.5 | 16.7 | 1.1 | 0.35 |
| 6 | 1.1 | 8.0 | 1.1 | 8.3 | 0.52 |
| 7 | 6.0 | 2.3 | 3.6 | 1.4 | 0.30 |

Figure 4.65 shows the lactide block length with increasing lactide feed, as calculated by Equation 2.4 (page 66). The theoretical value is calculated using Equation 2.5 on page 62. This value assumes a random copolymerisation, an observed block length lower than this value would indicate an alternating copolymerisation and an observed block length higher than this value would indicate a block copolymerisation.[20] With increasing percentage lactide in the feed, the average lactide block length steadily gets larger than the theoretical value. The caprolactone block lengths (shown in Figure 4.66) are mostly longer than the theoretical, but less noticeably so. This is partially due to lower conversions of caprolactone in each polymerisation.

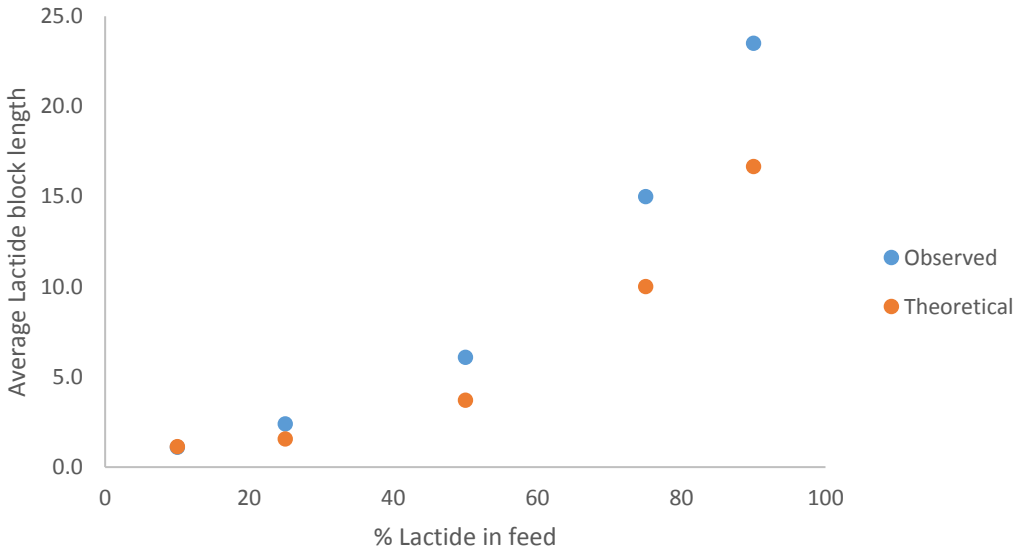


**Figure 4.65: Theoretical vs observed lactide block length with increasing lactide feed**

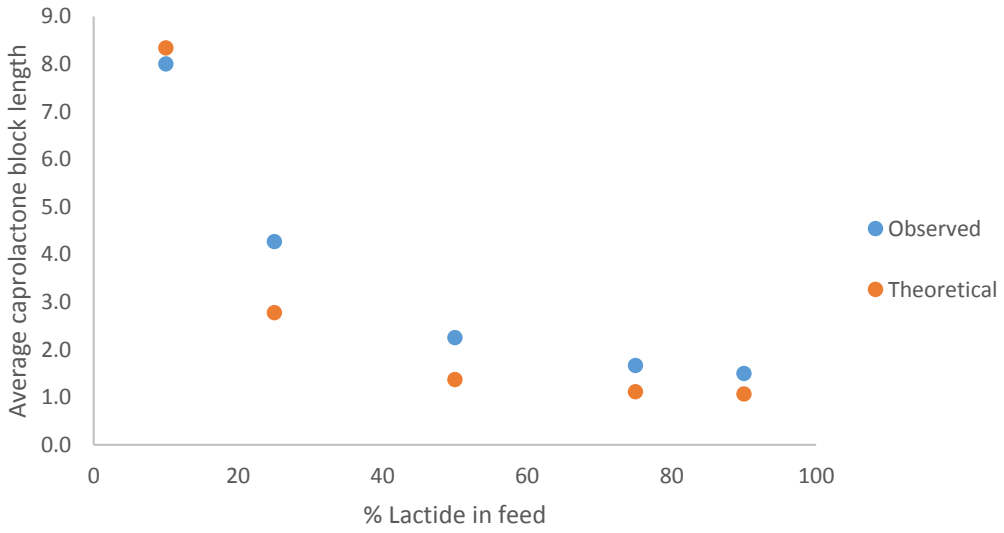


**Figure 4.66: Theoretical vs observed caprolactone block length with increasing lactide feed**

Another method of quantifying the blocky or random nature of the copolymer is using the randomness factor, R. For a truly random copolymer, R = 0.5, for a block copolymer R < 0.5 and for an alternating copolymer R > 0.5. In almost every polymer in Table 4.14, R is lower than 0.5, indicating a 'blocky' copolymer. This supports the conclusions from the block length analysis.

Figure 4.67 shows the initiation and propagation steps of the copolymerisation using Zr(**20**)O$^{i}$Pr. Lactide is preferentially consumed first, and the resulting polymer is blocky in nature. This suggests a chain-end control mechanism, as was observed with the polymerisation of *rac*-lactide. With insertion of one monomer, subsequent insertion of the same monomer is preferred.

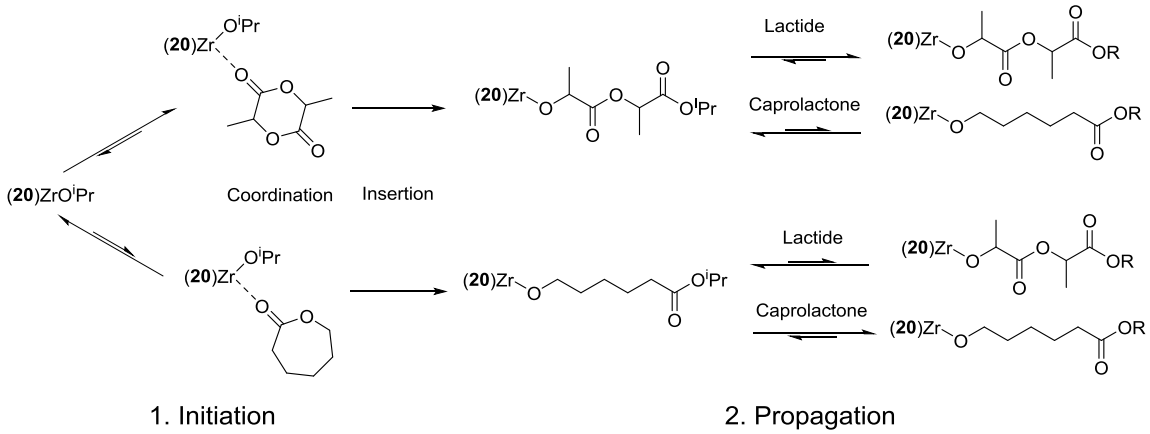


**Figure 4.67: Diagram of copolymer initiation and propagation**

As Zr(**20**)(O$^{i}$Pr)$_2$ is more active for a single monomer of lactide than for *rac*-lactide, the copolymerisations were trialled using only L-lactide with caprolactone. Table 4.15 shows the copolymerisation data. For each entry the loading was 100:1 monomer to initiator with a reaction time was 4 days, and the conversion of lactide reached 100 %.

When using L-lactide as the comonomer, the 'blocky' nature of the copolymer increases. This can be rationalised for Zr(**20**)(O$^{i}$Pr)$_2$ as this initiator is isoselective, so insertion of L-lactide into a growing L-lactide chain is preferred. This blockiness can be seen in the average block lengths and the randomness factors. For example, a copolymer produced using a 50:50 feed of monomers has an average lactide block length of 6 (which would be 2.5 for random copolymer) and an average caprolactone block length of 4 (which would be 1.7 if random). The randomness factor for this copolymer is 0.21, which is lower than the equivalent copolymer using *rac*-lactide (Table 4.14, entry 2) which has an R factor of 0.30.

**Table 4.15: Copolymerisation data for the ROP of L-lactide and caprolactone using Zr(20)($O^iPr$)$_2$ in toluene at 80 °C. Relative polymeric fractions determined by $^1$H NMR spectroscopy, average block lengths (L) calculated by Equation 2.5, randomness factor (R) calculated by Equation 2.6**

| LA:CL | Conv CL (%) | $M_n$ calc ($gmol^{-1}$) | $M_n$ ($gmol^{-1}$) | PDI | [PLA] | [PCL] | [LA-LA] | [CL-CL] | [LA-CL] | [CL-LA] |
|---|---|---|---|---|---|---|---|---|---|---|
| 50:50 | 83 | 11,991 | 17,550 | 1.08 | 0.60 | 0.40 | 0.49 | 0.31 | 0.10 | 0.10 |
| 75:25 | 99 | 12,903 | 6,100 | 1.18 | 0.83 | 0.17 | 0.77 | 0.11 | 0.06 | 0.06 |
| 25:75 | 99 | 12,903 | 1,750 | 2.40 | 0.24 | 0.76 | 0.14 | 0.66 | 0.10 | 0.10 |

| L(LA) | L(CL) | L(LA)random | L(CL)random | R |
|---|---|---|---|---|
| 6 | 4 | 2.5 | 1.7 | 0.21 |
| 13.8 | 2.8 | 5.9 | 1.2 | 0.21 |
| 2.4 | 7.6 | 1.3 | 4.2 | 0.27 |

Figure 4.68 shows the DSC for PLLA-co-PCL produced using a 50:50 monomer feed (first entry, Table 4.15). The melting point is 141 °C and the crystallisation temperature at 88 °C.

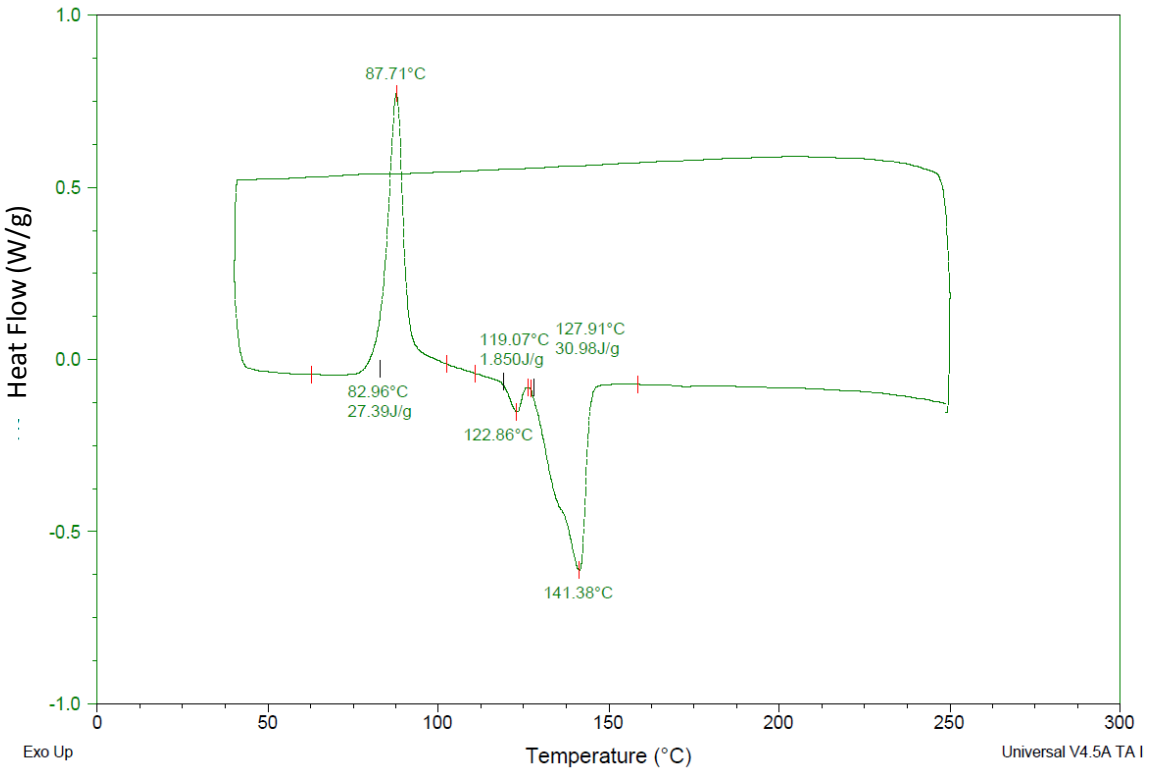


**Figure 4.68: DSC of PLLA-co-PCL produced using Zr(19)($O^iPr$)$_2$ at 50:50 monomer feed**

## 4.6.2 Carbon NMR spectroscopic analysis of copolymers

As explained in Chapter 2, $^{13}C\{^{1}H\}$ NMR can also be used to probe the nature of the copolymer. For example, analysis of the carbonyl region in the spectrum can reveal transesterification that has occurred during the copolymerisation, by appearance of a half lactide carbonyl resonance.

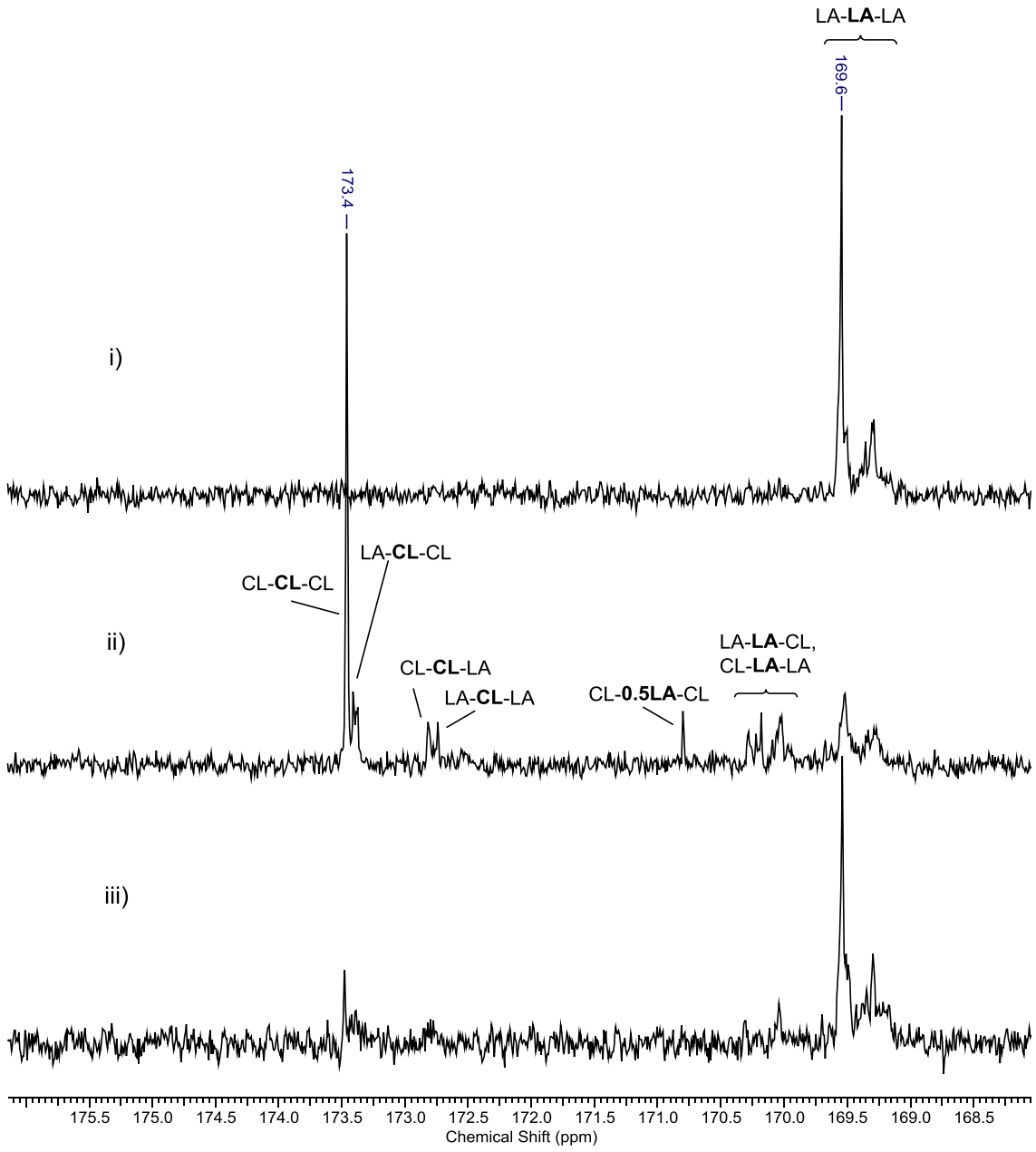


**Figure 4.69: $^{13}C\{^{1}H\}$ NMR spectrum of copolymer synthesised with 14Zr($O^{i}Pr$)$_2$ using i) 75:25 LA:CL monomer feed ii) 25:75 LA:CL monomer feed and iii) 50:50 LA:CL monomer feed. Resonances assigned according to literature[21, 22]**

Figure 4.69 shows the carbonyl carbon region of the $^{13}C\{^{1}H\}$ NMR spectra for the copolymers produced at 100:1 monomer to catalyst loading, at different monomer feed ratios. For the 75:25 feed of lactide to caprolactone (Table 4.14, entry 3), the dominant resonance in the spectrum is

at 169.6 ppm, the LA-**LA**-LA resonance. This is expected as the percentage of lactide-lactide linkages in the final polymer was 84 %. The CL-CL linkages make up only 4 % in the polymer and as such the CL-**CL**-CL carbonyl resonance is too weak to be observed in this spectrum. At a 25:75 lactide to caprolactone feed ratio (Table 4.14, entry 4) the dominant resonance is the CL-**CL**-CL carbonyl at 173.4 ppm, which is expected as the CL-CL linkages make up 48 % of the polymer. The resonance just below 171 ppm in this spectrum is for CL-**0.5LA**-CL, which indicates that the polymer is transesterified, due to the presence of half a lactide unit. Finally, for the 50:50 feed ratio (Table 4.14, entry 2), the CL-**CL**-CL carbonyl resonance is present but far weaker than the LA-**LA**-LA resonance. This is due not only to the lower ratio of caprolactone (27 %) in the final polymer but also that each lactide unit incorporates two carbonyl carbons, meaning the resonances will be twice as large for the lactide carbonyls.

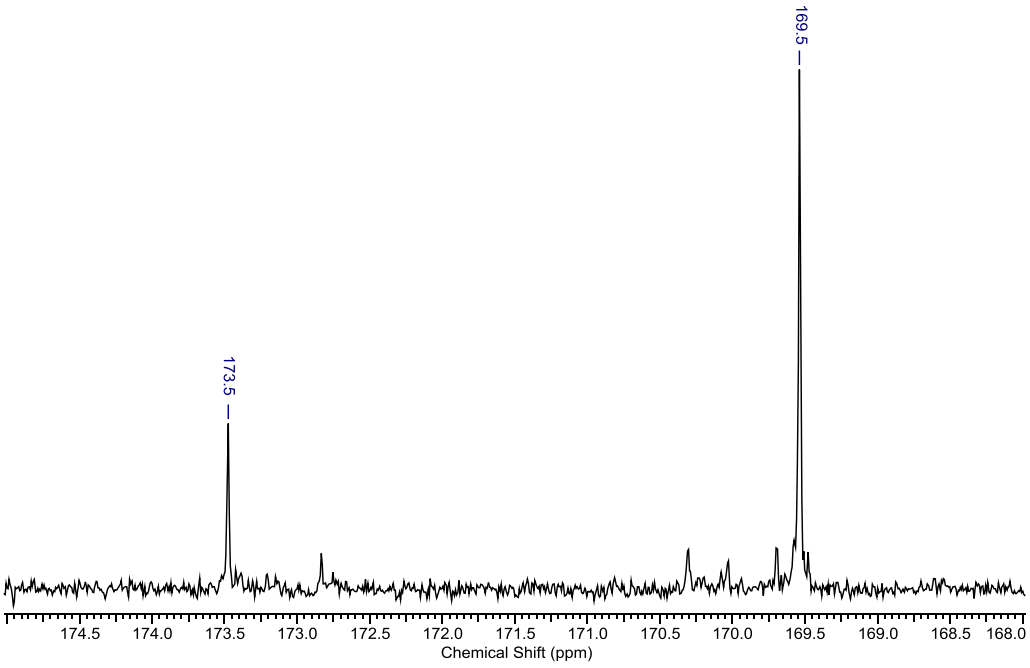


**Figure 4.70: Carbonyl region of $^{13}C\{^{1}H\}$ NMR spectrum**

Figure 4.70 shows the carbonyl region of the copolymer produced using a 50:50 mix of L-lactide and caprolactone (Table 4.15). This copolymer was more blocky than its analogue with *rac*-lactide and this is reflected in the $^{13}C\{^{1}H\}$ NMR, which has two intense resonances for the predominant CL-CL-CL (173.5 ppm) and LA-LA-LA (169.5 ppm) triads. No transesterification resonances are visible in this spectrum.

## 4.7 Conclusions

In this chapter, the relationship between the salen, salan and salalen metal complex structures with phenyl backbones were examined. It was found that the salen ligand **13**$H_2$ had an open but rigid structure, allowing two metal centres to be present in the complex in the case of aluminium, zirconium and hafnium. It is thought that the ligand 'opens' in order to steric clashes between the bulky *tert*-butyl substituent groups on the phenoxy moieties of **13**H, which provides the space for two metal centres to bind. However when zirconium *tert*-butoxide was employed, a monomeric species Zr(**13**)($O^tBu$)$_2$ was formed. This due to the bulkier *tert*-butoxide groups on the zirconium. In the case of the analogous salalen ligand **20**$H_2$, no dimeric species were observed on complexation with any of the metals used (aluminium, zirconium, hafnium) as the ligand was able to wrap around the single metal centre. In addition to these, some highly coloured complexes, $Al_2$(**16**)$_2Me_2$ and $Al_2$(**17**)$_2Me_2$, were synthesised using the salalen ligand precursors. Finally, an aluminium salan complex Al(**21**)Me was formed, which was mononuclear. The relative flexibility in the methylene bridge compared to its salen analogue allows for wrapping around a single metal centre.

When the salalen precursor complexes $Al_2$(**16**)$_2Me_2$, $Al_2$(**17**)$_2Me_2$ and Al(**19**)$Me_2$ were employed for the ROP of *rac*-lactide, no selectivity was observed, with $P_r$ values ranging 0.42-0.55. For $Al_2$(**16**)$_2Me_2$, two peaks were observed on the GPC trace, which is attributed to the presence of multiple initiating species in solution. For the melt polymerisation of lactide, the salen complexes $Zr_2$(**13**)($O^iPr$)$_6$ and $Hf_2$(**13**)($O^iPr$)$_6$ showed uncontrolled behaviour, with no stereoselectivity, poor molecular weight control and large PDI values, 1.22-2.04. The monomeric species Zr(**13**)($O^tBu$)$_2$ showed better molecular weight control, but still no stereoselectivity. The poor predictability of the dinuclear complexes is due to the high number of initiating groups per molecule. The molecular weight control of these dinuclear complexes was not much improved in solution at 80 °C, and still no stereoselectivity was observed. However, the dinuclear aluminium complex $Al_2$(**13**)$Me_4$ showed much better molecular weight control (PDI = 1.02-1.27) than its group 4 analogues, albeit with no stereoselectivity again.

For the aluminium salalen complex, Al(**20**)Me, at 100:1 loading in toluene at 80 °C, isoselectivity was observed ($P_r$ = 0.39). On reducing the temperature to 65 °C, the isoselectivity was enhanced, with $P_r$ = 0.36. However, long reaction times were required to achieve high conversions. The zirconium analogue of this salalen complex, Zr(**20**)($O^iPr$)$_2$, was found to produce isotactic PLA ($P_r$ = 0.21) to high conversion within one day in solution. Reduction of the solution temperature to 50 °C yielded highly isotactic PLA, with a $P_r$ value of 0.15. To put this into context, the analogous

zirconium salalen complex with an ethylene backbone produced polylactide with a $P_r$ value of 0.57 under the same conditions.[18] This indicates that the phenylene backbone of the initiator plays a vital role in the selectivity.

For the solution copolymerisation of *rac*-lactide and ε-caprolactone using Zr(**20**)($O^iPr$)$_2$, copolymer of a 'blocky' nature was produced. The blockiness of the copolymer was further enhanced when utilising L-lactide instead of *rac*-lactide as the comonomer.

## 4.8 Future work

In this project the salen and salalen ligands featured only *tert*-butyl phenoxy substituents, as the point of interest was the effect of the phenyl backbone on polymerisation. Future work could be carried out to investigate the effect of different substituents (examples in Figure 4.71) on the stereoselectivity and activity of the salalen complexes. It would also be interesting to further investigate the effect of ligand backbone, an example shown on the right in Figure 4.71.

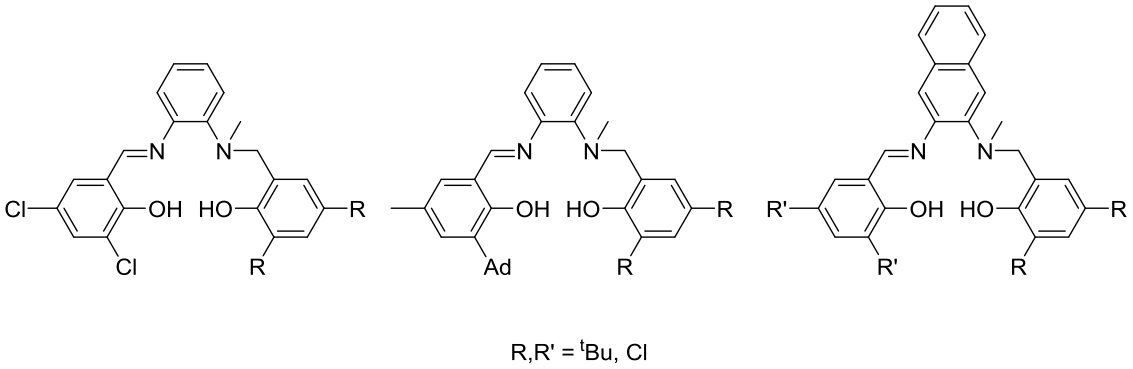


**Figure 4.71: Possible ligand variations for the salalen ligand**

The complexes $Zr_2$(**13**)$(O^iPr)_6$ and $Hf_2$(**13**)$(O^iPr)_6$ showed interesting results for the ring-opening polymerisation of *rac*-lactide both in the melt and in solution. From the polymerisation data obtained in this chapter, it was not clear as to whether the complex initiated one or two polymer chains per molecule. As this was not the primary focus of this chapter, there is scope for further studies on this initiator. Future work on this compound would include kinetic studies into the order of the reaction, in order to better understand the mechanism of polymerisation.

The initiator Al(**21**)Me was not active for the ROP of *rac*-lactide when using benzyl alcohol as a coinitiator. Future work would include trialling this initiator with less bulky coinitiators (e.g. isopropyl alcohol) or alternatively synthesising an aluminium alkoxide complex Al(**21**)OBn, which could be used under melt conditions, to provide a comparison of the polymerisation data of salan complexes to the salen and salalen complexes.

## 4.9 References


1. P. McKeown, M. G. Davidson, G. Kociok-Kohn and M. D. Jones, *Chem. Commun.*, 2016, **52**, 10431-10434.
2. E. L. Whitelaw, G. Loraine, M. F. Mahon and M. D. Jones, *Dalton Trans.*, 2011, **40**, 11469-11473.
3. S. L. Hancock, M. F. Mahon and M. D. Jones, *Dalton Trans.*, 2013, **42**, 9279-9285.
4. A. Pilone, N. De Maio, K. Press, V. Venditto, D. Pappalardo, M. Mazzeo, C. Pellecchia, M. Kol and M. Lamberti, *Dalton Trans.*, 2015, **44**, 2157-2165.
5. A. Pilone, K. Press, I. Goldberg, M. Kol, M. Mazzeo and M. Lamberti, *J. Am. Chem. Soc.*, 2014, **136**, 2940-2943.
6. A. Coletti, P. Galloni, A. Sartorel, V. Conte and B. Floris, *Catal. Today*, 2012, **192**, 44-55.
7. M. Zintl, F. Molnar, T. Urban, V. Bernhart, P. Preishuber-Pfluegl and B. Rieger, *Angew. Chem., Int. Ed.*, 2008, **47**, 3458-3460.
8. Y. Wang, Y. Qin, X. Wang and F. Wang, *Catal. Sci. Technol.*, 2014, **4**, 3964-3972.
9. B. Li, J. Lan, D. Wu and J. You, *Angew. Chem., Int. Ed.*, 2015, **54**, 14008-14012.
10. P. T. Anastas and J. C. Warner, *Green Chemistry: Theory and Practice*, Oxford University Press, New York, 1998.
11. S. Gendler, A. L. Zelikoff, J. Kopilov, I. Goldberg and M. Kol, *J. Am. Chem. Soc.*, 2008, **130**, 2144-2145.
12. H. Du, X. Pang, H. Yu, X. Zhuang, X. Chen, D. Cui, X. Wang and X. Jing, *Macromolecules*, 2007, **40**, 1904-1913.
13. A. L. Zelikoff, J. Kopilov, I. Goldberg, G. W. Coates and M. Kol, *Chem. Commun.*, 2009, 6804-6806.
14. T. K. Saha, V. Ramkumar and D. Chakraborty, *Inorg. Chem.*, 2011, **50**, 2720-2722.
15. M. A. Van Aelstyn, T. S. Keizer, D. L. Klopotek, S. Liu, M.-A. Munoz-Hernandez, P. Wei and D. A. Atwood, *Organometallics*, 2000, **19**, 1796-1801.
16. A. Maisse-François, L. Azor, A.-L. Schmitt, A. Coquel, L. Brelot, R. Welter, S. Bellemin-Laponnaz and S. Dagorne, *J. Organomet. Chem.*, 2012, **696**, 4248-4256.
17. T. R. Forder and M. D. Jones, *New J. Chem.*, 2015, **39**, 1974-1978.
18. E. L. Whitelaw, M. D. Jones and M. F. Mahon, *Inorg. Chem.*, 2010, **49**, 7176-7181.
19. T. M. Ovitt and G. W. Coates, *J. Polym. Sci., Part A: Polym. Chem.*, 2000, **38**, 4686-4692.
20. M. Tessier and A. Fradet, in *e-Polymers*, 2003, vol. 3, p. 391.
21. P. Vanhoorne, P. Dubois, R. Jerome and P. Teyssie, *Macromolecules*, 1992, **25**, 37-44.
22. N. Nomura, A. Akita, R. Ishii and M. Mizuno, *J. Am. Chem. Soc.*, 2010, **132**, 1750-1751.

# 5. Experimental

## 5.1 General considerations

All metal complex syntheses and characterisations were carried out using Schlenk and glove box techniques under a dry, inert atmosphere of argon. Dry solvents were obtained under an atmosphere of argon using a solvent purification system (SPS). All compounds were purchased from Sigma Aldrich and used as received unless otherwise stated.

$^{1}H$ and $^{13}C\{^{1}H\}$ NMR spectra were obtained using a Bruker 300 MHz or 400 MHz instrument. Samples were dissolved in $CDCl_3$, $C_6D_6$, $d_8$-toluene or $d_6$-DMSO. DOSY NMR experiments were run on a Bruker 500 MHz instrument by Tim Woodman or John Lowe.

Electrospray ionisation (ESI) Mass spectrometry was carried out using a MicroToF electrospray quadrupole time-of-flight mass spectrometer, with the sample dissolved in analytical grade methanol or acetonitrile at approximately 1 $\mu gmL^{-1}$ concentration. Spectra were recorded in positive loop injection mode. MALDI-ToF spectrometry was carried out by the EPSRC National Mass Spectrometry Service Centre in Swansea, or by either Tom Forder, Andy Russell or Paul McKeown at the University of Bath. MALDI-ToF mass spectra at the University of Bath were determined on a Bruker Autoflex speed instrument using *trans*-2-[3-(4-tert-butylphenyl)-2-methyl-2-propenylidene]malononitrile (DCTB) as the matrix and ionised using NaOAc.

For Chapters 2 and 3, GPC analyses were carried out on a Polymer Laboratories PL-GPC 50 integrated system using a 5 µm 300 x 7.5 mm column at 35 °C at a flow rate of 1 $mLmin^{-1}$. Samples were dissolved in tetrahydrofuran (THF) at a concentration of 2 $mgmL^{-1}$. The refractive index of the polymers were referenced to 11 polystyrene standards of narrow molecular weight, ranging from $M_w$ 615-568000 Da. For Chapter 4, GPC analyses were carried out on an Agilent 1260 GPC/SEC MDS using 2 PL MixedD 300 x 7.5 mm columns with a guard column of PL MixedD 50 x 7.5 mm. The mobile phase was GPC grade THF flowing at 1 $mLmin^{-1}$ at 35 °C. The polymers in this chapter were analysed by triple detection, using a differential refractive index detector, a viscometer detector and a dual angle light scattering detector.

All elemental analyses (carbon, hydrogen, nitrogen), including air sensitive samples, were carried out by Stephen Boyer at London Metropolitan University.

X-Ray Diffraction data was collected by Drs Matthew Jones, Mary Mahon or Gabriele Kociok-Kohn on a Nonius Kappa diffractometer at 150 K using Mo-Kα radiation (λ = 0.71073 Å) or a SuperNova, EOS detector diffractometer using radiation CuKα (λ = 1.54184 Å) or Mo-Kα (λ =

0.71073 Å). All structures were solved by direct methods and refined on all $F^2$ data using the SHELXL-97 02014 suite of programs, with hydrogen atoms included in idealised positions and refined using the riding model.

DSC analyses were recorded on a TA Instruments DSC Q20. The sample was heated at 40 °C for 1 minute, heating ramped to 250 °C at 10 °C $min^{-1}$, held at 250 °C for 1 minute, cooled to 40 °C at 10 °C $min^{-1}$, held at 40 °C for 1 minute then finally heated to 250 °C at 10 °C $min^{-1}$.

## 5.2 Polymerisation techniques

*Rac*-Lactide was purified by recrystallisation in dry toluene obtained from the SPS then sublimed twice prior to use. ε-caprolactone was distilled over $CaH_2$. Both monomers were stored in the glovebox under argon prior to use. Polymers were characterised as follows: conversion calculated from relative integration of monomer and polymer resonances in $^1H$ NMR spectrum of crude polymer mixture, $M_n$ and PDI determined by GPC, where possible tacticity determined by homonuclear decoupled $^1H$ NMR spectroscopy in $CDCl_3$ with the sample concentration approx. 10 $mgmL^{-1}$.

### Solvent polymerisation

1.0 g lactide was added to an ampoule with a Young's cap in 10 mL solvent, either toluene, dichloromethane (DCM) or THF, with the appropriate amount of initiator and 1 equivalent benzyl alcohol (unless otherwise stated) per metal centre in the initiator if required. Once complete, methanol (1-2 drops) was added to quench the reaction. The solvent was removed *in vacuo* and a crude NMR sample taken to determine conversion. The polymer was then washed with methanol (3 x 10 mL) to remove any remaining lactide and dried under high vacuum before analysis *via* NMR spectroscopy and GPC.

### Solvent-free polymerisation

1.0 g of *rac*-lactide was added to an ampoule with a Young's cap, typically at a 300:1 ratio of monomer to initiator. The ampoule was heated to 130 °C to melt the *rac*-lactide (or 100 °C if only L- or D- lactide used). Once complete (as determined by cessation of stirring by the stirrer bar), the polymer was dissolved in 10 mL DCM and a couple of drops methanol added to quench the reaction. Solvent was removed *in vacuo* and a crude NMR sample taken to determine conversion. The polymer was then washed with methanol (3 x 10 mL) to remove any remaining monomer and dried under high vacuum before analysis *via* NMR spectroscopy and GPC.

### Polymerisation of caprolactone

0.77 mL caprolactone was added to an ampoule with a Young's cap in 10 mL toluene with the appropriate amount of initiator and 1 equivalent benzyl alcohol (unless otherwise stated) per metal centre in the initiator. Once complete, methanol (1-2 drops) was added to quench the reaction. The solvent was removed *in vacuo* and a crude NMR sample taken to determine conversion. The polymer was then washed with methanol (3 x 10 mL) to remove any remaining lactide and dried under high vacuum before analysis *via* NMR spectroscopy and GPC.

### Copolymerisation of lactide and caprolactone

An ampoule was charged with appropriate amounts of each monomer and initiator. Benzyl alcohol was added as required (e.g. 7.2 µL, 1 equivalent at 100:1 loading) and the mixture dissolved in toluene (10 mL) and heated to 80 °C. Once complete, methanol (1-2 drops) was added to quench the reaction. The solvent was removed *in vacuo* and a crude NMR sample taken to determine conversion of each monomer. The polymer was then washed with methanol (3 x 10 mL) to remove any remaining lactide and dried under high vacuum before analysis *via* NMR spectroscopy and GPC.

### Kinetic study of polymerisation

A Young's NMR tube was charged with 50 mg of *rac*-lactide and dissolved in 0.5 mL $d_8$ toluene. A stock solution of initiator dissolved in $d_8$ toluene (and benzyl alcohol if required) was prepared. Typically, this would be the required mass of initiator multiplied by 10 and dissolved in 1 mL solvent. To the NMR tube, 0.1 mL of the stock solution was added. The overall volume is 0.6 mL, and the concentration of lactide in the sample is 0.58 M. The sample was heated to 80 °C inside a Bruker 400 MHz NMR instrument. $^1$H NMR spectra were taken at minute-scale intervals and conversion with time determined by relative integration of monomer and polymer methine resonances.

## 5.3 Experimental for Chapter 2

### 5.3.1 Ligand preparation

**1**$H_2$

1,5-diaminonaphthalene (5.0 g, 31.6 mmol) was dissolved in methanol (50 mL) and salicylaldehyde (7.72 g, 63.2 mmol) dissolved in methanol (50 mL) was added. The mixture was stirred until a mustard yellow precipitate formed, which was filtered and dried (9.86 g, 26.9 mmol, 85 %).

$^1$H NMR ($CDCl_3$): 7.01 (2H, t, J = 7.5 Hz, Ar-H) 7.12 (2H, d, J = 7.9 Hz, Ar-H), 7.27 (2H, d, J = 7.2 Hz, Ar-H), 7.47 (4H, m, Ar-H) 7.58 (2H, t, J = 7.5 Hz, Ar-H), 8.23 (2H, d, J = 8.3 Hz, Ar-H), 8.74 (2H, s, N=CH), 13.33 (2H, br. s, OH)

$^{13}$C{$^1$H} NMR ($CDCl_3$): 114.9 (Ar-C) 117.4 (Ar-H) 119.3 (Ar-H) 119.5 (Ar-H) 122.3 (Ar-H) 126.6 (Ar-H) 128.9 (Ar-H) 132.5 (Ar-H) 133.6 (Ar-C) 146.3 (Ar-N) 161.2 (Ar-OH) 163.9 (N=CH)

m/z $[C_{24}H_{18}N_2O_2 + H]^+$ Calculated: 367.1447 $gmol^{-1}$ Found: 367.1456 $gmol^{-1}$

**2**$H_2$

1,5-diaminonaphthalene (3.0 g, 19.0 mmol) was dissolved in methanol (50 mL) and 3,5-di-tert-butyl-salicylaldehyde (8.89 g, 37.9 mmol) dissolved in methanol (50 mL) was added. The mixture was refluxed at 80 °C for 18 hours and the yellow precipitate was then filtered and dried (11.0 g, 18.6 mmol, 98 %).

$^1$H NMR ($CDCl_3$): 1.28 (18H, s, $C(CH_3)_3$), 1.46 (18H, s, $C(CH_3)_3$), 7.16 (1H, s, Ar-H), 7.18 (1H, s, Ar-H), 7.23 (2H, d, J = 2.3 Hz, Ar-H) 7.44 (2H, d, J = 2.6 Hz, Ar-H), 7.50 (2H, dt, J = 1.1 Hz, Ar-H), 8.15 (2H, d, J = 8.3 Hz, Ar-H) 8.67 (2H, s, N=CH), 13.63 (2H, br. s, OH)

$^{13}$C{$^1$H} NMR ($CDCl_3$): 29.5 ($C(\mathbf{C}H_3)_3$) 31.5 ($C(\mathbf{C}H_3)_3$) 34.3 ($\mathbf{C}(CH_3)_3$) 35.2 ($\mathbf{C}(CH_3)_3$) 114.9 (Ar-C) 118.7 (Ar-H) 122.1 (Ar-H) 126.5 (Ar-H) 127.0 (Ar-H) 128.4 (Ar-H) 128.9 (Ar-H) 137.1 (Ar-H) 140.8 (Ar-C) 146.5 (Ar-N) 158.4 (Ar-OH) 165.0 (N=CH)

m/z $[C_{40}H_{50}N_2O_2 + H]^+$ Calculated: 591.3945 $gmol^{-1}$ Found: 591.4065 $gmol^{-1}$

**3**$H_2$

1,5-diaminonaphthalene (2.0 g, 12.6 mmol) was dissolved in methanol (50 mL) and salicylaldehyde (4.84 g, 25.3 mmol) dissolved in methanol (50 mL) was added. The mixture was stirred until an orange precipitate formed, which was filtered and dried (6.22 g, 12.3 mmol,

98 %). Compound incalcitrant. No NMR or mass spectrometry data obtained due to very poor solubility.

$C_{24}H_{14}N_2O_2Cl_4$ Calculated: C 57.17 % H 2.80 % N 5.56 % Found: C 57.30 % H 2.67 % N 5.64 %

**4**H

1-aminonaphthalene (5.0 g, 34.9 mmol) was dissolved in methanol (30 mL) and salicylaldehyde (4.26 g, 34.9 mmol) was added. The precipitate was filtered, washed with methanol (3 x 10 mL) and dried to yield an orange solid (3.42 g, 13.8 mmol, 40 %).

$^1$H NMR (400 MHz, $CDCl_3$) δ ppm 7.01 (td, *J*=7.5, 1.0 Hz, 1 H, Ar-H) 7.14 (dd, *J*=8.8, 0.5 Hz, 1 H, Ar-H) 7.19 (dd, *J*=7.3, 1.0 Hz, 1 H, Ar-H) 7.43 - 7.49 (m, 2 H, Ar-H) 7.52 (dd, *J*=8.3, 7.3 Hz, 1 H, Ar-H) 7.58 (dt, *J*=9.5, 3.3 Hz, 1 H, Ar-H) 7.81 (d, *J*=8.3 Hz, 1 H, Ar-H) 7.91 (dt, *J*=9.5, 3.5 Hz, 1 H, Ar-H) 8.25 - 8.35 (m, 1 H, Ar-H) 8.71 (s, 1 H N=CH) 13.44 (br. s, 1 H, OH)

$^{13}$C{$^1$H} NMR (400 MHz, $CDCl_3$) δ ppm 114.0 (Ar-H) 117.3 (Ar-H) 119.2 (Ar-H) 119.5 (Ar-C) 123.2 (Ar-H) 125.9 (Ar-H) 126.5 (Ar-H) 126.7 (Ar-H) 126.9 (Ar-H) 127.9 (Ar-H) 128.2 (Ar-C) 132.4 (Ar-H) 133.4 (Ar-H) 133.9 (Ar-C) 146.2 (Ar-N) 161.2 (Ar-OH) 163.6 (N=CH)

m/z $[C_{17}H_{13}NO + H]^+$ Calculated: 248.1031 $gmol^{-1}$ Found: 248.1060 $gmol^{-1}$

**5**H

1-aminonaphthalene (5.0 g, 34.9 mmol) was dissolved in methanol (30 mL). 3,5-di-*tert*-butyl-salicylaldehyde (8.18 g, 34.9 mmol) was dissolved in methanol and added to the first solution. The precipitate was filtered, washed with methanol (3 x 10 mL) and dried to yield a yellow solid (8.35 g, 23.3 mmol, 67 %).

$^1$H NMR (400 MHz, $CDCl_3$) δ ppm 1.43 (s, 9 H, $C(CH_3)_3$) 1.62 (s, 9 H, $C(CH_3)_3$) 7.22 (dd, *J*=7.3, 1.0 Hz, 1 H, Ar-H) 7.36 (d, *J*=2.5 Hz, 1 H, Ar-H) 7.51 - 7.56 (m, 1 H, Ar-H) 7.57 - 7.65 (m, 3 H, Ar-H) 7.81 (d, *J*=8.3 Hz, 1 H, Ar-H) 7.90 - 7.95 (m, 1 H, Ar-H) 8.34 - 8.40 (m, 1 H, Ar-H) 8.78 (s, 1 H, N=CH) 13.78 (br. s, 1 H, OH)

$^{13}$C{$^1$H} NMR (400 MHz, $CDCl_3$) δ ppm 29.5 ($C(\mathbf{C}H_3)_3$) 31.5 ($C(\mathbf{C}H_3)_3$) 34.2 ($\mathbf{C}(CH_3)_3$) 35.2 ($\mathbf{C}(CH_3)_3$) 114.0 (Ar-H) 118.6 (Ar-H) 123.4 (Ar-H) 125.9 (Ar-H) 126.3 (Ar-H) 126.5 (Ar-C) 126.6 (Ar-H) 126.9 (Ar-H) 127.8 (Ar-H) 128.2 (Ar-H) 128.3 (Ar-C) 134.0 (Ar-C) 138.0 (Ar-C) 140.7 (Ar-C) 146.5 (Ar-N) 158.4 (Ar-OH) 164.7 (CH=N)

m/z $[C_{25}H_{29}NO + H]^+$ Calculated: 360.2283 $gmol^{-1}$ Found: 360.2328 $gmol^{-1}$

**6**H

1-aminonaphthalene (5.0 g, 34.9 mmol) was dissolved in methanol (30 mL). 3,5-dichloro-salicylaldehyde (6.67 g, 34.9 mmol) was dissolved in methanol and added to the first solution. The precipitate was filtered, washed with methanol (3 x 10 mL) and dried to yield an orange solid (10.16 g, 32.3 mmol, 93 %).

$^{1}$H NMR (400 MHz, $CDCl_3$) δ ppm 7.21 (dd, *J*=7.4, 0.9 Hz, 1 H, Ar-H) 7.35 (d, *J*=2.3 Hz, 1 H, Ar-H) 7.48 - 7.54 (m, 2 H, Ar-H) 7.55 - 7.62 (m, 2 H, Ar-H) 7.84 (d, *J*=8.3 Hz, 1 H, Ar-H) 7.87 - 7.93 (m, 1H, Ar-H) 8.20 - 8.27 (m, 1 H, Ar-H) 8.64 (s, 1 H, N=CH) 14.35 (br. s, 1 H, OH)

$^{13}$C{$^{1}$H} NMR (400 MHz, $CDCl_3$) δ ppm 114.1 (Ar-H) 120.5 (Ar-C) 122.9 (Ar-H) 123.6 (Ar-C) 125.8 (Ar-H) 126.9 (Ar-H) 128.0 (Ar-H) 128.0 (Ar-H) 129.8 (Ar-H) 132.9 (Ar-Cl) 134.0 (Ar-Cl) 144.6 (Ar-N) 155.9 (Ar-OH) 161.3 (CH=N)

m/z $[C_{17}H_{12}Cl_2NO + H]^+$ Calculated: 316.0296 $gmol^{-1}$ Found: 316.0260 $gmol^{-1}$

## 5.3.2 Preparation of metal complexes

$Al_2$(**1**)$Me_4$

**1**$H_2$ (2.0 g, 5.46 mmol) was dissolved in toluene (60 mL) and $AlMe_3$ (2 M in hexane, 5.46 mL, 10.9 mmol) was added slowly. Some solvent was removed under vacuum and the product crystallised from solution. The yellow crystals were filtered and dried under vacuum (0.76 g, 1.59 mmol, 29 %).

$^{1}$H NMR ($C_6D_6$): -0.39 (6H, br. s, $Al(CH_3)_2$), -0.27 (6H, br. s, $Al(CH_3)_2$), 6.53 (2H, m, Ar-H), 6.73 (2H, d, J = 7.2 Hz, Ar-H), 6.96 (2H, dd, $J_1$ = 7.2 Hz, $J_2$ = 1 Hz, Ar-H), 7.10 (1H, m, Ar-H), 7.58 (2H, d, J = 8.7 Hz, N=CH)

$^{13}$C{$^{1}$H} NMR ($C_6D_6$): -8.7 ($Al(CH_3)_2$) 118.2 (Ar-H) 119.5 (Ar-C) 122.3 (Ar-H) 123.1 (Ar-H) 123.6 (Ar-H) 127.0 (Ar-H) 128.2 (Ar-H) 128.3 (Ar-H) 128.5 (Ar-H) 128.6 (Ar-H) 129.6 (Ar-H) 136.1 (Ar-C) 139.2 (Ar-C) 143.8 (Ar-N) 166.5 (Ar-O) 174.3 (N=CH)

$C_{28}H_{28}N_2O_2Al_2$ Calculated: C 70.28 % H 5.90 % N 5.85 % Found: C 70.14 % H 5.78 % N 5.69 %

$Al_2$(**2**)$Me_4$

**2**$H_2$ (2.0 g, 3.38 mmol) was dissolved in toluene (60 mL) and $AlMe_3$ (2 M in hexane, 3.38 mL, 6.77 mmol) was added slowly. Some solvent was removed under vacuum and the product crystallised from solution. The yellow crystals were filtered and dried under vacuum (1.53 g, 2.18 mmol, 64 %).

$^{1}$H NMR ($C_6D_6$): -0.33 (6H, br. s, $Al(CH_3)_2$), -0.23 (6H, br. s, $Al(CH_3)_2$), 1.31 (18H, s, $C(CH_3)_3$), 1.65 (18H, s, $C(CH_3)_3$), 6.74 (2H, d, J = 2.6 Hz, Ar-H), 6.98 - 7.09 (6H, m, Ar-H) 7.10 - 7.15 (2H, m, Ar-H), 7.79 (2H, d, J = 2.6 Hz, N=CH)

$^{13}$C{$^{1}$H} NMR ($d_8$-Tol): -8.9 ($Al(CH_3)_2$) 29.6 ($C(\mathbf{C}H_3)_3$) 31.4 ($C(\mathbf{C}H_3)_3$) 34.3 ($\mathbf{C}(CH_3)_3$) 35.7 ($\mathbf{C}(CH_3)_3$) 118.9 (Ar-C) 122.1 (Ar-H) 123.3 (Ar-H) 126.7 (Ar-H) 129.6 (Ar-H) 129.9 (Ar-H) 133.7 (Ar-C) 137.8 (Ar-C) 139.6 (Ar-C) 141.3 (Ar-C) 143.8 (Ar-N) 163.4 (Ar-O) 174.8 (N=CH)

$C_{44}H_{60}N_2O_2Al_2$ Calculated: C 75.18 % H 8.60 % N 3.99 % Found: C 75.00 % H 8.62 % N 3.91 %

$Al_2$(**3**)$Me_4$

**3**$H_2$ (2.0 g, 3.97 mmol) was suspended in toluene (75 mL) and $AlMe_3$ (2 M in hexane, 3.96 mL, 7.93 mmol) was added slowly. Upon reaction with trimethylaluminium the solid dissolved fully. Some solvent was removed under vacuum and the product precipitated from solution. The yellow solid was filtered and dried under vacuum (1.81 g, 2.94 mmol, 74 %).

$^{1}$H NMR ($C_6D_6$): -0.48 (6H, br. s, $Al(CH_3)_2$), -0.37 (6H, br. s, $Al(CH_3)_2$), 6.44 (2H, s, Ar-H), 6.88 (2H, s, Ar-H), 6.96 (2H, d, J = 7.2 Hz, Ar-H), 7.10 (2H, t, J = 7.5 Hz, Ar-H), 7.31 (2H, d, J = 2.6 Hz, Ar-H), 7.45 (1H, s, N=CH), 7.48 (1H, s, N=CH)

$^{13}$C{$^{1}$H} NMR ($C_6D_6$): -8.9 ($Al(CH_3)_2$) 119.9 (Ar-C) 122.1 (Ar-H) 122.3 (Ar-H) 123.7 (Ar-H) 127.2 (Ar-H) 129.1 (Ar-H) 133.2 (Ar-Cl) 137.9 (Ar-Cl) 143.2 (Ar-N) 159.9 (Ar-O) 173.3 (N=CH)

$C_{28}H_{24}N_2O_2Al_2Cl_4$ Calculated: C 54.57 % H 3.93 % N 4.55 % Found: C 54.36 % H 3.93 % N 4.43 %

Al(**4**)$Me_2$

A solution of $AlMe_3$ (4.0 mL, 2 M in hexane, 8.09 mmol) was added slowly to **4**H (2.0 g, 8.09 mmol) dissolved in hexane (50 mL). Crystals formed in solution, and the solvent was removed by filtration. The crystals were dried under vacuum with stirring to yield a yellow powder (1.20 g, 3.94 mmol, 49 %).

$^{1}$H NMR (300 MHz, $d_8$-Tol) δ ppm -0.41 (br. s, 6 H, Al-$(CH_3)_2$) 6.49 (dq, *J*=7.9, 1.0 Hz, 2 H, Ar-H) 6.64 (dd, *J*=7.7, 1.7 Hz, 2 H, Ar-H) 7.01 (qd, *J*=8.7, 1.1 Hz, 2 H, Ar-H) 7.06 - 7.23 (m, 6 H, Ar-H) 7.44 (dd, *J*=8.3, 1.0 Hz, 1 H, Ar-H) 7.54 (td, *J*=7.2, 1.9 Hz, 2 H, Ar-H) 7.60 - 7.68 (m, 2 H, Ar-H)

$^{13}$C{$^{1}$H} NMR (300 MHz, $d_8$-Tol) δ ppm -9.1 (Al-$(CH_3)_2$) 117.5 (Ar-H) 119.1 (Ar-C) 120.7 (Ar-H) 122.6 (Ar-H) 123.1 (Ar-H) 125.3 (Ar-H) 126.9 (Ar-H) 127.2 (Ar-H) 128.1 (Ar-H) 128.2 (Ar-C) 128.5 (Ar-H) 134.8 (Ar-C) 135.6 (Ar-H) 138.3 (Ar-H) 143.1 (Ar-N) 166.1 (Ar-O) 173.7 (CH=N)

$C_{19}H_{18}AlNO$ Calculated: C 75.23 % H 5.98 % N 4.62 % Found: C 75.36 % H 5.88 % N 4.80 %

Al(**5**)$Me_2$

A solution of $AlMe_3$ (2.78 mL, 2 M in hexane, 5.56 mmol) was added slowly to **5**H (2.0 g, 5.56 mmol) dissolved in hexane (60 mL). Crystals formed in solution, and the solvent was removed by filtration. The crystals were dried under vacuum with stirring to yield a yellow powder (0.48 g, 1.16 mmol, 21 %).

$^1$H NMR (300 MHz, $d_8$-Tol) δ ppm -0.37 (br. s, 6 H, Al-$(CH_3)_2$) 1.28 (s, 9 H, C$(CH_3)_3$) 1.62 (s, 9 H, C$(CH_3)_3$) 6.71 (d, *J*=2.6 Hz, 1 H, Ar-H) 6.97 - 7.22 (m, 5 H, Ar-H) 7.47 (d, *J*=7.9 Hz, 1 H, Ar-H) 7.51 (s, 1 H, N=CH) 7.54 (dd, *J*=8.5, 0.9 Hz, 1 H, Ar-H) 7.66 (d, *J*=8.7 Hz, 1 H, Ar-H) 7.74 (d, *J*=2.6 Hz, 1 H, Ar-H)

$^{13}$C{$^1$H} NMR (400 MHz, $d_8$-Tol) δ ppm -9.1 (Al-$(CH_3)_2$) 29.6 (C(**C**$H_3)_3$) 31.4 (C(**C**$H_3)_3$) 34.2 (**C**$(CH_3)_3$) 35.7 (**C**$(CH_3)_3$) 118.9 (Ar-H) 120.8 (Ar-H) 123.3 (Ar-H) 126.9 (Ar-H) 127.2 (Ar-H) 128.0 (Ar-H) 128.4 (Ar-C) 129.7 (Ar-H) 133.3 (Ar-H) 134.9 (Ar-C) 139.3 (Ar-C) 141.3 (Ar-C) 143.4 (Ar-N) 163.3 (Ar-O) 174.5 (CH=N)

$C_{27}H_{34}AlNO$ Calculated: C 78.04 % H 8.25 % N 3.76 % Found: C 77.89 % H 8.11 % N 3.67 %

Al(**6**)$Me_2$

A solution of $AlMe_3$ (3.16 mL, 2 M in hexane, 6.33 mmol) was added slowly to **6**H (2.0 g, 6.33 mmol) dissolved in toluene (60 mL). Crystals formed in solution, and the solvent was removed by filtration. The crystals were dried under vacuum with stirring to yield a yellow powder (1.35 g, 3.63 mmol, 57 %).

$^1$H NMR (300 MHz, $d_8$-Tol) δ ppm -0.47 (br. s, 6 H, Al$(CH_3)_2$) 6.30 (d, *J*=2.6 Hz, 1 H, Ar-H) 6.94 - 7.00 (m, 2 H, Ar-H) 7.05 - 7.13 (m, 2 H, Ar-H) 7.22 (td, *J*=6.8, 3.0 Hz, 3 H, Ar-H) 7.45 (d, *J*=8.3 Hz, 1 H, Ar-H) 7.48 - 7.57 (m, 2 H, Ar-H)

$^{13}$C{$^1$H} NMR (300 MHz, $d_8$-Tol) δ ppm -9.2 (Al-$(CH_3)_2$) 119.7 (Ar-H) 120.5 (Ar-H) 121.4 (Ar-C) 122.8 (Ar-H) 125.3 (Ar-H) 127.2 (Ar-H) 127.4 (Ar-H) 127.8 (Ar-C) 127.9 (Ar-C) 128.6 (Ar-H) 128.7 (Ar-H) 132.7 (Ar-H) 134.8 (Ar-Cl) 137.0 (Ar-Cl) 142.5 (Ar-N) 159.4 (Ar-O) 172.6 (N=CH)

$C_{19}H_{16}AlNOCl_2$ Calculated: C 61.31 % H 4.33 % N 3.76 % Found: C 61.40 % H 4.27 % N 3.84 %

## 5.4 Experimental for Chapter 3

### 5.4.1 Ligand preparation

*tert*-butyl (2-aminocyclohexyl)carbamate: A solution of trans-1,2-diaminocyclohexane (10.0 g, 87.6 mmol) in DCM (50 mL) was cooled to 0 °C and a solution of di-*tert*-butyl dicarbonate (6.37 g, 29.2 mmol) in DCM (50 mL) was added dropwise over half an hour. The solution was warmed to room temperature and the solution was left to stir overnight. Additional DCM (50 mL) and water (50 mL) were added to dissolve the suspension. The organic phase was separated and the solvent removed *in-vacuo*. The resulting solid was dissolved in diethyl ether (50 mL) and water (50 mL). The solution was then acidified to pH 5 using 4 M HCl. The mixture was separated and the aqueous phase washed three times with diethyl ether (3 x 50 mL). 2 M NaOH was added to the aqueous layer until pH 10 was reached. The precipitate was extracted with ethyl acetate (3 x 50 mL). The organic phase was washed with brine (20 mL) and dried with $MgSO_4$. The solid was removed by filtration and the solvent was removed *in vacuo* to form a pale yellow solid, *tert*-butyl (2-aminocyclohexyl)carbamate (2.5 g, 11.7 mmol, 13 %). $^1$H NMR (400 MHz, $CDCl_3$) δ ppm 1.04 - 1.21 (m, 2 H, $CH_2$) 1.21 - 1.33 (m, 2 H, $CH_2$) 1.45 (s, 9 H, $C(CH_3)_3$) 1.65 (br. s, 2 H, $NH_2$) 1.67 - 1.74 (m, 2 H, $CH_2$) 1.91 - 2.07 (m, 2 H, $CH_2$) 2.34 (td, *J*=10.2, 3.8 Hz, 1 H, CH) 3.02 - 3.25 (m, 1 H, CH) 4.48 (br. s, 1 H, NH).

**7**H

*tert*-butyl (2-aminocyclohexyl)carbamate (2.50 g, 11.7 mmol) was dissolved in methanol and salicylaldehyde (1.42 g, 11.7 mmol) was added. The precipitate was filtered and washed with methanol (3 x 10 mL) to yield a yellow solid (2.89 g, 9.07 mmol, 77 %).

$^1$H NMR (400 MHz, $CDCl_3$) δ ppm 1.29 (s, 9 H, $C(CH_3)_3$) 1.32 - 1.51 (m, 3 H, $CH_2$, CH) 1.61 - 1.73 (m, 1 H, CH) 1.73 - 1.85 (m, 2 H, $CH_2$) 1.85 - 1.94 (m, 1 H, CH) 2.02 - 2.14 (m, 1 H, CH) 3.05 (br. s, 1 H, CH) 3.57 (d, *J*=1.0 Hz, 1 H, CH) 4.36 (br. s, 1 H, NH) 6.86 (td, *J*=7.5, 1.0 Hz, 1 H, Ar-H) 6.95 (d, *J*=8.3 Hz, 1 H, Ar-H) 7.23 (dd, *J*=7.7, 1.6 Hz, 1 H, Ar-H) 7.26 - 7.32 (m, 1 H, Ar-H) 8.33 (s, 1 H, N=CH) 13.28 (br. s, 1 H, OH)

$^{13}C\{^1H\}$ NMR (400 MHz, $CDCl_3$) δ ppm 23.9 ($CH_2$) 24.7 ($CH_2$) 28.1 ($C(\mathbf{C}H_3)_3$) 31.4 ($CH_2$) 33.2 ($CH_2$) 54.2 ($O\text{-}\mathbf{C}(CH_3)_3$) 72.3 (CH) 79.2 (CH) 117.0 (Ar-H) 118.4 (Ar-H) 118.7 (Ar-H) 131.3 (Ar-H) 132.2 (Ar-C) 155.1 (Ar-OH) 161.2 (N=CH) 164.0 (C=O)

m/z $[C_{18}H_{26}N_2O_3 + H]^+$ Calculated: 319.2022 $gmol^{-1}$ Found: 319.2007 $gmol^{-1}$

**8**H

*tert*-butyl (2-aminocyclohexyl)carbamate (1.35 g, 6.30 mmol) was dissolved in methanol (25 mL) and a solution of 3,5-di-*tert*-butyl-salicylaldhyde (1.48 g, 6.30 mmol) in methanol (25 mL) was added. The precipitate was filtered and washed with methanol (3 x 10 mL) to yield a yellow solid (1.83 g, 4.24 mmol, 67 %).

$^{1}$H NMR (400 MHz, $CDCl_3$) δ ppm 1.08 - 1.26 (m, 3 H, $CH_2$, CH) 1.31 (s, 18 H, $C(CH_3)_3$) 1.44 (s, 9 H, $C(CH_3)_3$) 1.63 - 1.84 (m, 4 H, $CH_2$) 1.90 (d, *J*=10.3 Hz, 1 H, CH) 2.09 (d, *J*=10.3 Hz, 1 H, CH) 3.08 (s, 1 H, CH) 3.53 - 3.65 (m, 1 H, CH) 4.39 (br. s, 1 H, NH) 7.09 (s, 1 H, Ar-H) 7.37 (d, *J*=2.5 Hz, 1 H, Ar-H) 8.38 (s, 1 H, N=CH) 13.48 (br. s, 1 H, OH)

$^{13}$C{$^{1}$H} NMR (400 MHz, $CDCl_3$) δ ppm 24.1 ($CH_2$) 24.8 ($CH_2$) 28.1 ($C(\mathbf{C}H_3)_3$) 29.4 ($C(\mathbf{C}H_3)_3$) 31.5 ($C(\mathbf{C}H_3)_3$) 33.5 ($\mathbf{C}(CH_3)_3$) 34.1 ($\mathbf{C}(CH_3)_3$) 35.0 ($CH_2$) 54.4 (O-$\mathbf{C}(CH_3)_3$) 72.3 (CH) 79.3 (CH) 117.8 (Ar-H) 125.9 (Ar-C) 126.7 (Ar-C) 136.6 (Ar-H) 139.8 (Ar-C) 155.2 (Ar-OH) 158.0 (N=CH) 165.2 (C=O)

m/z $[C_{26}H_{42}N_2O_3 + H]^+$ Calculated: 431.3274 $gmol^{-1}$ Found: 431.3268 $gmol^{-1}$

**9**H

*tert*-butyl (2-aminocyclohexyl)carbamate (2.08 g, 9.69 mmol) was dissolved in methanol (30 mL) and a solution of 3,5-di-chloro-salicylaldhyde (1.87 g, 9.69 mmol) in methanol (30 mL) was added. The precipitate was filtered and washed with methanol (3 x 10 mL) to yield a yellow solid (2.20 g, 5.70 mmol, 59 %).

$^{1}$H NMR (400 MHz, $CDCl_3$) δ ppm 1.31 (s, 9 H, $C(CH_3)_3$) 1.36 - 1.51 (m, 3 H) 1.53 - 1.72 (m, 2 H) 1.73 - 1.87 (m, 2 H, CH2) 1.93 (d, *J*=9.8 Hz, 1 H, CH) 2.06 (d, *J*=8.8 Hz, 1 H, CH) 3.24 (s, 1 H, CH) 3.54 (d, *J*=7.8 Hz, 1 H, CH) 4.43 (br. s, 1 H, NH) 7.13 (d, *J*=2.5 Hz, 1 H, Ar-H) 7.39 (d, *J*=2.5 Hz, 1 H, Ar-H) 8.24 (s, 1 H, CH=N) 14.41 (br. s, 1 H, OH)

$^{13}$C{$^{1}$H} NMR (400 MHz, $CDCl_3$) δ ppm 23.7 ($CH_2$) 24.5 ($CH_2$) 28.1 ($C(\mathbf{C}H_3)_3$) 31.2 ($CH_2$) 32.7 ($CH_2$) 53.8 (O-$\mathbf{C}(CH_3)_3$) 70.8 (N-CH), 79.4 (N-CH) 119.1 (Ar-H) 121.8 (Ar-H) 123.1 (Ar-C) 128.9 (Ar-Cl) 132.2 (Ar-Cl) 155.0 (Ar-OH) 157.6 (N=CH) 162.4 (C=O)

m/z $[C_{18}H_{24}Cl_2N_2O_3 + H]^+$ Calculated: 387.1242 $gmol^{-1}$ Found: 387.1234 $gmol^{-1}$

**10**H

**7**H (3.29 g, 10.3 mmol) was dissolved in THF (30 mL) and methanol (10 mL) and sodium borohydride (1.96 g, 51.6 mmol) was slowly added and stirred for 4 hours. The reaction was quenched with water (10 mL) and the solvent was partially removed *in vacuo* until some precipitate formed. Water (50 mL) was added to precipitate the rest of the product which was filtered and washed with water. The white solid was dissolved in methanol (60 mL) and formaldehyde (38 % in $H_2O$, 2.23 mL) was added and allowed to stir for 1 hour. The solvent was removed *in vacuo* and the solid redissolved in THF (30 mL) and methanol (30 mL) and cooled to 0 °C. Sodium borohydride (1.96 g, 51.6 mmol) was slowly added and the solution stirred for 1 hour. The reaction was quenched with water (10 mL) and the solvent partially removed *in vacuo*. Water (50 mL) was added to precipitate the product, which was filtered and washed with water. The white solid (1.11 g, 3.32 mmol) was dissolved in methanol (30 mL) and 3 M HCl then heated to 60 °C and stirred overnight. The mixture was neutralised with 3 M NaOH and the white precipitate extracted with ethyl acetate (30 mL x 3). The organic phase was washed with brine (20 mL) and dried with $MgSO_4$. The solution was filtered and the solvent removed *in vacuo*. The solid was dissolved in methanol (50 mL) and an excess of benzaldehyde (0.3 g, 28.3 mmol) was added. A white precipitate formed after 30 minutes, which was filtered and washed with cold methanol (3 x 10 mL) and dried to a white solid (0.338 g, 1 mmol, 10 %).

$^1$H NMR (400 MHz, $CDCl_3$) δ ppm 1.32 - 1.50 (m, 3 H, $CH_2$, CH) 1.66 - 1.74 (m, 2 H, $CH_2$) 1.80 (d, *J*=5.5 Hz, 1 H, CH) 1.89 (br. s, 1 H, CH) 1.98 (d, *J*=12.1 Hz, 1 H, CH) 2.18 (s, 3 H, N-$CH_3$) 3.09 (td, *J*=11.3, 3.3 Hz, 1 H, CH) 3.29 - 3.38 (m, 1 H, CH) 3.88 (d, *J*=4.8 Hz, 2 H, N-$CH_2$) 6.68 - 6.75 (m, 2 H, Ar-H) 6.93 (d, *J*=7.3 Hz, 1 H, Ar-H) 7.10 (td, *J*=7.7, 1.6 Hz, 1 H, Ar-H) 7.42 - 7.49 (m, 3 H, Ar-H) 7.78 - 7.87 (m, 2 H, Ar-H) 8.35 (s, 1 H, N=CH)

$^{13}$C{$^1$H} NMR (400 MHz, $CDCl_3$) δ ppm 23.4 ($CH_2$) 24.8 ($CH_2$) 34.3 ($CH_2$) 34.8 ($CH_2$) 58.71 (N-$CH_3$) 62.1 (N-CH) 66.9 (N-$CH_2$) 70.7 (N-CH) 116.2 (Ar-H) 118.5 (Ar-H) 122.2 (Ar-H) 128.3 (Ar-H) 128.3 (Ar-H) 128.5 (Ar-H) 129.0 (Ar-H) 129.7 (Ar-H) 130.5 (Ar-H) 136.2 (Ar-C) 158.3 (Ar-OH) 160.8 (N=CH)

m/z $[C_{21}H_{25}N_2O + H]^+$ Calculated: 323.2123 $gmol^{-1}$ Found: 323.2114 $gmol^{-1}$

**11**H

**8**H (2.0 g, 4.64 mmol) was dissolved in THF (30 mL) and methanol (10 mL) and sodium borohydride (0.18 g, 4.64 mmol) was slowly added and stirred for 1 hour. The reaction was quenched with water (10 mL) and the solvent was partially removed *in vacuo* until some

precipitate formed. Water (50 mL) was added to precipitate the rest of the product which was filtered and washed with water. The white solid was dissolved in ethanol (50 mL) and formaldehyde (38 % in $H_2O$, 0.96 mL, 13.9 mmol) was added and allowed to stir for 1 hour. The solvent was removed *in vacuo* and the solid redissolved in THF (30 mL) and methanol (30 mL) and cooled to 0 °C. Sodium borohydride (0.18 g, 4.64 mmol) was slowly added and the solution stirred for 1 hour. The reaction was quenched with water (10 mL) and the solvent partially removed *in vacuo*. Water (50 mL) was added to precipitate the product which was filtered and washed with water. The white solid (2.03 g, 4.54 mmol) was dissolved in methanol (30 mL) and 3 M HCl then heated to 60 °C and stirred overnight. The mixture was neutralised with 3 M NaOH and the purple oil extracted with ethyl acetate (30 mL x 3). The organic phase was washed with brine (20 mL) and dried with $MgSO_4$. The solution was filtered and the solvent removed *in vacuo*. The oil was dissolved in methanol (30 mL) and an small excess of benzaldehyde (0.3 g, 28.3 mmol) was added. A white precipitate formed after 1 hour, which was filtered and washed with cold methanol (3 x 10 mL) and dried to a white solid (0.65 g, 1.49 mmol, 32 %).

$^1$H NMR (400 MHz, $CDCl_3$) δ ppm 1.22 (s, 9 H, $C(CH_3)_3$) 1.28 (s, 9 H, $C(CH_3)_3$) 1.38 - 1.46 (m, 3 H, $CH_2$) 1.73 - 1.88 (m, 3 H, $CH_2$) 1.88 - 1.96 (m, 1 H, $CH_2$) 2.00 (d, *J*=9.54 Hz, 1 H, $CH_2$) 2.14 (s, 3 H, N-$CH_3$) 3.05 - 3.17 (m, 1 H, CH) 3.26 - 3.36 (m, 1 H, CH) 3.78 (d, *J*=13.30 Hz, 1 H, N-$CH_2$) 3.91 (d, *J*=12.55 Hz, 1 H, N-$CH_2$) 6.81 (d, *J*=2.01 Hz, 1 H, Ar-H) 7.15 (d, *J*=2.26 Hz, 1 H, Ar-H) 7.40 - 7.46 (m, 3 H, Ar-H) 7.85 - 7.90 (m, 2 H, Ar-H) 8.35 (s, 1 H, N=CH)

$^{13}$C{$^1$H} NMR (400 MHz, $CDCl_3$) δ ppm 24.8 ($CH_2$), 25.2 ($CH_2$), 29.3 (C(**C**$H_3$)$_3$), 31.7 (C(**C**$H_3$)$_3$), 34.0 (**C**$(CH_3)_3$), 34.6 ($CH_2$), 34.6 (**C**$(CH_3)_3$), 67.4 (N-$CH_3$), 70.8 (N-$CH_2$), 121.2 (Ar-C), 122.5 (Ar-H), 123.1 (Ar-H), 128.3 (Ar-H), 128.6 (Ar-H), 130.4 (Ar-H), 135.4 (Ar-C), 136.3 (Ar-C), 139.6 (Ar-C), 154.8 (Ar-OH), 160.9 (N=CH)

m/z $[C_{29}H_{42}N_2O + H]^+$ Calculated: 435.3331 $gmol^{-1}$ Found: 435.3505 $gmol^{-1}$

**12**H

**9**H (3.17 g, 8.20 mmol) was dissolved in THF (30 mL) and methanol (10 mL) and sodium borohydride (0.31 g, 8.20 mmol) was slowly added and stirred for 1 hour. The reaction was quenched with water (10 mL) and the solvent was partially removed *in vacuo* until some precipitate formed. Water (50 mL) was added to precipitate the rest of the product which was filtered and washed with water. The white solid was dissolved in methanol (50 mL) and formaldehyde (37 % in $H_2O$, 0.6 mL) was added and allowed to stir for 1 hour. The solvent was

removed *in vacuo* and the solid redissolved in THF (40 mL) and methanol (20 mL) and cooled to 0 °C. Sodium borohydride (0.31 g, 8.20 mmol) was slowly added and the solution stirred for 1 hour. The reaction was quenched with water (10 mL) and the solvent partially removed *in vacuo*. Water (50 mL) was added to precipitate the product, which was filtered and washed with water. The white solid (3.26 g, 8.08 mmol) was dissolved in methanol (30 mL) and 3 M HCl then heated to 60 °C and stirred overnight. The mixture was neutralised with 3 M NaOH and the white precipitate extracted with ethyl acetate (30 mL x 3). The organic phase was washed with brine (20 mL) and dried with $MgSO_4$. The solution was filtered and the solvent removed *in vacuo*. The solid (0.85 g, 2.80 mmol) was dissolved in methanol (20 mL) and benzaldehyde (0.28 mL, 2.80 mmol) was added to the solution, which was stirred until a precipitate formed. The solid was filtered, washed with methanol (3 x 5 mL) and dried. Yield 0.64 g, 1.65 mmol, 59 %.

$^{1}$H NMR (400 MHz, $CDCl_3$) δ ppm 1.32 - 1.52 (m, 3 H, $CH_2$) 1.61 - 1.76 (m, 2 H, $CH_2$) 1.77 - 1.84 (m, 1 H, $CH_2$) 1.86 - 1.92 (m, 1 H, $CH_2$) 1.95 (d, *J*=13.1 Hz, 1 H, $CH_2$) 2.20 (s, 3 H, N-$CH_3$) 2.96 - 3.11 (m, 1 H, CH) 3.33 (td, *J*=10.2, 5.0 Hz, 1 H, CH) 3.80 - 3.93 (m, 2 H, N-$CH_2$) 6.80 (d, *J*=2.5 Hz, 1 H, Ar-H) 7.20 (d, *J*=2.5 Hz, 1 H, Ar-H) 7.42 - 7.50 (m, 3 H, Ar-H) 7.81 - 7.90 (m, 2 H, Ar-H) 8.35 (s, 1 H, N=CH)

$^{13}$C{$^{1}$H} NMR (400 MHz, $CDCl_3$) δ ppm 24.4 ($CH_2$) 24.7 ($CH_2$) 25.2 ($CH_2$) 34.3 (N-$CH_3$) 34.7 ($CH_2$) 59.0 (N-$CH_2$) 67.2 (N-CH) 70.4 (N-CH) 121.5 (Ar-C) 122.7 (Ar-Cl) 124.4 (Ar-Cl) 126.5 (Ar-H) 128.3 (Ar-H) 128.5 (Ar-H) 130.7 (Ar-H) 136.1 (Ar-C) 153.3 (Ar-OH) 161.1 (N=CH)

m/z $[C_{21}H_{24}N_2OCl_2 + Na]^+$ Calculated: 413.1163 gmol$^{-1}$ Found: 413.1155 gmol$^{-1}$

## 5.4.2 Preparation of metal complexes

### Aluminium complexes

Al(**7**)$_2$Me

A solution of $AlMe_3$ (0.66 mL, 2 M in hexane, 1.32 mmol) was slowly added to **7**H (0.84 g, 2.64 mmol) dissolved in toluene (50 mL). Crystals formed in solution, and the solvent was removed by filtration. The crystals were dried under vacuum with stirring to yield a pale yellow powder (0.37 g, 0.54 mmol, 41 %). The complex was extremely insoluble in common deuterated organic solvents, characterisation was carried out by X-ray crystallography and elemental analysis only.

$C_{37}H_{53}AlN_4O_6$ Calculated: C 65.66 % H 7.89 % N 8.28 % Found: C 65.70 % H 7.98 % N 8.165 %

Al(**8**)$Me_2$

A solution of $AlMe_3$ (0.51 mL, 2 M in hexane, 1.03 mmol) was added to **8**H (0.50 g, 1.03 mmol) dropwise in 20 mL toluene and stirred for 30min. Solvent was removed *in vacuo* and redissolved in hexane. Crystals formed in solution, and the solvent was removed by filtration. The crystals were dried under vacuum with stirring to yield a pale yellow powder (0.23 g, 0.48 mmol, 47 %).

$^1$H NMR (300 MHz, $d_8$-Tol) δ ppm -0.36 (s, 3 H, Al-$CH_3$) -0.22 (s, 3 H, Al-$CH_3$) 0.82 - 1.09 (m, 4 H, $CH_2$) 1.18 (s, 9 H, $C(CH_3)_3$) 1.34 (s, 9 H, $C(CH_3)_3$) 1.37 - 1.47 (m, 3 H, $CH_2$, CH) 1.56 (s, 9 H, $C(CH_3)_3$) 1.89 (d, *J*=10.6 Hz, 1 H, CH) 2.98 (t, *J*=9.2 Hz, 1 H, CH) 3.32 - 3.52 (m, 1 H, CH) 3.90 (d, *J*=8.3 Hz, 1 H, NH) 7.06 (d, *J*=2.6 Hz, 1 H, Ar-H) 7.63 (d, *J*=2.6 Hz, 1 H, Ar-H) 7.88 (s, 1 H, N=CH)

$^{13}$C{$^1$H} NMR (300 MHz, $d_8$-Tol) δ ppm 1.4 (Al-$(CH_3)_2$) 25.0 ($CH_2$) 25.3 ($CH_2$) 28.1 (C(**C**$H_3$)$_3$) 29.6 (C(**C**$H_3$)$_3$) 31.6 (C(**C**$H_3$)$_3$) 32.1 ($CH_2$) 33.0 ($CH_2$) 34.2 (**C**$(CH_3)_3$) 35.6 (**C**$(CH_3)_3$) 53.0 (N-CH) 69.8 (N-CH) 79.0 (O-**C**$(CH_3)_3$) 118.8 (Ar-C) 129.5 (Ar-H) 131.6 (Ar-H) 138.6 (Ar-C) 140.7 (Ar-C) 154.9 (Ar-O) 162.3 (N=CH) 171.9 (C=O)

$C_{28}H_{47}AlN_2O_3$ Calculated: C 69.10 % H 9.73 % N 5.76 % Found: C 68.24 % H 9.67 % N 5.85 %

Al(**9**)$Me_2$

A solution of $AlMe_3$ (0.65 mL, 2 M in hexane, 1.29 mmol) was slowly added to **9**H (0.50 g, 1.29 mmol) dissolved in toluene (40 mL) and stirred for 30 min. Crystals formed in solution, and the solvent was removed by filtration. The crystals were dried under vacuum with stirring to yield a yellow powder (0.28 g, 0.63 mmol, 49 %).

$^1$H NMR (300 MHz, $d_8$-Tol) δ ppm -0.43 (s, 3 H, $AlCH_3$) -0.33 (s, 3 H, $AlCH_3$) 0.70 - 1.00 (m, 4 H, $CH_2$) 1.17 (s, 9 H, $C(CH_3)_3$) 1.27 - 1.41 (m, 2 H, $CH_2$) 1.46 (d, *J*=11.3 Hz, 1 H, CH) 1.78 (d, *J*=12.8 Hz, 1 H, CH) 2.93 (t, *J*=11.3 Hz, 1 H, CH) 3.33 - 3.50 (m, 1 H, CH) 3.85 (d, *J*=8.7 Hz, 1 H, NH) 6.83 (d, *J*=2.6 Hz, 1 H, Ar-H) 7.22 (d, *J*=2.6 Hz, 1 H, Ar-H) 7.65 (s, 1 H, N=CH)

$^{13}$C{$^1$H} NMR (300 MHz, $d_8$-Tol) δ ppm 24.8 ($CH_2$) 25.1 ($CH_2$) 28.0 (C(**C**$H_3$)$_3$) 32.1 ($CH_2$) 33.0 ($CH_2$) 52.3 (N-CH) 69.0 (N-CH) 79.5 (O-**C**$(CH_3)_3$) 120.1 (Ar-H) 121.0 (Ar-H) 127.4 (Ar-C) 132.2 (Ar-Cl) 135.8 (Ar-Cl) 155.0 (Ar-O) 158.7 (N=CH) 169.6 (C=O)

$C_{20}H_{29}AlCl_2N_2O_3$ Calculated: C 54.18 % H 6.59 % N 6.32 % Found: C 53.96 % H 6.65 %, N 6.23 %

Al(**9**)$_2$Me

A solution of $AlMe_3$ (0.26 mL, 2 M in hexane, 0.52 mmol) was slowly added to **9**H (0.40 g, 1.03 mmol) dissolved in toluene (40 mL). Crystals formed in solution, and the solvent was removed by filtration. The crystals were dried under vacuum with stirring to yield a pale yellow powder (0.077 g, 0.09 mmol, 18 %). The complex was extremely insoluble in common deuterated organic solvents, characterisation was carried out by X-ray crystallography and elemental analysis only.

$C_{37}H_{49}AlCl_4N_4O_6$ Calculated: C 54.56 % H 6.06 % N 6.88 % Found: C 54.51 % H 6.14 % N 6.80 %

Al(**11**-Me)Me

**11**H (0.2 g, 0.46 mmol) was dissolved in toluene (10 mL) and 2 M trimethylaluminium solution (0.23 mL, 0.46 mmol) slowly added. The solution turned from clear to pale yellow. The solvent was removed and the solid redissolved in hexane (10 mL). The resulting crystals were filtered and dried under vacuum. Yield 0.11 g, 0.21 mmol, 47 %.

$^1$H NMR (300 MHz, $C_6D_6$) δ ppm -0.94 (s, 3 H, Al-$CH_3$) 0.62 - 1.02 (m, 4 H, $CH_2$) 1.16 - 1.26 (m, 1 H, $CH_2$) 1.40 - 1.43 (m, 1 H, $CH_2$) 1.44 (s, 9 H, C($CH_3$)$_3$) 1.46 - 1.53 (m, 2 H, $CH_2$) 1.65 (s, 3 H, N-$CH_3$) 1.68 (d, *J*=6.40 Hz, 3 H, CH-C**H**$_3$) 1.72 (s, 9 H, C($CH_3$)$_3$) 2.14 - 2.25 (m, 1 H, CH) 2.55 (d, *J*=12.43 Hz, 1 H, N-$CH_2$) 3.04 (td, *J*=9.89, 3.58 Hz, 1 H, CH) 3.89 (d, *J*=12.43 Hz, 1 H, N-$CH_2$) 4.22 (q, *J*=6.40 Hz, 1 H, $CH_3$-C**H**) 6.88 (d, *J*=2.64 Hz, 1 H, Ar-H) 7.19 - 7.26 (m, 1 H, Ar-H) 7.42 (t, *J*=7.72 Hz, 2 H, Ar-H) 7.61 (d, *J*=2.64 Hz, 1 H, Ar-H) 7.77 (d, *J*=7.16 Hz, 2 H, Ar-H)

$^{13}$C{$^1$H} NMR (300 MHz, $C_6D_6$) δ ppm -12.3 (Al-$CH_3$) 21.4 ($CH_2$) 22.9 (CH-**C**$H_3$) 25.0 ($CH_2$) 26.1 ($CH_2$) 30.4 (C(**C**$H_3$)$_3$) 32.5 (C(**C**$H_3$)$_3$) 33.5 ($CH_2$) 34.7 (**C**($CH_3$)$_3$) 35.8 (**C**($CH_3$)$_3$) 39.4 (N-$CH_3$) 53.2 (N-$CH_2$) 55.7 (**C**H-$CH_3$) 59.0 (CH) 72.9 (CH) 122.2 (Ar-H) 125.1 (Ar-H) 125.2 (Ar-H) 127.5 (Ar-H) 128.3 (Ar-H) 129.4 (Ar-H) 139.0 (Ar-C) 139.3 (Ar-C) 150.1 (Ar-C) 156.9 (Ar-O)

Al(**12**)$Me_2$

A solution of $AlMe_3$ (0.23 mL, 2 M in hexane, 0.46 mmol) was slowly added to **12**H (0.18 g, 0.46 mmol) dissolved in toluene (10 mL). Crystals formed in solution, and the solvent was removed by filtration. The crystals were dried under vacuum with stirring to yield a white powder (0.13 g, 0.30 mmol, 65 %).

$^{1}$H NMR (400 MHz, $d_8$-Tol) δ ppm -0.37 (s, 3 H, Al-Me) -0.30 (s, 3 H, Al-Me) 1.02 - 1.18 (m, 3 H, $CH_2$) 1.25 - 1.30 (m, 1 H, $CH_2$) 1.39 - 1.48 (m, 2 H, $CH_2$) 1.53 (d, *J*=8.78 Hz, 2 H, $CH_2$) 1.74 (s, 3 H, N-Me) 2.28 (d, *J*=11.54 Hz, 1 H, CH) 2.97 - 3.08 (m, 1 H, CH) 4.01 (d, *J*=13.80 Hz, 1 H, N-$CH_2$) 4.60 (d, *J*=14.05 Hz, 1 H, N-$CH_2$) 6.35 (d, *J*=1.76 Hz, 1 H, Ar-H) 7.27 - 7.33 (m, 4 H, Ar-H) 7.68 (d, *J*=5.27 Hz, 2 H, Ar-H) 7.75 (s, 1 H, N=CH)

No $^{13}$C NMR data, compound only partially soluble in $d_8$ toluene.

$C_{23}H_{29}N_2OCl_2Al$ Calculated: C 61.75 % H 6.53 % N 6.15 % Found: C 61.67 % H 6.66 % N 6.26 %

## Zinc complexes

### Zn(**7**)$_2$

A solution of $ZnMe_2$ (1.57 mL, 1 M in hexane, 1.57 mmol) was slowly added to **7**H (1.0 g, 3.14 mmol) dissolved in toluene (50 mL). Crystals formed in solution and the solvent was removed by filtration. The crystals were dried under vacuum with stirring to yield a white powder (0.97 g, 1.39 mmol, 89 %). Compound very insoluble, $^{1}$H NMR data broad peaks in $d_6$-DMSO.

$^{1}$H NMR (400 MHz, $d_6$-DMSO) δ ppm 0.74 (d, *J*=10.8 Hz, 2 H, $CH_2$) 0.97 - 1.33 (m, 22 H, 2C$(CH_3)_3$, 2$CH_2$) 1.45 (br. s, 6 H, $CH_2$) 1.78 (br. s, 4 H, $CH_2$) 3.14 (br. s, 3 H, CH) 3.58 (br. s, 1 H, CH) 6.48 - 6.82 (m, 4 H, Ar-H) 7.07 - 7.33 (m, 4 H, Ar-H) 8.08 - 8.42 (m, 2 H, N=CH)

$^{13}$C{$^{1}$H} NMR (400 MHz, $d_6$-DMSO) δ ppm 21.1 ($CH_2$) 24.2 ($CH_2$) 27.9 (C(**C**$H_3)_3$) 28.1 (C(**C**$H_3)_3$) 52.8 (HN-CH) 71.6 (N-CH) 77.5 (O-**C**$(CH_3)_3$) 77.6 (O-**C**$(CH_3)_3$) 113.8 (Ar-H) 118.1 (Ar-H) 118.4 (Ar-H) 122.3 (Ar-H) 125.4 (Ar-H) 128.2 (Ar-H) 128.9 (Ar-H) 134.2 (Ar-H) 136.2 (Ar-C) 137.4 (Ar-C) 154.6 (Ar-O) 169.7 (N=CH) 170.0 (C=O) 170.7 (C=O)

$C_{36}H_{50}N_4O_6Zn$ Calculated: C 61.75 % H 7.20 % N 8.00 % Found: C 61.56 %, H 7.30 %, N 7.94 %

### Zn(**7**)Me

A solution of $ZnMe_2$ (0.94 mL, 1 M in hexane , 0.94 mmol) was slowly added to **7**H (0.30 g, 0.94 mmol) dissolved in toluene (20 mL). Crystals formed in solution and the solvent was removed by filtration. The crystals were dried under vacuum with stirring to yield a pale yellow powder (0.082 g, 0.21 mmol, 22 %).

$^{1}$H NMR (400 MHz, $d_8$-Tol) δ ppm -0.07 (s, 3 H, Zn-$CH_3$) 0.51 (qd, *J*=12.0, 3.5 Hz, 1 H, CH) 0.78 - 0.93 (m, 1 H, CH) 0.94 - 1.09 (m, 2 H, $CH_2$) 1.13 (s, 9 H, C$(CH_3)_3$) 1.18 - 1.31 (m, 3 H, $CH_2$, CH) 1.34 (br. s, 1 H, CH) 1.41 (d, *J*=11.0 Hz, 3 H, $CH_2$, CH) 1.61 - 1.78 (m, 2 H, $CH_2$) 3.66 (td, *J*=16.6,

8.8 Hz, 1 H, CH) 4.06 (d, *J*=8.5 Hz, 1 H, NH) 6.53 (t, *J*=6.8 Hz, 1 H, Ar-H) 6.93 (d, *J*=7.8 Hz, 1 H, Ar-H) 6.98 (s, 1 H, Ar-H) 7.02 (s, 1 H, Ar-H) 7.08 - 7.15 (m, 2 H, Ar-H) 7.19 - 7.25 (m, 1 H, Ar-H) 7.55 (s, 1 H, N=CH)

$^{13}C\{^{1}H\}$ NMR (400 MHz, $d_8$-Tol) δ ppm -13.9 (Zn-$CH_3$), 24.5 ($CH_2$) 25.2 ($CH_2$) 27.9 (C(**C**$H_3$)$_3$) 30.6 ($CH_2$) 32.7 ($CH_2$) 54.6 (HN-CH) 78.6 (N-CH) 81.8 (O-**C**($CH_3$)$_3$) 113.3 (Ar-H) 118.4 (Ar-H) 124.2 (Ar-H) 134.8 (Ar-H) 135.3 (Ar-C) 158.7 (Ar-O) 167.8 (N=CH)

$C_{19}H_{28}N_2O_3Zn$ Calculated: C 57.36 % H 7.09 % N 7.04 % Found: C 57.23 %, H 7.16 %, N 7.00 %

Zn(**9**)$_2$

A solution of $ZnMe_2$ (0.65 mL, 1 M in hexane, 0.65 mmol) was slowly added to **9**H (0.50 g, 1.29 mmol) dissolved in toluene (20 mL). The resulting crystals were filtered and dried under vacuum to produce a pale yellow powder (0.17 g, 0.20 mmol, 30 %).

$^{1}H$ NMR (400 MHz, $CDCl_3$) δ ppm 0.98 - 1.18 (m, 2 H, $CH_2$) 1.31 (s, 18 H, C($CH_3$)$_3$) 1.36 - 1.54 (m, 4 H, $CH_2$) 1.60 - 1.77 (m, 4 H, $CH_2$) 1.77 - 2.00 (m, 6 H, $CH_2$) 3.29 (br. s, 2 H, CH) 3.86 (br. s, 2 H, CH) 5.56 (br. s, 2 H, NH) 7.02 (d, *J*=2.8 Hz, 2 H, Ar-H0) 7.45 (d, *J*=2.8 Hz, 1 H, Ar-H) 8.20 (br. s, 2 H, N=CH)

$^{13}C\{^{1}H\}$ NMR (400 MHz, $CDCl_3$) δ ppm 24.4 ($CH_2$) 25.2 ($CH_2$) 28.2 (C(**C**$H_3$)$_3$) 33.8 ($CH_2$) 55.2 (N-CH) 79.3 (O**C**($CH_3$)$_3$) 79.5 (O**C**($CH_3$)$_3$) 117.8 (Ar-H) 118.8 (Ar-H) 127.4 (Ar-H) 129.0 (Ar-H) 133.0 (Ar-Cl) 133.8 (Ar-Cl) 155.3 (Ar-O) 155.6 (Ar-O) 163.0 (N=CH) 169.3 (C=O)

$C_{36}H_{46}Cl_4N_4O_6Zn$ Calculated: C 51.60 % H 5.53 % N 6.69 % Found: C 48.69 % H 5.46 % N 5.78 %

Zn(**10**)Me

A solution of $ZnMe_2$ (1.56 mL, 1 M in hexane, 1.40 mmol) was slowly added to **10**H (0.45 g, 1.40 mmol) dissolved in toluene (20 mL). Crystals formed in solution, and the solvent was removed by filtration. The crystals were dried under vacuum with stirring to yield a white powder (0.43 g, 1.06 mmol, 76 %). The $^{1}H$ NMR showed a mixture of diastereomers, the data below is for the major isomer.

$^{1}H$ NMR (400 MHz, $d_8$-Tol) δ ppm -0.63 (m, 3 H, Zn-$CH_3$) 0.60 - 0.78 (m, 3 H, $CH_2$) 1.25 (d, *J*=11.3 Hz, 1 H, $CH_2$) 1.33 - 1.43 (m, 2 H, $CH_2$) 1.51 (d, *J*=12.6 Hz, 2 H, $CH_2$) 1.97 (s, 3 H, N-$CH_3$) 2.45 - 2.57 (m, 1 H, CH) 2.59 - 2.71 (m, 1 H, CH) 3.01 (d, *J*=12.6 Hz, 1 H, N-$CH_2$) 3.98 (d, *J*=12.6 Hz, 1 H,

N-$CH_2$) 6.61 (td, *J*=7.2, 1.4 Hz, 1 H) 6.86 (dd, *J*=7.3, 1.8 Hz, 1 H) 7.15 - 7.18 (m, 1 H) 7.19 - 7.27 (m, 3 H) 7.61 (d, *J*=2.3 Hz, 1 H) 8.08 (d, *J*=7.3 Hz, 2 H)

$^{13}C\{^1H\}$ NMR (400 MHz, $d_8$-Tol) δ ppm -16.8 (Zn-$CH_3$) 21.8 ($CH_2$) 24.0 ($CH_2$) 24.5 ($CH_2$) 29.7 ($CH_2$) 38.0 (N-$CH_3$) 59.4 ($CH_2$-N) 60.4 (CH) 60.8 (CH) 113.3 (Ar-H) 121.1 (Ar-H) 122.0 (Ar-H) 128.5 (Ar-H) 129.9 (Ar-H) 130.9 (Ar-H) 132.5 (Ar-H) 134.6 (Ar-N) 164.7 (Ar-O) 168.4 (CH=N)

$C_{22}H_{28}N_2OZn$ Calculated: C 65.75 % H 7.02 % N 6.97 % Found: C 65.59 % H 7.18 % N 6.85 %

Zn(**12**)Me

A solution of $ZnMe_2$ (1.59 mL, 1 M in hexane, 1.59 mmol) was slowly added to **12**H (0.62 g, 1.59 mmol) dissolved in toluene (20 mL). Crystals formed in solution, and the solvent was removed by filtration. The crystals were dried under vacuum with stirring to yield a white powder (0.44 g, 0.92 mmol, 58 %). The $^1H$ NMR showed a mixture of diastereomers, the data below is for the major isomer.

$^1H$ NMR (400 MHz, $C_6D_6$) δ ppm -0.54 (s, 3 H, Zn-$CH_3$) 0.45 - 0.64 (m, 3 H, $CH_2$) 1.16 (d, *J*=12.6 Hz, 1 H, $CH_2$) 1.20 - 1.35 (m, 3 H, $CH_2$) 1.41 (d, *J*=11.0 Hz, 1 H, $CH_2$) 1.84 (s, 3 H, N-$CH_3$) 2.24 (t, *J*=11.4 Hz, 1 H, CH) 2.48 (t, *J*=10.3 Hz, 1 H, CH) 2.78 (d, *J*=12.8 Hz, 1 H, $CH_2$) 3.73 (d, *J*=12.8 Hz, 1 H, $CH_2$) 6.80 (s, 1 H, N=CH) 7.10 - 7.15 (m, 1 H, Ar-H) 7.33 (t, *J*=7.3 Hz, 2 H, Ar-H) 7.52 (s, 1 H, Ar-H) 7.57 (br. s, 1 H, Ar-H) 8.17 (d, *J*=7.5 Hz, 2 H, Ar-H)

$^{13}C\{^1H\}$ NMR (400 MHz, $d_8$-Tol) δ ppm -17.0 (Zn-$CH_3$) 21.7 ($CH_2$) 23.8 ($CH_2$) 24.3 ($CH_2$) 29.3 ($CH_2$) 37.9 (N-$CH_3$) 58.3 (CH) 59.9 (CH) 61.2 (N-$CH_2$) 124.1 (Ar-H) 125.8 (Ar-H) 129.3 (Ar-H) 130.0 (Ar-H) 130.3 (Ar-H) 132.8 (Ar-Cl) 134.2 (Ar-Cl) 162.1 (Ar-O) 165.4 (N=CH)

$C_{22}H_{26}N_2OCl_2Zn$ Calculated: C 56.13 % H 5.57 % N 5.95 % Found: C 56.04 % H 5.65 % N 5.89 %

## 5.5 Experimental for chapter 4

### 5.5.1 Ligand preparation

**13**$H_2$

3,5-di-*tert*-butyl-2-hydroxybenzaldehyde (4.55 g, 19.4 mmol) dissolved in methanol (25 mL) was added to o-phenylenediamine (1.05 g, 9.71 mmol) dissolved in methanol (25 mL) and the solution refluxed at 80 °C for 16 hours. The resulting yellow solid was filtered and washed with cold methanol (3 x 10 mL) and dried under vacuum (4.77 g, 8.82 mmol, 91 %)

$^1$H NMR (400 MHz, $CDCl_3$) δ ppm 1.34 (s, 18 H, $C(CH_3)_3$) 1.46 (s, 18 H, $C(CH_3)_3$) 7.23 (d, *J*=2.5 Hz, 2 H, Ar-H) 7.24 - 7.28 (m, 3 H, Ar-H) 7.30 - 7.34 (m, 2 H, Ar-H) 7.46 (d, *J*=2.5 Hz, 2 H, Ar-H) 8.68 (s, 2 H, N=CH) 13.54 (br. s, 2 H, OH)

$^{13}$C{$^1$H} NMR (400 MHz, $CDCl_3$) δ ppm 29.5 ($C(\mathbf{C}H_3)_3$) 31.5 ($\mathbf{C}(CH_3)_3$) 34.2 ($\mathbf{C}(CH_3)_3$) 35.1 ($\mathbf{C}(CH_3)_3$) 118.4 (Ar-C) 119.8 (Ar-H) 126.8 (Ar-H) 127.3 (Ar-H) 128.2 (Ar-H) 137.2 (Ar-C) 140.3 (Ar-C) 142.8 (Ar-N) 158.6 (Ar-OH) 164.7 (N=CH)

m/z $[C_{36}\ H_{48}\ N_2\ O_2 + Na]^+$ Calculated: 563.3613 gmol$^{-1}$ Found: 563.3619 gmol$^{-1}$

$C_{36}H_{48}N_2O_2$ Calculated: C 79.95 % H 8.94 % N 5.18 % Found: C 80.09 % H 9.06 % N 5.24 %

**14**$H_2$

N-methyl-1,2-phenylenediamine (1.28 g, 10.5 mmol) was dissolved in methanol (10 mL) and 3,5-di-*tert*-butyl-2-hydroxbenzaldehyde (2.46 g, 10.5 mmol) dissolved in methanol (30 mL) was added. The solution was stirred for 16 hours, and the resulting precipitate isolated by vacuum filtration and washed with ice cold methanol (3 x 10 mL). The yellow solid was dried (2.51 g, 7.42 mmol, 71 %).

$^1$H NMR (400 MHz, $CDCl_3$) δ ppm 1.35 (s, 9 H, $C(CH_3)_3$) 1.49 (s, 9 H, $C(CH_3)_3$) 2.95 (s, 3 H, $CH_3$) 4.46 (br. s, 1 H, NH) 6.68 - 6.77 (m, 2 H, Ar-H) 7.01 (dd, *J*=7.8, 1.5 Hz, 1 H, Ar-H) 7.21 (td, *J*=7.8, 1.5 Hz, 1 H, Ar-H) 7.24 (d, *J*=2.3 Hz, 1 H, Ar-H) 7.47 (d, *J*=2.5 Hz, 1 H, Ar-H) 8.63 (s, 1 H, N=CH) 13.31 (s, 1 H, OH)

$^{13}$C{$^1$H} NMR (400 MHz, $CDCl_3$) δ ppm 29.4 ($C(\mathbf{C}H_3)_3$) 30.5 ($N\text{-}CH_3$) 31.5 ($C(\mathbf{C}H_3)_3$) 34.2 ($\mathbf{C}(CH_3)_3$) 35.1 ($\mathbf{C}(CH_3)_3$) 110.0 (Ar-H) 116.8 (Ar-H) 117.9 (Ar-H) 118.7 (Ar-H) 126.8 (Ar-H) 127.9 (Ar-H) 128.0 (Ar-C) 135.6 (Ar-C) 136.9 (Ar-C) 140.8 (Ar-NH) 143.1 (Ar-N) 157.7 (N=CH) 163.5 (Ar-OH)

m/z $[C_{22}H_{30}N_2O + H]^+$ Calculated: 339.2436 gmol$^{-1}$ Found: 339.2453 gmol$^{-1}$

$C_{22}H_{30}N_2O$ Calculated: C 78.06 % H 8.93 % N 8.27 % Found: C 78.17 % H 9.03 % N 8.25 %

**15**$H_2$

3,5-dichlorosalicylaldehyde (1.56 g, 8.18 mmol) was dissolved in methanol (15 mL) was added to N-methyl-1,2-diaminophenylene (1.0 g, 8.19 mmol) dissolved in methanol (15 mL) and stirred for 30 min. The bright orange precipitate was filtered and washed with cold methanol (3 x 10 mL). 1.86 g, 6.3 mmol, 77 %.

$^1$H NMR (400 MHz, $CDCl_3$) δ ppm 2.93 (s, 3 H, $CH_3$) 4.38 (br. s, 1 H, NH) 6.69 - 6.78 (m, 2 H, Ar-H) 7.04 (dd, *J*=7.8, 1.3 Hz, 1 H, Ar-H) 7.26 (dq, *J*=7.5, 1.5 Hz, 1 H, Ar-H) 7.33 (d, *J*=2.5 Hz, 1 H, Ar-H) 7.47 (d, *J*=2.5 Hz, 1 H, Ar-H) 8.55 (s, 1 H, N=CH) 13.96 (s, 1 H, OH)

$^{13}$C{$^1$H} NMR (400 MHz, $CDCl_3$) δ ppm 30.3 ($CH_3$) 110.6 (Ar-H) 116.8 (Ar-H) 117.8 (Ar-H) 120.8 (Ar-H) 122.6 (Ar-Cl) 123.7 (Ar-Cl) 129.5 (Ar-H) 129.6 (Ar-H) 132.4 (Ar-C) 133.5 (Ar-N) 143.4 (Ar-NH) 155.2 (Ar-OH) 159.3 (N=CH)

m/z $[C_{14}H_{12}N_2OCl_2 + H]^+$ Calculated: 295.0405 gmol$^{-1}$ Found: 295.0259 gmol$^{-1}$

**16**$H_2$

N-phenyl-1,2-phenylenediamine (1.0 g, 5.43 mmol) was dissolved in methanol (20 mL). 3,5-ditertbutylsalicylaldehyde (1.27 g, 5.43 mmol) dissolved in methanol (30 mL) was added and the reaction stirred for 18 hours. The yellow precipitate was filtered and washed with ice cold methanol (3 x 10 mL). 1.26 g, 3.13 mmol, 58 %.

$^1$H NMR (400 MHz, $CDCl_3$) δ ppm 1.35 (s, 9 H, $C(CH_3)_3$) 1.48 (s, 9 H, $C(CH_3)_3$) 6.25 (s, 1 H, Ar-H) 6.92 (td, *J*=7.5, 1.3 Hz, 1 H, Ar-H) 7.02 (tt, *J*=6.0, 1.0 Hz, 1 H, Ar-H) 7.13 (dd, *J*=7.9, 1.4 Hz, 1 H, Ar-H) 7.18 (td, *J*=6.8, 1.0 Hz, 1 H, Ar-H) 7.20 - 7.24 (m, 2 H, Ar-H) 7.27 (d, *J*=2.5 Hz, 1 H, Ar-H) 7.30 - 7.38 (m, 3 H, Ar-H) 7.49 (d, *J*=2.3 Hz, 1 H, Ar-H) 8.68 (s, 1 H, N=CH) 13.24 (s, 1 H, OH)

$^{13}$C{$^1$H} NMR (400 MHz, $CDCl_3$) δ ppm 29.4 ($C(\mathbf{C}H_3)_3$) 31.5 ($C(\mathbf{C}H_3)_3$) 34.2 ($\mathbf{C}(CH_3)_3$) 35.1 ($\mathbf{C}(CH_3)_3$) 114.8 (Ar-H) 118.6 (Ar-H) 118.9 (Ar-H) 119.8 (Ar-H) 120.1 (Ar-H) 122.0 (Ar-C) 126.9 (Ar-C) 127.4 (Ar-H) 128.3 (Ar-H) 129.4 (Ar-H) 137.0 (Ar-C) 137.5 (Ar-N) 137.5 (Ar-NH) 140.9 (Ar-OH) 142.1 (N=CH)

m/z $[C_{27}H_{32}N_2O + H]^+$ Calculated: 401.2592 gmol$^{-1}$ Found: 401.2555 gmol$^{-1}$

**17**$H_2$

N-phenyl-1,2-phenylenediamine (1.0 g, 5.43 mmol) was dissolved in methanol (20 mL). 3,5-dichlorosalicylaldehyde (1.04 g, 5.43 mmol) dissolved in methanol (30 mL) was added and the reaction stirred for 30 min. The red/orange precipitate was filtered and washed with ice cold methanol (3 x 10 mL). Yield 1.78 g, 4.98 mmol, 92 %.

$^1$H NMR (400 MHz, $CDCl_3$) δ ppm 6.10 (s, 1 H, NH) 6.94 (dq, *J*=6.5, 1.0 Hz, 1 H, Ar-H) 7.04 (t, *J*=7.3 Hz, 1 H, Ar-H) 7.14 (dd, *J*=7.9, 1.4 Hz, 1 H, Ar-H) 7.18 (dd, *J*=7.5, 1.0 Hz, 2 H, Ar-H) 7.22 (dq, *J*=7.0, 1.0 Hz, 1 H, Ar-H) 7.29 - 7.38 (m, 4 H, Ar-H) 7.49 (d, *J*=2.5 Hz, 1 H, Ar-H) 8.61 (s, 1 H, N=CH) 13.79 (s, 1 H, OH)

$^{13}$C{$^1$H} NMR (400 MHz, $CDCl_3$) δ ppm 115.7 (Ar-H) 118.8 (Ar-H) 120.3 (Ar-H) 120.4 (Ar-H) 120.7 (Ar-H) 122.6 (Ar-H) 122.7 (Ar-H) 123.8 (Ar-H) 128.9 (Ar-H) 129.4 (Ar-Cl) 129.8 (Ar-Cl) 132.7 (Ar-H) 135.7 (Ar-C) 138.2 (Ar-N) 141.5 (Ar-NH) 155.3 (Ar-OH) 160.5 (CH=N)

m/z $[C_{19}H_{14}N_2OCl_2 + H]^+$ Calculated: 357.0561 $gmol^{-1}$ Found: 357.0357 $gmol^{-1}$

**18**H

Salicylaldehyde (0.99 g, 8.19 mmol) was added to N-methyl-1,2-phenylenediamine (1.0 g, 8.19 mmol) dissolved in methanol (10 mL) and the solution stirred for 16 hours at room temperature. The yellow precipitate was filtered and washed with 10 mL ice cold methanol (1.47 g, 6.55 mmol, 79 %).

$^1$H NMR (400 MHz, $CDCl_3$) δ ppm 4.08 (s, 3 H, $CH_3$) 7.00 (dq, *J*=7.3, 0.5 Hz, 1 H, Ar-H) 7.18 (dd, *J*=8.3, 1.3 Hz, 1 H, Ar-H) 7.31 - 7.47 (m, 4 H, Ar-H) 7.74 (dd, *J*=8.0, 1.5 Hz, 1 H, Ar-H) 7.76 - 7.80 (m, 1 H, Ar-H) 12.99 (s, 1 H, OH)

$^{13}$C{$^1$H} NMR (400 MHz, $CDCl_3$) δ ppm 33.1 (N-$CH_3$) 109.5 (Ar-H) 113.1 (Ar-H) 118.1 (Ar-H) 118.6 (Ar-H) 118.9 (Ar-H) 123.0 (Ar-H) 123.3 (Ar-C) 127.1 (Ar-H) 131.5 (Ar-N) 140.4 (Ar-N) 151.6 (C=N) 159.0 (Ar-OH)

m/z $[C_{14}H_{12}N_2O + Na]^+$ Calculated: 247.0847 $gmol^{-1}$ Found: 247.0832 $gmol^{-1}$

**19**H

N-phenyl-1,2-phenylenediamine (1.0 g, 5.43 mmol) was dissolved in 10 mL methanol and salicylaldehyde (0.66 g, 5.43 mmol) was added. The solution was stirred for 16 hours until a precipitate formed. This was filtered and washed with ice cold methanol to yield a grey

powder (0.93 g, 3.24 mmol, 60 %).

$^{1}$H NMR (400 MHz, $CDCl_3$) δ ppm 6.54 (ddd, *J*=8.2, 7.2, 1.3 Hz, 1 H, Ar-H) 6.86 (dd, *J*=8.0, 1.5 Hz, 1 H, Ar-H) 7.08 - 7.13 (m, 2 H, Ar-H) 7.22 - 7.31 (m, 2 H, Ar-H) 7.37 (ddd, *J*=8.2, 7.2, 1.3 Hz, 1 H, Ar-H) 7.40 - 7.46 (m, 2 H, Ar-H) 7.60 - 7.67 (m, 2 H, Ar-H) 7.83 (dt, *J*=7.9, 0.9 Hz, 1 H, Ar-H) 13.55 (br. s, 1 H, OH)

$^{13}$C{$^{1}$H} NMR (400 MHz, $CDCl_3$) δ ppm 110.4 (Ar-H) 112.3 (Ar-H) 118.0 (Ar-H) 118.0 (Ar-H) 118.6 (Ar-H) 123.4 (Ar-H) 123.7 (Ar-H) 127.3 (Ar-H) 127.9 (Ar-H) 129.5 (Ar-H) 130.4 (Ar-C) 131.4 (Ar-H) 136.5 (Ar-H) 137.1 (Ar-N) 140.0 (Ar-N) 150.8 (Ar-OH) 159.6 (C=N)

m/z $[C_{19}H_{14}N_2O + Na]^+$ Calculated: 309.0998 gmol$^{-1}$ Found: 309.1004 gmol$^{-1}$

**20**$H_2$

**14**$H_2$ (2.08 g, 6.13 mmol) was dissolved in THF (20 mL) and 3,5-di-*tert*-butyl-2-hydroxybenzyl bromide (1.83 g, 6.13 mmol) dissolved in THF (20 mL) was added. Triethylamine (0.85 mL, 6.13 mmol) was added to the solution which was then refluxed for 3 hours at 80 °C. The precipitate was removed by vacuum filtration and the solvent of the filtrate removed by rotary evaporation. The oil was redissolved in dichloromethane (10 mL) and washed over silica. The solvent was removed by rotary evaporation and the yellow solid recrystallised in hexane (20 mL). Yellow crystals 1.25 g, 2.24 mmol, 37 %.

$^{1}$H NMR (400 MHz, $CDCl_3$) δ ppm 1.32 (s, 9 H, $C(CH_3)_3$) 1.36 (s, 9 H, $C(CH_3)_3$) 1.39 (s, 9 H, $C(CH_3)_3$) 1.49 (s, 9 H, $C(CH_3)_3$) 2.71 (s, 3 H, N-$CH_3$) 4.32 (s, 2 H, $CH_2$) 6.96 (d, *J*=2.3 Hz, 1 H, Ar-H) 7.10 (dd, *J*=7.8, 1.3 Hz, 1 H, Ar-H) 7.19 - 7.23 (m, 1 H, Ar-H) 7.24 (d, *J*=2.5 Hz, 1 H, Ar-H) 7.26 (d, *J*=2.3 Hz, 1 H, Ar-H) 7.28 - 7.34 (m, 2 H, Ar-H) 7.50 (d, *J*=2.5 Hz, 1 H, Ar-H) 8.63 (s, 1 H, N=CH) 10.07 (s, 1 H, OH) 13.00 (s, 1 H, OH)

$^{13}$C{$^{1}$H} NMR (400 MHz, $CDCl_3$) δ ppm 29.5 ($C(\mathbf{C}H_3)_3$) 29.7 ($C(\mathbf{C}H_3)_3$) 31.5 ($C(\mathbf{C}H_3)_3$) 31.7 ($C(\mathbf{C}H_3)_3$) 34.2 ($\mathbf{C}(CH_3)_3$) 34.2 ($\mathbf{C}(CH_3)_3$) 34.9 ($\mathbf{C}(CH_3)_3$) 35.2 ($\mathbf{C}(CH_3)_3$) 42.8 (N-$CH_3$) 59.8 ($CH_2$) 118.5 (Ar-C) 120.4 (Ar-H) 120.8 (Ar-H), 121.0 (Ar-C) 123.1 (Ar-H) 123.7 (Ar-H) 125.5 (Ar-H) 127.0 (Ar-H) 128.3 (Ar-H) 135.9 (Ar-C) 137.2 (Ar-C) 140.5 (Ar-C) 140.5 (Ar-C) 145.1 (Ar-N) 145.4 (Ar-N) 154.2 (Ar-OH) 158.2 (Ar-OH) 165.3 (CH=N)

m/z $[C_{37}H_{52}N_2O_2 + Na]^+$ Calculated: 579.3926 gmol$^{-1}$ Found: 579.3957 gmol$^{-1}$

$C_{37}H_{52}N_2O_2$ Calculated: C 79.81 % H 9.41 % N 5.03 % Found: C 79.94 % H 9.52 % N 4.94 %

**21**$H_2$

N,N-dimethyl-1,2-phenylenediamine (0.97 g, 7.12 mmol) was dissolved in 10 mL THF and 3,5-di-*tert*-butyl-2-hydroxybenzyl bromide (4.26 g, 14.2 mmol) dissolved in 30 mL THF was added. Triethylamine (1.99 mL, 14.2 mmol) was added to the solution, which was then refluxed for 16 hours at 70 °C. The precipitate was removed by vacuum filtration and the solvent of the filtrate removed by rotary evaporation. The oil was redissolved in dichloromethane (20 mL) and washed over silica. The solvent was removed by rotary evaporation and the pink solid used with no further purification. 2.34 g, 4.08 mmol, 57 %.

$^1$H NMR (400 MHz, $CDCl_3$) d ppm 1.27 (s, 18 H, $C(CH_3)_3$) 1.34 (s, 18 H, $C(CH_3)_3$) 2.72 (s, 6 H, N-$CH_3$) 4.05 (s, 4 H, $CH_2$) 6.86 (d, *J*=2.51 Hz, 2 H, Ar-H) 7.18 - 7.22 (m, 4 H, Ar-H) 7.39 (dd, *J*=5.90, 3.64 Hz, 2 H, Ar-H) 9.73 (s, 2 H, OH)

$^{13}$C{$^1$H} NMR (400 MHz, $CDCl_3$) δ ppm 29.6 (C(**C**$H_3$)$_3$) 31.6 (C(**C**$H_3$)$_3$) 34.1 (**C**$(CH_3)_3$) 34.9 (**C**$(CH_3)_3$) 44.1 (N-$CH_3$) 60.9 ($CH_2$) 121.5 (Ar-C) 122.8 (Ar-H) 123.1 (Ar-H) 124.6 (Ar-H) 126.1 (Ar-H) 136.0 (Ar-C) 140.6 (Ar-C) 148.0 (Ar-N) 153.5 (Ar-O)

m/z: $[C_{38}H_{57}N_2O_2 + H]^+$ Calculated: 573.4420 gmol$^{-1}$ Found: 573.4464 gmol$^{-1}$

## 5.5.2 Preparation of metal complexes

$Al_2$(**13**)$Me_4$

**13**$H_2$ (0.30 g, 0.55 mmol) was dissolved in hexane (20 mL) and 2 M trimethylaluminium (0.55 mL, 1.1 mmol) solution added slowly. The resulting crystals were isolated and dried under vacuum (0.18 g, 0.28 mmol, 51 %).

$^1$H NMR (400 MHz, $C_6D_6$) δ ppm -0.26 (d, *J*=1.0 Hz, 12 H, Al-$CH_3$) 1.16 (s, 18 H, $C(CH_3)_3$) 1.47 (s, 18 H, $C(CH_3)_3$) 6.81 - 6.89 (m, 2 H, Ar-H) 6.95 (s, 2 H, Ar-H) 7.28 - 7.34 (m, 2 H, Ar-H) 7.54 (s, 2 H, Ar-H) 7.99 (s, 2 H, N=CH)

$^{13}$C{$^1$H} NMR (400 MHz, $C_6D_6$) δ ppm -8.1 (Al-$CH_3$) 29.9 (C(**C**$H_3$)$_3$) 31.5 (C(**C**$H_3$)$_3$) 34.4 (**C**$(CH_3)_3$) 35.8 (**C**$(CH_3)_3$) 119.2 (Ar-C) 127.0 (Ar-H) 130.3 (Ar-H) 134.4 (Ar-H) 140.1 (Ar-C) 141.0 (Ar-C) 141.2 (Ar-C) 163.5 (Ar-O) 176.4 (N=CH)

$C_{40}H_{58}N_2O_2Al_2$ Calculated: C 73.59 % H 8.95 % N 4.29 % Found: C 73.39 % H 9.11 % N 4.33 %

$Zr_2$(**13**)($O^iPr$)$_6$

**13**$H_2$ (1.0 g, 1.8 mmol) was dissolved in 30 mL toluene with $Zr(O^iPr)_4.{}^iPrOH$ (1.43 g, 3.70 mmol) and stirred for 16 hours. The toluene was removed and the orange solid dissolved in hexane (20 mL). This was concentrated to produce a precipitate which was filtered and dried under vacuum (0.60 g, 0.56 mmol, 31 %).

$^1$H NMR (400 MHz, $C_6D_6$) δ ppm 1.15 (d, *J*=6.3 Hz, 6 H, CH-C**H**$_3$) 1.17 (s, 18 H, C(CH$_3$)$_3$) 1.18 (d, *J*=5.5 Hz, 6 H, CH-C**H**$_3$) 1.24 (d, *J*=6.5 Hz, 6 H, CH-C**H**$_3$) 1.27 (d, *J*=6.0 Hz, 6 H, CH-C**H**$_3$) 1.55 (dd, *J*=6.0, 0.5 Hz, 12 H, CH-C**H**$_3$) 1.74 (s, 18 H, C(CH$_3$)$_3$) 4.42 (spt, *J*=6.1 Hz, 2 H, C**H**-CH$_3$) 4.79 (spt, *J*=6.1 Hz, 2 H, C**H**-CH$_3$) 4.93 (m, *J*=6.5 Hz, 1 H, C**H**-CH$_3$) 4.99 (m, *J*=6.3 Hz, 1 H, C**H**-CH$_3$) 6.96 - 7.00 (m, 4 H, Ar-H) 7.03 - 7.06 (m, 2 H, Ar-H) 7.12 (d, *J*=7.5 Hz, 1 H, Ar-H) 7.69 (d, *J*=2.8 Hz, 2 H, Ar-H) 8.02 (s, 2 H, N=CH)

$^{13}$C{$^1$H} NMR (400 MHz, $C_6D_6$) δ ppm 24.1 (CH-**C**H$_3$) 25.7 (CH-**C**H$_3$) 27.6 (CH-**C**H$_3$) 27.8 (CH-**C**H$_3$) 27.8 (CH-**C**H$_3$) 28.0 (CH-**C**H$_3$) 30.7 (C(**C**H$_3$)$_3$) 31.8 (C(**C**H$_3$)$_3$) 34.4 (**C**(CH$_3$)$_3$) 36.0 (**C**(CH$_3$)$_3$) 70.2 (**C**H-CH$_3$) 71.5 (**C**H-CH$_3$) 72.3 (**C**H-CH$_3$) 72.8 (**C**H-CH$_3$) 123.0 (Ar-H) 125.4 (Ar-H) 127.4 (Ar-C) 128.3 (Ar-H) 128.5 (Ar-C) 130.3 (Ar-H) 131.4 (Ar-C) 139.2 (Ar-C) 139.7 (Ar-C) 148.7 (Ar-N) 161.9 (Ar-O) 170.6 (N=CH)

$C_{54}H_{88}N_2O_8Zr_2$ Calculated: C 60.29 % H 8.25 % N 2.60 % Found: C 58.59 % H 8.53 % N 2.69 %

$Hf_2$(**13**)($O^iPr$)$_6$

**13**$H_2$ (0.50 g, 0.92 mmol) was dissolved in toluene (20 mL) with $Hf(O^iPr)_4.{}^iPrOH$ (0.77 g, 1.85 mmol) and stirred at 60 °C for 16 hours. The solvent was removed under vacuum and the orange solid redissolved in hexane (10 mL). The solution was concentrated to produce a precipitate which was filtered and dried under vacuum (0.29 g, 0.23 mmol, 25 %).

$^1$H NMR (400 MHz, $CDCl_3$) δ ppm 0.91 (d, *J*=6.8 Hz, 6 H, CH-C**H**$_3$) 0.98 (d, *J*=6.0 Hz, 6 H, CH-C**H**$_3$) 1.06 (d, *J*=6.0 Hz, 6 H, CH-C**H**$_3$) 1.27 (br. s, 9 H CH-C**H**$_3$) 1.28 (s, 18 H, C(CH$_3$)$_3$) 1.29 (br. s, 9 H, CH-C**H**$_3$) 1.51 (s, 18 H, C(CH$_3$)$_3$) 4.31 (spt, *J*=6.0 Hz, 2 H, C**H**-CH$_3$) 4.59 (spt, *J*=6.0 Hz, 2 H, C**H**-CH$_3$) 4.72 (m, *J*=6.5 Hz, 1 H, C**H**-CH$_3$) 4.83 (m, *J*=6.5 Hz, 1 H, C**H**-CH$_3$) 6.97 - 7.02 (m, 4 H, Ar-H) 7.26 - 7.29 (m, 2 H, Ar-H) 7.52 (d, *J*=2.5 Hz, 2 H, Ar-H) 7.98 (s, 2 H, N=CH)

$^{13}$C{$^1$H} NMR (400 MHz, $CDCl_3$) δ ppm 23.0 (CH-**C**H$_3$) 24.7 (CH-**C**H$_3$) 27.2 (CH-**C**H$_3$) 27.2 (CH-**C**H$_3$) 27.3 (CH-**C**H$_3$) 27.5 (CH-**C**H$_3$) 30.0 (C(**C**H$_3$)$_3$) 31.4 (C(**C**H$_3$)$_3$) 34.0 (**C**(CH$_3$)$_3$) 35.2 (**C**(CH$_3$)$_3$) 69.1 (**C**H-CH$_3$) 70.3 (**C**H-CH$_3$) 70.9 (**C**H-CH$_3$) 71.9 (**C**H-CH$_3$) 122.3 (Ar-C) 124.9 (Ar-H) 126.7 (Ar-H) 129.3 (Ar-H) 130.8 (Ar-H) 138.3 (Ar-C) 139.3 (Ar-C) 147.8 (Ar-N) 161.3 (Ar-O) 170.1 (N=CH)

$C_{54}H_{88}N_2O_8Hf_2$ Calculated: C 51.88 % H 7.09 % N 2.24 % Found: C 50.17 % H 7.22 % N 2.49 %

Zr(**13**)($O^tBu$)$_2$

**13**$H_2$ (0.50 g, 0.92 mmol) was dissolved in 20 mL toluene with zirconium *tert*-butoxide (0.35 g, 0.92 mmol). Solvent was removed and the crude orange solid used without further purification (0.69 g, 0.88 mmol, 97 %).

Two isomers present in solution, data presented for most abundant isomer.

$^1$H NMR (400 MHz, $CDCl_3$) δ ppm 0.66 (s, 18 H, $C(CH_3)_3$) 1.34 (s, 18 H, $C(CH_3)_3$) 1.51 (s, 18 H, $OC(CH_3)_3$) 7.24 (d, *J*=2.8 Hz, 2H, Ar-H) 7.34 (ddd, *J*=6.0, 3.3, 1.3 Hz, 4 H, Ar-H) 7.56 (d, 2H, *J*=2.8 Hz) 8.56 (s, 2 H, N=CH)

$^{13}$C{$^1$H} NMR (400 MHz, $CDCl_3$) δ ppm 29.6 ($C(\mathbf{C}H_3)_3$) 31.4 ($C(\mathbf{C}H_3)_3$) 32.2 ($OC(\mathbf{C}H_3)_3$) 34.0 ($\mathbf{C}(CH_3)_3$) 35.5 ($\mathbf{C}(CH_3)_3$) 72.9 ($O\mathbf{C}(CH_3)_3$) 116.9 (Ar-H) 122.9 (Ar-C) 127.5 (Ar-H) 127.9 (Ar-H) 129.6 (Ar-H) 131.9 (Ar-H) 137.9 (Ar-C) 139.2 (Ar-C) 143.4 (Ar-N) 162.7 (N=CH) 164.8 (Ar-O)

$C_{44}H_{64}N_2O_2Zr$ Calculated: C 68.08 % H 8.31 % N 3.61 % Found: C 67.99 % H 8.82 % N 3.66 %

$Al_2$(**16**)$_2Me_2$

**16**$H_2$ (0.34 g, 0.85 mmol) was dissolved in 10 mL toluene and trimethylaluminium solution (2 M, 0.42 mL, 0.85 mmol) was added slowly. The solution turned from yellow to a dark, vivid purple. The solvent was removed under vacuum and hexane added (20 mL). The resulting precipitate was filtered and dried under vacuum (0.17 g, 0.19 mmol, 44 %).

Several species present, data selected for main species.

$^1$H NMR (400 MHz, $C_6D_6$) δ ppm -0.47 (s, 6 H, $Al(CH_3)_2$) 1.19 (s, 18 H, $C(CH_3)_3$) 1.24 (s, 18 H, $C(CH_3)_3$) 6.50 - 6.56 (m, 3 H, Ar-H) 6.62 (d, *J*=2.26 Hz, 3 H, Ar-H) 6.71 (d, *J*=8.28 Hz, 2 H, Ar-H) 6.86 - 6.95 (m, 6 H, Ar-H) 7.02 (d, *J*=7.28 Hz, 3 H, Ar-H) 7.13 (d, *J*=8.53 Hz, 3 H, Ar-H) 7.33 (d, *J*=2.26 Hz, 2 H, Ar-H) 8.21 (s, 2 H, N=CH)

Satisfactory elemental analysis data could not be obtained for this compound, most likely due to the high sensitivity of the complex to air and moisture.

$Al_2$(**17**)$_2Me_2$

**17**$H_2$ (0.30 g, 0.84 mmol) was dissolved in 20 mL toluene and trimethylaluminium solution (2 M, 0.42 mL, 0.84 mmol) was added slowly. The solution turned from yellow to a dark, inky blue. The solvent was removed under vacuum and the crude powder was used for analysis and polymerisation (0.26 g, 0.33 mmol, 80 %).

$^1$H NMR (400 MHz, $C_6D_6$) δ ppm -0.22 (s, 6 H, $Al(CH_3)_2$) 6.26 (d, *J*=2.5 Hz, 2 H, Ar-H) 6.31 (ddd, *J*=8.0, 6.8, 1.6 Hz, 2 H, Ar-H) 6.46 (dd, *J*=8.2, 1.4 Hz, 2 H, Ar-H) 6.67 - 6.71 (m, 5 H, Ar-H) 6.74 (dd, *J*=8.5, 1.3 Hz, 2 H, Ar-H) 6.83 (ddd, *J*=8.5, 7.0, 1.4 Hz, 2 H, Ar-H) 6.88 (tt, *J*=7.4, 1.2 Hz, 2 H, Ar-H) 7.03 (t, *J*=7.8 Hz, 5 H, Ar-H) 7.20 (s, 2 H, N=CH)

$^{13}$C{$^1$H} NMR (400 MHz, $C_6D_6$) δ ppm 112.9 (Ar-H) 114.3 (Ar-H) 116.3 (Ar-H) 123.2 (Ar-H) 125.5 (Ar-H) 126.0 (Ar-C) 127.0 (Ar-H) 127.6 (Ar-H) 128.9 (Ar-H) 129.7 (Ar-H) 129.8 (Ar-H) 130.2 (Ar-H) 130.3 (Ar-H) 132.5 (Ar-Cl) 134.6 (Ar-Cl) 138.2 (Ar-N) 146.6 (Ar-N) 151.7 (Ar-N) 152.1 (Ar-O) 155.7 (N=CH)

Satisfactory elemental analysis data could not be obtained for this compound, most likely due to the high sensitivity of the complex to air and moisture.

Al(**19**)$Me_2$

**19**H (0.44 g, 1.54 mmol) was dissolved in toluene (20 mL) then trimethylaluminium solution (2 M, 0.77 mL, 1.54 mmol) was added slowly. The solution turned from green/grey to yellow. The resulting crystals were filtered and dried under vacuum (0.16 g, 0.46 mmol, 30 %).

$^1$H NMR (400 MHz, $d_8$-Tol) δ ppm -0.02 (s, 6 H, $Al(CH_3)_2$) 6.20 (t, *J*=7.7 Hz, 1 H, Ar-H) 6.37 (d, *J*=8.0 Hz, 2 H, Ar-H) 6.66 (d, *J*=8.3 Hz, 1 H, Ar-H) 6.61 (d, *J*=8.3 Hz, 1 H, Ar-H) 6.89 - 6.96 (m, 3 H, Ar-H) 6.96 - 7.12 (m, 5 H, Ar-H) 7.22 (d, *J*=8.3 Hz, 1 H, Ar-H) 7.84 (d, *J*=8.3 Hz, 1 H, Ar-H)

$^{13}$C{$^1$H} NMR (400 MHz, $d_8$-Tol) δ ppm -9.1 ($Al(CH_3)_2$) 111.2 (Ar-H) 112.2 (Ar-H) 116.3 (Ar-H) 116.7 (Ar-H) 123.6 (Ar-H) 124.7 (Ar-H) 125.2 (Ar-H) 127.6 (Ar-H) 129.6 (Ar-H) 130.3 (Ar-H) 134.1 (Ar-C) 136.0 (Ar-H) 136.6 (Ar-N) 136.9 (Ar-N) 151.6 (Ar-O) 164.5 (C=N)

$C_{21}H_{19}N_2OAl$ Calculated: C 73.67 % H 5.59 % N 8.18 % Found: C 73.51 % H 5.65 % N 8.08 %

Al(**20**)Me

**20**$H_2$ (0.50 g, 0.90 mmol) was dissolved in 20 mL toluene and 2 M trimethylaluminium solution (0.44 mL, 0.90 mmol) was added slowly. The solution was stirred for 2 hours, then solvent

removed. The solid was redissolved in 20 mL hexane. The resulting crystals were filtered to yield a yellow solid (0.29 g, 0.49 mmol, 54 %).

$^{1}$H NMR (400 MHz, $C_6D_6$) δ ppm -0.30 (s, 3 H, Al-$CH_3$) 1.37 (s, 9 H, C($CH_3$)$_3$) 1.45 (s, 9 H, C($CH_3$)$_3$) 1.76 (s, 9 H, C($CH_3$)$_3$) 1.81 (s, 9 H, C($CH_3$)$_3$) 2.26 (s, 3 H, N-$CH_3$) 3.00 (d, *J*=12.1 Hz, 1 H, CH) 4.13 (d, *J*=12.1 Hz, 1 H, CH) 6.36 (d, *J*=8.0 Hz, 1 H, Ar-H) 6.79 - 6.85 (m, 2 H, Ar-H) 6.94 (d, *J*=2.8 Hz, 3 H, Ar-H) 7.60 (d, *J*=2.5 Hz, 1 H, Ar-H) 7.81 (d, *J*=2.5 Hz, 1 H, Ar-H) 7.90 (s, 1 H, N=CH)

$^{13}$C{$^{1}$H} NMR (400 MHz, $C_6D_6$) δ ppm 30.7 (C(**C**$H_3$)$_3$) 30.8 (C(**C**$H_3$)$_3$) 31.8 (C(**C**$H_3$)$_3$) 32.5 (C(**C**$H_3$)$_3$) 34.6 (**C**($CH_3$)$_3$) 34.7 (**C**($CH_3$)$_3$) 36.0 (**C**($CH_3$)$_3$) 36.2 (**C**($CH_3$)$_3$) 41.1 (N-$CH_3$) 66.1 ($CH_2$) 119.3 (Ar-H) 119.8 (Ar-C) 121.0 (Ar-H) 123.3 (Ar-C) 124.7 (Ar-H) 124.7 (Ar-H) 127.5(Ar-H) 128.3 (Ar-H) 128.8 (Ar-H) 133.7 (Ar-H) 138.4 (Ar-C) 139.0 (Ar-C) 139.1 (Ar-C) 141.4 (Ar-C) 142.2 (Ar-N) 145.9 (Ar-N) 157.8 (Ar-O) 166.4 (N=CH) 168.3 (Ar-O)

$C_{38}H_{53}N_2O_2Al$ Calculated: C 76.47 % H 8.95 % N 4.69 % Found: C 76.25 % H 9.08 % N 4.60 %

Zr(**20**)(O$^{i}$Pr)$_2$

**20**$H_2$ (0.83 g, 1.49 mmol) was dissolved in 40 mL hexane and 10 mL toluene with zirconium isoproxide isopropanol complex (0.58 g, 1.49 mmol). The solution was stirred at 60 °C for 6 hours. The solution was concentrated by removal of solvent and the resulting crystals filtered (0.33 g, 0.43 mmol, 29 %).

$^{1}$H NMR (400 MHz, $CDCl_3$) δ ppm 0.69 (d, *J*=5.8 Hz, 3 H, CH-C**H**$_3$) 0.87 (d, *J*=6.0 Hz, 3 H, CH-C**H**$_3$) 1.09 (s, 9 H, C($CH_3$)$_3$) 1.11 (s, 9 H, C($CH_3$)$_3$) 1.29 (br. s, 6 H, CH-C**H**$_3$) 1.32 (s, 9 H, C($CH_3$)$_3$) 1.55 (s, 9 H, C($CH_3$)$_3$) 3.32 (s, 3 H, N-$CH_3$) 3.78 (d, *J*=12.1 Hz, 1 H, $CH_2$) 3.92 (quin, *J*=12.0 Hz, 1 H, C**H**-$CH_3$) 4.52 (quin, *J*=12.0 Hz, 1 H, C**H**-$CH_3$) 4.69 (d, *J*=12.1 Hz, 1 H, $CH_2$) 6.51 (d, *J*=2.0 Hz, 1 H, Ar-H) 6.96 (d, *J*=2.3 Hz, 1 H, Ar-H) 7.11 (d, *J*=2.3 Hz, 1 H, Ar-H) 7.14 - 7.21 (m, 1 H, Ar-H) 7.27 (t, *J*=1.0 Hz, 1 H, Ar-H) 7.37 (d, *J*=8.0 Hz, 1 H, Ar-H) 7.47 (d, *J*=7.8 Hz, 1 H, Ar-H) 7.53 (d, *J*=2.3 Hz, 1 H, Ar-H) 8.52 (s, 1 H, N=CH)

$^{13}$C{$^{1}$H} NMR (400 MHz, $CDCl_3$) δ ppm 26.5 (CH-**C**$H_3$) 26.7 (CH-**C**$H_3$) 27.3 (CH-**C**$H_3$) 27.3 (CH-**C**$H_3$) 29.5 (C(**C**$H_3$)$_3$) 29.6 (C(**C**$H_3$)$_3$) 31.4 (C(**C**$H_3$)$_3$) 31.6 (C(**C**$H_3$)$_3$) 33.7 (**C**($CH_3$)$_3$) 34.1 (**C**($CH_3$)$_3$) 34.6 (**C**($CH_3$)$_3$) 35.3 (**C**($CH_3$)$_3$) 48.8 (N-$CH_3$) 67.1 ($CH_2$) 69.8 (**C**H-$CH_3$) 70.8 (**C**H-$CH_3$) 116.3 (Ar-H) 122.0 (Ar-C) 122.7 (Ar-C) 123.2 (Ar-H) 123.4 (Ar-H) 124.7 (Ar-H) 127.6 (Ar-H) 127.9 (Ar-H) 129.7 (Ar-H) 131.0 (Ar-H) 135.8 (Ar-C) 136.5 (Ar-C) 138.7 (Ar-C) 139.1 (Ar-C) 144.5 (Ar-N) 144.8 (Ar-N) 160.1 (Ar-O) 161.2 (Ar-O) 161.9 (N=CH)

$C_{43}H_{64}N_2O_4Zr$ Calculated: C 67.58 % H 8.44 % N 3.67 % Found: C 67.44 % H 8.57 % N 3.56 %

Hf(**20**)($O^iPr$)$_2$

**20**$H_2$ (0.30 g, 0.54 mmol) was dissolved in toluene (20 mL) with $Hf(O^iPr)_4.{}^iPrOH$ (0.26 g, 0.54 mmol) and stirred. The solvent was removed *in vacuo* and the solid recrystallised in hexane (20 mL). The resulting orange crystals were filtered and dried (0.13 g, 0.16 mmol, 29 %).

$^1$H NMR (400 MHz, $CDCl_3$) δ ppm 0.70 (d, *J*=6.0 Hz, 3 H, CH-C**H**$_3$) 0.85 (d, *J*=6.0 Hz, 3 H, CH-C**H**$_3$) 1.07 (s, 9 H, C($CH_3$)$_3$) 1.09 (s, 9 H, C($CH_3$)$_3$) 1.29 (d, *J*=6.0 Hz, 6 H, CH-C**H**$_3$) 1.32 (s, 9 H, C($CH_3$)$_3$) 1.55 (s, 9 H, C($CH_3$)$_3$) 3.35 (s, 3 H, N-$CH_3$) 3.77 (d, *J*=12.3 Hz, 1 H, $CH_2$) 3.99 (spt, *J*=11.9 Hz, 1 H, C**H**-$CH_3$) 4.62 (spt, *J*=12.1 Hz, 1 H, C**H**-$CH_3$) 4.78 (d, *J*=12.1 Hz, 1 H, $CH_2$) 6.48 (d, *J*=2.5 Hz, 1 H, Ar-H) 6.97 (d, *J*=2.51 Hz, 1 H, Ar-H) 7.11 (d, *J*=2.5 Hz, 1 H, Ar-H) 7.14 - 7.21 (m, 1 H, Ar-H) 7.24 - 7.30 (m, 1 H, Ar-H) 7.38 (d, *J*=7.8 Hz, 1 H, Ar-H) 7.47 (dd, *J*=8.0, 1.3 Hz, 1 H, Ar-H) 7.57 (d, *J*=2.5 Hz, 1 H, Ar-H) 8.52 (s, 1 H, N=CH)

$^{13}$C{$^1$H} NMR (400 MHz, $CDCl_3$) δ ppm 26.7 (CH-**C**$H_3$) 26.9 (CH-**C**$H_3$) 27.5 (CH-**C**$H_3$) 27.5 (CH-**C**$H_3$) 29.5 (C(**C**$H_3$)$_3$) 29.6 (C(**C**$H_3$)$_3$) 31.4 (C(**C**$H_3$)$_3$) 31.6 (C(**C**$H_3$)$_3$) 33.7 (**C**($CH_3$)$_3$) 34.0 (**C**($CH_3$)$_3$) 34.6 (**C**($CH_3$)$_3$) 35.3 (**C**($CH_3$)$_3$) 49.4 (N-$CH_3$) 67.1 ($CH_2$) 69.5 (**C**H-$CH_3$) 70.5 (**C**H-$CH_3$) 116.2 (Ar-H) 121.9 (Ar-C) 122.9 (Ar-C) 123.5 (Ar-H) 123.5 (Ar-H) 124.7 (Ar-H) 127.9 (Ar-H) 128.0 (Ar-H) 129.7 (Ar-H) 131.3 (Ar-H) 136.3 (Ar-C) 136.4 (Ar-C) 139.2 (Ar-C) 139.3 (Ar-C) 144.4 (Ar-N) 144.6 (Ar-N) 160.4 (Ar-O) 161.6 (Ar-O) 161.9 (N=CH)

$C_{43}H_{64}N_2O_4Hf$ Calculated: C 60.66 % H 7.58 % N 3.29 % Found: C 60.79 % H 7.72 % N 3.42 %

Zr(**20**)($O^tBu$)$_2$

**20**$H_2$ (0.50 g, 0.90 mmol) was dissolved in 10 mL toluene with zirconium *tert*-butoxide (0.34 g, 0.90 mmol). The solution was concentrated under vacuum and stored overnight at 0 °C. The resulting yellow crystals were filtered and dried under vacuum (0.15 g, 0.19 mmol, 21 %).

$^1$H NMR (400 MHz, $C_6D_6$) δ ppm 1.05 (s, 9 H, C($CH_3$)$_3$) 1.23 (s, 9 H, C($CH_3$)$_3$) 1.32 (s, 9 H, C($CH_3$)$_3$) 1.39 (s, 9 H, C($CH_3$)$_3$) 1.63 (s, 9 H, OC($CH_3$)$_3$) 1.82 (s, 9 H, OC($CH_3$)$_3$) 3.16 (s, 3 H, N-$CH_3$) 3.33 (d, *J*=12.1 Hz, 1 H, $CH_2$) 4.71 (d, *J*=12.1 Hz, 1 H, $CH_2$) 6.49 - 6.58 (m, 2 H, Ar-H) 6.69 (t, *J*=7.5 Hz, 1 H, Ar-H) 6.83 - 6.93 (m, 2 H, Ar-H) 6.98 - 7.08 (m, 1 H, Ar-H) 7.28 (s, 1 H, Ar-H) 7.71 - 7.76 (m, 1 H, Ar-H) 8.03 (s, 1 H, N=CH)

$^{13}$C{$^1$H} NMR (400 MHz, $C_6D_6$) δ ppm 30.4 (C(**C**$H_3$)$_3$) 30.4 (C(**C**$H_3$)$_3$) 31.9 (C(**C**$H_3$)$_3$) 32.4 (C(**C**$H_3$)$_3$) 33.0 (C(**C**$H_3$)$_3$) 33.8 (C(**C**$H_3$)$_3$) 34.4 (**C**($CH_3$)$_3$) 34.6 (**C**($CH_3$)$_3$) 35.5 (**C**($CH_3$)$_3$) 36.2 (**C**($CH_3$)$_3$) 50.2 ($CH_3$) 68.0 ($CH_2$) 74.9 (O**C**($CH_3$)$_3$) 75.8 (O**C**($CH_3$)$_3$) 117.1 (Ar-H) 122.8 (Ar-C) 123.6 (Ar-H) 123.9 (Ar-C) 124.4 (Ar-H) 125.3 (Ar-H) 128.0 (Ar-H) 128.3 (Ar-H) 130.8 (Ar-H) 131.6 (Ar-H) 136.6 (Ar-C)

137.0 (Ar-C) 139.5 (Ar-C) 139.7 (Ar-C) 145.2 (Ar-N) 145.6 (Ar-N) 161.7 (Ar-O) 162.2 (Ar-O) 162.4 (N=CH)

$C_{45}H_{68}N_2O_4Zr$ Calculated: C 68.22 % H 8.65 % N 3.54 % Found: C 68.08 % H 8.47 % N 3.42 %

Al(**21**)Me

**21**$H_2$ (0.50 g, 0.87 mmol) was dissolved in 20 mL hexane and trimethylaluminium (2 M, 0.43 mL, 0.87 mmol) was slowly added. A white precipitate formed, which was filtered and dried under vacuum. Yield 0.27 g, 0.43 mmol, 50 %.

$^1$H NMR (400 MHz, $C_6D_6$) δ ppm -0.37 (s, 3 H, Al-$CH_3$) 1.47 (s, 18 H, C($CH_3$)$_3$) 1.84 (s, 18 H, C($CH_3$)$_3$) 2.20 (s, 6 H, N-$CH_3$) 3.39 (d, *J*=12.8 Hz, 2 H, $CH_2$) 4.15 (d, *J*=12.8 Hz, 2 H, $CH_2$) 6.62 - 6.71 (m, 2 H, Ar-H) 6.81 (dd, *J*=6.0, 3.3 Hz, 2 H, Ar-H) 6.92 (s, 2 H, Ar-H) 7.64 (s, 2 H, Ar-H)

$^{13}$C{$^1$H} NMR (400 MHz, $C_6D_6$) δ ppm 30.6 (N-$CH_3$) 30.8 (C(**C**H$_3$)$_3$) 32.6 (C(**C**H$_3$)$_3$) 34.7 (**C**(CH$_3$)$_3$) 36.0 (**C**(CH$_3$)$_3$) 66.2 ($CH_2$) 66.7 ($CH_2$) 118.7 (Ar-C) 120.7 (Ar-C) 122.1 (Ar-C) 122.6 (Ar-H) 123.4 (Ar-H) 124.2 (Ar-H) 125.0 (Ar-H) 128.3 (Ar-C) 128.5 (Ar-H) 128.9 (Ar-H) 137.7 (Ar-C) 138.0 (Ar-C) 138.7 (Ar-N) 146.1 (Ar-N)

$C_{39}H_{57}N_2O_2Al$ Calculated: C 76.43 % H 9.37 % N 4.57 % Found: C 76.40 % H 9.47 % N 4.64 %

# 6. Appendix

## 6.1 DOSY NMR data

**Table 6.01: Diffusion coefficients ($m^2s^{-1}$) for the DOSY NMR spectrum of Zr(13)($O^tBu)_2$ in $CDCl_3$ from section 4.3.1 on page 136**

| Peak name | F2 [ppm] | D [m2/s] | error |
|---|---|---|---|
| 1 | 8.570 | 6.02e-10 | 3.218e-12 |
| 2 | 8.339 | 5.00e-10 | 9.280e-12 |
| 3 | 8.247 | 4.61e-10 | 2.400e-11 |
| 4 | 7.534 | 6.00e-10 | 3.375e-12 |
| 5 | 7.363 | 5.84e-10 | 5.912e-12 |
| 6 | 7.219 | 5.69e-10 | 1.504e-11 |
| 7 | 7.030 | 4.01e-10 | 1.941e-11 |
| 8 | 6.877 | 4.78e-10 | 3.588e-12 |
| 9 | 0.089 | 8.09e-11 | 3.573e-12 |
| 10 | 0.648 | 6.04e-10 | 2.639e-12 |
| 11 | 0.875 | 6.03e-10 | 1.719e-11 |
| 12 | 1.482 | 6.05e-10 | 2.724e-12 |
| 13 | 1.347 | 6.18e-10 | 1.621e-11 |
| 14 | 1.185 | 4.91e-10 | 9.693e-12 |

## 6.2 Crystal data tables

Pages 210-234 contain crystal data and structure refinement for all solid-state crystal structures in this thesis, in order of appearance.

Crystal data and structure refinement for $Al_2$(**1**)$Me_4$.

| | |
|---|---|
| Identification code | k13mdj08 |
| Empirical formula | C35 H36 Al2 N2 O2 |
| Formula weight | 570.62 |
| Temperature | 150(2) K |
| Wavelength | 0.71073 Å |
| Crystal system, space group | monoclinic, $P2_1/c$ |
| Unit cell dimensions | a = 9.0890(3) Å α = 90 °<br>b = 19.1017(7) Å β =93.941(2)°<br>c = 9.1614(3) Å γ = 90 ° |
| Volume | 1586.80(9) $Å^3$ |
| Z, Calculated density | 2, 1.194 $Mg/m^3$ |
| Absorption coefficient | 0.124 $mm^{-1}$ |
| F(000) | 604 |
| Crystal size | 0.10 x 0.10 x 0.05 mm |
| Theta range for data collection | 3.08 to 25.06 ° |
| Limiting indices | -10<=h<=10, -22<=k<=22, -10<=l<=10 |
| Reflections collected / unique | 16164 / 2803 [R(int) = 0.0820] |
| Completeness to theta = 25.06 | 99.7 % |
| Max. and min. transmission | 0.9938 and 0.9877 |
| Refinement method | Full-matrix least-squares on $F^2$ |
| Data / restraints / parameters | 2803 / 0 / 219 |
| Goodness-of-fit on $F^2$ | 1.029 |
| Final R indices [I>2sigma(I)] | $R_1$ = 0.0622, $wR_2$ = 0.1401 |
| R indices (all data) | $R_1$ = 0.0969, $wR_2$ = 0.1595 |
| Largest diff. peak and hole | 0.640 and -0.310 e.$Å^{-3}$ |

Crystal data and structure refinement for $Al_2$(**2**)$Me_4$.

| | |
|---|---|
| Identification code | k13mdj11 |
| Empirical formula | C29 H38 Al N O |
| Formula weight | 443.58 |
| Temperature | 150(2) K |
| Wavelength | 0.71073 Å |
| Crystal system, space group | Monoclinic, $P2_1/a$ |
| Unit cell dimensions | a = 14.1650(3) Å α = 90 °<br>b = 13.0700(3) Å β = 101.7450(10) °<br>c = 14.7260(4) Å γ = 90 ° |
| Volume | 2669.24(11) $Å^3$ |
| Z, Calculated density | 4, 1.104 $Mg/m^3$ |
| Absorption coefficient | 0.096 $mm^{-1}$ |
| F(000) | 960 |
| Crystal size | 0.10 x 0.10 x 0.05 mm |
| Theta range for data collection | 3.61 to 25.02 ° |
| Limiting indices | -16<=h<=16, -15<=k<=15, -17<=l<=16 |
| Reflections collected / unique | 23401 / 4696 [R(int) = 0.0746] |
| Completeness to theta = 25.02 | 99.6 % |
| Max. and min. transmission | 0.9952 and 0.9905 |
| Refinement method | Full-matrix least-squares on $F^2$ |
| Data / restraints / parameters | 4696 / 0 / 298 |
| Goodness-of-fit on $F^2$ | 1.034 |
| Final R indices [I>2sigma(I)] | $R_1$ = 0.0562, $wR_2$ = 0.1340 |
| R indices (all data) | $R_1$ = 0.0869, $wR_2$ = 0.1518 |
| Largest diff. peak and hole | 0.618 and -0.270 e.$Å^{-3}$ |

Crystal data and structure refinement for Al(**4**)$Me_2$.

| | |
|---|---|
| Identification code | k13mdj13 |
| Empirical formula | C19 H16 Al Cl2 N O |
| Formula weight | 372.21 |
| Temperature | 150(2) K |
| Wavelength | 0.71073 Å |
| Crystal system, space group | Monoclinic, $P2_1/n$ |
| Unit cell dimensions | a = 7.14900(10) Å α = 90 °<br>b = 22.3190(3) Å β = 97.6340(10) °<br>c = 22.6950(4) Å γ = 90 ° |
| Volume | 3589.09(9) $Å^3$ |
| Z, Calculated density | 8, 1.378 $Mg/m^3$ |
| Absorption coefficient | 0.416 $mm^{-1}$ |
| F(000) | 1536 |
| Crystal size | 0.40 x 0.10 x 0.05 mm |
| Theta range for data collection | 3.62 to 25.04 ° |
| Limiting indices | -8<=h<=8, -26<=k<=26, -5<=l<=26 |
| Reflections collected / unique | 6296 / 6296 [R(int) = 0.0000] |
| Completeness to theta = 25.04 | 98.9 % |
| Max. and min. transmission | 0.9795 and 0.8513 |
| Refinement method | Full-matrix least-squares on $F^2$ |
| Data / restraints / parameters | 6296 / 0 / 438 |
| Goodness-of-fit on $F^2$ | 1.141 |
| Final R indices [I>2sigma(I)] | $R_1$ = 0.1419, $wR_2$ = 0.3520 |
| R indices (all data) | $R_1$ = 0.1621, $wR_2$ = 0.3607 |
| Largest diff. peak and hole | 1.015 and -1.217 e.$Å^{-3}$ |

Crystal data and structure refinement for Al(**6**)$Me_2$.

| | |
|---|---|
| Identification code | k13mdj14 |
| Empirical formula | C19 H18 Al N O |
| Formula weight | 303.32 |
| Temperature | 150(2) K |
| Wavelength | 0.71073 Å |
| Crystal system, space group | Monoclinic, *C*2/*c* |
| Unit cell dimensions | a = 14.2070(2) Å α = 90 °<br>b = 7.01600(10) Å β = 97.5650(10) °<br>c = 32.8480(6) Å γ = 90 ° |
| Volume | 3245.67(9) $Å^3$ |
| Z, Calculated density | 8, 1.241 $Mg/m^3$ |
| Absorption coefficient | 0.126 $mm^{-1}$ |
| F(000) | 1280 |
| Crystal size | 0.20 x 0.10 x 0.05 mm |
| Theta range for data collection | 3.55 to 27.44 ° |
| Limiting indices | -17<=h<=18, -9<=k<=9, -42<=l<=42 |
| Reflections collected / unique | 22280 / 3673 [R(int) = 0.0583] |
| Completeness to theta = 27.44 | 99.2 % |
| Max. and min. transmission | 0.9937 and 0.9753 |
| Refinement method | Full-matrix least-squares on $F^2$ |
| Data / restraints / parameters | 3673 / 0 / 201 |
| Goodness-of-fit on $F^2$ | 1.017 |
| Final R indices [I>2sigma(I)] | $R_1$ = 0.0430, $wR_2$ = 0.0981 |
| R indices (all data) | $R_1$ = 0.0709, $wR_2$ = 0.1117 |
| Largest diff. peak and hole | 0.245 and -0.249 e.$Å^{-3}$ |

Crystal data and structure refinement for **8**H.

| | |
|---|---|
| Identification code | e14mdj09 |
| Empirical formula | C78 H126 N6 O9 |
| Formula weight | 1291.85 |
| Temperature | 150(2) K |
| Wavelength | 0.71073 Å |
| Crystal system, space group | Monoclinic, $P2_1$ |
| Unit cell dimensions | a = 13.343(3) Å α = 90.0 °<br>b = 21.8390(16) Å β = 113.37(3) °<br>c = 14.986(4) Å γ = 90.0 ° |
| Volume | 4009(1) $Å^3$ |
| Z, Calculated density | 2, 1.070 $Mg/m^3$ |
| Absorption coefficient | 0.069 $mm^{-1}$ |
| F(000) | 1416 |
| Crystal size | 0.30 x 0.20 x 0.20 mm |
| Theta range for data collection | 3.58 to 26.37 ° |
| Limiting indices | -16<=h<=16, -25<=k<=27, -18<=l<=18 |
| Reflections collected / unique | 34693 / 14694 [R(int) = 0.0441] |
| Completeness to theta = 26.37 | 99.7 % |
| Max. and min. transmission | 0.9863 and 0.9796 |
| Refinement method | Full-matrix least-squares on $F^2$ |
| Data / restraints / parameters | 14694 / 1 / 919 |
| Goodness-of-fit on $F^2$ | 0.968 |
| Final R indices [I>2sigma(I)] | $R_1$ = 0.0500, $wR_2$ = 0.0766 |
| R indices (all data) | $R_1$ = 0.0932, $wR_2$ = 0.0882 |
| Absolute structure parameter | 0.7(7) |
| Largest diff. peak and hole | 0.168 and -0.184 e.$Å^{-3}$ |

Crystal data and structure refinement for **11**H.

| | |
|---|---|
| Identification code | s14mdj11 |
| Empirical formula | C21 H24 Cl2 N2 O |
| Formula weight | 391.32 |
| Temperature | 150(2) K |
| Wavelength | 1.54184 Å |
| Crystal system, space group | Triclinic, *P*-1 |
| Unit cell dimensions | a = 9.1107(5) Å α = 114.741(5) °<br>b = 11.4778(6) Å β = 109.741(5) °<br>c = 11.4950(6) Å γ = 92.704(4) ° |
| Volume | 1002.24(9) $Å^3$ |
| Z, Calculated density | 2,1.297 $Mg/m^3$ |
| Absorption coefficient | 3.000 $mm^{-1}$ |
| F(000) | 412 |
| Crystal size | 0.20 x 0.20 x 0.20 mm |
| Theta range for data collection | 4.35 to 71.95 ° |
| Limiting indices | -11<=h<=10, -11<=k<=14, -14<=l<=14 |
| Reflections collected / unique | 9249 / 3925 [R(int) = 0.0443] |
| Completeness to theta = 71.95 | 99.6 % |
| Absorption correction | None |
| Max. and min. transmission | 0.5853 and 0.5853 |
| Refinement method | Full-matrix least-squares on $F^2$ |
| Data / restraints / parameters | 3925 / 0 / 237 |
| Goodness-of-fit on $F^2$ | 1.040 |
| Final R indices [I>2sigma(I)] | $R_1$ = 0.0497, $wR_2$ = 0.1289 |
| R indices (all data) | $R_1$ = 0.0537, $wR_2$ = 0.1360 |
| Largest diff. peak and hole | 0.281 and -0.342 $e.Å^{-3}$ |

Crystal data and structure refinement for Al(**8**)$Me_2$.

| | |
|---|---|
| Identification code | k14mdj01 |
| Empirical formula | C28 H47 Al N2 O3 |
| Formula weight | 486.66 |
| Temperature | 150(2) K |
| Wavelength | 0.71073 Å |
| Crystal system, space group | Triclinic, *P*-1 |
| Unit cell dimensions | a = 10.9020(2) Å α = 68.800(1) °<br>b = 12.2590(2) Å β = 74.207(1) °<br>c = 12.6270(2) Å γ = 76.837(1) ° |
| Volume | 1498.16(4) $Å^3$ |
| Z, Calculated density | 2, 1.079 $Mg/m^3$ |
| Absorption coefficient | 0.096 $mm^{-1}$ |
| F(000) | 532 |
| Crystal size | 0.40 x 0.30 x 0.10 mm |
| Theta range for data collection | 3.54 to 27.64 ° |
| Limiting indices | -14<=h<=14, -15<=k<=15, -12<=l<=16 |
| Reflections collected / unique | 6849 / 6849 [R(int) = 0.0000] |
| Completeness to theta = 27.64 | 98.1 % |
| Absorption correction | Semi-empirical from equivalents |
| Max. and min. transmission | 0.9905 and 0.9627 |
| Refinement method | Full-matrix least-squares on $F^2$ |
| Data / restraints / parameters | 6849 / 0 / 324 |
| Goodness-of-fit on $F^2$ | 1.145 |
| Final R indices [I>2sigma(I)] | $R_1$ = 0.0844, $wR_2$ = 0.2271 |
| R indices (all data) | $R_1$ = 0.1026, $wR_2$ = 0.2360 |
| Extinction coefficient | 0.056(6) |
| Largest diff. peak and hole | 0.773 and -0.547 $e.Å^{-3}$ |

Crystal data and structure refinement for Al(**7**)$_2$Me.

| | | |
|---|---|---|
| Identification code | K14MDJ02 | |
| Empirical formula | C44 H61 Al N4 O6 | |
| Formula weight | 768.94 | |
| Temperature | 150(2) K | |
| Wavelength | 0.71073 Å | |
| Crystal system | Monoclinic | |
| Space group | $P2_1/n$ | |
| Unit cell dimensions | a = 11.1370(2) Å | α = 90° |
| | b = 19.3770(2) Å | β =104.421(1)° |
| | c = 21.5440(4) Å | γ = 90° |
| Volume | 4502.74(13) Å$^3$ | |
| Z | 4 | |
| Density (calculated) | 1.134 Mg/m$^3$ | |
| Absorption coefficient | 0.093 mm$^{-1}$ | |
| F(000) | 1656 | |
| Crystal size | 0.200 x 0.150 x 0.100 mm$^3$ | |
| Theta range for data collection | 3.606 to 26.010° | |
| Index ranges | -13<=h<=13, -23<=k<=23, -26<=l<=26 | |
| Reflections collected | 45683 | |
| Independent reflections | 8835 [R(int) = 0.0686] | |
| Completeness to theta = 25.242° | 99.6 % | |
| Refinement method | Full-matrix least-squares on F$^2$ | |
| Data / restraints / parameters | 8835 / 0 / 551 | |
| Goodness-of-fit on F$^2$ | 1.018 | |
| Final R indices [I>2sigma(I)] | $R_1$ = 0.0438, $wR_2$ = 0.0960 | |
| R indices (all data) | $R_1$ = 0.0709, $wR_2$ = 0.1095 | |
| Extinction coefficient | n/a | |
| Largest diff. peak and hole | 0.175 and -0.233 e.Å$^{-3}$ | |

Crystal data and structure refinement for Al(**9**)$_2$Me.

| | |
|---|---|
| Identification code | k14mdj03 |
| Empirical formula | C44 H57 Al Cl4 N4 O6 |
| Formula weight | 906.72 |
| Temperature | 150(2) K |
| Wavelength | 0.71073 Å |
| Crystal system, space group | Orthorhombic, *Pcnn* |
| Unit cell dimensions | a = 11.90830(10) Å α = 90 °<br>b = 17.4722(2) Å β = 90 °<br>c = 22.2286(3) Å γ = 90 ° |
| Volume | 4624.98(9) Å$^3$ |
| Z, Calculated density | 4, 1.302 Mg/m$^3$ |
| Absorption coefficient | 0.325 mm$^{-1}$ |
| F(000) | 1912 |
| Crystal size | 0.20 x 0.10 x 0.10 mm |
| Theta range for data collection | 3.67 to 27.47 ° |
| Limiting indices | -15<=h<=15, -22<=k<=22, -28<=l<=28 |
| Reflections collected / unique | 78650 / 5295 [R(int) = 0.0748] |
| Completeness to theta = 27.47 | 99.7 % |
| Max. and min. transmission | 0.9682 and 0.9379 |
| Refinement method | Full-matrix least-squares on F$^2$ |
| Data / restraints / parameters | 5295 / 43 / 295 |
| Goodness-of-fit on F$^2$ | 1.022 |
| Final R indices [I>2sigma(I)] | $R_1$ = 0.0536, $wR_2$ = 0.1367 |
| R indices (all data) | $R_1$ = 0.0776, $wR_2$ = 0.1526 |
| Largest diff. peak and hole | 0.749 and -0.530 e.Å$^{-3}$ |

Crystal data and structure refinement for Al(**9**)$Me_2$.

| | |
|---|---|
| Identification code | h14mdj01 |
| Empirical formula | C20 H29 Al Cl2 N2 O3 |
| Formula weight | 443.33 |
| Temperature | 150(2) K |
| Wavelength | 0.71073 Å |
| Crystal system, space group | Monoclinic, $P2_1/a$ |
| Unit cell dimensions | a = 17.4860(3) Å α = 90 °<br>b = 6.31700(10) Å β = 106.1450(10)°<br>c = 21.5380(3) Å gamma = 90 ° |
| Volume | 2285.24(6) $A^3$ |
| Z, Calculated density | 4, 1.289 $Mg/m^3$ |
| Absorption coefficient | 0.345 $mm^{-1}$ |
| F(000) | 936 |
| Crystal size | 0.20 x 0.10 x 0.10 mm |
| Theta range for data collection | 3.52 to 27.48 ° |
| Limiting indices | -22<=h<=21, -7<=k<=8, -27<=l<=27 |
| Reflections collected / unique | 37262 / 5203 [R(int) = 0.0499] |
| Completeness to theta = 27.48 | 99.4 % |
| Max. and min. transmission | 0.9663 and 0.9342 |
| Refinement method | Full-matrix least-squares on $F^2$ |
| Data / restraints / parameters | 5203 / 0 / 262 |
| Goodness-of-fit on $F^2$ | 1.042 |
| Final R indices [I>2sigma(I)] | $R_1$ = 0.0361, $wR_2$ = 0.0985 |
| R indices (all data) | $R_1$ = 0.0464, $wR_2$ = 0.1082 |
| Largest diff. peak and hole | 0.309 and -0.549 e.$Å^{-3}$ |

Crystal data and structure refinement for $Zn(\mathbf{7})_2$.

| | |
|---|---|
| Identification code | h14mdj04 |
| Empirical formula | C25 H33 N2 O3 Zn0.50 |
| Formula weight | 442.22 |
| Temperature | 150(2) K |
| Wavelength | 0.71073 Å |
| Crystal system, space group | Monoclinic, $P2_1/n$ |
| Unit cell dimensions | a = 12.7520(5) Å α = 90 °<br>b = 13.4860(7) Å β = 98.867(3) °<br>c = 28.1480(12) Å γ = 90 ° |
| Volume | 4782.9(4) $Å^3$ |
| Z, Calculated density | 8, 1.228 $Mg/m^3$ |
| Absorption coefficient | 0.564 $mm^{-1}$ |
| F(000) | 1888 |
| Crystal size | 0.20 x 0.20 x 0.10 mm |
| Theta range for data collection | 3.63 to 27.58 ° |
| Limiting indices | -16<=h<=16, -17<=k<=17, -36<=l<=36 |
| Reflections collected / unique | 54781 / 10827 [R(int) = 0.0789] |
| Completeness to theta = 27.58 | 97.7 % |
| Absorption correction | Semi-empirical from equivalents |
| Max. and min. transmission | 0.9457 and 0.8955 |
| Refinement method | Full-matrix least-squares on $F^2$ |
| Data / restraints / parameters | 10827 / 0 / 566 |
| Goodness-of-fit on $F^2$ | 1.114 |
| Final R indices [I>2sigma(I)] | $R_1$ = 0.0684, $wR_2$ = 0.1765 |
| R indices (all data) | $R_1$ = 0.0978, $wR_2$ = 0.1930 |
| Largest diff. peak and hole | 0.758 and -0.512 $e.Å^{-3}$ |

Crystal data and structure refinement for Zn(**9**)$_2$.

| | |
|---|---|
| Identification code | s14mdj13 |
| Empirical formula | C18 H23 Cl2 N2 O3 Zn0.50 |
| Formula weight | 418.97 |
| Temperature | 150(2) K |
| Wavelength | 1.54184 Å |
| Crystal system, space group | Monoclinic, *C*2/*c* |
| Unit cell dimensions | a = 17.5578(13) Å α = 90 °<br>b = 12.1110(9) Å β = 109.517(11) °<br>c = 19.742(2) Å γ = 90 ° |
| Volume | 3956.8(6) Å$^3$ |
| Z, Calculated density | 8, 1.407 Mg/m$^3$ |
| Absorption coefficient | 3.744 mm$^{-1}$ |
| F(000) | 1744 |
| Crystal size | 0.10 x 0.05 x 0.03 mm |
| Theta range for data collection | 4.52 to 72.97 ° |
| Limiting indices | -20<=h<=21, -15<=k<=9, -24<=l<=24 |
| Reflections collected / unique | 14645 / 3843 [R(int) = 0.0627] |
| Completeness to theta = 72.97 | 97.2 % |
| Max. and min. transmission | 0.9122 and 0.7059 |
| Refinement method | Full-matrix least-squares on F$^2$ |
| Data / restraints / parameters | 3843 / 0 / 238 |
| Goodness-of-fit on F$^2$ | 1.051 |
| Final R indices [I>2sigma(I)] | $R_1$ = 0.0601, $wR_2$ = 0.1582 |
| R indices (all data) | $R_1$ = 0.0798, $wR_2$ = 0.1747 |
| Largest diff. peak and hole | 0.838 and -0.481 e.Å$^{-3}$ |

Crystal data and structure refinement for Zn(**10**)Me.

| | |
|---|---|
| Identification code | k14mdj06 |
| Empirical formula | C22 H28 N2 O Zn |
| Formula weight | 401.83 |
| Temperature | 150(2) K |
| Wavelength | 0.71073 Å |
| Crystal system, space group | Monoclinic, *C*2/*c* |
| Unit cell dimensions | a = 18.6250(6) Å α = 90 °<br>b = 9.4360(3) Å β = 112.2230(10) °<br>c = 24.5720(9) γ = 90 ° |
| Volume | 3997.6(2) $A^3$ |
| Z, Calculated density | 8, 1.335 $Mg/m^3$ |
| Absorption coefficient | 1.241 $mm^{-1}$ |
| F(000) | 1696 |
| Crystal size | 0.20 x 0.10 x 0.10 mm |
| Theta range for data collection | 3.95 to 25.04 ° |
| Limiting indices | -22<=h<=22, -11<=k<=11, -29<=l<=29 |
| Reflections collected / unique | 15606 / 15613 [R(int) = 0.0000] |
| Completeness to theta = 25.04 | 99.0 % |
| Max. and min. transmission | 0.8859 and 0.7894 |
| Refinement method | Full-matrix least-squares on $F^2$ |
| Data / restraints / parameters | 15613 / 0 / 238 |
| Goodness-of-fit on $F^2$ | 1.019 |
| Final R indices [I>2sigma(I)] | $R_1$ = 0.0644, $wR_2$ = 0.1463 |
| R indices (all data) | $R_1$ = 0.0956, $wR_2$ = 0.1662 |
| Largest diff. peak and hole | 0.499 and -0.512 e.$Å^{-3}$ |

Crystal data and structure refinement for Zn(**11**)Me.

| | |
|---|---|
| Identification code | s14mdj16 |
| Empirical formula | C22 H26 Cl2 N2 O Zn |
| Formula weight | 470.73 |
| Temperature | 150(2) K |
| Wavelength | 1.54184 Å |
| Crystal system, space group | Orthorhombic, $P2_12_12_1$ |
| Unit cell dimensions | a = 9.37080(10) Å α = 90 °<br>b = 9.77470(10) A β = 90 °<br>c = 23.9564(3) Å γ = 90 ° |
| Volume | 2194.33(4) $Å^3$ |
| Z, Calculated density | 4, 1.431 $Mg/m^3$ |
| Absorption coefficient | 3.904 $mm^{-1}$ |
| F(000) | 984 |
| Crystal size | 0.10 x 0.10 x 0.05 mm |
| Theta range for data collection | 4.89 to 72.02 ° |
| Limiting indices | -11<=h<=11, -12<=k<=12, -18<=l<=29 |
| Reflections collected / unique | 24550 / 4298 [R(int) = 0.0596] |
| Completeness to theta = 72.02 | 99.6 % |
| Max. and min. transmission | 0.8287 and 0.6962 |
| Refinement method | Full-matrix least-squares on $F^2$ |
| Data / restraints / parameters | 4298 / 0 / 255 |
| Goodness-of-fit on $F^2$ | 1.008 |
| Final R indices [I>2sigma(I)] | $R_1$ = 0.0454, $wR_2$ = 0.1181 |
| R indices (all data) | $R_1$ = 0.0458, $wR_2$ = 0.1187 |
| Absolute structure parameter | 0.52(2) |
| Largest diff. peak and hole | 0.563 and -0.492 $e.Å^{-3}$ |

Crystal data and structure refinement for Al(**11**)$Me_2$.

| | |
|---|---|
| Identification code | e15mdj10 |
| Empirical formula | C23 H29 Al Cl2 N2 O |
| Formula weight | 447.36 |
| Temperature | 150(2) K |
| Wavelength | 0.71073 Å |
| Crystal system | Monoclinic |
| Space group | $P2_1/n$ |
| Unit cell dimensions | a = 13.526(3) Å α= 90°<br>b = 11.7800(3) Å β=112.964(15)°<br>c = 15.6277(12) Å γ = 90° |
| Volume | 2292.7(5) $Å^3$ |
| Z | 4 |
| Density (calculated) | 1.296 $Mg/m^3$ |
| Absorption coefficient | 0.338 $mm^{-1}$ |
| F(000) | 944 |
| Crystal size | 0.30 x 0.20 x 0.20 $mm^3$ |
| Theta range for data collection | 3.32 to 26.37°. |
| Index ranges | -16<=h<=16, -14<=k<=14, -18<=l<=19 |
| Reflections collected | 16241 |
| Independent reflections | 4684 [R(int) = 0.0287] |
| Completeness to theta = 26.37° | 99.8 % |
| Max. and min. transmission | 0.9354 and 0.9053 |
| Refinement method | Full-matrix least-squares on $F^2$ |
| Data / restraints / parameters | 4684 / 0 / 265 |
| Goodness-of-fit on $F^2$ | 1.034 |
| Final R indices [I>2sigma(I)] | $R_1$ = 0.0361, $wR_2$ = 0.0902 |
| R indices (all data) | $R_1$ = 0.0468, $wR_2$ = 0.0966 |
| Largest diff. peak and hole | 0.369 and -0.307 e.$Å^{-3}$ |

Crystal data and structure refinement for **20**$H_2$.

| | |
|---|---|
| Identification code | MDJ37A |
| Empirical formula | C40 H59 N2 O2 |
| Formula weight | 599.89 |
| Temperature | 150(2) K |
| Wavelength | 1.54184 Å |
| Crystal system | Monoclinic |
| Space group | $P2_1/c$ |
| Unit cell dimensions | a = 14.03560(10) Å α= 90° |
| | b = 17.71280(10) Å β= 108.8450(10)° |
| | c = 15.61540(10) Å γ = 90° |
| Volume | 3674.04(5) $Å^3$ |
| Z | 4 |
| Density (calculated) | 1.085 $Mg/m^3$ |
| Absorption coefficient | 0.500 $mm^{-1}$ |
| F(000) | 1316 |
| Crystal size | 0.200 x 0.150 x 0.100 $mm^3$ |
| Theta range for data collection | 3.327 to 66.596° |
| Index ranges | -16<=h<=16, -21<=k<=21, -18<=l<=18 |
| Reflections collected | 56336 |
| Independent reflections | 6492 [R(int) = 0.0334] |
| Completeness to theta = 66.596° | 100.0 % |
| Refinement method | Full-matrix least-squares on $F^2$ |
| Data / restraints / parameters | 6492 / 21 / 429 |
| Goodness-of-fit on $F^2$ | 1.060 |
| Final R indices [I>2sigma(I)] | $R_1$ = 0.0591, $wR_2$ = 0.1638 |
| R indices (all data) | $R_1$ = 0.0627, wR2 = 0.1671 |
| Extinction coefficient | n/a |
| Largest diff. peak and hole | 0.701 and -0.569 e.$Å^{-3}$ |

Crystal data and structure refinement for $Zr_2$(**13**)($O^iPr$)$_6$.

| | | |
|---|---|---|
| Identification code | e15mdj24 | |
| Empirical formula | C143 H216 N4 O16 Zr4 | |
| Formula weight | 2612.06 | |
| Temperature | 150(2) K | |
| Wavelength | 0.71073 Å | |
| Crystal system | Triclinic | |
| Space group | *P*-1 | |
| Unit cell dimensions | a = 10.6100(3) Å | α= 101.501(2)° |
| | b = 13.4662(3) Å | β= 90.510(2)° |
| | c = 27.2278(7) Å | γ =107.840(2)° |
| Volume | 3618.57(17) Å$^3$ | |
| Z | 1 | |
| Density (calculated) | 1.199 Mg/m$^3$ | |
| Absorption coefficient | 0.339 mm$^{-1}$ | |
| F(000) | 1390 | |
| Crystal size | 0.300 x 0.300 x 0.300 mm$^3$ | |
| Theta range for data collection | 3.351 to 30.254° | |
| Index ranges | -14<=h<=14, -17<=k<=18, -38<=l<=35 | |
| Reflections collected | 37526 | |
| Independent reflections | 18460 [R(int) = 0.0204] | |
| Completeness to theta = 25.242° | 99.7 % | |
| Refinement method | Full-matrix least-squares on $F^2$ | |
| Data / restraints / parameters | 18460 / 42 / 858 | |
| Goodness-of-fit on $F^2$ | 1.041 | |
| Final R indices [I>2sigma(I)] | $R_1$ = 0.0417, $wR_2$ = 0.0876 | |
| R indices (all data) | $R_1$ = 0.0577, $wR_2$ = 0.0962 | |
| Extinction coefficient | n/a | |
| Largest diff. peak and hole | 1.032 and -0.596 e.Å$^{-3}$ | |

Crystal data and structure refinement for $Hf_2$(**13**)($O^iPr$)$_6$.

| | |
|---|---|
| Identification code | s16mdj36 |
| Empirical formula | C63 H109 Hf2 N2 O8 |
| Formula weight | 1379.50 |
| Temperature | 150.01(10) K |
| Wavelength | 1.54184 Å |
| Crystal system, space group | Triclinic, *P*-1 |
| Unit cell dimensions | a = 15.0674(3) Å α = 89.944(2)°<br>b = 15.3066(3) Å β = 65.437(2)°<br>c = 16.2254(4) Å γ = 87.572(2)° |
| Volume | 3399.81(14) Å$^3$ |
| Z, Calculated density | 2, 1.348 Mg/m$^3$ |
| Absorption coefficient | 5.913 mm$^{-1}$ |
| F(000) | 1418 |
| Crystal size | 0.220 x 0.200 x 0.150 mm |
| Theta range for data collection | 2.890 to 70.074 ° |
| Limiting indices | -18<=h<=16, -16<=k<=18, -19<=l<=19 |
| Reflections collected / unique | 26427 / 12915 [R(int) = 0.0231] |
| Completeness to theta = 25.06 | 100.0 % |
| Max. and min. transmission | 1.00000 and 0.53561 |
| Refinement method | Full-matrix least-squares on F$^2$ |
| Data / restraints / parameters | 12915 / 27 / 805 |
| Goodness-of-fit on F$^2$ | 1.055 |
| Final R indices [I>2sigma(I)] | $R_1$ = 0.0291, $wR_2$ = 0.0698 |
| R indices (all data) | $R_1$ = 0.0351, $wR_2$ = 0.0741 |
| Largest diff. peak and hole | 1.221 and -0.907 e.Å$^{-3}$ |

Crystal data and structure refinement for $Al_2$(**13**)$Me_4$.

| | |
|---|---|
| Identification code | s16mdj30 |
| Empirical formula | C40 H58 Al2 N2 O2 |
| Formula weight | 652.84 |
| Temperature | 150(2) K |
| Wavelength | 1.54184 Å |
| Crystal system | Orthorhombic |
| Space group | *F*dd2 |
| Unit cell dimensions | a = 39.9899(3) Å α = 90° |
| | b = 21.8307(2) Å β = 90° |
| | c = 9.34980(10) Å γ = 90° |
| Volume | 8162.45(13) $Å^3$ |
| Z | 8 |
| Density (calculated) | 1.062 $Mg/m^3$ |
| Absorption coefficient | 0.885 $mm^{-1}$ |
| F(000) | 2832 |
| Crystal size | 0.30 x 0.25 x 0.20 $mm^3$ |
| Theta range for data collection | 4.42 to 70.07° |
| Index ranges | -48<=h<=48, -26<=k<=26, -11<=l<=9 |
| Reflections collected | 32891 |
| Independent reflections | 3639 [R(int) = 0.0275] |
| Completeness to theta = 70.07° | 100.0 % |
| Max. and min. transmission | 0.8429 and 0.7772 |
| Refinement method | Full-matrix least-squares on $F^2$ |
| Data / restraints / parameters | 3639 / 1 / 216 |
| Goodness-of-fit on $F^2$ | 1.089 |
| Final R indices [I>2sigma(I)] | $R_1$ = 0.0238, $wR_2$ = 0.0652 |
| R indices (all data) | $R_1$ = 0.0239, $wR_2$ = 0.0653 |
| Absolute structure parameter | 0.00(2) |
| Largest diff. peak and hole | 0.159 and -0.145 e.$Å^{-3}$ |

Crystal data and structure refinement for $Al_2$(**16**)$_2Me_2$.

| | | |
|---|---|---|
| Identification code | e16mdj02 | |
| Empirical formula | C28 H33 Al N2 O | |
| Formula weight | 440.54 | |
| Temperature | 150(2) K | |
| Wavelength | 0.71073 Å | |
| Crystal system | Monoclinic | |
| Space group | *I*2/a | |
| Unit cell dimensions | a = 14.0323(3) Å | α = 90° |
| | b = 20.2988(6) Å | β = 90.120(2)° |
| | c = 16.9186(4) Å | γ = 90° |
| Volume | 4819.1(2) Å$^3$ | |
| Z | 8 | |
| Density (calculated) | 1.214 Mg/m$^3$ | |
| Absorption coefficient | 0.107 mm$^{-1}$ | |
| F(000) | 1888 | |
| Crystal size | 0.30 x 0.20 x 0.20 mm$^3$ | |
| Theta range for data collection | 3.34 to 26.37° | |
| Index ranges | -17<=h<=16, -24<=k<=25, -21<=l<=21 | |
| Reflections collected | 29329 | |
| Independent reflections | 4920 [R(int) = 0.0210] | |
| Completeness to theta = 26.37° | 99.7 % | |
| Max. and min. transmission | 0.9790 and 0.9687 | |
| Refinement method | Full-matrix least-squares on F$^2$ | |
| Data / restraints / parameters | 4920 / 0 / 297 | |
| Goodness-of-fit on F$^2$ | 0.991 | |
| Final R indices [I>2sigma(I)] | $R_1$ = 0.0336, $wR_2$ = 0.0912 | |
| R indices (all data) | $R_1$ = 0.0381, $wR_2$ = 0.0952 | |
| Largest diff. peak and hole | 0.296 and -0.241 e.Å$^{-3}$ | |

Crystal data and structure refinement for Al(**19**)$Me_2$.

| | | |
|---|---|---|
| Identification code | e15mdj13 | |
| Empirical formula | C21 H19 Al N2 O | |
| Formula weight | 342.36 | |
| Temperature | 150(2) K | |
| Wavelength | 0.71073 Å | |
| Crystal system | Monoclinic | |
| Space group | $P2_1/c$ | |
| Unit cell dimensions | a = 9.3200(9) Å | α = 90°. |
| | b = 8.4251(4) Å | β =98.838(15)° |
| | c = 23.276(4) Å | γ = 90°. |
| Volume | 1806.0(4) $Å^3$ | |
| Z | 4 | |
| Density (calculated) | 1.259 $Mg/m^3$ | |
| Absorption coefficient | 0.123 $mm^{-1}$ | |
| F(000) | 720 | |
| Crystal size | 0.20 x 0.20 x 0.05 $mm^3$ | |
| Theta range for data collection | 3.30 to 25.02° | |
| Index ranges | -10<=h<=11, -10<=k<=10, -27<=l<=27 | |
| Reflections collected | 12768 | |
| Independent reflections | 3167 [R(int) = 0.0323] | |
| Completeness to theta = 25.02° | 99.8 % | |
| Max. and min. transmission | 0.9939 and 0.9759 | |
| Refinement method | Full-matrix least-squares on $F^2$ | |
| Data / restraints / parameters | 3167 / 0 / 228 | |
| Goodness-of-fit on $F^2$ | 1.023 | |
| Final R indices [I>2sigma(I)] | $R_1$ = 0.0460, $wR_2$ = 0.0998 | |
| R indices (all data) | $R_1$ = 0.0625, $wR_2$ = 0.1071 | |
| Largest diff. peak and hole | 0.662 and -0.364 e.$Å^{-3}$ | |

Crystal data and structure refinement for Al(**20**)Me.

| | |
|---|---|
| Identification code | s15mdj29 |
| Empirical formula | C38 H53 Al N2 O2 |
| Formula weight | 596.80 |
| Temperature | 150(2) K |
| Wavelength | 1.54184 Å |
| Crystal system | Monoclinic |
| Space group | $P2_1/c$ |
| Unit cell dimensions | a = 9.36640(10) Å α = 90°<br>b = 29.9373(2) Å β = 105.9740(10)°<br>c = 13.10040(10) Å γ = 90° |
| Volume | 3531.57(5) $Å^3$ |
| Z | 4 |
| Density (calculated) | 1.122 $Mg/m^3$ |
| Absorption coefficient | 0.750 $mm^{-1}$ |
| F(000) | 1296 |
| Crystal size | 0.1 x 0.01 x 0.05 $mm^3$ |
| Theta range for data collection | 4.59 to 71.91° |
| Index ranges | -11<=h<=10, -36<=k<=34, -16<=l<=16 |
| Reflections collected | 49141 |
| Independent reflections | 6932 [R(int) = 0.0234] |
| Completeness to theta = 71.91° | 99.9 % |
| Refinement method | Full-matrix least-squares on $F^2$ |
| Data / restraints / parameters | 6932 / 0 / 402 |
| Goodness-of-fit on $F^2$ | 1.036 |
| Final R indices [I>2sigma(I)] | $R_1$ = 0.0337, $wR_2$ = 0.0863 |
| R indices (all data) | $R_1$ = 0.0353, $wR_2$ = 0.0874 |
| Largest diff. peak and hole | 0.252 and -0.298 $e.Å^{-3}$ |

Crystal data and structure refinement for Zr(**20**)($O^iPr$)$_2$.

| | | |
|---|---|---|
| Identification code | s14mdj27 | |
| Empirical formula | C51 H48 N4 O4 Zr | |
| Formula weight | 872.15 | |
| Temperature | 150(2) K | |
| Wavelength | 1.54184 Å | |
| Crystal system | Monoclinic | |
| Space group | $P2_1/c$ | |
| Unit cell dimensions | a = 16.0477(7) Å | α= 90° |
| | b = 26.2712(13) Å | β= 101.817(4)° |
| | c = 10.5861(4) Å | γ = 90° |
| Volume | 4368.4(3) Å$^3$ | |
| Z | 4 | |
| Density (calculated) | 1.326 Mg/m$^3$ | |
| Absorption coefficient | 2.456 mm$^{-1}$ | |
| F(000) | 1816 | |
| Crystal size | 0.20 x 0.10 x 0.05 mm$^3$ | |
| Theta range for data collection | 4.59 to 70.14° | |
| Index ranges | -19<=h<=11, -31<=k<=31, -12<=l<=12 | |
| Reflections collected | 15003 | |
| Independent reflections | 8042 [R(int) = 0.0444] | |
| Completeness to theta = 67.684° | 97.0 % | |
| Max. and min. transmission | 0.8870 and 0.6394 | |
| Refinement method | Full-matrix least-squares on $F^2$ | |
| Data / restraints / parameters | 8042 / 0 / 587 | |
| Goodness-of-fit on $F^2$ | 1.125 | |
| Final R indices [I>2sigma(I)] | $R_1$ = 0.0501, $wR_2$ = 0.0958 | |
| R indices (all data) | $R_1$ = 0.0689, $wR_2$ = 0.1022 | |
| Largest diff. peak and hole | 0.916 and -0.615 e.Å$^{-3}$ | |

Crystal data and structure refinement for Zr(**20**)($O^tBu$)$_2$.

| | |
|---|---|
| Identification code | s16mdj42 |
| Empirical formula | C97 H144 N4 O8 Zr2 |
| Formula weight | 1676.59 |
| Temperature | 150.01(10) K |
| Wavelength | 1.54184 Å |
| Crystal system | Monoclinic |
| Space group | $P2_1/n$ |
| Unit cell dimensions | a = 14.68480(10) Å α = 90° |
| | b = 22.36270(10) Å β =113.500(1)° |
| | c = 15.72650(10) Å γ = 90° |
| Volume | 4736.11(6) Å$^3$ |
| Z | 2 |
| Density (calculated) | 1.176 Mg/m$^3$ |
| Absorption coefficient | 2.219 mm$^{-1}$ |
| F(000) | 1796 |
| Crystal size | 0.200 x 0.150 x 0.100 mm$^3$ |
| Theta range for data collection | 3.485 to 73.431° |
| Index ranges | -18<=h<=18, -25<=k<=27, -19<=l<=19 |
| Reflections collected | 108679 |
| Independent reflections | 9516 [R(int) = 0.0254] |
| Completeness to theta = 67.684° | 100.0 % |
| Absorption correction | Semi-empirical from equivalents |
| Max. and min. transmission | 1.00000 and 0.83542 |
| Refinement method | Full-matrix least-squares on F$^2$ |
| Data / restraints / parameters | 9516 / 0 / 539 |
| Goodness-of-fit on F$^2$ | 1.069 |
| Final R indices [I>2sigma(I)] | $R_1$ = 0.0236, $wR_2$ = 0.0615 |
| R indices (all data) | $R_1$ = 0.0241, $wR_2$ = 0.0618 |
| Extinction coefficient | n/a |
| Largest diff. peak and hole | 0.536 and -0.330 e.Å$^{-3}$ |

Crystal data and structure refinement for Hf(**20**)($O^iPr$)$_2$.

| | | |
|---|---|---|
| Identification code | e16mdj08 | |
| Empirical formula | C91 H140 Hf2 N4 O8 | |
| Formula weight | 1775.04 | |
| Temperature | 150(2) K | |
| Wavelength | 0.71073 Å | |
| Crystal system | Monoclinic | |
| Space group | $P2_1/n$ | |
| Unit cell dimensions | a = 14.665(4) Å | α = 90° |
| | b = 22.490(3) Å | β = 114.16(2)° |
| | c = 15.545(3) Å | γ = 90° |
| Volume | 4677.8(17) Å$^3$ | |
| Z | 2 | |
| Density (calculated) | 1.260 Mg/m$^3$ | |
| Absorption coefficient | 2.269 mm$^{-1}$ | |
| F(000) | 1844 | |
| Crystal size | 0.250 x 0.200 x 0.090 mm$^3$ | |
| Theta range for data collection | 3.322 to 28.386° | |
| Index ranges | -19<=h<=17, -29<=k<=29, -20<=l<=20 | |
| Reflections collected | 70175 | |
| Independent reflections | 10594 [R(int) = 0.0671] | |
| Completeness to theta = 25.242° | 99.7 % | |
| Absorption correction | Analytical | |
| Max. and min. transmission | 0.958 and 0.899 | |
| Refinement method | Full-matrix least-squares on F$^2$ | |
| Data / restraints / parameters | 10594 / 111 / 602 | |
| Goodness-of-fit on F$^2$ | 1.089 | |
| Final R indices [I>2sigma(I)] | $R_1$ = 0.0625, $wR_2$ = 0.1132 | |
| R indices (all data) | $R_1$ = 0.1041, $wR_2$ = 0.1269 | |
| Extinction coefficient | n/a | |
| Largest diff. peak and hole | 2.280 and -0.892 e.Å$^{-3}$ | |